ACRH-16

ARGONNE CANCER RESEARCH HOSPITAL
950 EAST FIFTY-NINTH STREET · CHICAGO 37 · ILLINOIS

Semiannual Report to
THE ATOMIC ENERGY COMMISSION

SEPTEMBER 1961

LEON O. JACOBSON, M.D.
Editor

MARGOT DOYLE, Ph.D.
Associate Editor

OPERATED BY THE UNIVERSITY OF CHICAGO
UNDER
CONTRACT AT-(11-1)-69

DISCLAIMER

LEGAL NOTICE

Price $2.75. Available from the Office of
Technical Services, Department of Commerce,
Washington 25, D.C.

ACRH-16

ARGONNE CANCER RESEARCH HOSPITAL
950 EAST FIFTY-NINTH STREET · CHICAGO 37 · ILLINOIS

Semiannual Report to

THE ATOMIC ENERGY COMMISSION

SEPTEMBER 1961

LEON O. JACOBSON, M.D.
Editor

MARGOT DOYLE, Ph.D.
Associate Editor

OPERATED BY THE UNIVERSITY OF CHICAGO
UNDER
CONTRACT AT-(11-1)-69

TABLE OF CONTENTS

THE USE OF I^{125} TO INCREASE ISOTOPE SCANNING RESOLUTION*

By

H. Endlich,† P. V. Harper, R. N. Beck, W. D. Siemens,
and K. A. Lathrop

The probability of detecting a "cold" lesion in an organ such as the liver or thyroid by isotope scanning depends on both the absolute count rate and the contrast on target—non-target ratio over the lesion. The contrast ratio, especially in a large organ like the liver, is considerably reduced by high-energy radiation originating in the tissues beneath the cold lesion and penetrating through it to the collimator system. It occurred to us that the contrast ratio could be increased considerably by the use of a radiation source emitting low energy gamma radiation or x-radiation, since photons originating deep in the organ would be largely attenuated before reaching the detector, while photons originating from more superficial regions would still be detectable.[1-3]

Using conventional methods with I^{131} rose bengal or colloidal gold^{198} for liver scans, practical considerations limit the collimator design to a field of view approximately 1 inch in diameter, and the detection of cold nodules much smaller becomes virtually impossible.[4,5] In the thyroid, where the mass of tissue surrounding the cold nodule is much smaller and the available photon flux is higher, a collimator with a field of view 5 to 6 mm in diameter at the focus may be used, and cold nodules of this size may be demonstrated under favorable conditions.[6] One of the principal objectives of this investigation was to evaluate the possible improvement in resolution which might be obtained by using lower energy photon emitters.

EXPERIMENTAL

Two apparently suitable sources of low energy radiation are palladium-103, whose principal radiations, the rhodium $K\alpha$ and $K\beta$ photons, have energies of 20.2 and 23 KEV, and iodine-125, whose observable photon radiations are the tellurium $K\alpha$ and $K\beta$ lines with energies of 27.4 and 31.2 KEV respectively, and the small unconverted fraction of the 35.4 KEV gamma. The narrow-beam half-value layers for these radiations are very nearly 1.0 cm and 2.0 cm, respectively, in tissue.[3,7]

A variety of phantoms was constructed to represent the liver and thyroid containing cold lesions of various sizes and locations. These phantoms were made of slabs of 12 per cent gelatin, 4 x 1/2 inch, and contained the isotope in solution with cylindrical Lucite plugs to represent the cold nodules. Figure 1 shows count rate profiles across 6 such liver phantoms containing palladium-103, iodine-125, and iodine-131, and having lesions 1 x 1 inch in two locations, one on the surface of the liver and the other 1 inch below the surface. In both cases, 1 inch of overlying tissue was present, and the thickness of the liver was 4 inches. A 2 x 2 inch sodium iodide crystal with a 5 mil beryllium window was used with the same collimator for all measurements.

*This paper has been accepted for publication in the Am. J. Roentgenol., Rad. Therapy, and Nucl. Med.

†Department of Radiology, University of Chicago.

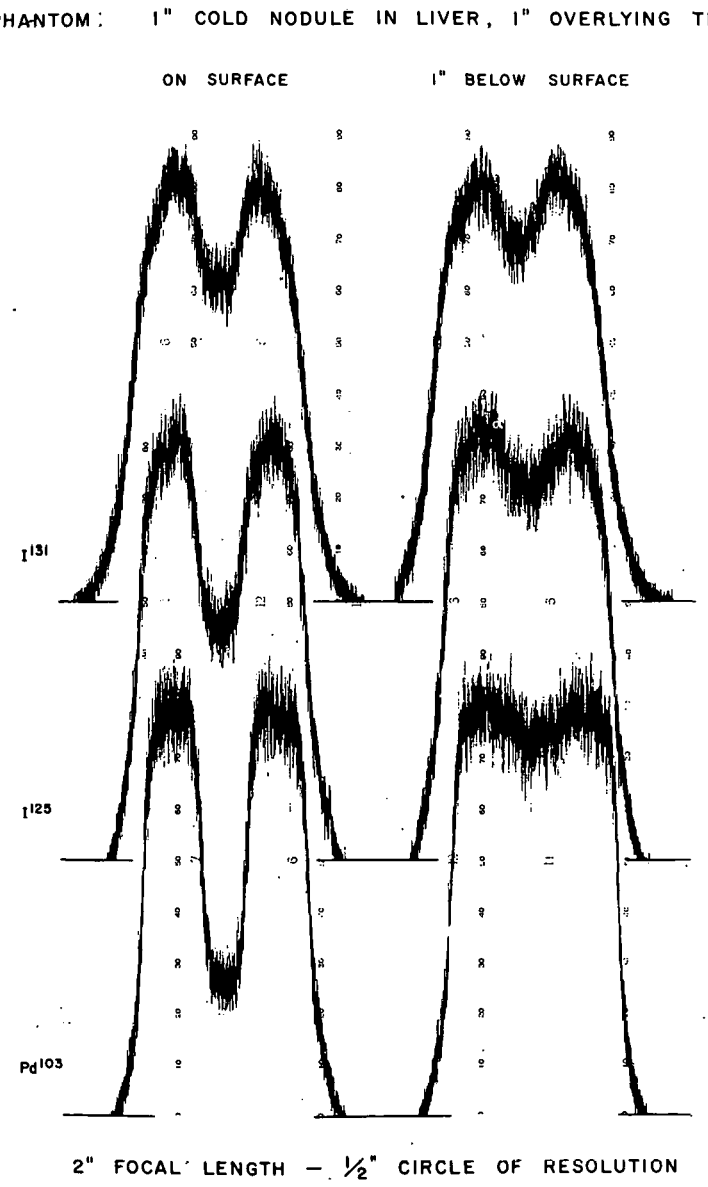

Figure 1. Count rate profiles across liver phantoms containing I^{131}, I^{125}, and Pd^{103}.

The collimator, which had a 2-inch focal length and a 1/2-inch circle of view at the focus was designed so that 1 per cent of the observed counts for I^{131} represented 364 KEV photons which had penetrated the collimator septa. The focal point of the collimator traversed the center of the "lesion" during the scan. A single channel pulse height analyzer was used to observe the principal photopeak of each isotope.

Similar measurements were made on thyroid phantoms constructed of 1/2-inch slabs of gelatin containing either I^{125} or I^{131}. These were sandwiched between 1 inch of overlying and 4 inches of underlying untagged gelatin representing the other tissues of the neck. The 1-inch diameter Lucite plugs representing the cold lesions extended entirely through the 1/2-inch active

layer so that the collimator over the lesion was not looking directly at any of the radioactive material and registered only scattered photons.

The contrast ratios and relative count rates observed in these phantoms, normalized to the same isotope concentration, are shown in Table 1. We had feared that the radiations from I^{125}, which are attenuated to a substantial degree by scatter rather than absorption, might produce an intense background of scattered radiation. As can be seen, especially in thyroid phantoms, while this phenomenon exists, it is somewhat less than the background from Compton scatter of the high energy photons of I^{131}.

Table 1

OBSERVED CONTRAST RATIOS

	Liver phantoms			Thyroid phantoms	
	Contrast ratio		Relative count rates over normal tissue for equal isotope density	Contrast ratio	Relative count rates over normal tissue for equal isotope density
	Lesion on surface	Lesion 1" below surface			
I^{131}	.77	.87	100	.34	100
I^{125}	.58	.91	58	.30	85
Pd^{103}	.35	.96	4	-	-

Since the probability of detecting a lesion within a given time depends on the count rate as well as on the contrast, the attenuation in overlying tissue becomes critical at the lower energies. Under the conditions shown in Figure 1, the one inch of overlying tissue produces a reduction in count rate to 79 per cent for I^{131}, to 45 per cent for I^{125} and to 21 per cent for Pd^{103} This attenuation nullifies to a considerable extent the useful increase in contrast.

The difficulty in producing a palladium compound with properties suitable for liver scanning has virtually eliminated the use of this material at the present time. Palladium phthalocyanine sulfonate was found to have a biological half time of about 12 days in the liver. In comparison, the half-life of iodine-tagged rose bengal is a few hours.

The respective radiation dosages[3,4] of I^{125} and I^{131} are compared in Table 2. The energy from I^{125} available for producing ionization is the sum of the 35.4 KEV gamma transition and the energy of the tellurium excited state following K or L capture. This amounts to an average of 62.3 KEV per disintegration with 41.3 KEV as K and γ photons. The remaining 21.0 KEV appears as soft fluorescent photons, conversion electrons and Auger electrons, which are absorbed close to their point of origin and may be considered in dose calculations as β radiation.

Using specially designed detectors, the radiation of I^{125} may be detected several times more efficiently than those of I^{131}. Collimators may be designed[8] which are approximately 3 times as efficient for I^{125} as for I^{131} for the same configuration and field of view. Virtually all the photons from I^{125} penetrate the beryllium window, interact with the sodium iodide detector crystal and appear in the photopeak, while approximately 50 per cent of the photons from I^{131} have Compton interactions in the crystal and do not appear in the photopeak.[9] In addition, I^{125}

Table 2

COMPARATIVE RADIATION DOSAGE

Isotope	Rads per μcd/g			Total organ dose (rads)		
	Thyroid	Liver	Total body	Thyroid 30 μc/30 g	Liver 200 μc/1.5 kg	Total body 5 μc/70 kg
I^{131}	120	152	200	103	.210	.010
I^{125}	130	192	272	58	.035	.014
			AGENT	Iodide	Rose bengal	Iodinated albumin
			Biol. half-life	50 days	2 hours	17 days

produces 1.8 times as many detectable photons per disintegration as does I^{131}.

In an attempt to bring all these different factors together for comparison under optimal conditions, the relative statistical detection efficiency was computed* for the cold nodules in the liver and thyroid phantoms described above, based on equal radiation dosage and scan time. The observed count rates were weighted according to the above mentioned factors, and the results are shown in Table 3. The values in Table 3 may be interpreted in several ways. For instance,

Table 3

RELATIVE STATISTICAL DETECTION EFFICIENCY

For cold nodules in phantoms for same scan time and radiation dosage

	Liver		Thyroid
	Lesion on surface	Lesion 1" below surface	
I^{131}	1.00	.30	1
I^{125}	21	.80	5.5

*Consider the count rate C_L over a cold lesion and C_t over the surrounding tissue. In time T, $C_L T$ and $C_t T$ counts will be accumulated over these regions. A statistical measure of the difference between these two counts is the number Z of standard deviations of the difference contained in the difference. Since Poisson formulation may be applied, the standard deviation of the difference is $\sqrt{C_t T + C_L T}$ and

$$Z = \frac{C_t T - C_L T}{\sqrt{C_t T + C_L T}}$$

Rearranging: $$T = \frac{Z^2\left(\frac{C_L}{C_t} + 1\right)}{C_t\left(\frac{C_L}{C_t} - 1\right)^2}$$

T is thus the time required for a count over each region long enough to establish the existence of a difference with $Z\delta$ confidence. T depends both on the contrast ration C_L/C_T and the absolute count rate C_T. The reciprocal of T is taken as a measure of the statistical detection efficiency.

in the liver phantom with the cold nodule on the surface shown in column 1, the lesion could be detected 21 times faster using the I^{125} for the same radiation dosage as with I^{131} or it could be detected in the same time for 1/21 of the radiation dosage or, using the same scan time and radiation dosage as with I^{131}, a collimator with a sharper focus and resultant lower efficiency could be used to increase the resolution of the resulting picture.

In considering this increase in resolution, it is difficult to arrive at a precise descriptive criterion. Each situation appears to have its own special requirements. Since in both thyroid and liver scanning the lesions of interest are voids, the criterion chosen was the smallest void which could be detected with 2δ confidence from the count rates over the void and the surrounding tissue. In the case of the thyroid the void was assumed to extend entirely through the gland as in the experiments described. In the case of the liver, the void was assumed to have a depth equal to its diameter, and the field of view of the collimator was assumed to equal the diameter of the void. The diameter of the circle of view of the collimator at its focus thus becomes the measure of resolution, and the counting statistics determine the smallest usable collimator.

Using the same parameters as in Table 3, it can be shown that with I^{125} a cold nodule of approximately one half the diameter should be detectable in either the thyroid or liver without exceeding the radiation dosage and scanning time used with I^{131}. The effect of reducing the diameter of the "circle of view at the focus" to one-half reduces the counting efficiency of the collimator by a factor of 4 or more depending on the configuration of the region of view. Since the time permitted for viewing a region of this size during a scan is likewise reduced by a factor of 4 when the scan time is kept constant, the opportunity for the detector system to accumulate a statistically valid count over such a lesion is reduced by a factor of 16 or more, thus requiring at least a 4th power increase in the emitted detectable photon flux at the surface of the body or an appropriate increase in contrast or both, if statistical validity is to be maintained. These conditions are apparently achieved by substituting I^{125} for I^{131}.

The absolute dimensions of the smallest detectable lesions were estimated using the above criteria together with the efficiencies of optimal collimators.[8] Assuming, for the thyroid, 1 inch of overlying tissue, a 15-minute scan time, 100 cm^2 for the area scanned, and 100 rads for dose to the gland, a lesion 6.1 mm in diameter should be detectable with I^{131}, and 3.6 mm in diameter with I^{125}.

For the liver, with 1 inch overlying tissue, using a scan time of 30 minutes, 600 cm^2 for area scanned, and 200 mrad for radiation dosage, lesions 17 mm in diameter on the surface and 21 mm in diameter 1 inch below the surface should be detectable with I^{131}. The corresponding figures for I^{125} are 9 mm and 21 mm. These numbers are, of course, based on the assumption that the liver is not moving with respiration, and must be interpreted with this reservation.

The size of a detectable lesion by this statistical criterion thus appears to be consistent with the experience gained by other investigators using I^{131} for liver and thyroid scanning and we are hopeful that the predicted figures for I^{125} may be realistic.

CLINICAL MATERIAL

The principal deterrent to the clinical and experimental use of iodine-125 has been its lack of availability. The commercially available I^{125} produced by the cyclotron bombardment of tellurium is expensive and heavily contaminated with the undesirable 13-day iodine-126. The alternative method of producing iodine-125 by the neutron activation of xenon-124 has been developed

in our laboratory to the point where curie quantities with less than 2 per cent contamination have been produced, and it now appears feasible to consider the clinical use of this material on a substantial scale.[3,7]

As special detection equipment is not yet available for routine scanning of iodine-125, conventional unmodified equipment was used, and iodine-125 was substituted for iodine-131, microcurie for microcurie. Under these circumstances the radiation dosage to the patient except under the most unfavorable circumstances was still less than that of I^{131}. (See Table 2.)

In the present study, comparative thyroid scans with iodine-125 and iodine-131 were made on ten patients, and comparative liver scans, using iodine-tagged rose bengal likewise were made on ten patients. All patients were selected on the basis of clinically suspected pathology. In all cases, iodine-125 was used first, followed by iodine-131, in order to prevent the low energy Compton scatter from the iodine-131 interfering with the low energy photons from iodine-125. Pulse height analysis was used for both isotopes so that only the 364 KEV photopeak was observed for iodine-131 and the 27 to 35 KEV photopeak for iodine-125. The equipment was the Picker Magna-scanner as described by Herring,[10] the 19-hole collimator being used for the liver scans and the 31-hole collimator for the thyroid scans. The thyroid patients were scanned 24 hours after administration of 50 microcuries of isotope. Those patients in whom the liver was scanned were given iodine-125- and iodine-131-labeled rose bengal in doses of 3 μc per kg, without previous administration of untagged rose bengal.

As was expected, the count rates with iodine-125 averaged somewhat lower for the liver scans—1,200 to 1,500 counts per minute with iodine-125 and 3,000 to 4,000 counts per minute with iodine-131. This is not surprising since special detectors were not used for the iodine-125 and the attenuation of radiation in the aluminum can of the crystal alone accounts for an additional loss of 40 per cent in count rate. Nevertheless, even under these circumstances, representative liver scans (Figures 2 and 3) show a remarkably improved visualization of surgically demonstrated hepatic metastases.

In general, the thyroid scans closely resembled those obtained with I^{131}. Cold nodules are better delineated, however, even though the count rates are lower, as observed in Figure 4 which illustrates the thyroid scans of a patient with multinodular nontoxic goiter. The many nodules are clearly demonstrated with iodine-125, but almost not at all with iodine-131. The gross pathological specimen is seen in Figure 5.

DISCUSSION

The single most consistent observation made in comparing scans made with the two isotopes is the over-all increase in contrast in scans with I^{125}. It should be pointed out that the increased contrast in cold nodules demonstrated in the liver and thyroid is not entirely equivalent to the criteria for resolution presented in the earlier part of this paper. In the clinical cases the count rates far exceed the minimal values required for "statistical detection of a lesion." The isotope contrast becomes prominent under these circumstances and produces a greatly improved picture.

It is interesting to speculate, and work is in progress at the moment to determine, how much further the picture can be improved by sharpening the collimator focus and sacrificing count rate. It is also possible that by judicious application of background cutoff techniques the collimator focus may be sharpened in effect without as much loss in count rate. At the present time

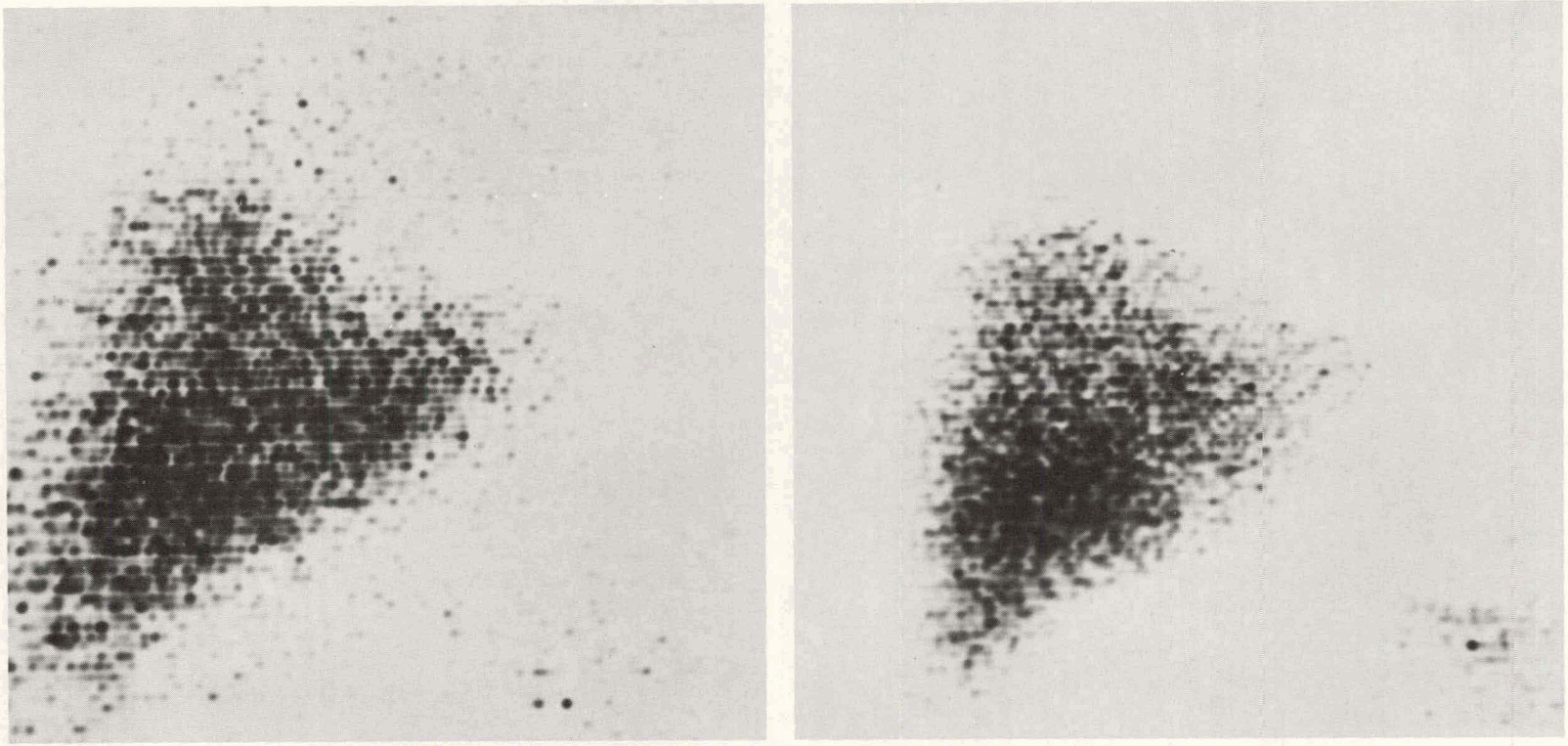

Figure 2. Rose bengal liver scans of the same patient using I^{125} on left, I^{131} on right, with demonstration of surgically proven metastases by I^{125} which are practically invisible using I^{131} (Picker Magna-scanner, 19-hole collimator).

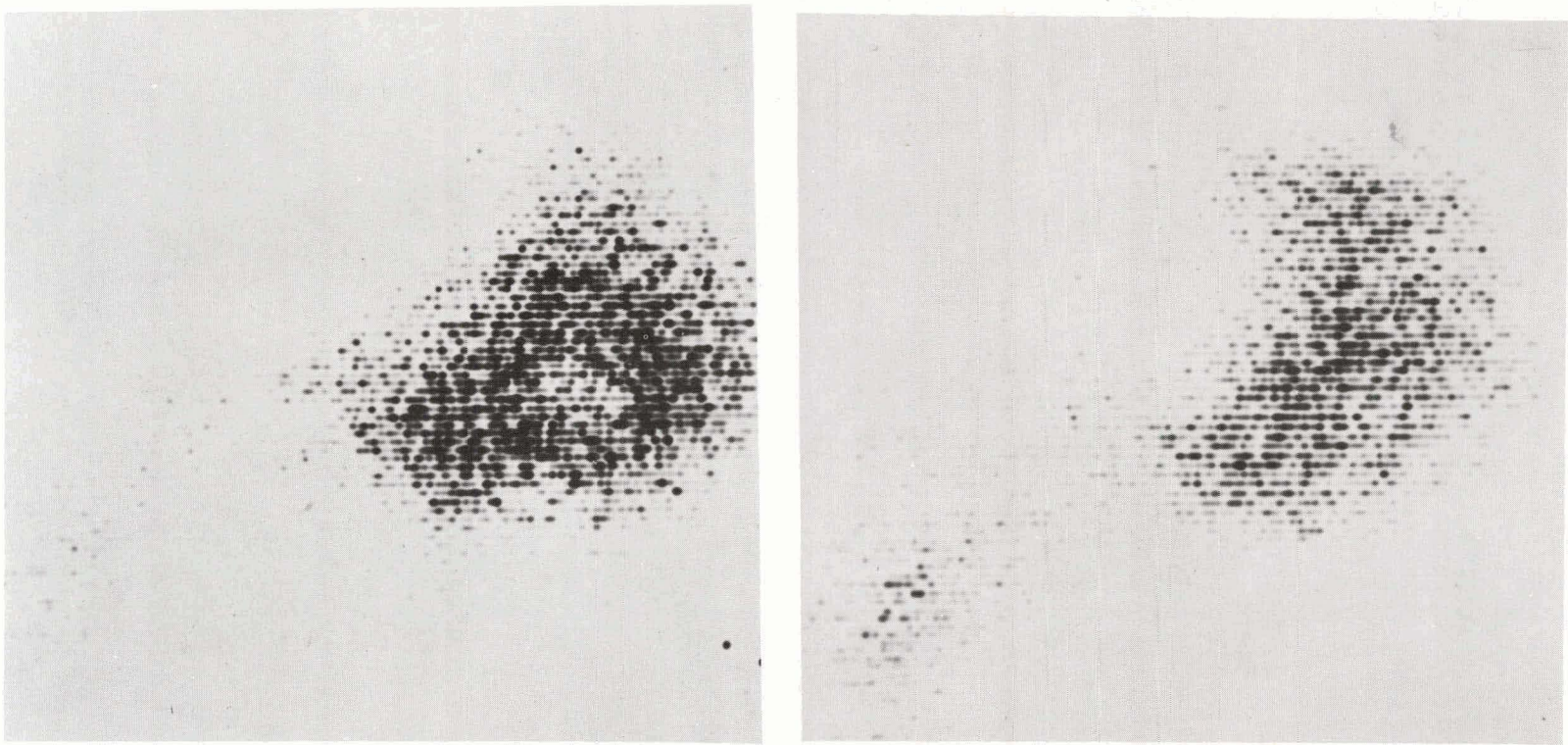

Figure 3. Demonstration of lesion using I^{125} rose bengal liver scan (left) which is practically invisible with I^{131} (right).

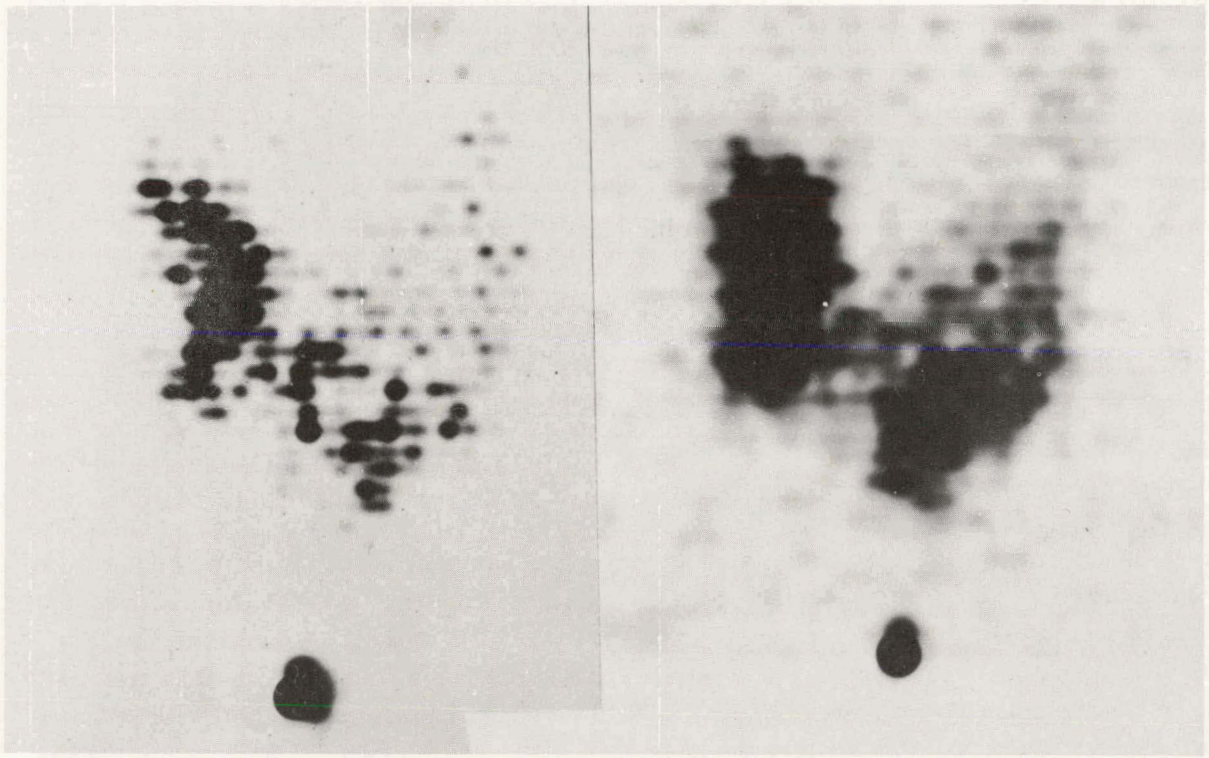

Figure 4. I^{125} (left) and I^{131} (right) scans of multinodular thyroid, 15 μc in gland (Picker Magna-scanner using 31-hole collimator).

Figure 5. Surgical specimen of thyroid shown in Figure 4.

it seems completely justifiable to use I^{125} with the equipment available since, even under these unfavorable circumstances, iodine-125 appears to be as good as or better than I^{131} in terms of producing a more clearly resolved scan of the thyroid and the liver.

The methods of contrast now in use, background cutoff, and video or photographic manipulation,[11-13] should be complementary to the "built in" contrast in I^{125} scans. It is characteristic of all these methods that some information must be sacrificed at least temporarily in order that other information may be accessible. I^{125} is no exception to the rule, as is seen in Table 3. While the possibility of detecting a lesion much beneath the surface of the liver is reduced to a relatively much greater extent than with the penetrating radiation of I^{131}, it is a matter of practical experience that such lesions, unless quite large, are much more difficult to detect by any type of scanning technique. It is obvious that to be most effective the liver scan should be circumferential rather than planar, as suggested by Kuhl,[14] and under these circumstances a collimator with shorter focus and higher efficiency would be more effective, giving clearer pictures of the entire "visible" surface of the liver, and permitting visualization of lesions on the lateral and posterior aspects of the liver, at present hidden in a frontal, planar scan. The use of more efficient, shorter focus collimators introduces divergence into the region of view to a greater extent although the divergence beyond the focal point is of little importance because photons originating at this depth are largely attenuated in the overlying tissue. This circumstance and the much larger area to be looked at in a circumferential scan suggest that multiple detectors would probably achieve the best results.

While the relatively low radiation dosage to the liver produced by tagged rose bengal permits justification of efforts to increase the resolution of the liver scan, this position is not so readily tenable in thyroid scanning, and it would appear wise to expend a considerable portion of the advantage gained from the use of I^{125} in reducing the radiation dosage to the gland resulting from this procedure.

Other advantages accruing from the use of I^{125} are the long shelf life (60 day half-life), low shielding requirements, and low background possible when a thin crystal is used.[1-3,7,15]

LITERATURE CITED

1. Harper, P. V., K. A. Lathrop, and R. Beck. Rad. Res., 12:65, 1960 (Abstract).
2. Harper, P. V. V° Congresso Internazionnle per L'Energia Nucleare, 2:245, Guigno 1960.
3. Harper, P. V., W. D. Siemens, K. A. Lathrop, and H. Endlich. Argonne Cancer Research Hospital Report to the Atomic Energy Commission ACRH-15, March 1961.
4. Firedell, H. L., W. J. MacIntyre, and A. M. Rejali. Am. J. Roentgenol. Rad. Therapy and Nuclear Med., 77:455, 1957.
5. Donato, L., M. F. Becchini, and S. Panichi. Medical Radioisotope Scanning, published by the International Atomic Energy Agency, Karntner Ring. Vienna, Austria 1959, p. 87.
6. Endlich, H. L. Am. J. of Roentgenol. Rad. Therapy and Nuclear Med. (In Press.)
7. Harper, P. V., W. D. Siemens, K. A. Lathrop, and H. Endlich. J. Nucl. Med. (In Press.)
8. Beck, R. J. Nucl. Med., October 1961.
9. Miller, W. F., J. Reynolds, and W. J. Snow. Physics and Mathematics A. E. C. Research and Development Reprint, ANL - 5902 August 1958.

10. Herring, C. E. J. Nucl. Med., 1:83, 1960.

11. Bender, M. A., and M. Blau. J. Nucl. Med., June 1959 (Abstract 21).

12. Bender, M. A., and M. Blau. Int. J. Appl. Radiat., 4:154, 1959.

13. MacIntyre, W. J., A. M. Rejali, J. H. Christie, F. S. Gott, and T. S. Houser. Int. J. Appl. Radiat., 3:193, 1958.

14. Kuhl, D. E. Radiology, 71:875, 1958.

15. Myers, W. G., and J. C. Vanderleeden. J. Nucl. Med., 1:149, 1960.

FOCAL IONIZING RADIATION OF THE POSTERIOR OCULAR SEGMENT*

By

F. W. Newell,† O. Choi,† N. A. Book,† P. V. Harper, and A. Simkus†

Most data concerning the effects of focal ionizing irradiation on the posterior ocular segment have been derived from experience treating intraocular malignancy by means of locally applied radium,[1-3] radon seeds[1,3] and, more recently, the artificially produced isotopes cobalt-60[1,2] and tantalum-182.[4] Stallard,[1] in the 1951 William McKenzie Memorial Lecture, reviewed much of the early literature concerning the topic and Desjardins'[1a] 1931 review covers much of the general experience related to radiation effects upon the eye. Generally, because the physical factors relating to the energy of the radiation are incomplete, most early studies are solely of historical interest.

The effects of ionizing radiation applied to the entire eye rather than to a localized area have been the subject of a number of studies.[5-7]

Newell, Harper, and Kõistenen[8] have described the effects of yttrium-90 seeds upon the posterior ocular segment, this being the only report concerning the use of an isotope emitting beta rays solely.

In the present study, polyethylene envelopes, as described by Newell and Harper,[9] were attached to the sclera of rabbits. The envelopes were then filled with radioactive iodine of different activities. The effects of this radiation were studied ophthalmoscopically and histologically at various intervals after the implantation.

TECHNIQUE

Male pigmented and albino rabbits weighing between 2.5 and 3.0 kg were used. The animals were anesthetized with intravenous pentobarbital and ocular instillation of tetracaine hydrochloride. The eye was rotated superiorly and a conjunctival incision was made near the inferior limbus (Figure 1). The inferior rectus and inferior oblique muscles, which insert near to each other, were severed at their insertions and the sclera exposed. The polyethylene envelope was sutured to the globe at about the equator and the muscles reattached at their insertions. A pursestring catgut suture was passed through the conjunctiva but not tied. The envelope was then filled with the previously prepared radioactive solution and the excess tubing excised by means of a heated hemostat. The pursestring suture was drawn up and tied.

The immediate inflammatory reaction was minimal. The localization of the radioactive iodine in the envelope was confirmed by the absence of radiation from the thyroid gland region as measured by a Geiger-Mueller probe. Ophthalmoscopic study was made at weekly intervals after pupillary dilation with Neosynephrine until the animal was killed. The fellow eye was not treated.

---

*Summary of a paper appearing in Am. J. Ophthalmol. 50:1216, 1960.

†Department of Surgery, University of Chicago. This investigation was supported in part by a research grant, B-1869, from the National Institute of Neurological Diseases and Blindness of the National Institutes of Health, Public Health Service.

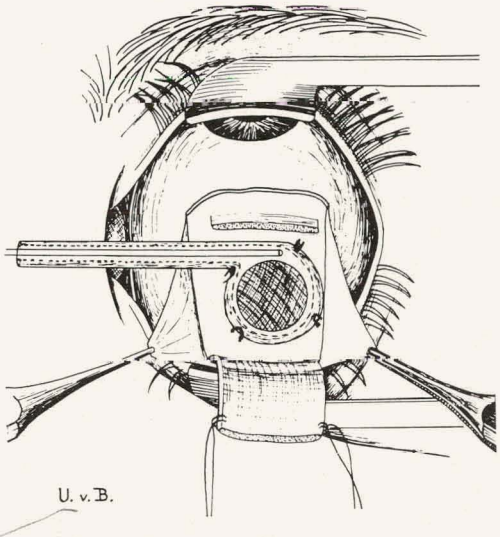

Figure 1. Method of applying the envelope to the sclera. A human eye is depicted.

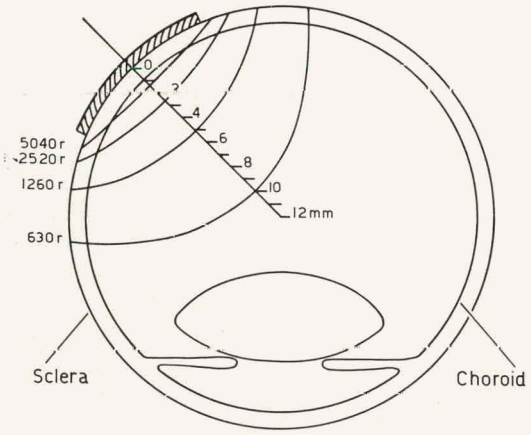

Figure 2. Calculated isodose curves showing gamma ray dosage surrounding a 1.0 cm^2 plane applicator containing 1.0 mc iodine-131, assuming complete decay, inverse square attenuation, and no absorption.

The dosage factors used in animal studies are shown in Table 1. Figure 2 indicates the calculated dosage at various distances from a 1.0 cm^2 applicator assuming complete decay, inverse square attenuation, no absorption, and a gamma radiation level of 2.18 r/mc/hr at 1.0 cm. Rabbits were killed at intervals varying from one week to 58 weeks after implantation in the dosage range from 0.18 mc/cm^2 to 1.5 mc/cm^2. In the range of 2.0 mc/cm^2 animals were studied at intervals of 1, 2, 3, 6, 12, 22, and 26 weeks after implantation.

The iodine usually must be concentrated prior to use for focal irradiation. A volume of 5.0 to 10 ml of I^{131} which has an activity of about 20 per cent in excess of that required is placed in a conical centrifuge tube. To it is added 2.0 mg of potassium iodide as a carrier. The iodine is then precipitated as silver iodide with a 50 per cent excess of silver nitrate. The solution is acidified with 10 per cent nitric acid, digested for one hour at 70°C and then centrifuged. The supernatant is decanted and the precipitated silver iodide is dried with a stream of air in the

Table 1

DOSAGE FACTORS USED IN ANIMAL STUDIES
(Area blotter = 0.28 cm^2)

Dosage I^{131} (mc)	Isotope density (mc/cm^2)	Gamma-radiation dosage* (1.0 cm from source) (r)	Mg hr radium equivalent
0.05	0.18	113	13
0.18	0.64	403	26
0.28	1.0	630	72
0.42	1.5	945	108
0.56	2.0	1260	144

*Dosage is calculated for a mean life of 280 hr.

dark at room temperature. The centrifuge tube containing the isotope is handled at all times in a lead-shielded container to minimize exposure.

The silver iodide is prepared for placement in the implant by dissolving it in a sufficient volume of saturated potassium iodide to yield the desired number of millicuries per unit volume.

To fill the implant, approximately 50 cm of polyethylene tubing (PE-10 Clay-Adams), previously calibrated, is placed in a lead container with the free ends outside. To one end is attached a syringe and the tubing is entirely filled with elemental mercury. A small quantity of nonradioactive potassium iodide is then drawn into the tubing. The tubing is then placed in the radioactive solution and a volume of 0.01 ml is withdrawn. The portion of the tubing which has been dipped in the solution is usually markedly radioactive and is cut off and discarded. Using gloved hands, a one-inch-long 27-gauge needle with the hub removed is insinuated into the tubing for delivery of the radioactive solution to the tubing within the envelope.

The first polyethylene envelopes used were evacuated and heat sealed, and the vacuum caused filling of the envelope when connected with the tubing containing the I^{131}. Failure to seal the envelope adequately, or puncture of the envelope with a surgical instrument, led to wetting of the contained blotter with body fluids and irregular distribution of the isotope. Additionally a break in the envelope would permit the isotope to be distributed to body fluids. (Because of this possibility patients are routinely administered sodium iodide intravenously prior to filling of the envelope, to block the thyroid gland from the radioactive iodine.)

At present, polyethylene envelopes (Figure 3) are made by means of an aluminum mold at 250° F by the machine shop at Argonne Cancer Research Hospital. Prior to sealing, a 6.0 mm circular disc of eight-ply cellulose blotting material is enclosed in the envelope. It was found that 0.01 cc of fluid completely saturates the blotting paper. The envelope is filled by means of a fine No. 10 polyethylene tubing (Clay-Adams) and, when the envelope is filled, the implant is sealed, using a curved hemostat with flat surfaces heated to 300° F.

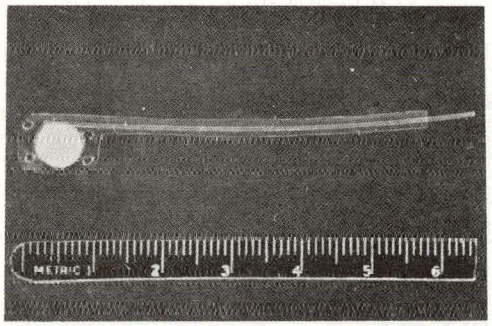

Figure 3. Polyethylene envelope with enclosed 6.0 mm circular disc of absorbent material. After filling with iodine-131, the tubing is cut off with a heated clamp which seals the envelope.

The blotting material used in these studies was cellulose distributed under the trade-name "S-'Wipe's" and manufactured by the General Cellulose Company, Inc., of Garwood, New Jersey. Eight thicknesses were used and when wet these measured 0.5 mm in thickness. The selection of the blotting paper is not too critical except that, if it is too thick, considerable changes in the geometry of the radiation field are introduced. If the solution does not wet the entire blotting paper, the distribution will be irregular and the isodose curve distorted.

Polyethylene compounds vary considerably in their reactivity to radiation and chemicals. To ensure safety the polyethylene used was tested for reactivity in the anterior chamber of a rabbit eye. No tissue reaction was evident nine months after implantation. The material currently being used is polyethylene sheeting 0.04 mm in thickness.

RESULTS

Ophthalmoscopic changes were noted consistently only in animals in which the isotope density was 1.5 mc/cm^2 or more. This dosage corresponded to 945-1260 r in air 1.0 cm from the source and to 108-144 mg/hr radium equivalent.

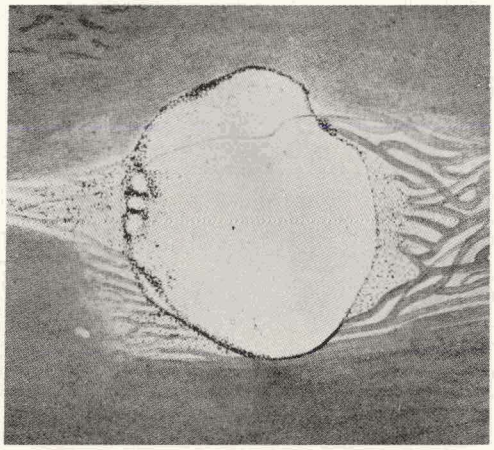

Figure 4. The fundus lesion in a pigmented rabbit seven weeks after the instillation of 2.0 mc/cm^2.

In animals receiving 2.0/mc/cm^2, initial ophthalmoscopic changes of an ill-defined grayish-white elevation over the site of implantation were noted two and three weeks after the procedure. These lesions developed into well-defined, sharply circumscribed and slightly elevated whitish areas over which were scattered numerous dark-brown pigmented dots (Figure 4). In the periphery of the area, choroidal blood vessels were evident. No hemorrhages were noted at any time.

The ophthalmoscopic changes in animals receiving 1.5 mc/cm^2 were similar but the initial changes were not observed until five or six weeks after implantation.

Consistent ophthalmoscopic changes were not observed in animals receiving 1.0 mc/cm^2. Rarely, an ill-defined slightly pale area was noted over the implantation site seven to nine weeks after the procedure. In animals receiving 0.64 mc/cm^2 or less, ophthalmoscopic changes did not occur.

HISTOLOGIC CHANGES

The rabbits were killed at intervals after implantation with intravenous pentobarbital sodium and the eye having the polyethylene implant was enucleated immediately. Following fixation in neutral formalin solution, nasal and temporal calottes were removed and the eye was embedded in paraffin. Serial sections were stained with periodic acid-Schiff, alcian blue, and toluidine blue in addition to hematoxylin and eosin.

There were no histologic lesions demonstrated in animals receiving between 0.18 and 0.64 mc/cm^2 of radiation. The eyes were enucleated from eight to 58 weeks after instillation of radioactive iodine in the implanted envelopes.

Of 11 animals treated with 0.90 to 1.0 mc/cm^2 of radiation, histologic changes occurred in four. Three of these animals were killed at eight weeks after implantation and one was followed for 58 weeks. The affected animals showed thinning of the choroid adjacent to the envelope and no changes in the pigment epithelium. The layer of rods and cones was degenerated and rarefied and only loose, pale-staining fragments were present. The external limiting membrane and outer nuclear layer in the corresponding area were thinned and there was a decrease in cell population (Figure 5). In the animal killed at 58 weeks, in addition to the changes just described, the pigment epithelium was flattened and there was rarefaction of the outer plexiform and inner nuclear layers.

In all animals receiving an application of 1.50-2.0 mc/cm^2, definite ophthalmoscopic and

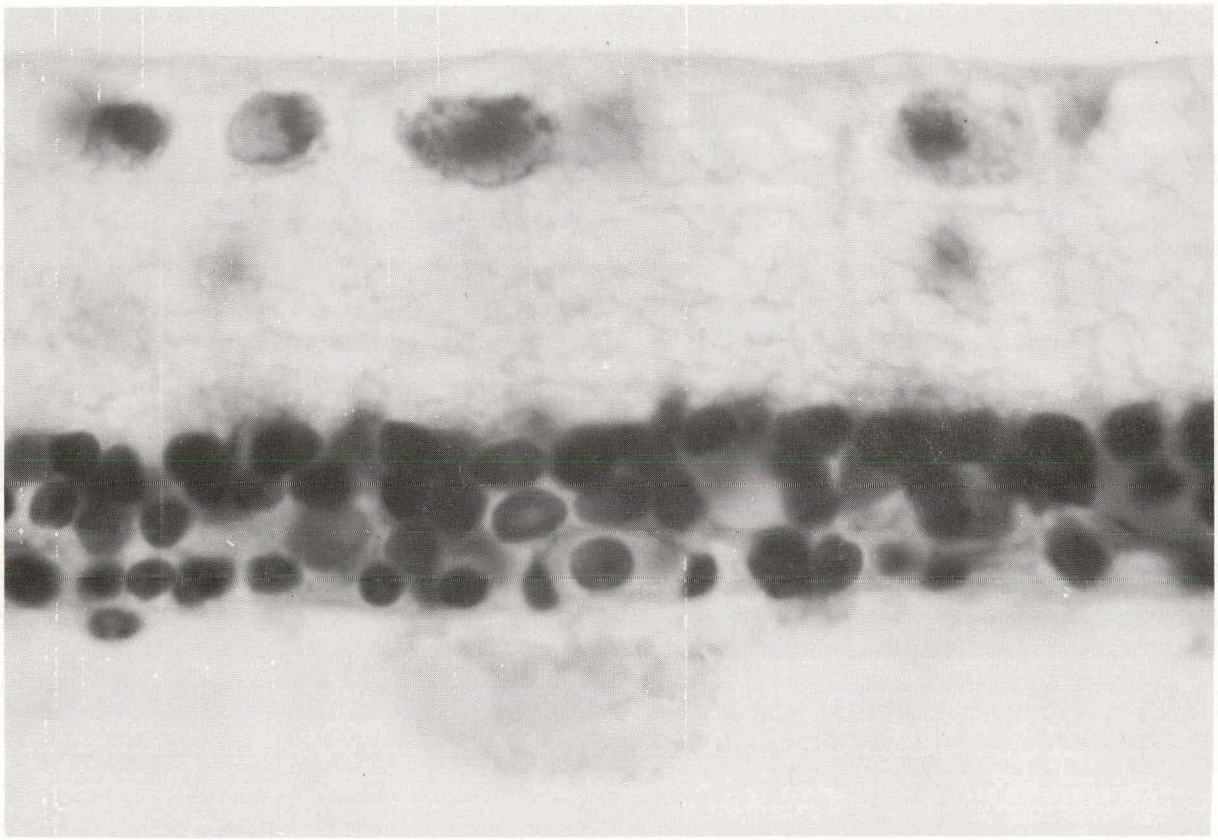

Figure 5. Destruction of the outer retinal layers with preservation of the internal in an animal killed eight weeks after the implantation of 0.9 mc/cm^2. (Hematoxylin-eosin, x 1425.)

histologic changes occurred. After one week the layer of rods and cones was destroyed and there was thinning of the corresponding outer nuclear layer. The remainder of the eye appeared normal (Figure 6).

After 12 to 26 weeks the choroid was nearly entirely destroyed with few or no blood vessels remaining. The pigment epithelium was thinned and the remaining cells were flat and degenerated and of a spindle rather than cuboidal shape. In some areas there was migration of the pigment epithelium into the region of the degenerated retina (Figure 7). After eight weeks, the remaining retina consisted of a rarefied inner nuclear layer and a few ganglion cells (Figure 8).

Hemorrhages were not observed at any time. There was no phagocytosis or cellular infiltration noted. Lens opacities were not observed and the retina on the side of the eye directly opposite to the site of implantation was not affected.

DISCUSSION

The plastic envelope described, although well tolerated by the ocular tissues, is far from satisfactory. The thin polyethylene is easily perforated by fixation forceps and, in man, the posterior scleral sutures may be difficult to insert. If not adequately sutured the envelope does not conform to the scleral curvature and the retina receives less than the calculated radiation.

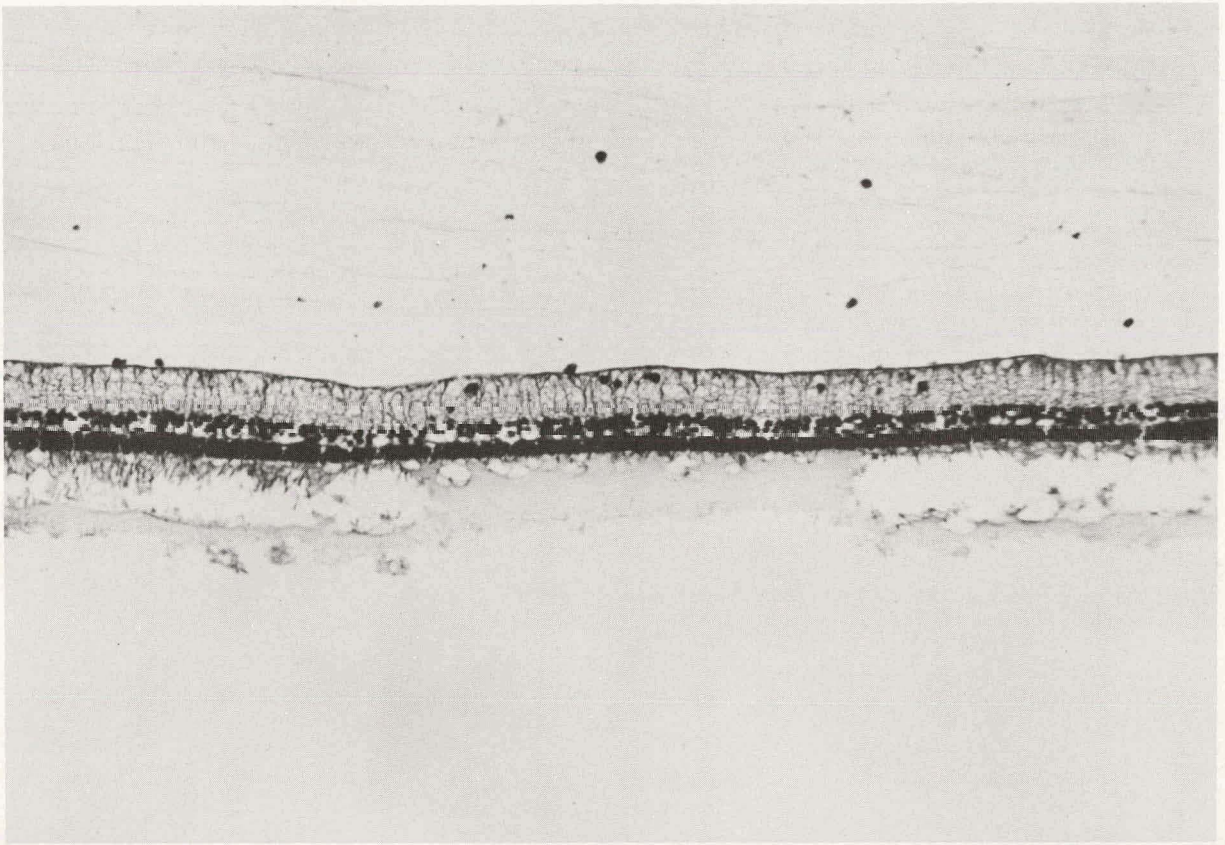

Figure 6. Destruction of the layer of rods and cones and rarefaction of the outer nuclear layer in animal killed one week after the implantation of 2.0 mc/cm^2. (Hematoxylin-eosin, x 190.)

Studies indicate that the radioactive iodine is evenly distributed, an essential factor in dosimetry so that there are no "hot spots" of concentrated radioactivity. It may be well also to shield the surface of the envelope not in contact with the globe to minimize radiation to extraocular orbital structures. A thin foil of either lead or platinum would be effective. Conversely, there were no radiation effects observed in either Tenon's capsule or the overlying rectus muscles with the envelopes used without shielding.

The absence of morphologic evidence of radiation injury to the sclera was somewhat surprising, inasmuch as iodine-131 decays by the emission of both beta particles and gamma rays. The beta particles have maximal energies of 0.60 mev (87.2 per cent), 0.335 mev (9.3 per cent), 0.250 mev (2.6 per cent) and 0.815 mev (0.7 per cent) and an average energy of 0.199 mev. The effect of the beta radiation arising in this application is to cause a very high cauterizing dose within 1.0 mm of the implant. The other radiation effects arise from gamma ray emission. Harper, et al.[10] have implanted envelopes containing iodine-131 adjacent to major blood vessels without causing histologic alteration. It is believed unlikely that delayed scleral radiation injury will be observed with this technique. Radiation cataract was not observed but this may well be due to an inadequate period of observation.

If the technique of focal irradiation is to be maximally useful, the isotope used should be

inexpensive and easily available. We believe that it is desirable to permit the implant to remain in position and not to have to remove it after therapy. Table 2 indicates the dosage factors relating to various common isotopes. If the roentgens per hour per curie 1.0 cm from the source are known, the Paterson and Parker tables may be used in calculation of dosage and comparison of radiation with radium.

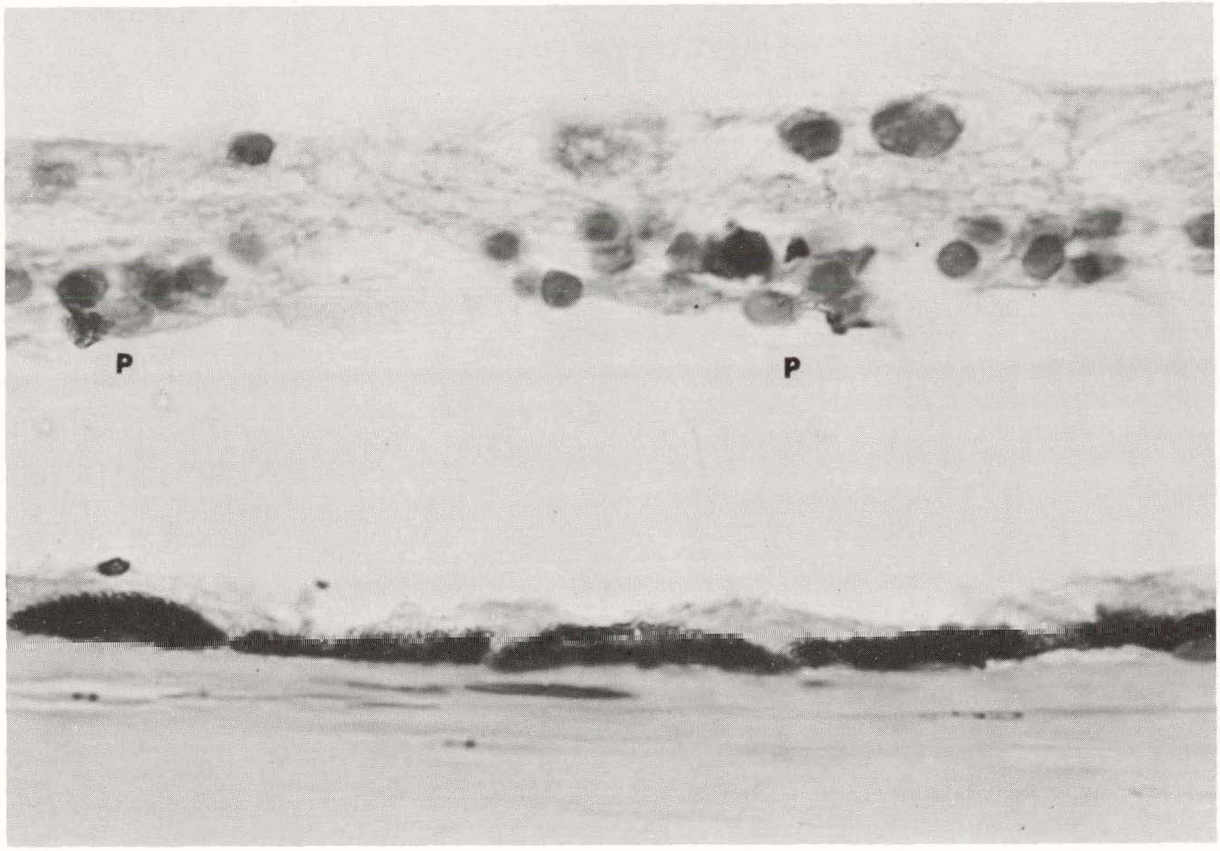

Figure 7. Destruction of the choroid and migration of pigment epithelial cells (P) into surviving retina in animal receiving 2.0 mc/cm^2 with eye enucleated after 12 weeks. (Alcian blue, x 1085.)

In addition the isotope must be soluble enough to be distributed in the polyethylene envelope and in the event of escape from the envelope must not have undesirable biologic actions. (It should be noted that, when these envelopes are used in man, the thyroid is protected by a prior dose of intravenous potassium iodide.) With these considerations iodine seems to be the most satisfactory isotope for this application.

The cytologic changes observed in the rabbits reported here are generally comparable to other experimental studies of the effects of ionizing radiation upon the posterior ocular segment. Cibis and his co-workers irradiated the entire eye using a variety of sources but mostly x-radiation. A dose rate of 630 r/min in air and 275 r/min in vitreous was used. This corresponds to a dose rate of 0.077 r/min at a distance of 1.0 cm from the applicator when iodine-131 is used. It must be remembered, however, that inverse square attenuation resulted in a

much higher dose near the retina. However, even if the retina was 1.25 mm from the source the maximum radiation was 0.616 r/min.

In the dosage used here, acute vascular congestion and systemic radiation effects, as observed by Cibis, et al., did not occur. The outer retinal layers, particularly the layer of rods and their nuclei, appeared much more sensitive to ionizing radiation than either the remainder

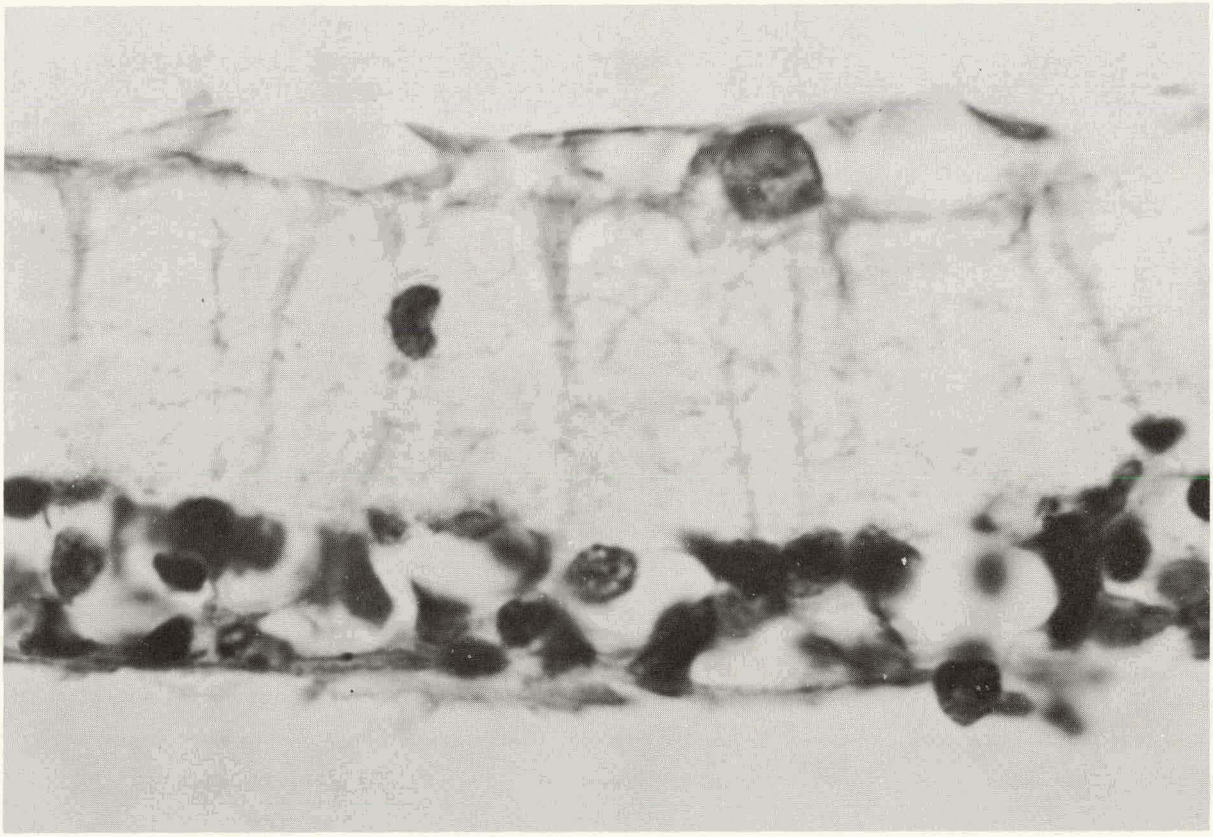

Figure 8. Thinning of the retina in rabbit with implantation of 2.0 mc/cm^2 with eye enucleated after 26 weeks. The layer of rods has disappeared entirely and there is a decrease in the number of cells in the inner nuclear and ganglion cell layer. (Hematoxylin-eosin; x 1425.)

of the retina or the choroid. The cytologic changes were a direct result of ionization and did not occur because of interference with the retinal blood supply.

Previous studies of the effects of locally applied radiation to the posterior ocular segment have arisen mostly from instances of unsuccessful therapy of human malignancy. In these cases there is usually no correlation of factors of dosage and histologic change. However, the report of Tamler, Winter, and Toch[11] is unusually detailed and should be repeated in other eyes in which radiation dosage is known.

The dosimetry of radiation of tissues adjacent to implanted radioactive substances is most inaccurate. The isodose curves shown in Figure 1 indicate that, in the region closest to the source, a variation of dosage of a mm can result in a variation of dosage of thousands of roentgens. However, if one considers the applicator having a half-thickness of 0.5 mm and the thick-

Table 2

CALCULATED GAMMA RADIATION LEVELS FOR ONE mc OF SOME RADIOISOTOPES

Isotope	r/hr/mc (A) at 1.0 cm	Mean life (B)	Total dose (D)
Radium (0.5 mm pt filtration)	8.4	2284 yr	1.68×10^8 r
Radon	8.4	133 hr	1117 r
Cobalt-60	13.5 (E)	7.6 yr	8.66×10^6
Gold-198	2.48	93 hr	223 r
Iodine-131	2.31	280 hr	630 r
Iridium-192	5.1 (C)	101 da	1.24×10^4 r
Tantalum-182	6.13 (C)	159 da	2.34×10^4 r

A. From Overman, R. T., and H. M. Clark, Radioisotope Techniques, New York, McGraw-Hill, 1960.

B. The time required for the disintegration rate to decrease by the factor e^{-1}:

$$\frac{\text{half-life}}{0.693} = \text{half-life} \times 1.443$$

C. Lederman, M., and W. K. Sinclair, Radioactive isotopes for beta and gamma ray applicators. In Therapeutic Use of Artificial Isotopes (Paul F. Hahn, ed.), New York, John Wiley & Sons, 1956.

D. Assuming complete decay, no absorption, inverse square attenuation, a plane applicator measured at a distance of 1.0 cm.

E. By calculation from Stallard's data the value for cobalt-60 with the shielding used by him is about 9.0 r/hr/mc at 1.0 cm.

ness of the choroid and sclera to be 1.5 mm, the minimum dose causing rod damage in this series was 3,300 r, and a dosage of 2,400 r did not cause histologic changes. This is assuming, however, that the radioactive source was immediately adjacent to the sclera, an assumption not confirmed by the absence of beta particle damage to the sclera. If it is assumed that the radiation source was 3.0 mm from the retina rather than 2.0 mm, the dosage factors conform closely to those of Cibis, et al.: 2,040 r caused radiation injury and 1,510 r did not.

Focal ionizing radiation of the posterior globe has been used in the treatment of retinoblastoma, metastatic carcinoma, and malignant melanoma of the choroid. In assessing the effects in retinoblastoma the outstanding results of Reese and his co-workers[12] using x-radiation and intracarotid antitumor agents, particularly triethylene melamine, must be considered. It seems likely, however, that, if less than one third of the retina is involved, either method of radiation will be successful. Focal ionizing radiation has as its advantages a single application of an easily controlled, high dose of radiation precisely localized to the area to be treated, without involvement of overlying structures. It could thus be used in instances in which both eyes are present, as in the occurrence of the tumor in the offspring of retinoblastoma survivors. The chief disadvantage of focal ionizing radiation is failure to sterilize minute nests of tumor too small to be seen. Additionally, in tumors located in the anterior globe, a cataractogenic dose of radiation may be administered.

The chief advantage of x-radiation is in the accumulated experience with this mode of therapy. However, to achieve the excellent results reported by Reese considerable attention must be

directed to the appropriate mechanical devices designed to direct the x-radiation. If such appliances are not available, focal ionizing radiation would appear to offer considerable advantage.

The best method of treating metastatic carcinoma of the choroid is open to question. Generally such tumors are sensitive to radiation and cataract is not a problem in view of the limited life expectancy, so that conventional x-radiation can be used in adequate dosage without extraordinary precaution. However, focal ionizing radiation may be just as effective and applied with less difficulty.

Stallard,[13] in 1959, reported the use of radioactive applications in the treatment of malignant melanoma of the choroid. Forty-five patients were treated, with success in 25. He points out that it is too early to assess the results.

The reports in the literature suggest strongly that in retinoblastoma, if conventional radiation therapy has been used without success, it is extremely unlikely that focal ionizing radiation will preserve the eye. Many of the instances of unsuccessful local application of ionizing radiation involve eyes in which initial x-radiation did not arrest the process.

From the studies reported here it is believed that focal ionizing radiation with iodine-131 will give results comparable to those obtained with radium, cobalt-60 or radon applicators. The chief advantage in the use of iodine-131 is in permanent placement of the implant so that it does not have to be removed. It is believed that a concentration of 2.0 mc/cm^2 of iodine-131 should be used with appropriate precaution so that the implant is in close contact with the sclera overlying the area to be treated.

LITERATURE CITED

1. Stallard, H. B. Brit. J. Ophth., 36:245, 1952; Brit. J. Ophth., 36:313, 1952.

1a. Desjardins, A. U. Am. J. Roentgenol., 26:639, 787, 921, 1931.

2. Williams, I. G. Am. J. Roentgenol., 77:786, 1957.

3. Stallard, H. B. AMA Arch. Ophth., 51:573, 1954.

4. Lederman, M., and W. K. Sinclair. In Hahn, F. P. (ed), Therapeutic Use of Artificial Isotopes, New York, John Wiley & Sons, 1956.
Lederman, M. Brit. J. Radiol., 29:1, 1956.
Trott, N. G., and B. M. Wheatley. Brit. J. Radiol., 29:13, 1956.

5. Chalupecky, H. Zentralbl. f. prakt. Augenh., 21:334, 1897. (Cited by: Lascassagne, A., and G. Gricouroff, Action of Radiation on Tissues, New York, Grune & Stratton, Inc., 1958.)

6. Cibis, P. A., W. K. Noell, and B. Eichel. AMA Arch. Ophth., 53:651, 1955.
Cibis, P. A., and D. V. L. Brown. Am. J. Ophth., 40:84, 1955.
Noell, W. K., B. Eichel, and P. A. Cibis. Fed. Proc., 13:106, 1954.
Brown, D. V. L., P. A. Cibis, and J. E. Pickering. AMA Arch. Ophth., 54:249, 1955.

7. Kent, S. P., and A. A. Swanson. Radiation Res., 6:111, 1957.
Kent, S. P. Radiation Res., 10:380, 1959.

8. Newell, F. W., P. V. Harper, and A. Köistenen. Am. J. Ophth., 42:85, 1956.

9. Newell, F. W., and P. V. Harper. Am. J. Ophth., 44:222, 1957.

10. Harper, P. V., W. E. Adams, E. E. Schwartz, K. A. Lathrop, and R. W. Harrison. Surg. Forum, 6:419, 1956.
Harper, P. V., K. A. Lathrop, R. W. Harrison, C. G. Thurston, T. T. Kennedy, and J. F. Mullan. Surgery, 40:270, 1956.

11. Tamler, E., F. C. Winter, and P. Toch. AMA Arch. Ophth., 58:647, 1957.

12. Reese, A. B. Tumors of the Eye, New York, Hoeber, 1957.
Reese, A. B., G. Hyman, G. Merriam, A. Forrest, and M. Klegerman. Am. J. Ophth., 43: 865, 1957.

13. Stallard, H. B. Tr. Ophth. Soc. U. Kingdom, 79:373, 1959.

THE PATHOGENESIS OF GOUT*

By

L. B. Sørensen

Since Garrod's original observation[1] in 1848 that excessive amounts of serum uric acid were present in gouty patients, there has been widespread agreement that gout is attributable to a sustained accumulation of uric acid in the body. The author believes that if a patient has a sufficient degree of hyperuricemia for a long enough period he will eventually develop gout, irrespective of the nature of the hyperuricemia. This, then, implies that the clinical syndrome of gout comprises several distinct entities. The accumulation of uric acid must result from a disturbance in the normal equilibrium between the production of uric acid on one hand and the elimination of urate on the other. As a consequence, hyperuricemia will occur in the following circumstances:

(1) When the production of urate is so great that, even though the routes of elimination are of normal capacity, they are inadequate to handle the excessive load.

(2) When the capacity for elimination of uric acid is so reduced that a normal-sized production of uric acid cannot be disposed of.

For a discussion of the normal pathways in the metabolism of uric acid, the reader is referred to a recent review of the subject published by the author.[2]

Isotopic techniques permit accurate measurements of the miscible pool and turnover rate of uric acid. The miscible pool is defined as the quantity of urates in the body capable of mixing promptly with intravenously-injected isotope-labeled uric acid. The miscible pool averages about 1200 mg in normal males. The turnover rate is a measure of the fraction of all the uric acid which is replaced per unit time. The endogenous urate production amounts to 600 to 700 mg per day in healthy males.

The metabolism of uric acid is diagrammatically outlined in Figure 1.

An excessive intake of purines does not ordinarily play any role in the pathogenesis of gout, although in the days when the treatment of pernicious anemia consisted of oral administration of as much as one pound of fresh liver daily, acute gout occasionally developed in such patients after several weeks of treatment.[3,4] It is of interest that when normal subjects were fed uric acid precursors (4 g of ribose nucleic acids daily for 3 to 5 days) their plasma urate levels increased to the range found in patients with gout.[5]

Neither does extrarenal elimination play a role in the development of hyperuricemia; on the contrary, there appears to be a compensatory increase in the extrarenal excretion of uric acid in many patients with hyperuricemia. Figure 2 shows that in two patients with impaired kidney function, the recovery from urine of intravenously injected uric acid-C^{14} amounted to only 24 and 29 per cent of the administered dose after 7 days. The extrarenal excretion is low

*This paper has been accepted in part for publication in Arch. Int. Med.

in patients with Wilson's disease, where there is a functional impairment in the renal reabsorption of uric acid by the tubules.

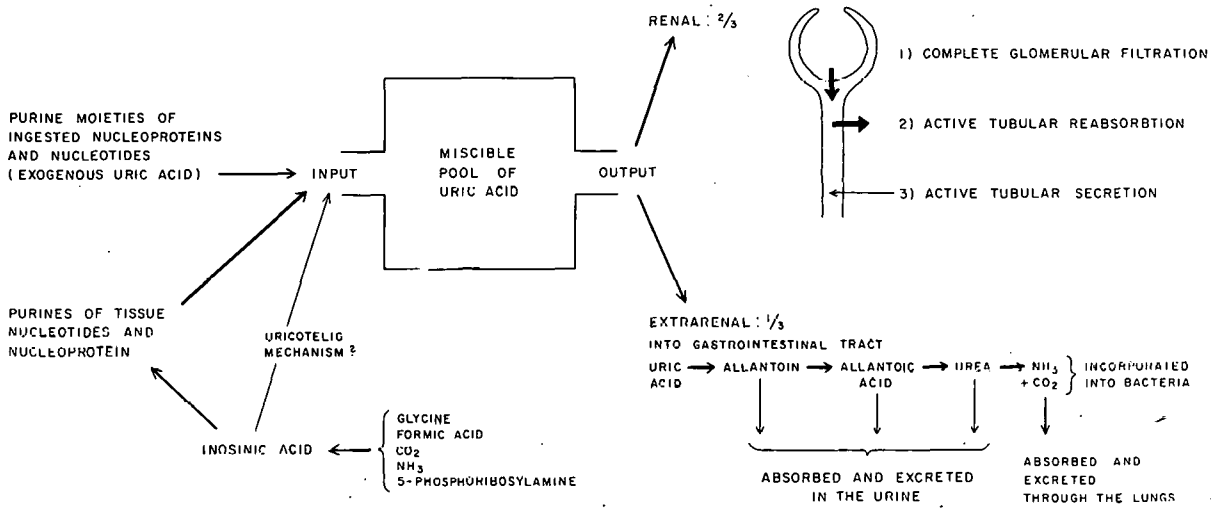

Figure 1. Diagram representing the metabolism of uric acid in man.

The author believes that the following scheme represents adequately the various types of gout.

Primary gout	metabolic type;	characterized by overproduction of uric acid due to an increased vestige of the shunt mechanism whereby precursors enter the purine nucleus of uric acid.
	renal type;	characterized by the excretion in the bladder urine of a smaller percentage of the filtered urate load (tubular dysfunction).
Secondary gout	metabolic type;	characterized by overproduction of uric acid due to an increased turnover of nucleoproteins, e.g., in the bone marrow in certain diseases of the hematopoietic system.
	renal type;	due to decreased glomerular filtration rate.
	a third type;	due to drugs blocking the tubular secretion of urate.

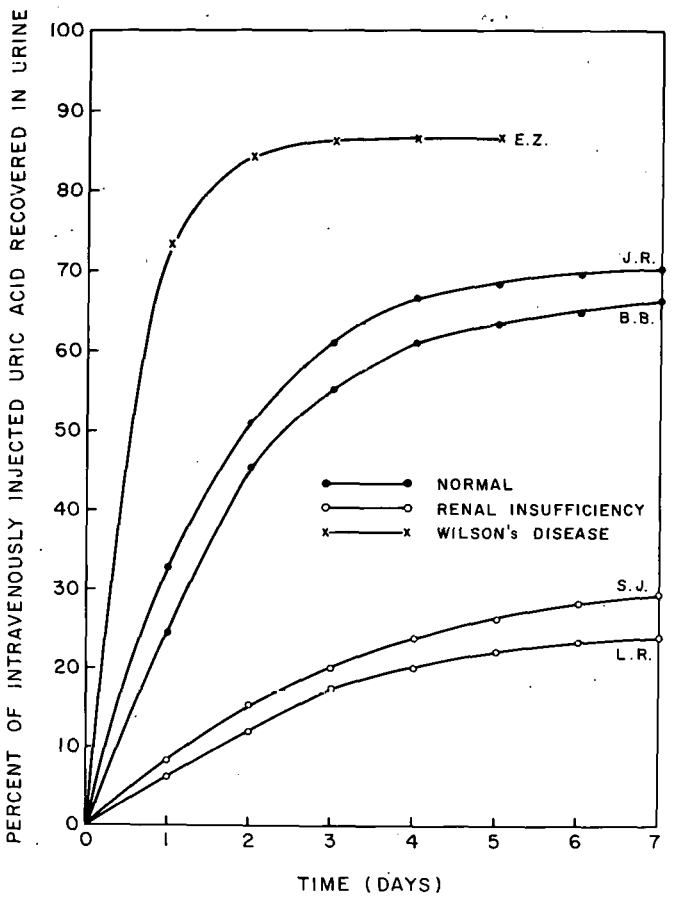

Figure 2. The cumulative recovery from urine of uric acid-C^{14} injected intravenously into 2 normal subjects (J.R. and B.B.), 2 patients with renal insufficiency (L.R. and S.J.) and 1 patient with hepatolenticular degeneration (E.Z.).

EXPERIMENTAL AND DISCUSSION

In the following section abstracts of cases in each group will be presented as well as a report of studies in which C^{14}-labeled uric acid and glycine were employed. The enzymatic spectrophotometric method of Praetorius was used for the determination of uric acid in plasma and urine.[6] The experimental technique for the determination of uric acid pool and turnover are described elsewhere.[2] In the glycine experiments glycine labeled with C^{14} in the 1-position was dissolved in 500 ml of sterile saline and the solution passed through a bacteriological fritted glass filter disc into an infusion bottle before being administered intravenously over a period of 60 minutes. Urine was collected in 12-hour portions for a minimum of 7 days. Radioassay was performed in a vibrating reed electrometer after wet oxidation of uric acid in a vacuum combustion line. The patients were maintained on a diet essentially free of purines, but with sufficient protein to maintain N-balance. Standard clearance methods utilizing bladder washouts were employed for the renal function studies. Inulin was determined by the diphenyl-

amine method of Harrison[7] with modifications as described by Smith.[8]

Primary metabolic gout. Under this term may be classified an inborn error in the purine metabolism, the most significant manifestation of which is an overproduction of uric acid and—in the absence of impaired renal function—an augmentation in urinary uric acid. Patients with this disease have an increased incorporation of glycine into uric acid. Three cases are reviewed below.

C.C., a 23-year-old male had experienced 5 attacks of acute gouty arthritis. A maternal uncle suffered from gout. No tophi were found on physical examination or by x-rays. The concentration of uric acid in the plasma was 11.4 to 11.6 mg per cent. There was a blood urea nitrogen of 12 mg per cent and a urea clearance of 58 ml per minute.

J.K. was a 38-year-old male with a history of acute recurrent arthritis of 3 years duration. Tophi were absent. The plasma urate concentration was 8.0 to 8.8 mg per cent. Urea clearance was 70 ml per minute with a blood urea nitrogen of 10 mg per cent.

A.D. was a 46-year-old male who presented a most severe case of chronic tophaceous gout. The first attack of articular distress occurred at the age of 22. Three of his 4 brothers and 3 maternal uncles suffered from gout. Extensive tophaceous involvement of fingers, elbows and knees was noted on physical examination. Numerous osseous tophi and tophaceous destruction of practically all the joints of hands, feet, elbows and knees were demonstrated at x-ray examination. The plasma urate concentration ranged from 10.3 to 12.5 mg per cent. The blood urea nitrogen was 11 mg per cent and the urea clearance 68 ml per minute.

The results of the uric acid pool and turnover studies in these patients and in a normal subject included for comparison, appear in Figures 3 and 4 and Table 1.

Patient C.C. had a miscible pool of uric acid of 2907 mg and a turnover rate of 1203 mg daily. There was no evidence of urate deposits and the logarithm of the decreasing isotope concentration followed a straight line. His urinary uric acid excretion averaged 899 mg per 24 hours or 75 per cent of the turnover. At the end of 9 days 75.8 per cent of the injected C^{14} had been recovered in urinary uric acid.

Similar values were obtained in the case of J.K. who had a miscible pool of 2178 mg and a daily urate production of 1163 mg.

Although hundreds of grams of uric acid were present in the solid phase in patient A.D., his miscible pool was no higher than those of the 2 patients without tophi. From Figure 4 it is seen that the semilogarithmic plot of the isotope concentration against time is not a straight line, as would be expected if the isotope dilution were due solely to the formation of endogenous uric acid. This is due to the fact that a continuous process of dissolution and precipitation of uric acid takes place in those areas of tophi in contact with the body fluids. This process results in a dilution of isotope in the miscible pool which is indistinguishable from the dilution incident to the endogenous formation of new non-isotopic molecules of uric acid. In tophaceous gout, therefore, a patient's turnover cannot be calculated from the initial decrease in the isotope concentration.

To determine the uptake of isotope in the solid phase a tophus was excised from patient A.D. 4.2 days after the injection of uric acid-C^{14}, at a time when the isotope concentration in the miscible pool of uric acid was approximately 3350 DPM of C^{14} per mg of uric acid.

The over-all specific activity of C^{14} in this tophus was 176 DPM per mg of uric acid or 5.3 per cent that of the miscible pool at the same time. On the 13th day the isotope concentra-

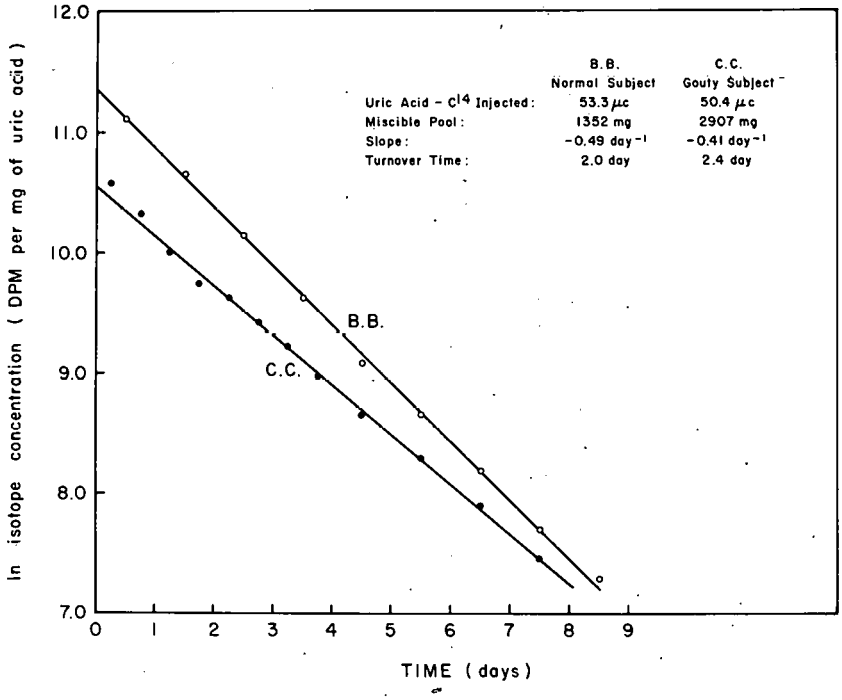

Figure 3. Hemilogarithmic plots of the isotope concentration in urinary uric acid against time for a normal subject (B.B.) and a patient with primary metabolic gout (C.C.)

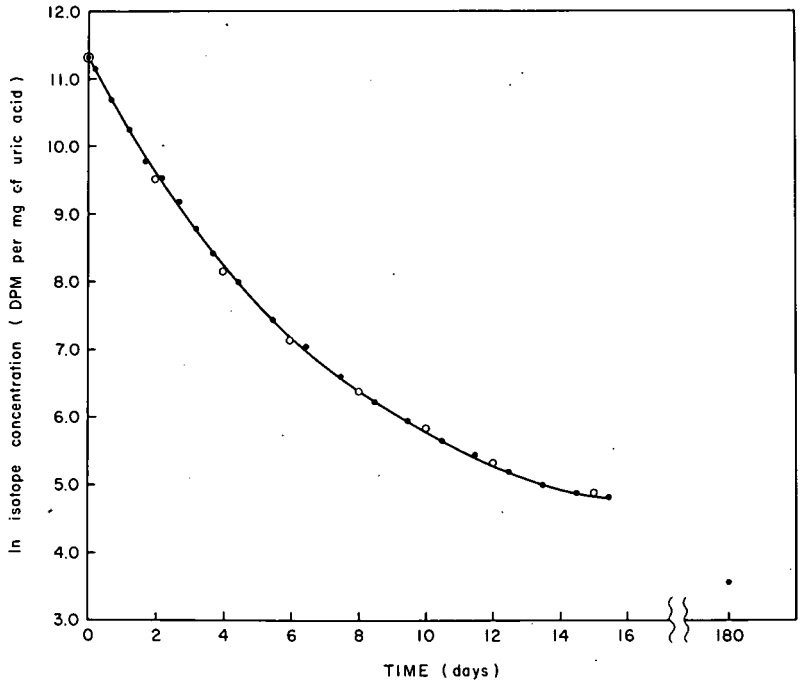

Figure 4. Hemilogarithmic plot of the isotope concentration in urinary uric acid against time for a patient with chronic tophaceous gout (A.D.).

Table 1

URIC ACID MISCIBLE POOL, DAILY TURNOVER AND URINARY RECOVERY OF INTRAVENOUSLY INJECTED URIC ACID-2-C^{14} IN THREE PATIENTS WITH PRIMARY METABOLIC GOUT AND IN ONE NORMAL SUBJECT

Case	Plasma uric acid (mg %)	Miscible pool (mg)	Turnover (mg/day)	Urinary uric acid (mg/day)	Extrarenal elimination (mg/day)	Renal excretion (% of turnover)	Recovery from urine of injected uric acid (% of dose)
Normal	5.2	1352	662	427	235	64.4	67.6 (9 days)
C.C.	11.4-11.6	2907	1203	899	304	74.9	75.8 (9 days)
J.K.	8.0- 8.8	2178	1163	744	419	64.0	68.4 (11 days)
A.D.	10.5-12.5	2397	(1185)	790	(395)	66.7	49.0 (16 days)

tion in the miscible pool of uric acid had reached a similar value.

The steady-state system for uric acid in a tophaceous gout patient can be pictured as a two-compartment system, the soluble pool of uric acid, and the readily exchangeable areas of tophi in contact with the body fluids (Figure 5). Between these 2 compartments there is a measurable exchange of uric acid. If it is assumed that this system is in a steady state during the relatively

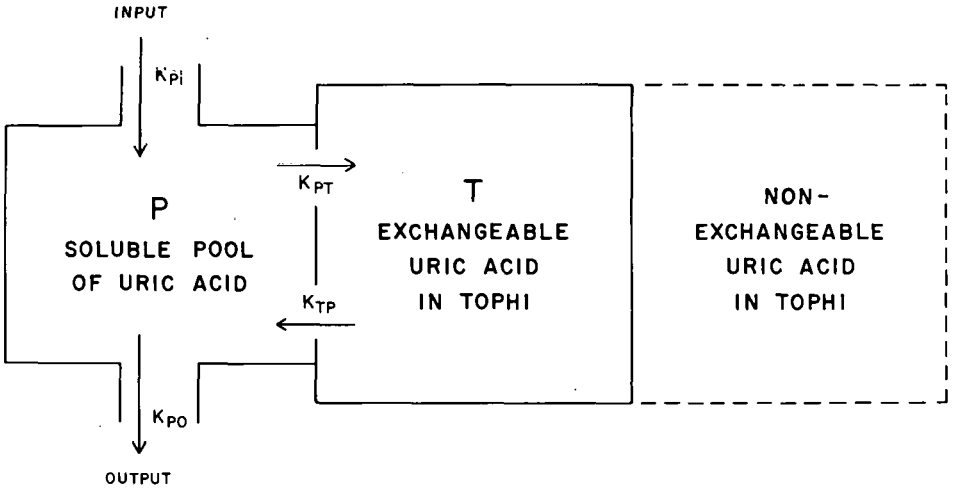

Figure 5. Simplified diagram of a two-compartment system for uric acid in a tophaceous gout patient.

short duration of the experiment then $K_{Pi} = K_{Po}$ and $K_{PT} = K_{TP}$. The differential equations describing the system are

$$\frac{dP^*}{dt} = - K_{Po} \left(\frac{P^*}{P}\right) - K_{PT} \left(\frac{P^*}{P}\right) + K_{TP} \left(\frac{T^*}{T}\right),$$

$$\text{and } \frac{dT^*}{dt} = K_{PT} \left(\frac{P^*}{P}\right) - K_{TP} \left(\frac{T^*}{T}\right)$$

The solution of the differential equation for P yields

$$\frac{P^*}{P} = C_1 e^{\alpha t} + C_2 e^{\beta t}$$

Treatment of the experimental curve according to this expression yields

$$\frac{P^*}{P} = 4.39 \cdot e^{-.004 \cdot t} + 6.93 \cdot e^{-.149 \cdot t}$$

as the best fit. The open circles on the graph in Figure 4 show the closeness of the fit.

If the rate of formation of urate is known, the transfer constants may be calculated. As mentioned above, the endogenous production cannot be determined directly from the experimental curve; however, a fairly accurate estimate can be obtained from knowledge of the renal function and the urinary output of uric acid. Since this patient's urate clearance was in the normal range, it was felt that the renal excretion of urate would constitute approximately 2/3 of the total elimination. This would correspond to a daily turnover of 1185 mg. Based on this value the following rate constants were obtained:

endogenous production:	0.494 · P =	1185	mg/day
rate of transport into tophi:	0.340 · P =	815	mg/day
rate of transport from tophi:	0.0012 · T =	815	mg/day

The amount of uric acid in the tophaceous compartment participating in this exchange is, therefore, some 300 times the size of the soluble pool.

As a result of this fairly rapid exchange a large proportion of isotopic uric acid is initially introduced into tophi and since the quantity of exchangeable uric acid in tophi is several hundred times the miscible pool of uric acid, the release of isotope from tophaceous compartment occurs at a slow rate. This impression was further supported by the fact that C^{14} continued to be detectable in urinary uric acid for months. On the 180th day after the injection of uric acid-C^{14}, at a time when the patient had been on a uricosuric regimen for 5 months, a 24-hour urine specimen was shown to contain 1755 mg of uric acid and 61,000 DPM of C^{14}.

The establishment of a smaller miscible pool of uric acid in a tophaceous gouty subject by administration of a uricosuric drug, results in altered and more favorable rates of exchange between soluble and solid uric acid molecules, the eventual outcome of which is a reduction in the size of tophi. Five months after patient A.D. had been started on a uricosuric drug regimen, he had a urinary uric acid excretion which exceeded the endogenous production by more than 500 mg daily. At the same time his plasma urate concentration was 9.1 mg per cent; therefore, maintenance of an elevated plasma urate level in this patient is not an indication of a poor uricosuric response, but rather signifies that uric acid is readily mobilized from the tophaceous compartment.

Studies on the mechanism of overproduction of urate in this condition have revealed a more extensive and more rapid incorporation of precursor products such as glycine, aminoimidazolecarboxamide and formate into uric acid.[9-13]

The concentration of C^{14} in urinary uric acid following the intravenous injection of a single tracer dose of glycine-1-C^{14} into subjects C.C. and A.D. are plotted as a function of time in Figure 6. In a normal subject the isotope concentration in urinary uric acid reaches a maximum after 2-1/2 days and declines slowly thereafter. This indicates that the isotope is derived predominantly from a large pool of uric acid precursors having a slow turnover rate.

In the 2 gouty subjects the isotope concentration rises rapidly to a maximum in half-a-day, attaining a value 4 to 6 times that seen in the normal subject. This is followed by a fairly rapid decline. The configuration of this curve would indicate a more direct relationship between precursor and product in the gouty than in the normal subject.

The cumulative recovery of C^{14} in urinary uric acid has been plotted in Figure 7. At the end of 7 days, approximately 0.40 and 0.52 per cent of the C^{14} previously injected as glycine

had been excreted as uric acid by the two gouty subjects. These values were 5 and 6-1/2 times the corresponding figure for the normal subject.

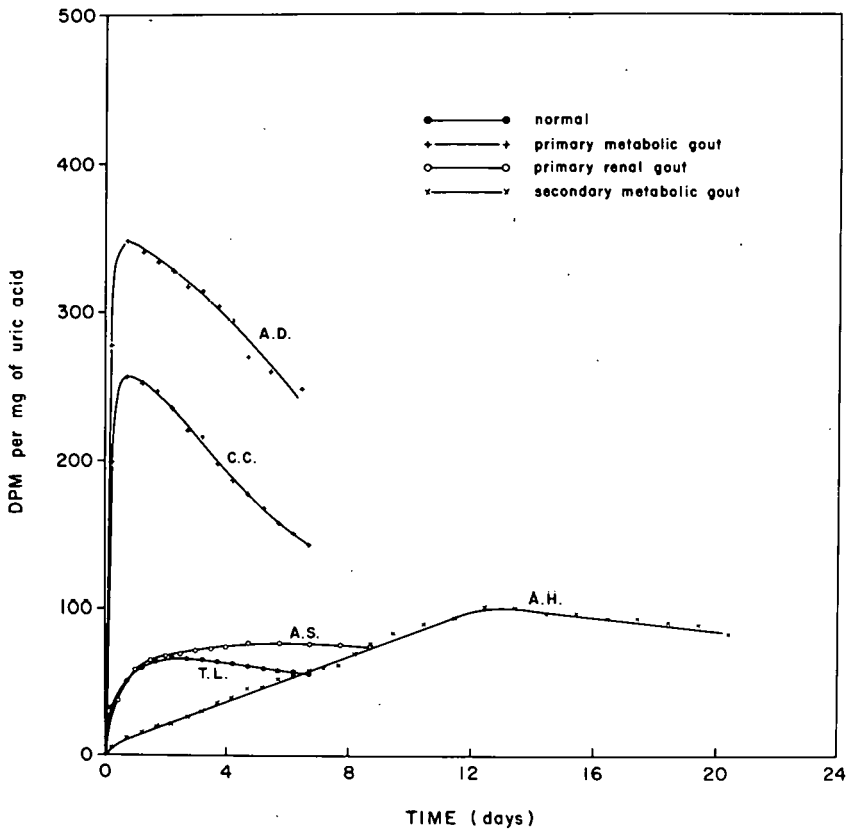

Figure 6. The isotope concentration in urinary uric acid against time following injection at zero time of 100 μc of glycine-1-C^{14}.

Primary renal gout. This disturbance is characterized by hyperuricemia due to a dysfunction in the enzymatic transport mechanism of urate through the renal tubules. A smaller percentage of the filtered urate load is excreted in the bladder urine by these subjects. By maintenance of elevated plasma urate levels the urinary urate output may be within the normal range, or, if there is a compensatory augmentation in the extrarenal excretion of uric acid, it may be decreased. There is a normal-sized production of uric acid.

Three out of 12 patients with primary gout studied by the writer could be classified in this category. In all cases there was a negative history for previous kidney disease, and a family history of gouty arthritis could not be extracted. The blood picture was entirely normal. The glomerular filtration rate as estimated by the renal clearance of inulin or creatinine was either normal or only slightly decreased.

The results of the pool and turnover studies with uric acid-C^{14} are seen in Table 2. In all cases there was a moderately elevated miscible pool, but the daily urate production was in the normal range. The urinary output of uric acid and the fraction of injected uric acid-C^{14} which

was recovered from urine were below normal.

Following the intravenous administration of glycine-C^{14} into patient A.S. no excessive incorporation of C^{14} into uric acid was found (Figures 6 and 7). Maximum isotope concentration in urinary uric acid was reached on the 4th day. At the end of 7 days 0.08 per cent of the administered C^{14} had been recovered in urinary uric acid. This study indicates clearly that not all cases of primary gout are characterized by over-incorporation of labeled glycine into uric

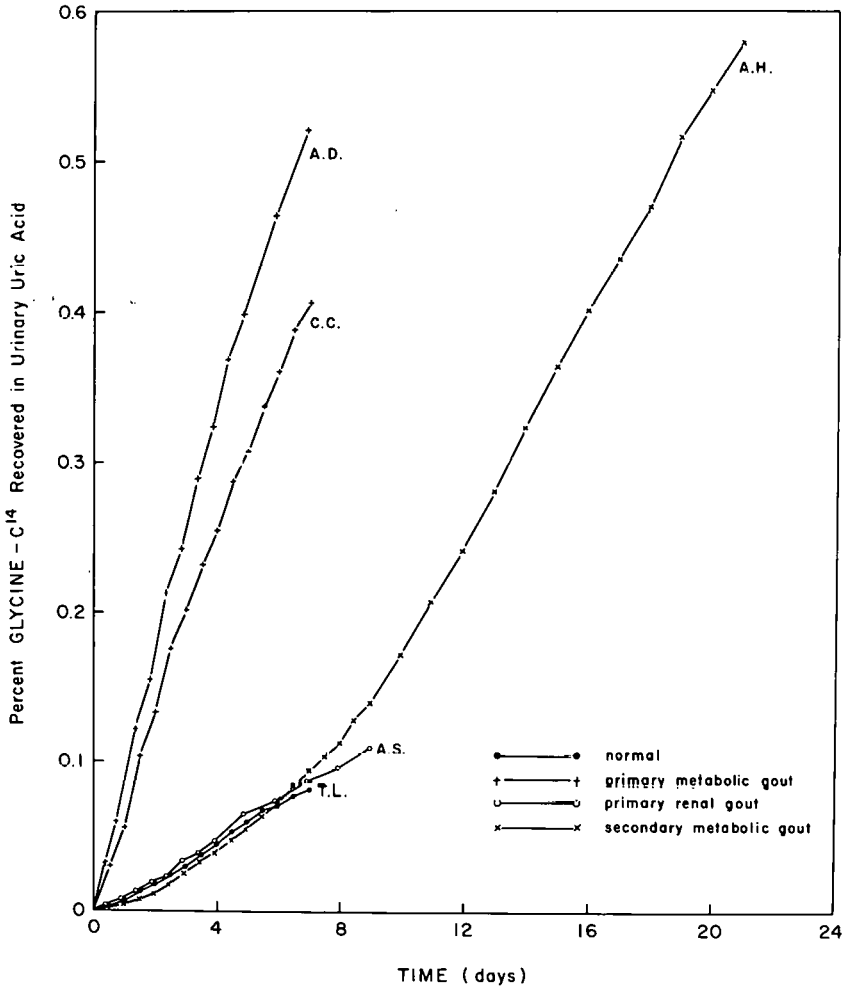

Figure 7. The cumulative recovery of C^{14} in urinary uric acid after intravenous administration of 100 μc of glycine-1-C^{14}.

acid, and is in accordance with the findings of other investigators.[9,14,15] Excessive incorporation of glycine is usually confined to those gouty subjects who have abnormally high urinary outputs of uric acid.

A specific abnormality in the renal handling of uric acid in patient A.S. was demonstrated by the performance of discrete renal functional studies. The results of inulin and urate clearance studies are listed in Table 3. The glomerular filtration rate is within the normal range.

Table 2

URIC ACID MISCIBLE POOL, DAILY TURNOVER AND URINARY RECOVERY OF INTRAVENOUSLY INJECTED URIC ACID-2-C^{14} IN THREE PATIENTS WITH PRIMARY RENAL GOUT

Case	Duration of symptoms years	Stage	Plasma uric acid (mg %)	Miscible pool (mg)	Turnover (mg/day)	Urinary uric acid (mg/day)	Recovery from urine of injected uric acid (% of dose)
A.S.	6	acute recurrent arthritis, + osseous tophi	9.3	1962	679	319	43.8 (9 days)
B.S.	10	acute recurrent arthritis, 0 tophi	9.9	1809	597	325	44.6 (7 days)
S.M.	20	chronic arthritis +++ tophi	10.0	1783	578	261	44.5 (10 days)

Table 3

SIMULTANEOUS INULIN AND URIC ACID CLEARANCES IN A PATIENT (A.S.) WITH PRIMARY RENAL GOUT

(Clearances corrected to 1.73 sq m surface area)

Experiment No.	Collection period (min)	Urine flow (cc/min)	Plasma		Urine		Clearances		Clearance ratio
			Inulin (mg/cc)	Urate (mg/cc)	Inulin (mg/cc)	Urate (mg/cc)	Inulin (cc/min)	Urate (cc/min)	Urate/Inulin
1	22	3.18	0.1028	0.0784	4.868	0.140	137	5.19	0.038
2	21	2.76	0.1035	0.0728	5.138	0.151	125	5.22	0.042
3	20	3.50	0.1083	0.0750	4.263	0.119	125	5.07	0.040

The uric acid clearance and the proportion of filtered uric acid excreted by this patient are definitely reduced. The normal uric acid clearance is 7 to 10 ml per minute. These data indicate that accumulation of uric acid in this patient is caused by an intrinsic defect in the renal excretion of urate, which can be regarded as a dysfunction in the tubular transport mechanism of urate consisting either in an increased tubular reabsorption or in a decreased tubular secretion of uric acid.

Of interest in this connection are the recent findings by Nugent and Tyler,[5] who upon oral purine loading of normal subjects found that the non-gouty subjects reabsorbed a smaller proportion of their filtered uric acid and achieved a uric acid clearance and a uric acid excretion rate well above the levels observed in the gouty subjects. The authors conclude that abnormal renal excretion of uric acid is one important cause of hyperuricemia in some patients with gout.

Secondary metabolic gout. This disturbance is inherent to an increased formation or destruction of cells and as a result an increased metabolism of nucleic acids, the eventual outcome of which is an enhancement of the production of uric acid. Clinical gouty arthritis is a well recognized phenomenon in patients afflicted with a number of blood dyscrasias.

One case of secondary metabolic gout is included in this material. In this instance acute gout developed 16 years after polycythemia vera had been diagnosed.

Studies with C^{14}-labeled uric acid revealed a threefold increase in the size of the miscible pool and in the turnover of uric acid. The miscible pool was found to be 3806 mg with a plasma urate level of 16.1 mg per cent. The daily endogenous production of uric acid was no less than 1667 mg of which 1314 mg or 78.8 per cent was excreted through the kidneys. At the end of 11 days 72.2 per cent of the injected uric acid-C^{14} had been excreted with the urine, a figure which agrees well with the ratio between the mean daily urinary urate excretion and the computed daily turnover. One year prior to this study the patient had been placed upon a regimen of 0.5 g of probenecid twice daily, which was continued throughout the study. On this program an excellent uricosuric response was observed and although there was some impairment in the renal function, his kidneys were capable of eliminating close to 80 per cent of the totally formed urate.

When glycine-1-C^{14} was injected into this patient the pattern of C^{14}-incorporation into uric acid was quite different from those observed either in normal subjects or in patients with primary gout (Figure 6). The curve rises slowly and does not exceed normal until the 6th day. The maximum value is first reached on the 13th day, after which time the curve falls off slowly. Figure 7 illustrates the cumulative excretion of C^{14} as urinary uric acid expressed as the percentage of the total dose initially administered. By the end of a week 0.095 per cent had been recovered, and at the end of 3 weeks the recovery was 0.58 per cent.

Polycythemia vera is the blood disorder most frequently associated with clinical gouty arthritis, the incidence varying from 2.0 to 8.8 per cent. Other blood dyscrasias occasionally complicated by secondary gout include leukemia, myeloid metaplasia and hemolytic anemias. A review of the coexistence of gout and blood dyscrasias has been given by Talbott.[16] Of special interest is the excessive urate production following radiotherapy or the administration of chemotherapeutic agents which cause destruction of cells with subsequent liberation of large amounts of nucleoproteins. An elevated urinary output of uric acid may prove to be a valuable index for the efficiency of chemical agents in the control of cancer.

Secondary renal gout. In this condition there is a normal-sized production of uric acid, and hyperuricemia arises as a consequence of an insufficient amount of effectively functioning renal tissue. Glomerular insufficiency is the most common cause of hyperuricemia and typical bouts of gouty arthritis are not unusual in patients with long-continued uremia.[17,18] Some writers[18,19] suggest that latent gout may be made manifest by renal disease. Addis[17] implies, as does the author, that renal insufficiency may give rise to true secondary gout. The reason why overt gout does not complicate this condition as often as one might expect, may be that many patients do not outlast the initial stage of asymptomatic hyperuricemia. Three cases of gouty arthritis secondary to glomerular insufficiency are reviewed below.

L.B., a 63-year-old male is known to have had arterial hypertension and chronic pyelonephritis for 8 years. During the past 3 years he has experienced 7 or 8 episodes of acute gouty arthritis.

The blood pressure was 220/120 mm Hg. The blood urea nitrogen ranged from 38 to 49 mg per cent with a urea clearance of 8 ml per minute. Moderate amounts of protein, casts, white blood cells and bacteria were present in the urine. The plasma uric acid concentration ranged between 15 and 16 mg per cent.

The miscible pool of uric acid was found to contain 2233 mg; 22.8 per cent of this was replaced daily, requiring the introduction into the pool of 509 mg of new endogenous uric acid each day. The mean daily urinary uric acid excretion was 316 mg or 62.2 per cent of the turnover value. At the end of 8 days, 51.9 per cent of the injected C^{14} had been recovered in urinary uric acid. Patient L.B., therefore, has a normal-sized production of uric acid. The occurrence of gout several years after the diagnosis of chronic pyelonephritis had been made tends to indicate that hyperuricemia and gouty arthritis resulted as a consequence of renal insufficiency.

L.R. was a 51-year-old male with chronic nephropathy of undetermined type. He had a history of albuminuria for 12 years. Urine analysis revealed small amounts of red blood cells, white blood cells, hyaline casts and intracellular double refractile fat. Urea clearance varied from 16 to 40 ml per minute. Shortly before the pool and turnover study with labeled uric acid he experienced his first episode of acute gouty arthritis. The plasma urate concentration was 10.5 mg per cent. The size of the pool was determined as 2521 mg with a daily turnover of 731 mg. The average daily urinary uric acid excretion was 215 mg, or 29.4 per cent of the turnover. By the end of 7 days, 24.0 per cent of the injected C^{14} had been recovered from urinary uric acid.

The third patient, H.S., was a 70-year-old male, who died from longstanding arteriosclerotic cardiovascular disease and chronic renal failure. Ten months prior to death he experienced his first episode of acute articular distress. At this time plasma uric acid was 12.4 mg per cent and the blood urea nitrogen 29 mg per cent. Subsequently typical acute gouty attacks recurred in both feet with increasing frequency.

The autopsy findings included acute myocardial infarction, old and recent cerebrovascular accidents, severe ulcerated atherosclerosis of the aorta and its branches, chronic renal disease and gouty tophi on both metatarsophalangeal areas. Microscopically both kidneys exhibited all the stigmata of severe arterial and arteriolar nephrosclerosis, but none of the changes of gouty nephrosis. Urates could not be demonstrated in small pieces of papillary tissue which had

been fixed in absolute alcohol and examined in polarized light or after staining by the method of Schultz-Smith.

The specific renal lesion[20] in gout characterized by overproduction of uric acid consists of microtophaceous urate deposits in the lumen of the collecting tubules or in the interstices of the pyramids. The tubular epithelium about the casts of the crystals may be partly or completely destroyed. Foreign body giant cells are present about the periphery of the crystals, which may be surrounded by interstitial fibrosis and lymphocytic reaction. In a small proportion of cases the pyramidal urate deposits become so great that they cause obstruction of the ducts of Bellini with resulting atrophy and fibrosis of the tubules.

Drug-induced gout. In recent years there have been several reports of cases of acute gouty arthritis precipitated by certain drugs, including pyrazinamide[21] and chlorothiazide,[22-24] which are thought to cause inhibition of renal tubular secretion of uric acid.[25] One case is reported below.

W.B., a 62-year-old male, had had hypertensive cardiovascular disease with cardiomegaly for more than 10 years. In August 1958 chlorothiazide (750 mg/day) was added to his antihypertensive program. One year later he developed typical acute gouty arthritis of his left wrist and carpal joints. The plasma uric acid concentration was 9.6 mg per cent. The daily dose of chlorothiazide was subsequently reduced to 250 mg and two weeks later the plasma urate level had fallen to 7.5 mg per cent.

While the patient was maintained on 250 mg of chlorothiazide daily, his endogenous uric acid production was determined by means of C^{14}-labeled uric acid. The miscible pool of uric acid was moderately elevated, being 1659 mg. The daily turnover rate was 37.1 per cent the size the miscible pool, or 615 mg which is in the normal range. The average daily urinary uric acid excretion was 217 mg, or 35.3 per cent of the total elimination. At the end of 7 days 34.3 per cent of the injected C^{14} had been recovered in urinary uric acid.

The hyperuricemic action of chlorothiazide was studied in an additional patient. This subject received uric acid-C^{14} intravenously. Beginning 4 days later, 250 mg of chlorothiazide was administered orally every 8 hours for 3 days. The results are shown in Figure 8. The slope of the isotope dilution curve against time remained unchanged indicating that chlorothiazide does not enhance the catabolism of nucleoproteins. Administration of the drug for 3 days resulted in an elevation of plasma uric acid of 1.3 mg per cent. Concomitantly there was a decrease in the urinary uric acid output, which on the third day was 100 mg lower than the baseline value. The low plasma levels of chlorothiazide obtained with oral administration of the drug inhibit the renal tubular secretion of uric acid, thus causing hyperuricemia.

A paradoxical response is produced by giving 0.5 g of chlorothiazide intravenously. The transient uricosuric effect of chlorothiazide, also noted by Januszewicz et al.,[26] is clearly illustrated in Figure 9 and Table 4. Simultaneous urate and inulin clearance studies were performed. After passage of 3 control periods to establish baseline values for the glomerular filtration rate and urate clearance, 0.5 g of chlorothiazide was injected intravenously. This was followed by a prompt and significant uricosuric response, which lasted for about 80 minutes. The urate clearance rose from 11 ml/minute during the control period to 28.2 ml/minute during the first 25 minutes following the intravenous injection. A 10 per cent reduction in the glomerular filtration rate followed the administration of chlorothiazide. A similar effect was noted by Januszewicz et al.,[26] who suggested that chlorothiazide exerted a direct action on

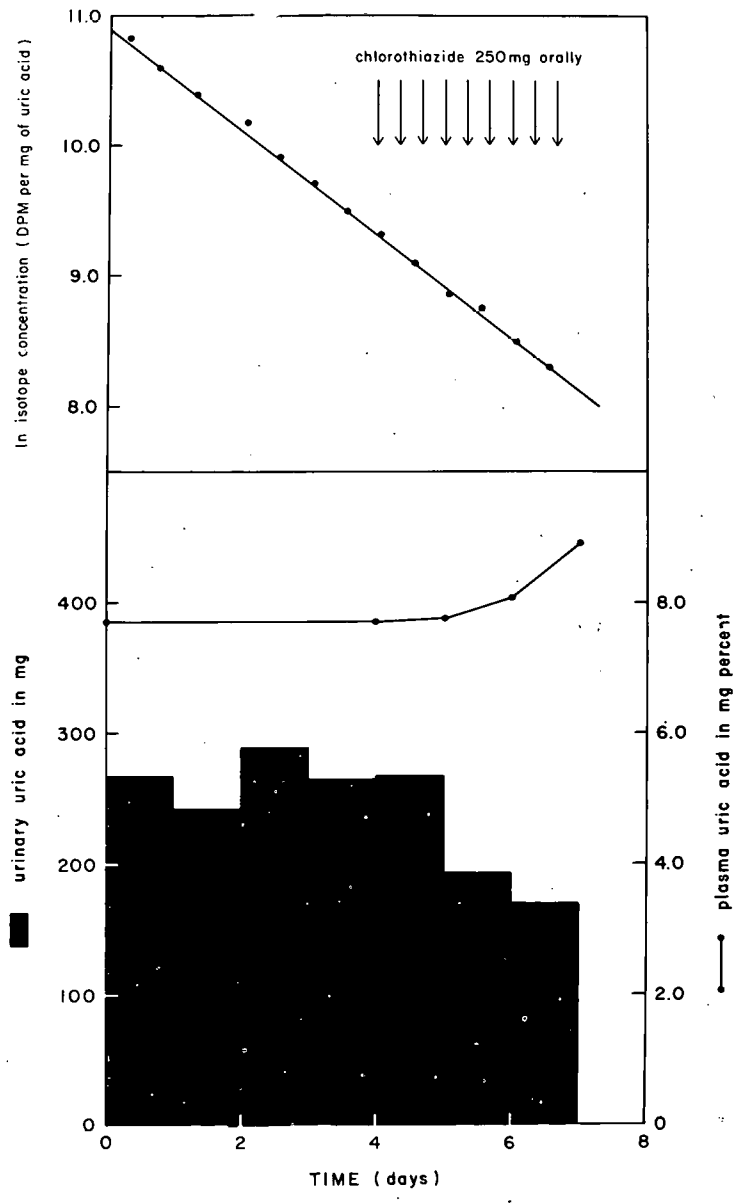

Figure 8. Upper. Hemilogarithmic plot of the isotope concentration in urinary uric acid against time. Beginning on the 4th day 250 mg of chlorothiazide was administered orally every 8 hours for 3 days. Lower. The effect of orally-administered chlorothiazide on the plasma urate level and the urinary acid excretion.

Table 4

SIMULTANEOUS INULIN AND URIC ACID CLEARANCES IN A PATIENT WHO RECEIVED 0.5 g OF CHLOROTHIAZIDE INTRAVENOUSLY 82 MINUTES AFTER THE START OF EXPERIMENT

(Body surface area: 1.73 sq m)

Experiment No.	Collection period (min)	Urine flow (cc/min)	Plasma		Urine		Clearances		Clearance ratio
			Inulin (mg/cc)	Urate (mg/cc)	Inulin (mg/min)	Urate (mg/min)	Inulin (cc/min)	Urate (cc/min)	Urate/Inulin
1	0- 24.5	2.86	0.195	0.0544	19.67	0.582	101	10.7	0.106
2	24.5- 51.0	3.89	0.175	0.0544	18.17	0.598	104	11.0	0.106
3	51.0- 79.5	3.44	0.162	0.0544	17.16	0.617	106	11.3	0.107
4	79.5-105.5	12.50	0.151	0.0527	15.44	1.487	102	28.2	0.276
5	105.5-127.0	10.60	0.144	0.0509	13.33	1.002	93	19.7	0.212
6	127.0-158.5	9.11	0.138	0.0510	13.21	0.743	96	14.6	0.152
7	158.5-192.5	5.94	0.133	0.0517	12.08	0.537	91	10.4	0.114

the renal vasculature.

These experiments indicate that the effect of chlorothiazide upon the excretion of uric acid is similar to the effect of uricosuric drugs such as salicylates, probenecid and phenylbutazone.[27] Small doses of these drugs inhibit the tubular excretory mechanism for urate, resulting in the retention of urate. When larger doses are given, tubular reabsorption of urate is also suppressed, the net effect then being uricosuria.

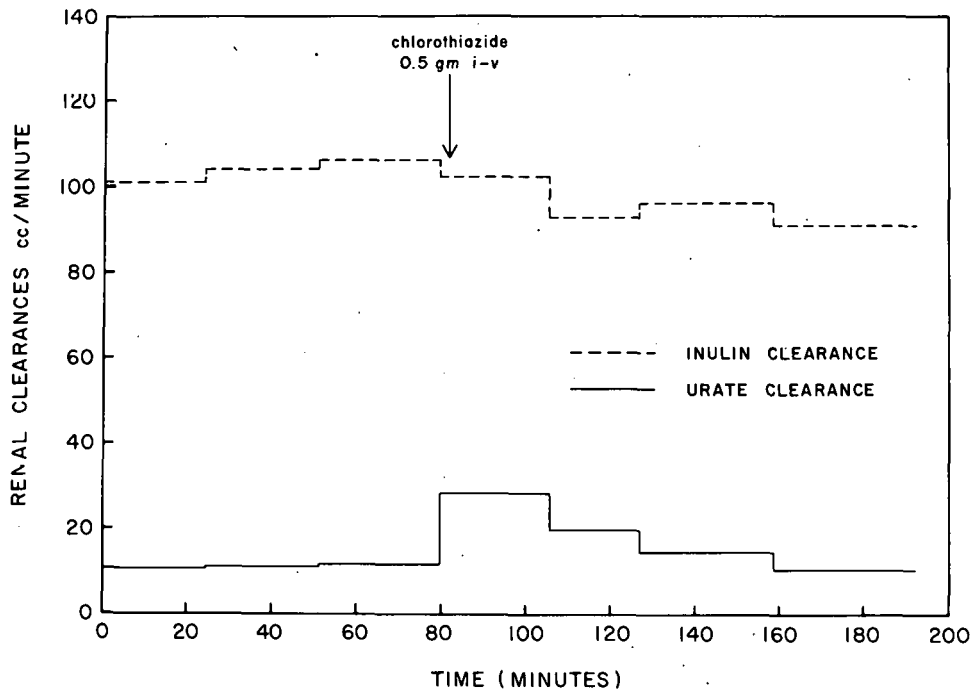

Figure 9. The effect of intravenously-injected chlorothiazide on inulin and urate clearances. 0.5 g of chlorothiazide was administered at 80 minutes time.

ACKNOWLEDGMENT

The author is indebted to the following doctors in Billings Hospital, University of Chicago Clinics, and wishes to express his appreciation for their help: L. O. Jacobson, R. J. Hasterlik, A. Kappas, and G. W. LeRoy; C. Newton, R. Levine and F. Straus.

LITERATURE CITED

1. Garrod, A. B. Tr. Roy. Med.-Chir. Soc. London, 31:83, 1848.
2. Sørensen, L. B. Scandinav. J. Clin. and Lab. Invest. Supplementum, 54, 1960.
3. Spence, J. C. Lancet, 2:1026, 1927.
4. Sears, W. G. Lancet, 1:24, 1933.
5. Nugent, C. A., and F. H. Tyler. J. Clin. Invest., 38:1890, 1959.

6. Praetorius, E. Scandinav. J. Clin. and Lab. Invest., 1:222, 1949.

7. Harrison, H. E. Proc. Soc. Exptl. Biol. and Med., 49:111, 1942.

8. Smith, H. W. Principles of Renal Physiology, New York, Oxford University Press, 1956.

9. Benedict, J. D., T. F. Yu, E. J. Bien, A. B. Gutman, and D. Stetten, Jr. J. Clin. Invest., 32:775, 1953.

10. Muller, A. F., and W. Bauer. Proc. Soc. Exptl. Biol. and Med., 82:47, 1953.

11. Wyngaarden, J. B. J. Clin. Invest., 36:1508, 1957.

12. Seegmiller, J. E., L. Laster, and D. Stetten, Jr. Ninth International Congress on Rheumatic Diseases, II:207, 1957.

13. Spilman, E. L. Fed. Proc., 13:302, 1954.

14. Wyngaarden, J. B. Metabolism, 7:374, 1958.

15. Seegmiller, J. E., L. Laster, and L. V. Liddle. Metabolism, 7:376, 1958.

16. Talbott, J. H. Medicine, 38:173, 1959.

17. Addis, T. Glomerular Nephritis, Diagnosis and Treatment, New York, Macmillan Co., 1948, p. 139.

18. Merrill, J. P. The Treatment of Renal Failure, New York and London, Grune and Stratton, Inc., 1955, p. 62.

19. Bauer, W., and E. Calkins. Gout. In Duncan, G. G.: Diseases of Metabolism, Philadelphia and London, W. B. Saunders, 1959, 4th ed., p. 666.

20. Allen, A. C. The Kidney, Medical and Surgical Diseases, New York, Grune and Stratton, Inc., 1951, p. 286.

21. Cullen, J. H., L. J. A. Early, and J. M. Fiore. Am. Rev. Tuberc., 74:289, 1956.

22. Oren, B. G., M. Rich, and M. S. Belle. J. A. M. A., 168:2128, 1958.

23. Healey, L. A., G. J. Magid, and J. L. Decker. New England J. Med., 261:1358, 1959.

24. Freeman, R. B., and G. G. Duncan. Metabolism, 9:1107, 1960.

25. Monroe, K. E., L. H. Grant, A. A. Sasahara, and D. Littman. New England J. Med., 261:290, 1959.

26. Januszewicz, W., H. O. Heinemann, F. E. Demartini, and J. H. Laragh. New England J. Med., 261:264, 1959.

27. Yu, T. F., and A. B. Gutman. Proc. Soc. Exptl. Biol. and Med., 90:542, 1955.

ROENTGEN DIAGNOSIS OF PANCREATIC DISEASE*

By

R. D. Moseley, Jr.

Until recent years, plain abdominal films and regular gastroduodenal roentgen examination were essentially the only radiologic techniques applied to the diagnosis of diseases of the pancreas.[1-4] A great increase in interest in the problems of diagnosis of diseases of this organ has been evidenced of late by the development of a variety of techniques designed to investigate the pancreas. Among these techniques may be mentioned operative pancreatography,[5] pancreatic angiography,[6] pneumoretroperitoneal pancreatography,[7] intravenous cholangiography,[8] percutaneous direct cholangiography,[9] and splenoportography.[7] In addition, considerable research effort has been expended in the development—as yet unsuccessful—of compounds for the direct opacification of the pancreas.[10-12] Until these efforts are successful, we will be limited to the indirect methods of visualization, which are the basis both of the older and the more recent methods mentioned above and which are attended with great diagnostic difficulty, from the standpoint of both overdiagnosis as well as underdiagnosis.

Before discussing the newer techniques and the present status of direct visualization research, the status of the most commonly employed technique—gastroduodenal examination—will be assessed.

Because localization of masses depends on the types of extrinsic deformity of the gastrointestinal tract, the accuracy of diagnosis of pancreatic disease by this method is, unfortunately, not high. For instance, an identical deformity of the body of the stomach may be produced by both pancreatic tumor and by hepatoma.

Widening of the duodenal loop has long been a standard radiologic sign of pancreatic mass. This finding almost routinely occurs late in the development of the lesion when surgical intervention is least likely to be successful.

While the "reverse 3 sign" or epsilon (ϵ) sign in the second portion of the duodenum is probably always indicative of abnormality, it is not possible by the presence of this sign to differentiate pancreatic neoplasm from pancreatitis. An impression in the duodenal bulb resulting from a dilated common duct particularly associated with mucosal abnormalities in the second portion of the duodenum is a relatively reliable sign of pancreatic neoplasm but is not frequently encountered in these patients.

The most commonly overlooked findings are small areas of invasion and mucosal irregularity in the second portion of the duodenum.

Attempts to diagnose acute and chronic pancreatitis are frequently made on the basis of plain abdominal films. An accumulation of gas in a segment of the small bowel (Figure 1)—a localized adynamic ileus—is frequently associated with acute pancreatitis. Unfortunately the borderland between normal and abnormal here is very indistinct, and the roentgen findings alone will not support a diagnosis.

---

*This paper appears in the Arch. Int. Med. 107:31, 1961, Jan.

Figure 1. "Sentinel" loop of dilated small bowel as a result of localized adynamic ileus in a case of acute pancreatitis.

The presence of calculi within the parenchyma and ducts of the gland is, of course, diagnostic of chronic calcareous pancreatitis.

Operative pancreatography by the transduodenal approach (Figure 2) has in recent years been advocated in the diagnosis of pancreatic disease. Certainly this technique is our nearest current approach to direct visualization of the pancreas. It is unfortunate that this is an operative technique, since this factor so markedly limits its usefulness.

We have found the transduodenal approach technically difficult and, on those infrequent occasions when we utilize this method, use the technique of injection into the ducts following excision of the tail of the pancreas (Figure 3A).

Parenchymal visualization (Figure 3B) follows the second injection via this route as well as in the originally described technique.

In a modification of this technique, pancreatic cysts may be injected at operation (Figure 4) with demonstration of the pathologic morphology of the cyst itself as well as its relation to the pancreatic duct system and surrounding structures.

The great hopes held for the technique of angiography of the pancreatic vessels have not been practically realized. While the pancreaticoduodenal artery can be visualized using percutaneous femoral puncture catheter techniques, the criteria for diagnosis of pancreatic disease by this method have not been developed.

The technique of pneumoretroperitoneal pancreatography, in which the stomach and duodenum are opacified with orally administered organic iodine compounds (Gastrografin), the biliary

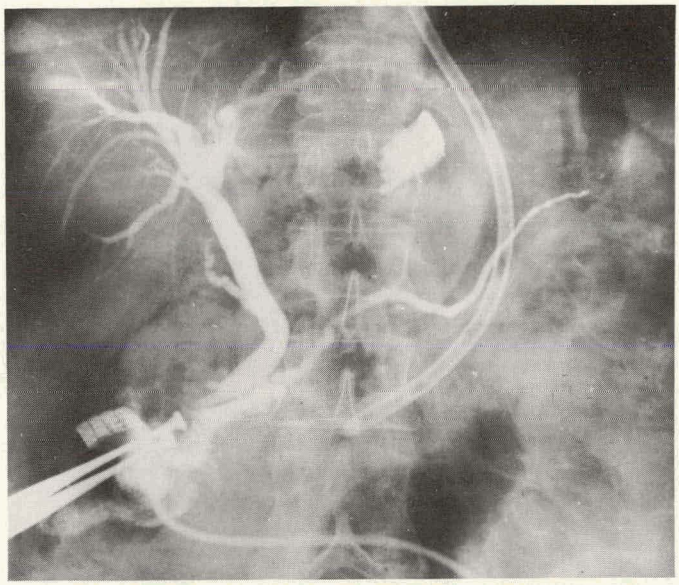

Figure 2. Transduodenal operative pancreatogram demonstrating the duct of Wirsung as well as portions of the biliary system.

and urinary tracts visualized with intravenously administered medium (Duografin) and the retroperitoneal potential space filled with carbon dioxide (Figure 5), makes it possible in many instances to outline the pancreas and to detect lesions producing an increase in size of this organ.

Body section radiography is an important adjunct to this procedure in that obscuration of details of overlying structures frequently makes prominent details that would otherwise be hidden. For instance, deviation of the course of the opacified common duct by neoplasm (Figure 6)

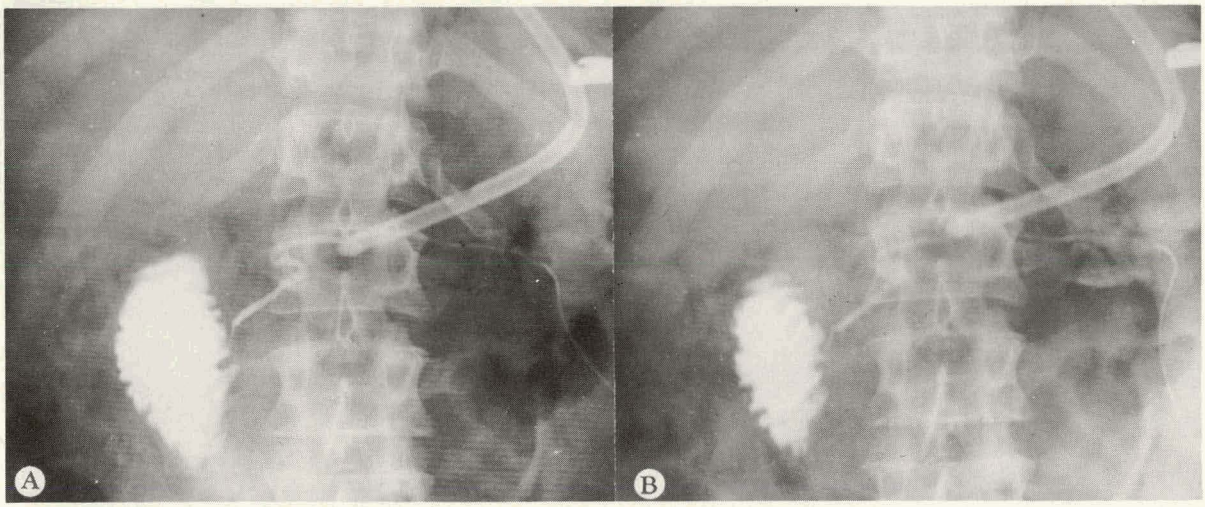

Figure 3. A, operative pancreatogram with injection through polyethylene catheter introduced into sectioned duct in tail of pancreas; B, second injection demonstrates parenchymal opacification.

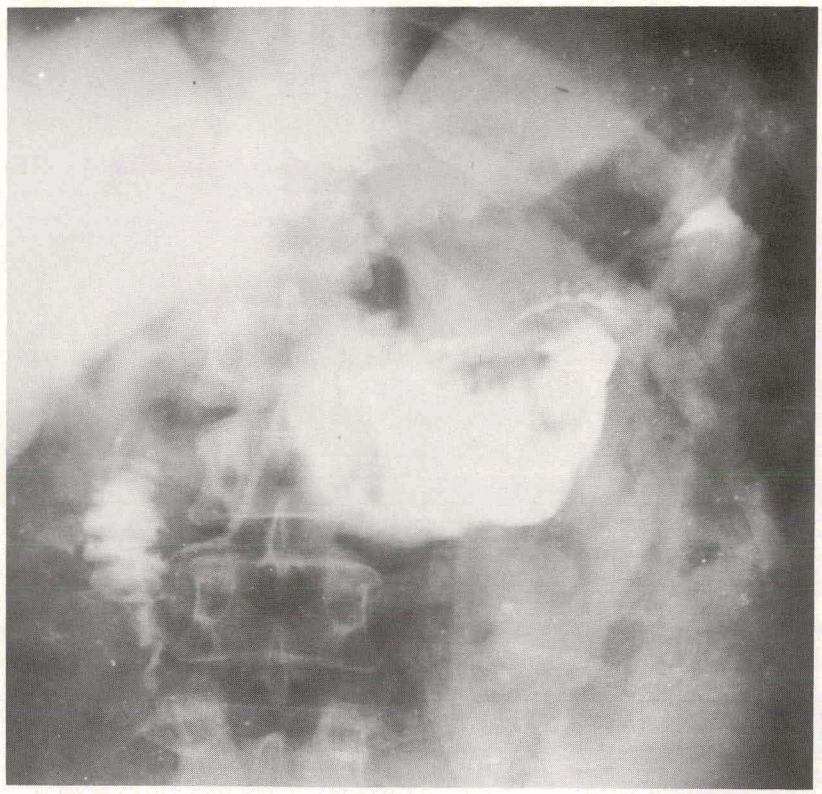

Figure 4. Opacification of pancreatic ducts and large pancreatic cyst following injection of opaque material in the cyst.

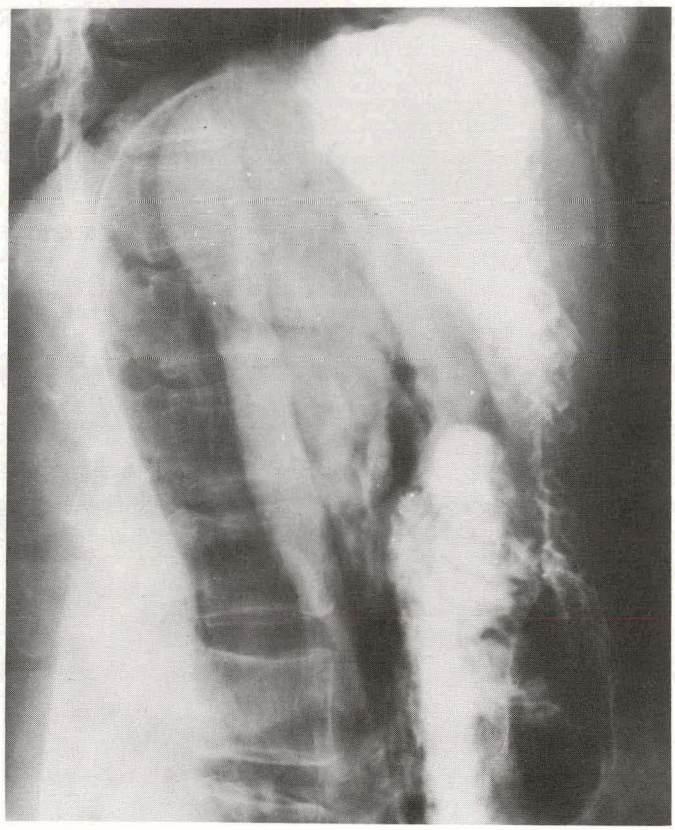

Figure 5. Normal pancreas demonstrated by pneumoretroperitoneal pancreatography.

Figure 6. Deviation of the opacified common duct by carcinoma of the uncinate process of the head of the pancreas—pneumoretroperitoneal pancreatogram.

is made much more apparent by laminography.

This visualization of the biliary tract and of the urinary tract (Figure 7, A and B) as a part of this technique is frequently quite helpful diagnostically because of the displacement of these visualized structures by masses in the pancreas.

The large pancreatic mass (Figure 8) can be easily visualized by this technique. Unfortunately small lesions or lesions which produce no significant alteration of the size of the pancreas are difficult or impossible to outline by this method.

Intravenous cholangiography (Figure 9) may be used to give indirect evidence of pancreatic disease—particularly of inflammatory lesions. The gallbladder ordinarily does not opacify on intravenous cholangiography in the presence of acute cholecystitis. In the presence of pancreatitis, visualization of the gallbladder will occur in approximately two-thirds of the cases. Thus the technique is useful but not infallible in the differentiation of acute cholecystitis and pancreatitis.

Percutaneous direct cholangiography by the transhepatic route is a technique which, in highly selected cases, may be useful in the diagnosis of pancreatic disease, particularly neoplasm (Figure 10). Where, due to intense jaundice, other techniques for visualization of the biliary tract fail, percutaneous cholangiography may be indicated. Unfortunately the method is not with-

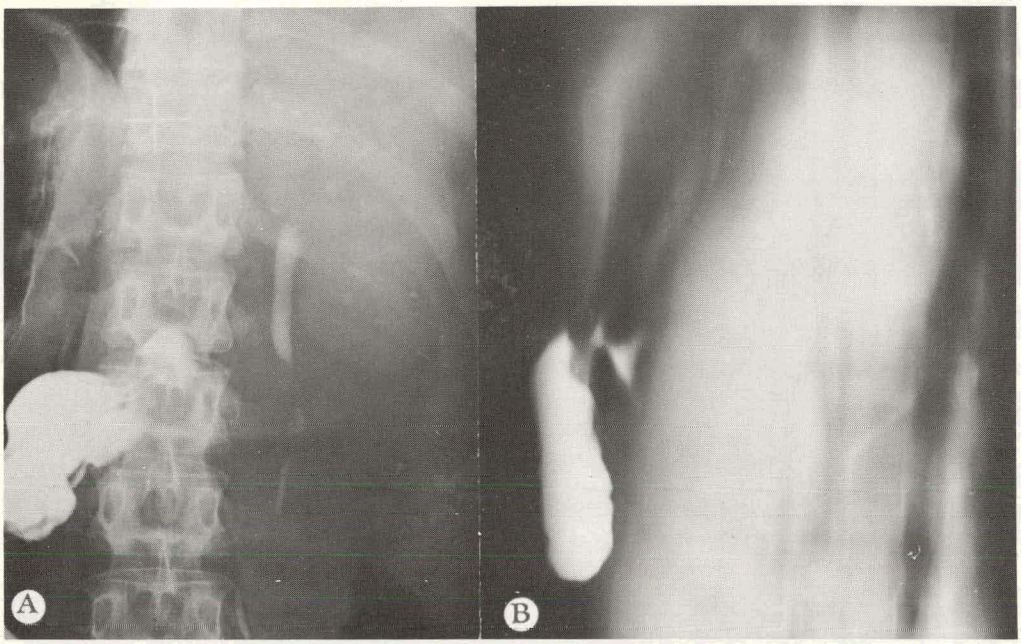

Figure 7. (A and B). Displacement of the right ureter by pancreatic neoplasm—pneumoretroperitoneal pancreatogram.

Figure 8. Large pancreatic neoplasm—pneumoretroperitoneal pancreatogram.

Figure 9. Intravenous cholangiogram with excellent visualization of gallbladder and bile ducts in a patient with acute pancreatitis.

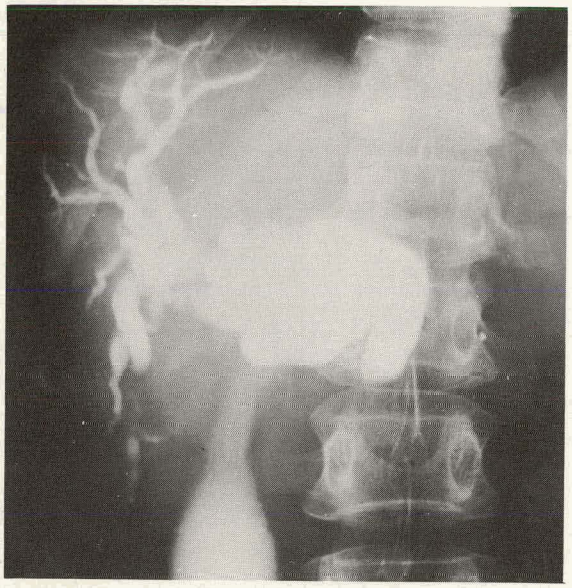

Figure 10. Percutaneous transhepatic cholangiogram: obstruction of common duct due to pancreatic neoplasm.

out danger, especially the danger of bile peritonitis, and thus its usefulness is limited.

Splenoportography may be used as an aid in estimating the retroperitoneal invasiveness of pancreatic neoplasm and as a procedure for evaluation of operability. If the splenoportal venous system is intact, operative approaches are ordinarily technically easier. Invasion of these veins (Figure 11) or their complete occlusion makes the outlook for other than palliative operative procedures less hopeful.

It is apparent from this discussion of both older and newer procedures for the radiologic investigation of the pancreas that until an agent can be developed for direct visualization of this organ following oral or intravenous administration and that as long as we must depend on indirect technique, our accuracy in the diagnosis of pancreatic disease will not be at a satisfactory level.

Many substances for direct visualization of the pancreas (Table) ranging from acridine compounds to zinc compounds are currently under investigation. The compounds so far selected are based on experimental evidence of selective excretion of such materials by the pancreas and on the possibility of altering these compounds, usually by the substitution of iodine atoms, in order to make them opaque to x-rays.

Until we have such compounds available, radiologic diagnosis of pancreatic disease will rest on the unsubstantial base of our presently available techniques of gastroduodenal examinations, operative pancreatography, pancreatic angiography, pneumoretroperitoneal pancreatography, intravenous cholangiography, percutaneous direct cholangiography, and splenoportography.

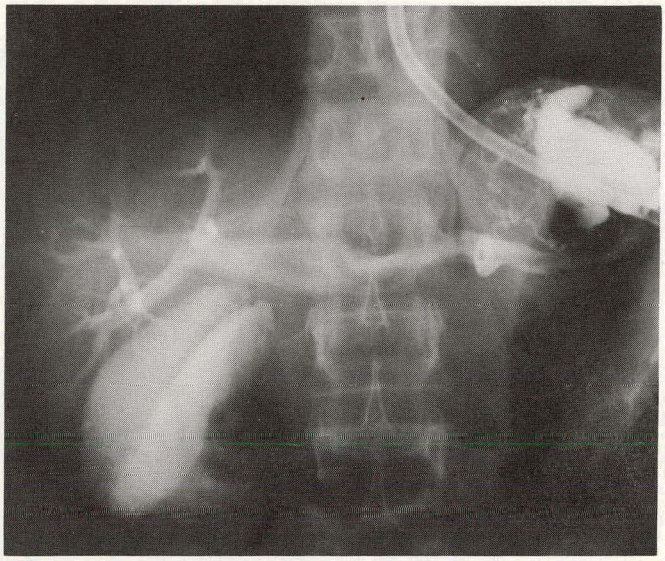

Figure 11. Splenoportogram, showing compression and invasion of splenoportal veins by pancreatic neoplasm.

Table

SUBSTANCES FOR DIRECT VISUALIZATION OF THE PANCREAS

Acridine orange
Acridine red
Alloxan
Basic fuchsin
Berberine (and other derivatives of extracts of Colombo root)
Pyronin B
Rhodamine B
Zinc compounds (halogenated organic compounds)

LITERATURE CITED

1. Beeler, J. W., and B. R. Kirklin. Am. J. Roentgenol., 67:576, 1952.
2. Case, J. T. Am. J. Roentgenol., 44:485, 1940.
3. Hodes, P. J., E. P. Pendergrass, and N. J. Winston. Radiology, 62:1, 1954.
4. Larsen, K. A., and A. Pedersen. Acta radiol., 45:459, 1956.
5. Doubilet, H., M. H. Poppel, and J. H. Mulholland. Radiology, 64:325, 1955.
6. Ödman, P. Acta radiol. Suppl., 159, 1958.
7. Moseley, R. D., Jr. Am. J. Roentgenol., 80:967, 1958.
8. Johnson, H. C., Jr., B. D. Minor, J. A. Thompson, and H. S. Weens. New England J. Med., 260:158, 1959.

9. Carter, R. F., and G. M. Saypol. J.A.M.A., 148:253, 1952.

10. Shapiro, R. Radiology, 69:690, 1957.

11. Nardi, G. L., and J. H. Seipel. S. Forum, 6:381, 1955.

12. White, T. T., and D. F. Magee. Radiology, 72:238, 1959.

DETERMINATION OF RADIOTRACER STABILITY OF TRITIUM-LABELED COMPOUNDS IN BIOLOGICAL STUDIES*

By

G. T. Okita and J. L. Spratt †

Reviews of recent literature indicate that many investigators are ignoring the possibility that tritium atoms may exchange with hydrogen atoms when tritium-labeled compounds are used in biological studies. Even purification of labeled compounds to constant specific activity or purification by gas-liquid chromatography does not preclude the possibility of tritium exchange.

The purpose of this report is to stress the necessity of establishing biological radiotracer stability of tritiated compounds which are to be employed in biological investigations, and to describe some of the methods devised to establish this condition.

Before tritium-labeled compounds can be tested for biological tracer stability, radiochemical purity must be established. Difficulties in purifying certain tritiated compounds have been reported by various investigators.[1-5]

Recently, Rothchild of New England Nuclear Corporation conducted a survey[3] to determine the number of investigators who were not able to purify their labeled compounds to constant specific activity after utilizing their Wilzbach tritiation service.[6] As indicated in Table 1, out of a total of 83 scored replies, 13 compounds could not be purified to constant specific activity.

Certain unsaturated compounds also have been shown to be contaminated by their dihydro derivative after all the usual criteria for radiochemical purity have been satisfied, such as constant specific activity with recrystallization, fractional crystallization, occurrence of a single spot with corresponding radioactivity using various paper chromatographic solvent systems, and stoichiometric agreement between compound and radioactivity upon preparation of chemical derivatives.

Table 2 illustrates the difficulty Misra and Woods[4] encountered in purifying H^3-morphine, and Werbin et al.[5] had in purifying H^3-β-sitosterol. In both cases Wilzbach-labeled compounds were initially purified to a constant specific activity and resolved as a single spot using three different paper chromatographic solvent systems. Final purification was achieved only after the use of an additional purification procedure which resolved the parent compound from the dihydro contaminant.

However, even if a tritiated compound satisfies the usual criteria of radiochemical purity, this is still no guarantee that the compound can then be used as a reliable biochemical tracer. Since all biological systems are aqueous systems, the possibility of tritium atoms exchanging

---

*This paper was presented at the International Atomic Energy Agency Symposium on the Detection and Use of Tritium in the Physical and Biological Sciences, Vienna, Austria, May 1961, and will appear in the Proceedings of the Symposium.

†Department of Pharmacology, University of Chicago. Present address: Department of Pharmacology, State University of Iowa, Iowa City, Iowa.

Table 1

Compounds labeled	Purified to constant specific activity	Not purified to constant specific activity	Don't know
Amino acids and polypeptides	2	1	-
Aromatics	12	1	3
Carbohydrates	3	-	3
Hydrocarbons	9	2	3
Lipids	4	4	-
Nucleosides and pyrimidines	3	1	1
Steroids	14	1	1
Other compounds	4	3	8
Total	51	13	19

From survey by S. Rothchild, Atomlight, No. 16, p. 6, Jan. 1961.

Table 2

Compounds*	Final procedure employed for purification	Contaminant	Reference
Morphine	Paper chromatography using buffered paper	Dihydromorphine	Misra and Woods Nature, 185:304, 1960
β-sitosterol	Prepared epoxide derivative	Dihydrositosterol	Werbin, Chaikoff and Imada Arch. Biochem. 89:213, 1960

*Recrystallization to constant specific activity and paper chromatography using at least three different solvent systems.

with hydrogen atoms is readily appreciated. Furthermore, in addition to this problem of physical exchange within a biological system, there is the additional possibility that isotopic dilution will be mediated by specific enzymatic hydrogen transfer systems under equilibrium conditions. For example, it is possible that DPN and TPN, acting as hydrogen acceptors can replace tritium for hydrogen under equilibrium conditions with a resultant drop in specific activity which is not due to dilution of the labeled compound by net synthesis from non-labeled endogenous sources. Therefore, the one remaining criterion of a biological tracer compound, i.e., biological radiotracer stability, must still be verified before valid biological experimentation can be undertaken.

METHODS AND DISCUSSION

Following are some of the methods that can be utilized for establishing radiotracer stability of tritiated compounds. Other methods may be employed, depending upon the nature of the

experiment in which the H^3-labeled material will be used.

Method 1. Exogenous compounds which do not undergo isotopic dilution by endogenous synthesis, such as tritium-labeled drugs, can be investigated by this method. It consists of the demonstration that there is no diminution in specific activity when the labeled material is reisolated from in vitro or in vivo biological systems. Achor[7] used this method in our laboratory to confirm the biological stability of H^3-morphine labeled by the Wilzbach procedure. The purified morphine which had a constant specific activity of 8.32 c/mg was administered intraperitoneally to rats in a dose of 35 mg/kg. The comparable specific activity of 8.36 c/mg for the morphine isolated from the urine confirmed the biological stability of the material.

Method 2. Endogenous biochemical compounds which may undergo isotopic dilution can be tested for tritium radiotracer stability when the same compound labeled with carbon-14 is available. Since the labeled carbon atoms are not exchangeable, the stability of the tritiated compound is indicated if the biological experimental data parallel those obtained with the C^{14} compound. This approach was used in comparing the biological half-life of radiochemically pure H^3-cholesterol prepared by the catalytic exchange method of Fukushima and Gallagher[8] to that of cholesterol-4-C^{14} (New England Nuclear Corporation). A single intravenous dose containing both H^3-cholesterol and C^{14}-cholesterol was administered to a patient. At various time intervals following injection, the plasma-free cholesterol was isolated and the H^3 and C^{14} radioactivity determined by a double-label counting technique using a liquid scintillation spectrometer.[9] Comparison of the logarithm of specific activity vs time for both C^{14} and H^3 compound gave identical results. Such a duplication of biological half-life or other experimental parameters can also be performed by administering each isotopic compound separately in different animals or at different times.

Method 3. The determination of the H^3 to C^{14} isotope ratio in a mixture of the same compound labeled with both isotopes can be used to verify the biological stability of both exogenous and endogenous compounds.

Identical isotope ratio before administration of the double-labeled material and after isolation from the biological system demonstrates tritium stability. This method is particularly applicable where isolation of minute amounts of material necessitate the use of non-radioactive carrier compound. An application of this method was employed in confirming the biological stability of the heart drug, digitoxin, which had been labeled with tritium by the Wilzbach procedure. Radiochemically pure H^3-digitoxin was mixed with biosynthetically-labeled C^{14}-digitoxin prepared in our laboratory.[10] The H^3 to C^{14} isotope ratio of digitoxin was determined and then injected intravenously into two rats. Unchanged digitoxin was isolated and purified from the urine and feces collected over the first 24 hours. The isotope ratio for the individually assayed H^3 and C^{14} solutions before injection was compared to the isotope ratio of the double-labeled drug isolated from the excreta, the latter being performed by double-label counting.[9] The isotope ratios for the injected and recovered digitoxin shown in Table 3 are in good agreement and demonstrate the radiotracer stability of the tritiated compound.

Method 4. LaBrosse has suggested a method wherein a distillate of urine following administration of a tritium-labeled compound is assayed for tritium that may have exchanged with H^1 of body water.[11] Assuming that an adequate amount of radiotracer is administered to compensate for the tremendous effect of diluting any exchanged tritium by total-body water, lack of radioactivity in the distillate indicates stability of the tritium label. In applying this method,

LaBrosse could not find any measurable radioactivity in urine distillate following the administration of d,l-epinephrine-7-H^3 to humans. He therefore concluded that the tritium on the 7-position was biologically stable. This method can also be applied to in vitro systems by radioassay of the distillate of the incubation medium. The method is obviously not suitable for compounds in which the tritium atoms are normally metabolized to body water by usual biochemical reactions.

Table 3

CONFIRMATION OF BIOLOGICAL STABILITY OF DIGITOXIN

H^3/C^{14} isotope ratio of digitoxin before administration	4.48
H^3/C^{14} isotope ratio of digitoxin recovered from excreta	4.41

LITERATURE CITED

1. Nystrom, R. F., and D. E. Simko. "Atomlight," New England Nuclear Corporation, Boston, January, 1959.
2. Bradlow, L. W., D. K. Fukushima, and T. F. Gallagher. "Atomlight," New England Nuclear Corporation, Boston, September, 1959.
3. Rothchild, S. "Atomlight," New England Nuclear Corporation, Boston, January, 1961.
4. Misra, A. L., and L. A. Woods. Nature, 185:304, 1960.
5. Werbin, H., I. L. Chaikoff, and M. R. Imada. Arch. Biochem., 89:213, 1960.
6. Wilzbach, K. E. J. Am. Chem. Soc., 79:1013, 1957.
7. Achor, L. B. J. Pharmacol. Exptl. Therap., 122:1A, 1958.
8. Fukushima, D. K., and T. F. Gallagher. J. Biol. Chem., 198:871, 1952.
9. Okita, G. T., J. J. Kabara, F. Richardson, and G. V. LeRoy. Nucleonics, 15:111, 1957.
10. Okita, G. T., F. E. Kelsey, E. J. Walaszek, and E. M. K. Geiling. J. Pharmacol. Exptl. Therap., 110:244, 1954.
11. LaBrosse, E. H. Proceedings of the Symposium on Advances in Tracer Applications of Tritium. New York City, October 1958, p. 22.

IN VIVO BIOCHEMICAL CHANGES DURING SPONTANEOUS CARCINOGENESIS I. METABOLIC PATTERNS OF EXPIRATORY $C^{14}O_2$ FOLLOWING ADMINISTRATION OF BICARBONATE, ACETATE AND GLUCOSE*

By

E. A. Ezz† and G. T. Okita

In 1923, Warburg[1] reported that cancer cells have a decreased oxidative metabolism and an increased anaerobic metabolism as compared to normal growing cells. In 1956, he reported that experimental evidence has accumulated to show that the ratio of glycolysis to aerobic respiration in the production of energy is quantitatively related to the degree of malignancy.[2,3] He further postulates that the origin of cancer is due to an irreversible injury to respiration followed by a long intracellular struggle for existence by adaptation of lost respiratory energy with fermentative energy which ultimately results in conversion of highly differentiated normal cells into undifferentiated cancer cells. Greenstein[4] showed that cancer tissues, regardless of the tissue of origin, tend to converge to a common enzymatic pattern. He also suggested that the biochemical characters of the tissues of tumor-bearing animals gradually change towards those of tumor tissue. Nakahara and Fukuoka[5,6] were able to separate from tumor tissues a cell-free extract which they labeled toxohormone. Injection of toxohormone into normal animals produced metabolic effects similar to those occurring in tumor bearing animals.

The present study is an attempt to evaluate possible biochemical changes occurring during the process of spontaneous carcinogenesis as well as during tumor development in intact unanesthetized animals. These changes were investigated by following expiratory $C^{14}O_2$ patterns‡ in normal, "precancerous," and tumor-bearing animals following the administration of C^{14}-labeled intermediates. Mice of high cancer strain which develop spontaneous mammary tumors were utilized in preference to tumor transplants to avoid the occurrence of metabolic alterations which might result from immunological responses to tumor inoculation.[7]

This approach of evaluating expiratory $C^{14}O_2$ patterns has proven to be a useful method for investigating in vivo metabolic changes which occur under various physiological and metabolic conditions. It has been employed in our laboratory by LeRoy et al.[8,9] for biochemical studies on humans, and by Kabara et al.[10,11] in studies of metabolic patterns of expiratory $C^{14}O_2$ in tumor-bearing CF_1 mice following the injection of C^{14}-labeled intermediates. Harmon, Kirk and Talbert[12] have determined the effect of cancer and fasting on the oxidation of labeled acetate, glucose and glycine to $C^{14}O_2$.

---

*Presented in part at the Annual Meeting of the American Society for Pharmacology and Experimental Therapeutics, Seattle, Washington, August, 1960.

†Submitted in partial fulfillment of the requirements for the degree of Doctor of Philosophy at the University of Chicago. Present address: University of Alexandria, Faculty of Medicine, Alexandria, U.A.R.

‡Graphical plots of specific activity, C^{14}-radioactivity, or per cent of injected C^{14} in expired $C^{14}O_2$ as a function of time.

This communication presents data which indicate the occurrence of biochemical changes in intact "precancerous" and tumor-bearing animals compared to those in normal virgin control animals.

MATERIALS AND METHODS

Female C3H/AN mice were used since they have a high degree of susceptibility to spontaneous mammary tumors.[13] The C3H/AN mice were obtained from Cumberland View Farms and studies made of the following experimental groups: (1) three-month-old virgin females known to have the mammary tumor milk factor, (2) retired exbreeders, approximately 12 months old, which had produced at least 5 litters and had no detectable mammary tumors, (3) exbreeders with single tumors, and (4) exbreeders with multiple tumors. The non-tumor C3H/AN exbreeders were included as a source of "precancerous" animals since they develop hyperplastic alveolar nodules in their mammary glands which are regarded as precancerous lesions.[14-16] As a result, we were able to investigate the possibility that biochemical changes occur before the onset of tumor in the "precancerous" stage. Special care was taken to include only tumor-bearing animals with firm, non-necrotic and non-deteriorating tumors. Single-tumor bearing animals had tumors between 0.5 to 1.5 cm in diameter, while multiple-tumor animals had two or more tumors of which at least one was larger than 0.5 cm in diameter.

The C^{14}-labeled intermediates used for the metabolic study were obtained from Tracerlab, Inc. and New England Nuclear Corp. Radio-chemical purity of the compounds was established by a paper strip scan of the chromatographed labeled compound. Radioactivity was reassayed using a vibrating reed electrometer-ionization chamber. The intermediates chosen are those involved in carbohydrate metabolism. Sodium bicarbonate-C^{14} was used to obtain information on bicarbonate pool size and turnover rates since the bicarbonate pool is the final common passage for most of the carbon-containing intermediates, and therefore may affect expiratory $C^{14}O_2$ patterns of other C^{14}-intermediates. Acetate-1-C^{14} was used because of the important role it plays in carbohydrate metabolism. The use of glucose-1-C^{14} and glucose-6-C^{14} enabled us to measure the relative proportions of carbohydrates metabolized via the Embden-Myerhof pathway and by the direct oxidative hexose monophosphate pathway by comparing differences in the rates of liberated $C^{14}O_2$. In the glycolytic pathway, C-1 and C-6 are metabolized in the same manner, being converted to the methyl carbon of pyruvic acid. In the direct oxidative pathway, C-1 is promptly eliminated as $C^{14}O_2$ while C-6 is not.

All C^{14}-labeled intermediates were prepared as sterile solutions in normal saline to prevent bacterial decomposition, and were reassayed from time to time. The intermediates were administered intraperitoneally in the following doses per gram body weight: bicarbonate-C^{14}, 0.005 μc; acetate-1-C^{14}, 0.01 μc; glucose 1-C^{14} and glucose-6-C^{14}, 0.03 μc.

The instrument used for the expiratory $C^{14}O_2$ studies was designed by LeRoy, Okita et al.[8] and built by the Argonne Cancer Research Hospital electronics shop. It monitors continuously $C^{14}O_2$ radioactivity, the amount of CO_2 in expired air, and the specific activity of expired $C^{14}O_2$. Simultaneous monitoring of specific activity of $C^{14}O_2$ is important since it excludes physiological artifacts which occur in C^{14} radioactivity and CO_2 curves resulting from excitement or other physiologically active or inactive states. Since the apparatus was designed originally for work on humans some modifications were necessary to adapt it for studies on mice. As shown in Figure 1, the instrument is composed of an animal chamber through which a steady

air flow pushes the expired air via a water trap and a radiation detector (4 π window-flow Geiger counter) to $C^{12}O_2$ gas analyzer. The C^{14} radioactivity, CO_2, and the specific activity of $C^{14}O_2$ in expired air are registered simultaneously on a multi-channel recorder. Both radiation detector and gas analyzer are calibrated before each run.

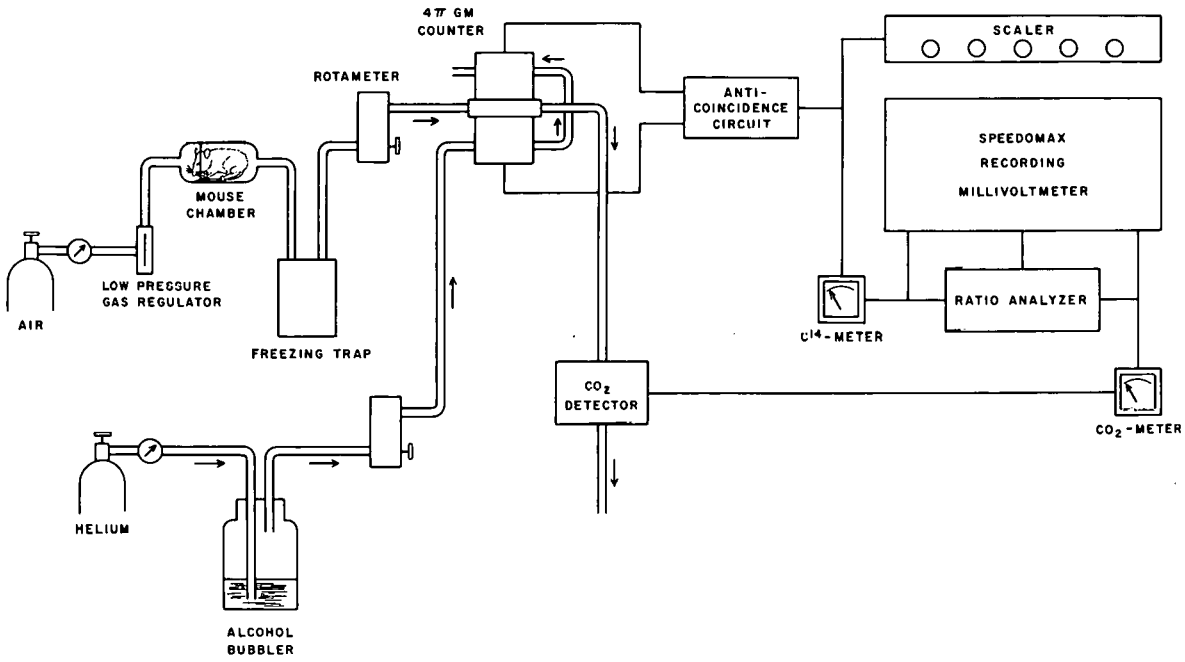

Figure 1. Schematic block diagram of continuous $C^{14}O_2$ monitoring apparatus.

All mice were fasted 8-14 hours. Before injection of the intermediates each mouse was placed in the animal chamber for approximately 30 minutes to familiarize it with the chamber. Immediately after injection, the mice were returned to the animal chamber and expiratory $C^{14}O_2$, CO_2 and the specific activity of $C^{14}O_2$ were recorded continuously. The experimental period was 1 hour for the bicarbonate-C^{14} run, 1.5 hour for the acetate-1-C^{14}, and 2 hours for glucose-1-C^{14} and glucose-6-C^{14}. Longer periods were not employed in order to minimize recycling of $C^{14}O_2$ from secondary products. The parameters calculated were (1) DPM of C^{14} in expired air per gram weight as a function of time and (2) cumulative per cent of injected radioactivity recovered as expired $C^{14}O_2$. For each group of animals mean values ± S.D. of DPM/gram at selected time intervals were plotted as differential curves on rectangular coordinates. The area under the differential curve at successive time intervals was measured with a planimeter, converted into per cent of dose recovered, and integrated over the experimental period to give the cumulative or integral curve. Significant differences were determined by student's "t" test and indicated by "p" values.

The kinetic data of the miscible body bicarbonate pool were calculated from the specific activity values after administration of bicarbonate-C^{14}. Pool size, biological half-time and turnover rates were calculated on a Univac digital computer using conventional methods.[16] These calculations are necessary since changes in bicarbonate pool size lead to either greater or lesser dilution of $C^{14}O_2$ specific activity, and thus diminish or increase the peak values of

the differential curves. Similarly, an increase in the turnover rate leads to a shift of the curve to the left with earlier and higher peak values, while a decrease leads to delayed and lower peak values. In general the respiratory $C^{14}O_2$ pattern following administration of a C^{14}-labeled intermediate, depends on the rate at which the intermediate is catabolized to $C^{14}O_2$, and the size of the bicarbonate pool and its turnover rate.

RESULTS

The results of the pool size, half-time and turnover rates of the miscible body bicarbonate pool for the various experimental groups are shown in Table 1. There is no significant difference in pool size or half-time between virgins, exbreeders, and multiple tumor mice. In animals with single tumors, the pool size is 2.2 times larger than in virgins ($P < 0.01$). Biological half-time, also, is more than twice as long in animals with single tumors ($P < 0.005$). The turnover rate (mM/hour) is moderately lower only for the multiple tumor group.

Table 1

KINETICS OF MISCIBLE BODY BICARBONATE POOL

Experimental group (N)	Pool size (mM)	Half time (Minutes)	Turnover rate (mM/hour)
Virgins (10)	0.82 ± 0.21 (S.D.)	6.27 ± 1.06	5.56 ± 1.60
Exbreeders (9)	0.76 ± 0.03	7.22 ± 0.45	4.4 ± 0.34
Single Tumor-bearers (13)	1.81 ± 1.05 ($P < 0.01$)	13.2 ± 5.83 ($P < 0.005$)	5.5 ± 1.33
Multiple Tumor-bearers (6)	0.73 ± 0.34	7.3 ± 1.92	3.8 ± 1.38 ($P < 0.025$)

P value for difference in mean values between various groups and virgins. Only P values less than 0.05 are shown.

The results of the differential expiratory $C^{14}O_2$ curves following the administration of sodium bicarbonate-C^{14}, sodium acetate-1-C^{14}, glucose-1-C^{14}, and glucose-6-C^{14} to the various experimental groups are shown in Figure 2. Data on the per cent of the injected dose recovered over the experimental period are shown in Table 2.

The bicarbonate-C^{14} curves in Figure 2 show a decrease in peak values for exbreeders and tumor animals in comparison to virgin controls. The cumulative data in Table 2 also show a reduction in the per cent of the injected dose recovered for the exbreeder and single tumor group, but not for the multiple tumor group.

In the acetate-1-C^{14} differential curves there is a significant decrease ($P < 0.05$) in the peak value of the tumor animals in comparison to the virgin controls. Although the decrease in the peak value of the exbreeder group is not statistically significant from that of the virgins, the sequence of peak values follows the same trends noted for bicarbonate curves. From the

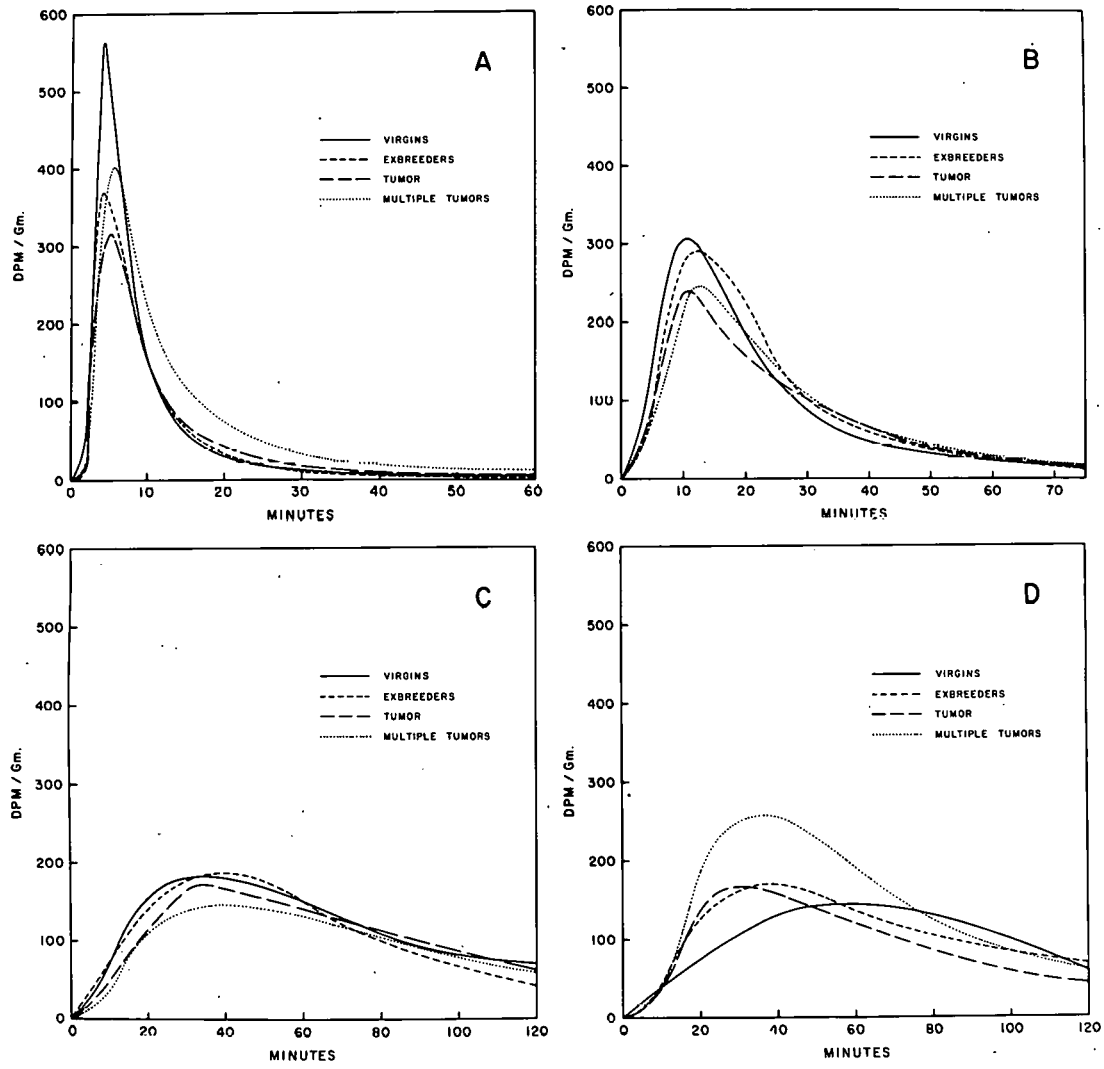

Figure 2. Effects of carcinogenesis on rates of excretion of expiratory $C^{14}O_2$ following administration of bicarbonate-C^{14} (A), acetate-1-C^{14} (B), glucose-1-C^{14} (C), and glucose-6-C^{14} (D).

cumulative acetate-1-C^{14} data we find that there is no significant difference between the cumulative per cent recovered in virgins and exbreeders. The per cent of the injected dose recovered in tumor animals, however, is significantly lower than in virgins and exbreeders.

The glucose-1-C^{14} curves exhibit the general trend noticed in the rising portion of the bicarbonate-C^{14} and acetate-1-C^{14} curves, i.e., the curve for the virgins is higher than that for the exbreeders and both are higher than the tumor bearers. In addition it can be seen that the peak values for both tumor bearers and exbreeders are shifted to the right. The cumulative data indicate that the tumor groups show a slight reduction when compared to virgin controls.

Differential curves for glucose-6-C^{14} show that the peak values for exbreeders and single tumor animals are slightly higher than for virgins, while the multiple tumor values are approximately 50 per cent higher. Of greater importance is the marked shift to the left for both tumor-groups and exbreeker peaks, the single-tumor group being shifted the most ($P < 0.01$). It is sig-

Table 2

PER CENT OF INJECTED C^{14}-LABELED INTERMEDIATE OXIDIZED TO EXPIRED $C^{14}O_2$

Experimental group	Bicarbonate (0-12 min) (N)	Acetate-1-C^{14} (0-20 min) (N)	Glucose-1-C^{14} (0-60 min) (N)	Glucose-6-C^{14} (0-60 min) (N)
Virgins	35.2 ± 8.4 (10)	19.8 ± 1.2 (7)	13.3 ± 0.9 (5)	9.8 ± 0.89 (6)
Exbreeders	27.3 ± 8.4 ($P < 0.05$) (9)	18.9 ± 7.3 (8)	13.3 ± 0.76 (7)	13.3 ± 4.6 ($P < 0.05$) (9)
Single Tumor-bearers	28.8 ± 8.2 ($P < 0.05$) (13)	15.8 ± 1.5 ($P < 0.005$) (11)	11.5 ± 2.0 ($P < 0.05$) (10)	13.7 ± 3.6 ($P < 0.005$) (4)
Multiple Tumor-bearers	34.1 ± 1.8 (6)	15.6 ± 6.1 (8)	10.5 ± 7.36 (4)	18.0 ± 4.3 ($P < 0.005$) (4)

P values are for differences in mean values between various groups and virgins. Only P values less than 0.05 are shown.

nificant that the shift of the peak to the left for the tumor groups occurs despite the increase in bicarbonate pool size which would tend to shift the peak in the opposite direction.

The ratios of the per cent $C^{14}O_2$ recovered after glucose-1-C^{14} and glucose-6-C^{14} for the various experimental groups are presented in Table 3. These ratios are an index of the relative amount of carbohydrate metabolized via the direct oxidative pathway and that metabolized via the glycolytic pathway. A decrease in the ratio of G-1/G-6 indicates an increase in glycolysis and/or a decrease in oxidative pathway. From Table 3 it will be noted that this ratio shows a rank order arrangement between the various experimental groups, the virgins having the highest values, followed in sequence by exbreeders and single tumor-bearing animals, the multiple tumor mice having the lowest value.

Table 3

RATIO OF GLUCOSE-1-C^{14}/GLUCOSE-6-C^{14} RECOVERED AS EXPIRED $C^{14}O_2$

Experimental group	G-1/G-6 ratio
Virgins	1.36
Exbreeders	0.998
Single Tumor-bearers	0.840
Multiple Tumor-bearers	0.582

DISCUSSION

Significant biochemical changes were noted between non-tumor "precancerous" and spontaneous tumor-bearing animals. In vivo biochemical effects were demonstrated in intact, non-anesthetized female C3H/AN mice by comparing continuous expiratory $C^{14}O_2$ patterns following

intraperitoneal administration of C^{14}-labeled intermediates.

The most striking metabolic change observed was an increase in glycolysis in exbreeder, tumor, and multiple tumor animals as evidenced by an earlier peak-time in the expiratory $C^{14}O_2$ differential curves after the administration of glucose-6-C^{14}. The cumulative data indicated approximately a one-third increase in the per cent of $C^{14}O_2$ recovered from glucose-6-C^{14} for exbreeder and single-tumor animals, and almost a twofold increase in the multiple-tumor group, in comparison to virgin controls. Oxidative metabolism of glucose-1-C^{14} via the hexose monophosphate pathway was decreased for both the single and multiple tumor groups in terms of the per cent of $C^{14}O_2$ recovered. A slight delay in the peak-time of the glucose-1-C^{14} differential curves for exbreeder and tumor animals was also observed. The decrease in oxidative metabolism with an appreciable increase in fermentative mechanisms for intact tumor bearing animals is in agreement with the in vitro results first reported by Warburg[1-3] for tumor tissues.

Relative changes in glucose metabolism were demonstrated by comparing ratios of glucose-1-C^{14}/glucose-6-C^{14} oxidized to $C^{14}O_2$. Rank order arrangement of ratio values with the non-tumor virgins having the highest value and the multiple-tumor group having the lowest value indicate that not only does biochemical change occur in single and multiple tumor groups, but that biochemical effects of spontaneous carcinogenesis can be demonstrated even before the onset and development of grossly observable tumors as shown in "precancerous" exbreeder animals. Furthermore, the ratio values as well as expiratory $C^{14}O_2$ patterns suggest that total body metabolism has been altered in the "cancer state" since the metabolic changes noted are greater than those which can be accounted for by the relatively small size of the tumor mass per se. This is in accordance with Greenstein's postulation[4] that "the biochemical characters of tissues of tumor-bearing animals gradually change towards those of tumor tissue." In addition to supporting this hypothesis, our data also extend it, since the biochemical characters of "precancerous" animals gradually change toward those of tumor-bearing animals.

The possibility that the biochemical changes demonstrated in our study are the result of "aging" can be ruled out for the following reasons: (1) the age of all exbreeder, single-tumor, and multiple-tumor animals was approximately 12 months, yet the G-1/G-6 ratios were in decreasing order of magnitude and not identical; (2) when a comparison is made between virgin control animals having the mammary tumor milk factor and those without it, but of the same age, the latter group has a higher ratio value of 1.48 which places it at the head of the rank order;[18,19] (3) ratio values obtained for the same tumor bearing animals before and after ovariectomy demonstrate that the ovariectomized values are similar to virgin control values.[18,19] In each case biochemical changes were detected in experimental groups of approximately the same age. "Aging" can therefore be ruled out as a variable responsible for our experimental results.

CONCLUSIONS

Some of the most significant findings noted in our study are: (1) demonstration of in vivo biochemical differences between spontaneous tumor and non-tumor C3H/AN mice, (2) evidence that biochemical characters similar to those present in tumor-bearing animals occur even before the onset of tumor formation as shown in "precancerous" mice, (3) confirmation of in vitro results of others by the demonstration of an increase in glycolysis with a decrease in di-

rect oxidative metabolism in intact spontaneous tumor-bearing animals, (4) demonstration of biochemical differences noted in tumor-bearing animals as being the result of changes in total body metabolism rather than due to metabolic changes in the tumor mass itself, and (5) evidence that there is a direct relationship between the state of carcinogenesis and metabolic alterations.

ACKNOWLEDGMENTS

The authors wish to express their sincere thanks and appreciation to Dr. G. V. LeRoy for his constructive criticism and suggestions during the course of this study.

LITERATURE CITED

1. Warburg, O. Biochem. Zeitschr., 142:317, 1923.
2. Warburg, O. Science, 123:309, 1956.
3. Warburg, O. Science, 124:269, 1956.
4. Greenstein, J. P. In Biochemistry of Cancer, 2nd Ed., New York: Academic Press, Inc., 1954, pp. 327 et seq. and 507 et seq.
5. Nakahara, W., and F. Fukuoka. Japan Med. J., 1:271, 1948.
6. Nakahara, W. Adv. Cancer Res., 5:157, 1958.
7. Furth, J. Cancer Res., 19:241, 1959.
8. LeRoy, G. V. Radiocarbon and Medical Research. Argonne Cancer Research Hospital Semiannual Report, 10:86, 1958.
9. LeRoy, G. V., G. T. Okita, E. C. Tocus, and D. Charleston. Int. J. App'd Rad'n and Iso., 7:273, 1960.
10. Kabara, J. J., G. T. Okita, and G. V. LeRoy. Federation Proc., 16:310, 1957.
11. Kabara, J. J. The Biogenesis and Metabolism of Cholesterol in Normal and Tumor Mice. Ph.D. Thesis, University of Chicago, 1959.
12. Harmon, D. H., M. R. Kirk, and B. M. Tolbert. Am. J. Physiol., 196:265, 1959.
13. Heston, W. E. Mammary Tumors in Mice. Publication of American Association for Advancement of Science No. 22, 1945, p. 63.
14. Gardener, W. U., L. C. Strong, and C. M. Smith. Am. J. Cancer, 37:510, 1939.
15. Huseby, R. A., and J. J. Bittner. Cancer Res., 6:240, 1946.
16. Muhlbock, O., W. Tengbergen, and T. G. Van Rijssel. J. N. Cancer Instit., 13:505, 1952.
17. Aronoff, S. Techniques of Radiobiochemistry, Ames, Iowa, The Iowa State College Press, 1956, p. 75.
18. Ezz, E. A., and G. Okita. Pharmacologist, 2:75, 1960.
19. Ezz, E. A., and G. Okita. Proceedings of the First International Pharmacological Meeting, Stockholm, Sweden, August, 1961.

URIDINE NUCLEOTIDE INCORPORATION INTO PIGEON LIVER MICROSOME RIBONUCLEIC ACID*

By

D. B. Straus† and E. Goldwasser

The role of nucleotides as precursors of ribonucleic acid in animal tissues has been well documented.[1-4] Aside from the formation of polymers by the enzyme polynucleotide phosphorylase,[5] only one preliminary report of net synthesis of polyribonucleotides in cell-free systems has been made.[6] Hilmoe and Heppel[7] have demonstrated the phosphorolysis of added polyadenylic acid by a partially purified enzyme system from guinea pig liver nuclei but were unable to obtain incorporation of adenosine diphosphate into RNA. The incorporation of mononucleotides into the RNA of nuclear,[7-11] microsomal,[3,11] and supernatant[11-13] fractions of cell-free systems has been described. All of these systems apparently utilize nucleoside triphosphates as the direct precursors of RNA.

Some of these systems incorporate nucleotides nonterminally[3,8,9,12] whereas the others[10,11,13] involve terminal addition of nucleoside triphosphates to RNA. The nonterminal incorporation of adenosine monophosphate, under conditions of oxidative phosphorylation, into cytoplasmic RNA of pigeon liver has previously been reported by one of us.[1]

Herbert et al.[3] have shown that orotic acid is first converted to uridine monophosphate and the latter is then incorporated into rat liver microsomal RNA presumably after conversion to uridine diphosphate or UTP. It seemed pertinent to determine the phosphorylation level of the nucleotide which was the direct precursor of microsomal RNA since most cytoplasmic RNA is in this fraction and because this RNA may serve as templates for the biosynthesis of proteins. In this study the conditions required for nucleotide incorporation into pigeon liver microsomal RNA have been determined and a comparison made between UMP, UDP, and UTP as RNA precursors. The quantities of terminal and nonterminal incorporation have been determined, as well as some of the other properties of the system.

EXPERIMENTAL PROCEDURE

Materials. Orotic acid-6-C^{14} was purchased from the Volk Radiochemical Company. $H_3P^{32}O_4$ was obtained from Oak Ridge National Laboratory. Crystalline bovine plasma albumin, crystalline trypsin, and recrystallized RNase were obtained from Armour and Company. Recrystallized lysozyme was purchased from Pentex Biochemicals, and pyruvate kinase from C. F. Boehringer and Sons. All other reagents were the best commercially available grade.

Protein determination. The method of Lowry et al.[14] was used for protein determination. Crystalline bovine plasma albumin was used as the standard.

*This paper appears in J. Biol. Chem., 236:849, 1961. It is taken, in part, from the thesis submitted by David B. Straus in partial fulfillment of the requirements for the degree of Doctor of Philosophy, University of Chicago.

†Present address, Department of Chemistry, Princeton University, Princeton, New Jersey.

RNA determination. RNA was determined by the orcinol method of Dische and Schwartz[15] modified in that samples were kept at 100° for 15 minutes. The standard used was RNA isolated from pressed bakers' yeast by the method of Cresthield et al.[16]

Aliquots of microsome suspensions were precipitated in the cold and washed 5 times with 0.5 M $HClO_4$. Lipids were removed by extraction with ethanol, ether, and chloroform 2:2:1 (volume for volume), and the residue dried before addition of 0.3 M KOH. Hydrolysis was carried out at 37° for 18 hours, after which the acid-insoluble portion and K^+ ions were removed by precipitation with cold $HClO_4$, and the acid-soluble fraction analyzed for RNA as mixed 2'(3')-nucleotides.

Synthesis of UMP^{32} and UMP-6-C^{14}. UMP^{32} was synthesized by a new method, the reaction of $H_3P^{32}O_4$ with 2',3'-O-isopropylidene uridine and N,N'-dicyclohexylcarbodiimide in a homogeneous p-dioxane system. The specific radioactivity of the UMP^{32} was 5.0×10^7 cpm per μmole. Details of this synthesis will be described elsewhere.

Orotic acid-6-C^{14} (1.5 mc per mmole) was enzymically converted to UMP-6-C^{14} by use of mixed orotidine-5'-P pyrophosphorylase and carboxylase in the 25 to 57 per cent ethanol fraction of an autolysate of dried brewers' yeast according to the method of Lieberman et al.[17] The UMP-6-C^{14} was isolated by ion exchange chromatography on a Dowex 1-Cl^- column.

Synthesis of labeled UDP and UTP. ATP was used as the donor for the enzymic phosphorylation of UMP^{32} by the nucleotide kinase mixture isolated from brewers' yeast autolysates according to the method of Lieberman et al.[18] The reaction mixture, containing both adenosine and uridine nucleotides was fractionated on Dowex 1-Cl^- with the use of 0.003 M HCl and increasing concentrations of NaCl as eluants. UDP^{32} and UTP^{32} were collected in tubes containing about 150 μmoles of NH_4OH (final pH 5).* The uridine nucleotides were converted to the potassium salt and concentrated on small columns of Dowex 1-Cl^- at 4°.[19] These columns were eluted with 0.01 M HCl-0.35 M KCl; the eluant volume used gave a 2500:1 ratio of chloride to nucleotide. Eluates were neutralized with KOH, concentrated, and analyzed spectrophotometrically.

For the C^{14}-labeled UMP, another phosphorylation method was necessary. UMP-6-C^{14} was converted to the pyridinium salt and this salt phosphorylated with tri-n-butylammonium phosphate and N,N'-dicyclohexylcarbodiimide according to the method of Smith and Khorana.[20] The product mixture was fractionated on Dowex 1-Cl^-. UTP-6-C^{14} was concentrated as described for the P^{32}-labeled uridine nucleotides.

All labeled nucleotides were characterized spectrophotometrically and by cochromatography with authentic standards with the use of 2:1 isopropanol-1 per cent $(NH_4)_2SO_4$ as solvent and Whatman No. 1 paper previously soaked in 1 per cent $(NH_4)_2SO_4$ and dried.[21] Radioautographs of the chromatograms were made and in all cases radioactivity was found to be associated exclusively with the ultraviolet quenching spot of the appropriate standard; no other radioactive areas were found on the chromatograms.

The chemical phosphorylation of nucleoside monophosphates has not been successful, in our hands, with quantities of starting material less than about 20 μmoles. The enzymic phosphorylation, in contrast, requires the separation of ATP, used in excess, from the desired nucleotides; this is difficult when more than about 20 μmoles of monophosphate starting material

*In this study, nucleotide P^{32} was always in the ester position.

are used. Despite the more complex separation problem, the enzymic phosphorylation is much faster than the chemical synthesis. Both methods give comparable yields of UTP (50 to 70 per cent) and UDP (20 to 30 per cent) based on UMP.

Isolation and washing of pigeon liver microsomes. Pigeons were decapitated, the livers rapidly removed, weighed, placed on ice, and minced. Minces were mixed with 4 volumes of homogenization medium,* in a hydraulic homogenizer[22] and the suspension rapidly forced through a 42 μ annular orifice. Initial homogenates were rapidly rehomogenized to obtain maximal cell breakage.

Nuclei, unbroken cells, erythrocytes, and connective tissue were sedimented by centrifugation at 600 x g† for 10 minutes. The cytoplasmic fraction was then centrifuged for 15 minutes at 15,000 x g to sediment mitochondria. Microsomes, contaminated with glycogen, were sedimented by centrifugation of the 15,000 x g supernatant for 60 minutes at 90,000 x g.

The supernatant fraction was carefully decanted and tubes wiped dry while still inverted. The microsomes were washed by suspending the residue in fresh homogenization medium followed by recentrifugation for 25 minutes at 90,000 x g. Other subcellular fractions were similarly washed. All operations were carried out at 0-4° after weighing the liver.

Homogenates and nuclear and cytoplasmic fractions were stained and examined microscopically. No evidence could be found for disruption of nuclei, and identifiable nucleoli were absent from the cytoplasmic fraction.

The washed microsomal fraction was homogenized in a Potter-Elvehjem homogenizer with rehomogenization medium to give 0.8 to 1.2 g equivalents per ml. In some cases the rehomogenization medium was the same as that used for initial homogenization whereas in others this medium contained $MgCl_2$, buffer at the same concentration, and pH used for incorporation experiments.

Removal of bound nucleotides from microsomes. Evidence has been obtained showing that microsomes bind nucleotides (see "Results"). To remove these nucleotides, the 15,000 x g supernatant was made 1.6×10^{-3} M in ATP and 8×10^{-4} M in pyrophosphate buffer, pH 7.7, before the initial sedimentation of microsomes. The microsomes were washed 3 times with ATP and PP_i (8×10^{-4} M ATP and 1.6×10^{-3} M PP_i buffer, 8×10^{-5} M ATP and 8×10^{-4} M PP_i buffer, 8×10^{-5} M PP_i buffer). The final pellets were rinsed several times with small volumes of homogenization medium and then rehomogenized as described for microsomes.

The ATP-pyrophosphate washing procedure removes most of the bound nucleotides as well as 20 to 40 per cent of the total RNA, and 10 to 20 per cent of total protein; the RNA-protein ratio is lowered from 0.16 to 0.12. Removal of ribonucleoprotein particles and RNA from rat liver microsomes with more concentrated pyrophosphate buffers has previously been reported by Sachs.[23]

Incorporation experiments. Except where otherwise indicated, incubation mixtures were 0.05 M Tris·HCl buffer at various pH values, and 0.25 M sucrose; they contained 0.1 μmole labeled uridine nucleotide and, usually, 0.1 μmole each of the corresponding cytidine, adenosine, and guanosine nucleotides. An ATP-generating system consisting of 1.0 μmole P-enolpyruvate

*The homogenization medium was 0.004 M $MgCl_2$, 0.035 M KCl, 0.25 M sucrose, 0.04 M Tris·HCl, pH 7.6.

†All gravitational fields refer to the average radius at which the field was applied.

and 5 μg pyruvate kinase was used in most cases. Details of each incubation mixture are given in the tables describing the experiments. Mixtures were made up complete except for microsomes, or other subcellular fraction, and labeled uridine nucleotide. After a brief preincubation at 37°, microsomes were added, followed within 10 seconds by labeled uridine nucleotide at zero time. At the end of the incubation period, samples were placed in an ice bath and made 0.5 M with perchloric acid. Zero time control samples were made up and processed similarly except that $HClO_4$ was added before the microsomes and they were kept at 0°. The acid-insoluble residues were washed with $HClO_4$ and lipids were removed as described above.

Extraction of RNA from protein nucleates by pyrophosphate. The extraction of RNA from microsome protein nucleates by the method of Davidson and Smellie[24] gave low and varying recoveries of RNA and could not be used. It was found, however, that extraction of protein nucleates with 0.1 M $Na_3HP_2O_7$, pH 7.7, gave nearly quantitative separation of RNA and protein.

Protein nucleates were suspended in 0.1 M pyrophosphate buffer, pH 7.7, and incubated 60 minutes at 37° followed by 5 minutes at 100°. Samples were cooled and centrifuged to remove protein. The average recovery of RNA in the supernatants was 97 per cent in a large number of experiments. Protein contamination was estimated to range from 10 to 20 μg per mg of RNA although some nonprotein contaminant might have contributed significantly to the very slight absorbency in the Lowry method.[14]

RNA and PP_i were separated by precipitating the RNA with 3.5 volumes of 8:1 (volume for volume) absolute ethanol-70 per cent $HClO_4$ at -18°, allowing 1 to 2 hours before centrifugation. After two washings with ethanol-perchloric acid and two with acetone, recoveries of RNA were about 70 to 80 per cent.

Separation of bound nucleotides from RNA. Zero time control acid-insoluble fractions were frequently found to be more radioactive than corresponding incubated samples. It seemed clear that all radioactivity in the zero time samples resulted from the binding of labeled 5'-uridine nucleotides to the precipitated microsomes. Many different procedures were tried in attempts to eliminate these bound nucleotides.

Repeated washing of acid-insoluble protein nucleates with $HClO_4$ (0.25 to 1.0 M) does not remove bound radioactivity. Extraction of RNA from protein nucleates with 10 per cent NaCl,[24] or pyrophosphate buffer, pH 7.7, solubilizes the bound nucleotides as well as the RNA. However, the nucleotides could not be completely separated from RNA in such extracts by: (a) dialysis against water, (b) dialysis against 1 per cent water suspensions of Dowex 1-Cl^-, (c) electrodialysis, (d) precipitation and washing of extracted RNA with ethanol or ethanol-$HClO_4$, (e) differential adsorption of nucleotides onto Norit A,[11] and (f) differential elution of RNA from Norit A with phenol.[25] All of these procedures lower the ratio of zero time radioactivity to incubated sample radioactivity but none eliminate zero time bound nucleotides or even reduce the zero time radioactivity to the level of the incubated samples except at the expense of large losses of RNA (70 to 90 per cent). The failure of dialysis and ethanol precipitation procedures indicated that the 5'-nucleotides in NaCl and pyrophosphate extracts of microsome protein nucleates were present bound to some larger molecule. In model experiments, virtually all labeled nucleotide could be separated from yeast RNA by these procedures but considerable radioactivity remained bound to such proteins as bovine plasma albumin. Probably the nucleotides are bound to traces of protein which are solubilized in the extraction procedures. A suitable, isolable, RNA derivative or a more effective RNA purification procedure was needed. Methods of achieving both

aims were developed which eliminate zero time radioactivity.

Phosphorus from nucleotides incorporated into RNA appears in 2'(3')-nucleotides after alkaline hydrolysis of RNA; separation of these RNA derivatives from any 5'-nucleotides in the alkaline hydrolysate affords an unambiguous determination of nucleotide incorporation into RNA. A paper chromatographic solvent system, 6:3:1 absolute ethanol-2 per cent (weight for volume) $H_3BO_3NH_4OH$ (density 0.9), was developed which separates 2'(3')-nucleotides from 5'-nucleotides. Pertinent R_F values are (Whatman No. 3MM, descending): 0.55, 0.52, 0.54, 0.45 for 2'(3')-UMP, 2'(3')-AMP, 2'(3')-CMP, and 2'(3')-GMP; 0.34, 0.29, 0.34 and 0.23 for the corresponding 5'-nucleotides; 0.24 for UDP; and 0.21 for UTP.

The total RNA, derived from protein nucleates by pyrophosphate extraction and acid-alcohol precipitation, was hydrolyzed with 0.100 ml of 0.3 M KOH (18 hours, 37°), neutralized with Dowex 50W-H^+, and chromatographed with the borate solvent. The 2'(3')-nucleotide area, readily visible under ultraviolet light, was cut out and eluted overnight in 0.01 M HCl. Aliquots of the eluates were analyzed for radioactivity and RNA (as mixed 2'(3')-nucleotides). Alternatively, protein nucleates were hydrolyzed directly, the hydrolysates acidified with $HClO_4$, centrifuged, and then neutralized with KOH or tri-n-heptylamine in chloroform before chromatography. Perchlorate ion retards migration of nucleotides in the borate solvent and its removal as $KClO_4$ or tri-n-heptylammonium perchlorate is necessary.

The chromatographic separation of 2'(3')- and 5'-nucleotides with the borate solvent has been carried out both on alkaline hydrolysates of RNA (Procedure 1-A) and protein nucleates (Procedure 1-B).

The second method (Procedure 2) for eliminating zero time radioactivity was based on the observation of Metzenberg[26] that RNA formed an insoluble salt with the cationic detergent cetyltrimethylammonium bromide. Protein nucleates were extracted with pyrophosphate and the RNA-free acid precipitated with ethanol-$HClO_4$ as described. The RNA residue was mixed with 2.0 ml of 0.01 M cetyltrimethylammonium chloride and the flocculent precipitate which formed was collected by centrifugation. The residue was washed twice with 0.01 M detergent, twice with water, and once with acetone. At this stage the zero time cetyltrimethylammonium RNA was still slightly radioactive, but bound nucleotide was almost completely removed by dissolving the residue in ethanol followed by reprecipitation of the RNA-free acid with ethanol-$HClO_4$. After removing $HClO_4$ with acetone the residue was dissolved in 0.05 M NH_4OH and aliquots taken for determination of RNA and radioactivity.

When freshly prepared, cetyltrimethylammonium chloride solutions may gel in the cold, therefore the procedure must be carried out at room temperature. However, this tendency to gel disappears on aging, and the work may be carried out at 4°. The recovery of RNA with the use of the complete procedure was 70 to 80 per cent and was not affected by the use of aged detergent solutions. Perchlorate ion also forms a water-insoluble, ethanol-soluble, cetyltrimethylammonium salt and must be completely removed before addition of detergent.

Radioactivity determinations. Aliquots of samples containing P^{32} were dried in aluminum cups, and counted using a proportional type gas flow counting tube (10 per cent methane, 90 per cent argon) with an aluminized Mylar window.

C^{14} samples were counted as infinitely thin layers (< 0.1 mg per cm^2) in aluminum cups with an internal gas flow Geiger counter. The counting error for both C^{14} and P^{32} determinations was 3 per cent or less.

RESULTS

Binding of nucleotides to subcellular fractions from pigeon liver. The zero time binding of UTP to the various subcellular fractions from pigeon liver and of all three uridine nucleotides to microsomes was measured and the results are presented in Tables 1 and 2.

Table 1

UTP BINDING AT ZERO TIME*

Subcellular fraction	Binding of UTP^{32}	
	Specific	Total bound
	mμmoles/mg RNA	mμmoles
Mitochondria (Mt)	1.6	0.8
Microsomes (Mc)	8.9	5.9
Supernatant (S)	52.3	30.3
Mt + Mc	6.1	7.1
Mt + S	26.4	27.5
Mc + S	34.8	43.2
Mt + Mc + S	10.9	34.6
Nuclei (N)	5.8	3.6
Cytoplasm (C)	19.5	55.5
N + C	15.4	53.4

*Samples for cytoplasmic fractions contained: 250 μmoles of Tris·HCl (pH 7.5), 0.1 μmole each of CTP, ATP, GTP, and UTP^{32} (2.5 x 10^6 cpm per μmole), 20 μmoles of $MgCl_2$, 175 μmoles of KCl, 1100 μmoles of NaCl, and 1250 μmoles of sucrose in a total volume of 5.0 ml. Mitochondria derived from 1 g of liver, microsomes from 0.9 g, and dialyzed supernatant fraction from 0.4 g of liver were used where indicated. PP_i extracts of zero time protein nucleates analyzed for RNA and radioactivity.

Samples for nuclei and whole cytoplasm contained: 300 μmoles of Tris·HCl (pH 7.5), 0.1 μmole each of CTP, ATP, GTP, and UTP^{32} (1.3 x 10^6 cpm per μmole), 25 μmoles of $MgCl_2$, 210 μmoles of KCl, 1100 μmoles of NaCl, and 1550 μmoles of sucrose in a total volume of 6.2 ml one gram equivalent of nuclei and 1.0 g equivalent of cytoplasm used where indicated. KOH hydrolysates of zero time protein nucleates analyzed for RNA and radioactivity.

It is clear that all subcellular fractions bind UTP^{32} firmly under these experimental conditions. Nuclei and mitochondria bind much less UTP^{32} than microsomes or supernatant and the two former fractions appear to lower the binding of the two latter when mixed with them. The mixture of microsomes and supernatant shows a greater total binding than the sum of the binding of individual fractions suggesting that there is some interaction between them.

The microsome fraction binds UTP most extensively, followed in order by UDP and UMP. The labeled substances bound were positively identified as UTP, UDP, and UMP by chromatography in the borate solvent and radioautography. Other experiments showed that zero time binding is constant between pH 7.0 and 9.0 but is much reduced at pH 6.1 and 5.5, indicating that the extent of binding is dependent on the valence of the nucleotide.

The increased binding of UTP which occurs when other nucleoside triphosphates are omitted from the zero time samples suggests that a given nucleotide is not bound to a site specific for

Table 2

ZERO TIME BINDING OF UMP, UDP, AND UTP TO MICROSOMES*

Experiment	Nucleotides[a]	Specific binding of uridine nucleotide
		mμmoles/mg RNA
A	UMP^{32} + 3 NMP	0.9
	UDP^{32} + 3 NDP	11.5
	UTP^{32} + 3 NTP	17.0
B	UTP^{32} + 3 NTP	8.5
	UTP^{32} alone	16.5
C	UTP^{32} + 3 NTP	2.1
	UTP^{32} alone	7.8

*In addition to the standard components, samples contained:

A. Eight and six-tenths micromoles of $MgCl_2$, 10 μmoles of $MnCl_2$, 325 μmoles of KCl, and 0.9 g equivalent of microsomes. UMP^{32} and UDP^{32} (0.08 μmole) and UTP^{32} (0.1 μmole) were used; specific activity of all uridine nucleotides was 8.5×10^6 cpm per μmole. Final volume was 2.14 ml, pH 7.6. PP_i extracts of zero time protein nucleates analyzed for RNA and radioactivity.

B. Nucleotides as indicated, 0.1 μmole of UTP^{32} (1.8×10^7 cpm per μmole), 9.4 μmoles of $MgCl_2$, 10.0 μmoles of $MnCl_2$, the ATP-generating system, 10.0 μmoles of spermidine·HCl, 330 μmoles of KCl, and 1.0 g equivalent of microsomes in a total volume of 2.34 ml, pH 7.6. KOH hydrolysates of zero times protein nucleates analyzed for RNA and radioactivity.

C. Nucleotides as indicated, 0.1 μmole of UTP^{32} (4.2×10^6 cpm per μmole), 20 μmoles of $MgCl_2$, the ATP-generating system, 336 μmoles of KCl, and 0.8 g equivalent of ATP-PP_i washed microsomes (3 washes) in a total volume of 2.47 ml, pH 7.6. PP_i extracts of zero time protein nucleates analyzed for RNA and radioactivity.

[a]NMP, NDP, and NTP refer to nucleoside mono-, di-, and triphosphates, respectively.

that nucleotide. Microsomes show a doubling in binding of UTP when CTP, ATP, and GTP are omitted; ATP-pyrophosphate-washed microsomes show a quadrupling when these nucleotides are omitted. This fact and the nonspecific binding suggest that ATP and pyrophosphate displace nucleotides bound to native microsomes.

In addition to nucleotide binding, Sachs[27] has reported that rat liver microsomes bind pyrophosphate and we have found that the binding of orthophosphate to pigeon liver microsomes is quite extensive. As much as 5 μmoles of added P_i^{32} could be recovered in the acid-washed, defatted, protein nucleate from 1 g equivalent of microsomes in a system containing 50 μmoles of P_i^{32} at pH 7.5. The binding of these polyvalent anion derivatives of phosphoric acid suggests that microsomes may bind other polyanions of biological importance such as amino acid transfer RNA.[28,29]

Comparison of UMP, UDP, and UTP as precursors of microsomal RNA. The incorporation of P^{32}-labeled UMP, UDP, and UTP, with mixtures of the corresponding cytidine, adenosine, and guanosine nucleotides, into microsomal RNA was measured. Results are presented in Table 3. It is clear that nucleoside triphosphates are the best precursors of RNA in this system. UTP^{32} incorporation is markedly increased by the addition of an ATP-generating system and

Table 3

COMPARISON OF NUCLEOSIDE MONO-, DI-, AND TRIPHOSPHATES AS PRECURSORS OF RNA IN PIGEON LIVER MICROSOMES*

Precursors	Uridine nucleotide incorporation	
	Specific	Total
	mμmoles/mg RNA	mμmoles
UMP^{32} + 3 NMP	0.007	<0.005
UDP^{32} + 3 NDP	0.10	0.08
UTP^{32} + 3 NTP	0.36	0.30
UTP^{32} + 3 NTP + generating system	0.56	0.46

*Incubation mixture the same as in Table 2,A. The ATP generating system used as indicated. Incubation for 10 minutes at 37°. One μmole additional P-enolpyruvate added after 5 minutes. Procedure 1-A used to process samples.

this is taken as further evidence that the triphosphates are the direct precursors of RNA in microsomes. Stimulation by the ATP-generating system suggested that enzyme(s) are present in microsomes which degrade the triphosphates and we found that microsomes do convert ATP to ADP; the initial specific activity is about 80 μmoles of P_i produced per mg of protein per hour.

We do not know whether the incorporation of UDP^{32} requires initial conversion to UTP^{32} or whether it also occurs by an independent route.

Time Course of UTP incorporation into microsomal RNA. The incorporation of UTP^{32} increases linearly for 10 minutes and then the specific activity of the microsomal RNA decreases precipitously to less than 15 per cent of the maximal incorporation by 60 minutes (Figure 1). Since the specific activity passes through a maximum, the newly labeled RNA must be degraded and released to the acid-soluble fraction more rapidly than the remainder of microsomal RNA.

Incubation of microsomes in homogenization medium for 2 hours at 37° results in a 12 per cent loss of acid-insoluble RNA which is completely recovered as acid-soluble nucleotides and nucleosides. Pigeon liver microsomes contain a nuclease and microsomal RNA does not appear to be a homogeneous substrate for this enzyme.

The nuclease activity explains the decrease in RNA radioactivity after 10 minutes but, since this enzyme is present at all times and may be active during the first 10 minutes of incubation, the actual incorporation reaction must proceed at a rate less than that of the degradative reaction after the first 10 minutes have elapsed. The synthesizing system must have used up or destroyed some essential component. Nucleoside triphosphates other than CTP, ATP, UTP, or GTP, such as pseudouridine triphosphate[30,31] or other minor constituents of RNA, small quantities of which may be bound to microsomes, could be used up by 10 minutes, or those RNA molecules required for incorporation (see below) may be degraded or used up.

Dependence of UTP incorporation into RNA on the presence of RNA. Preincubation of microsomes with pancreatic RNase strongly inhibits the incorporation of UTP^{32} into RNA (Table 4). No attempt was made to remove RNase before UTP^{32} addition to the incorporation system and it is possible that the inhibitory effect of the enzyme is due to rapid hydrolysis of the newly synthesized RNA and not to removal of RNA molecules required for incorporation. The data pre-

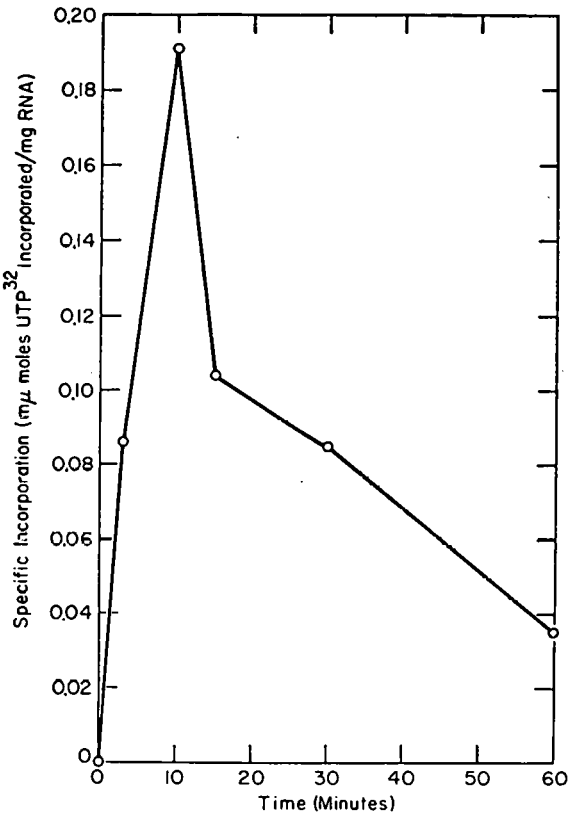

Figure 1. Time course of UTP incorporation into microsomal RNA. In addition to standard components, samples contained CTP, ATP, GTP, and UTP^{32} (2.3×10^6 cpm per μmole), 21 μmoles of $MgCl_2$, the ATP generating system, 310 μmoles of KCl, and 1.2 g equivalents of pigeon liver microsomes in a total volume of 1.74 ml, pH 7.8_5. Incubation for the indicated times at 37°; 1.0 μmole P-enolpyruvate added to remaining samples at the following times: 5 minutes, 15 minutes, and 45 minutes. Samples processed by Procedure 2.

sented in Table 4 show about the same inhibition of incorporation in Experiments A and B but the loss of RNA due to RNase in Experiment A was about 20 per cent, whereas that in Experiment B was only about 4 per cent. These data suggest, but do not definitely establish, that pancreatic RNase inhibits incorporation of UTP^{32} into microsomal RNA by degrading biologically active RNA molecules required for the process of incorporation.

It has been noted[32] that some of the effects of RNase may be due to its relatively high isoelectric point (pI) rather than to its specific enzymic activity. In this system, preincubation with lysozyme, which has an even higher pI, sometimes stimulates incorporation. This stimulation has not been reproducible but lysozyme has never been found to inhibit nucleotide incorporation into RNA.

UTP^{32} incorporation into microsomal RNA is completely inhibited by pyrophosphate but only inhibited 40 per cent by the same concentration of orthophosphate. Since nucleoside triphos-

Table 4

EFFECT OF RNase, LYSOZYME, P_i, PP_i, TRYPSIN, AND HEAT ON UTP INCORPORATION INTO MICROSOMAL RNA*

Experiment	Additions	Labeled UTP incorporation	
		Specific	Total
		mμmoles/mg RNA	mμmoles
A	None	0.56	0.46
	RNase	0.06	-[a]
	Lysozyme	0.96	0.79
	$K^+PO_4^-$ buffer, pH 7.6	0.31	0.28
	$Na_2KHP_2O_7$ buffer, pH 7.6	0.006	<0.005
	Heated microsomes (5 minutes, 100°)	<0.005	<0.005
B	None	0.28	0.18
	Trypsin	0.03	0.02
	RNase	0.04	0.02
C	None	0.13	0.28
	0.20 ml water at 10 minutes	0.09	0.18
	20 μmoles $Na_2KHP_2O_7$ buffer, pH 8.0 (0.20 ml) at 10 minutes	0.05	0.11

*In addition to the standard components, samples contained:

A. Same as in Table 2,A, except that ATP-generating system added. RNase (100 μg) and lysozyme (100 μg) preincubated 20 minutes with the complete system, without UTP^{32}, which was added at zero time. Microsome rehomogenate preincubated simultaneously at 37°. Twenty micromoles each of P_i and PP_i buffers, pH 7.6, used as indicated. Incubation 10 minutes at 37°. P-enolpyruvate (1.0 μmole) added at 5 minutes. Samples processed by Procedure 1-A.

B. Same as in Table 2,B, except that ATP generating system added; CTP, ATP, and GTP used. RNase (100 μg) and trypsin (100 μg) preincubated 15 minutes with the complete system, without UTP^{32}, which was added at zero time. Incubation 10 minutes at 37°. P-enolpyruvate (1.0 μmole) added at 5 minutes. Samples processed by Procedure 1-B.

C. UTP-6-C^{14} (1.6×10^6 cpm per μmole), 20 μmoles of $MgCl_2$, the ATP-generating system, 315 μmoles of KCl, and 1.1 g equivalent of microsomes in a total volume of 1.84 ml, pH 8.0. Control incubated 10 minutes and experimental samples 20 minutes at 37°. Additions as indicated. P-enolpyruvate (1.0 μmole) added to remaining samples at 5, 10, and 15 minutes. Samples processed by Procedure 2.

[a]Calculation of total incorporation not justifiable because of the loss of RNA to the acid soluble fraction.

phates are the direct precursors of RNA in microsomes, a pyrophosphorolysis of biologically active RNA would be expected. Pyrophosphate, added at the point of maximal incorporation, causes a reduction of incorporated UTP-6-C^{14} over and above the reduction due to the endogenous RNase. This reduction is probably due to pyrophosphorolysis. Pyrophosphate might also inhibit incorporation by chelation of Mg^{+2} required for incorporation (see below) and also for the structural integrity of the microsomes, or by displacement of nucleotides and RNA from the microsomes. Orthophosphate might act by analogous mechanisms, although its chelating and displacement activities would be lower than pyrophosphate.

Dependence of UTP incorporation into RNA on protein. Preincubation of microsomes with trypsin greatly inhibits incorporation of UTP^{32}. There is no incorporation when boiled microsomes are used (Table 4). These facts show that the incorporation is most likely an enzymic process. Purification of the enzyme responsible for RNA formation in microsomes is now being attempted.

Dependence of UTP incorporation into RNA on nucleotides. Early attempts to show that UTP^{32} incorporation into RNA was dependent on the presence of all four nucleoside triphosphates were unsuccessful (e.g. Table 5, 0). The finding of zero time nucleotide binding suggested that the microsomes might contain sufficient bound nucleoside triphosphates to synthesize

Table 5

UTP^{32} INCORPORATION INTO MICROSOME RNA DEPENDENCE ON NUCLEOTIDES*

Washes with ATP-PP_i	Nucleotides	Labeled UTP incorporation		Stimulation
		Specific	Total	
		mμmoles/mg RNA	mμmoles	%
0	UTP^{32} + 3 NTP	0.28	0.18	-18
	UTP^{32} alone	0.35	0.22	
3	UTP^{32} + 3 NTP	0.08	0.04_0	+14
	UTP^{32} alone	0.07	0.03_5	
4	UTP-6-C^{14} + 3 NTP	0.06	0.03_9	+50
	UTP-6-C^{14} alone	0.04	0.02_6	

*In addition to the standard components, samples contained:
0. Same as Table 2,B. Processing by Procedure 1-B.
3. Same as Table 2,C. Processing by Procedure 1-A.
4. Nucleotides as indicated, 0.1 μmole of UTP-6-C^{14} (1.7×10^6 cpm per μmole) the ATP-generating system, 22 μmoles of $MgCl_2$, 305 μmoles of KCl, and 1.0 g equivalent of ATP-PP_i-washed microsomes in a total volume of 1.84 ml, pH 8.0. Samples incubated 10 minutes at 37°; 1.0 μmole of P-enolpyruvate added at 5 minutes. Samples processed by Procedure 2.

RNA without requiring the addition of other nucleotides. The ATP-pyrophosphate washing procedure was designed to eliminate such bound nucleotides and experiments with these microsomes show that the incorporation of UTP is nucleotide dependent, although the stimulation of incorporation by added CTP, ATP, and GTP is not great. ATP-pyrophosphate-washed microsomes have a lower incorporation of UTP^{32} than microsomes isolated from the same homogenate but not so washed; this may be due to removal of required RNA (see above).

The demonstration of nucleotide dependence with ATP-pyrophosphate-washed microsomes, in contrast to the inability to demonstrate this with microsomes not washed in this way, confirms the previous conclusion, based on zero time binding, that native microsomes do bind nucleotides and that ATP and pyrophosphate can displace bound nucleotides.

pH optimum. The incorporation of UTP^{32} into microsomal RNA as a function of pH is presented in Figure 2. The optimal pH is about 8.0. One-half of the maximal activity is found at pH 7.5 and about 9.2.

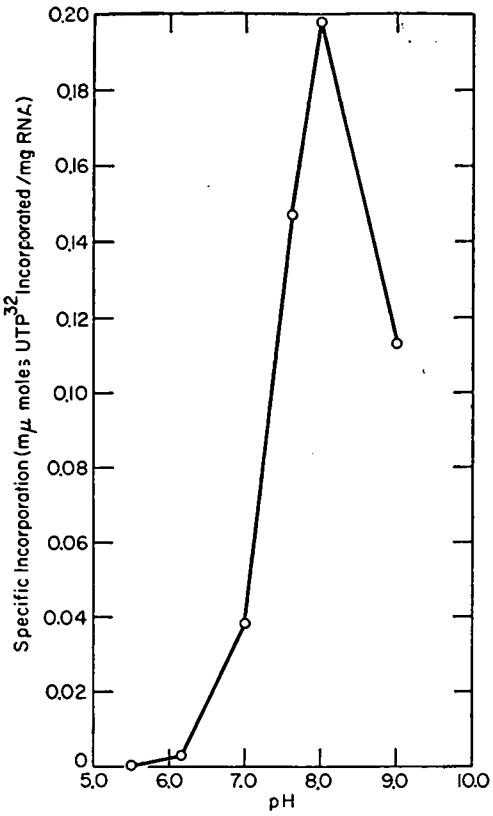

Figure 2. pH vs activity. Sample composition the same as in Table 2,C except that microsomes were used; CTP, ATP, and GTP added; 100 μmoles of potassium malonate buffers, pH 5.5_0 and 6.1_5, and 100 μmoles of Tris·HCl buffers, pH 7.0_0, 7.6_2, 8.0_0, and 9.0_0 used. Incubation for 10 minutes at 37° and 1.0 μmole P-enolpyruvate added after 5 minutes. Samples processed by Procedure 1-A.

Divalent cation requirement. Chung et al.[12] have reported that Mn^{+2} stimulates ATP-8-C^{14} incorporation into embryonic chicken liver supernatant RNA in the presence of an optimal quantity of Mg^{+2}. Both manganous and magnesium ions have been tested with the pigeon liver microsome system (Table 6). The stimulatory effect of these ions appears to be equal under the conditions used. The incorporation of UTP-6-C^{14} is inhibited 85 per cent when EDTA,* in amounts equivalent to the amount of $MgCl_2$ used, is added to the system; this amount of EDTA would not remove magnesium originally present in the microsomes. The EDTA inhibition suggests that there is an absolute requirement for a divalent cation, either Mg^{+2} or Mn^{+2}. No other divalent cations have been tested in this system.

Effect of spermidine·HCl on UTP incorporation into RNA. Chung et al.[12] also report that spermidine stimulates ATP-8-C^{14} incorporation into embryonic chicken liver supernatant RNA.

*The abbreviation used is: EDTA, ethylenediaminetetraacetic acid.

Table 6

EFFECT OF DIVALENT CATIONS ON LABELED-UTP INCORPORATION INTO MICROSOME RNA*

Experiment	Mg^{+2}	Mn^{+2}	EDTA, pH 8.0	Specific incorporation of labeled UTP
	μ moles	μ moles	μ moles	mμmoles/mg RNA
A	9.4			0.20
	9.4	10.0		0.28
B	8.6	10.0		0.46
	18.6			0.46
C		20.0		0.18
	20.0			0.15
D	20.0			0.13
	20.0		20.0	0.02

*In addition to the standard components, samples contained:
A. Same as Table 2,B, except divalent cations as indicated. Processing by Procedure 1-B.
B. Same as Table 2,A, except divalent cations as indicated and addition of ATP generating system. Processing by Procedure 1-A.
C. Same as Table 2,C, except divalent cations as indicated, CTP, ATP, GTP used, and microsomes instead of ATP-PP_i-washed microsomes. Processing by Procedure 1-A.
D. Same as Table 4,C, except EDTA as indicated. Samples processed by Procedure 2.

The addition of spermidine · HCl to the pigeon liver microsome system at a concentration of 0.004 M resulted in a 44 per cent inhibition of UTP^{32} incorporation.

Distribution of isotope in alkaline hydrolysates of RNA labeled by UTP^{32} and UTP-6-C^{14} incorporation. Nucleoside triphosphate ester phosphorus incorporated into RNA is recovered from an alkaline hydrolysate esterified in the 2' or 3' position of the nucleoside moiety which was adjacent to the incorporated nucleotide. A distribution of P^{32} among all the 2'(3')-nucleotides derived from RNA labeled by incorporation of a single ester-labeled nucleotide suggests nonterminal incorporation,[1,8] and labeling of only one 2'(3')-nucleotide suggests terminal incorporation.[2] Neither of these findings can be considered definitive. Terminal addition to a heterogeneous population of RNA molecules containing all four bases in terminal nucleoside moieties would result in labeling of all four 2'(3')-nucleotides. Nonterminal incorporation of a nucleotide in a position adjacent to a particular nucleoside moiety would appear as terminal addition by the randomization criterion.

Pigeon liver microsome RNA was labeled by incorporation of UTP^{32}, the RNA isolated by Procedure 2, hydrolyzed with KOH, and then fractionated by chromatography on Dowex 1-Cl^- by a modification of the method of Cohn.[19] P^{32} was found in all 2'(3')-nucleotides (Table 7). This finding is consistent with some nonterminal incorporation but the high proportion of the total incorporated radioactivity in 2'(3')-UMP is not consistent with random incorporation as

Table 7

ISOTOPE DISTRIBUTION IN ALKALINE HYDROLYSATES OF LABELED RNA

Substance[c]	RNA-P^{32}[a]			RNA-C^{14}[b]	
	Total cpm	% of total	Pairing frequency[d]	Total cpm	% of total
Nucleoside	0			22	5
Unidentified fraction	0			112	26
2'(3')-CMP	72	18	2.1	12	3
2'(3')-AMP	34	9	1.0		
2'(3')-UMP	218[e]	56	6.3	250	59
2'(3')-GMP	60	15	1.8		
Recovery	384	99		396	93

[a] RNA-P^{32} (389 cpm), 1.22 mg, used.

[b] RNA-C^{14} (426 cpm), 2.90 mg, used.

[c] Listed in order of elution from a Dowex 1-Cl^- column.

[d] The frequency of nucleoside pairs, . . . XpU . . ., in the labeled fraction of microsomal RNA relative to . . . ApU . . . in this fraction. X is cytidine (C), adenosine (A), uridine (U), or guanosine (G).

[e] This fraction chromatographed with carrier 5'-UMP with the use of the borate solvent. All radioactivity was found in the 2'(3')-UMP spot.

found with polynucleotide phosphorylase.[33]

The use of purine- or pyrimidine-base-labeled nucleotides, such as UTP-6-C^{14}, allows unequivocal determination of terminal and nonterminal incorporation.[13] Uridine isolated from alkaline hydrolysates of RNA would be labeled if UTP-6-C^{14} were added terminally whereas C^{14} would appear as 2'(3')-UMP if the nucleotide was incorporated nonterminally. Microsome RNA, labeled by incorporation of UTP-6-C^{14}, was isolated, hydrolyzed, and fractionated as for RNA-P^{32}. Most of the C^{14} was recovered in 2'(3')-UMP showing that the incorporation is largely nonterminal and not random.

The unidentified fraction indicated in Table 7 was eluted by 0.002 M HCl just before 2'(3')-CMP and after the column had been washed with 100 resin bed volumes of water, the last 80 volumes of which showed no absorption at 260 mμ. The ion exchange properties of this fraction suggest that it contains nucleotides since this volume of water usually elutes all nucleosides. Paper chromatography of this fraction with carrier uridine in the isopropanol-HCl solvent of Wyatt[34] showed that the radio activity migrated with the uridine. Insufficient material remained, however, to confirm this possible identity of the unidentified fraction radioactivity with uridine with the use of other chromatographic systems. Nucleoside-2',3'-cyclic phosphates would be eluted by the 0.002 M HCl from Dowex 1-Cl^- but a similar fraction found on chromatography of the RNA-P^{32} alkaline hydrolysate was not radioactive although radioactivity would be expected if this fraction contained nucleoside-2',3'-cyclic phosphates.

A similar, unidentified fraction was found by Hecht et al.[13] in the ion exchange chromatogram of the alkaline hydrolysate of supernatant RNA labeled terminally by incorporation of ATP-8-C^{14}. They suggested that this fraction was the dinucleotide adenylyl-(5',3')-cytidine phosphate

which was more resistant to alkaline hydrolysis than other phosphodiesters. The unidentified fraction found in the present work must be derived from UTP with microsomal RNA as a required intermediate. Work is in progress to determine the nature of this fraction.

DISCUSSION

All cell-free systems isolated from the tissues of higher animals which synthesize* RNA[8-13] utilize nucleoside triphosphates as direct precursors. The differences which exist between them, apart from species and cytological source of the enzymes, are chiefly with reference to nucleotide dependence, RNA dependence, and terminal or nonterminal addition. The synthesis of amino acid transfer RNA[13] is not dependent on the presence of four nucleoside triphosphates, utilizing only CTP and ATP, but is dependent on RNA which undergoes terminal addition; the calf thymus nuclei system of Hurwitz et al.[10] and the rat liver microsome system of Herbert[11] (which requires the presence of either nuclei or supernatant) are similar. RNA-synthesizing systems from embryonic chicken liver supernatant,[12] and the pigeon liver microsome system are nucleotide dependent, RNA dependent, and they show nonterminal incorporation; the rat liver microsome system described by Herbert et al.[3] may be similar. The rat liver nuclei system of Weiss[8] is nucleotide dependent, shows nonterminal incorporation, and is apparently DNA dependent. The calf thymus nuclei system of Edmonds and Abrams[9] is not nucleotide or RNA dependent and shows nonterminal incorporation.

The pigeon liver microsome system is clearly different from the embryonic chicken liver system of Chung et al.[12] in that the effect of divalent cations, pH optima, and the effects of spermidine are different. Except for the DNA dependence, there are no apparent qualitative differences, with regard to the criteria listed, between the microsome system and the rat liver nuclei system of Weiss.[8]

There appear to be several RNA-synthesizing systems in cells of higher animals and even within certain subcellular particulate fractions.

The firm binding of nucleotides,[11,35] pyrophosphate,[27] and orthophosphate to rat and pigeon liver microsomes may have physiological significance in that such binding would provide a means of concentrating biologically active polyanions at enzymic sites where they are utilized. In view of the binding of nucleotides to all subcellular fractions, caution must be used in the interpretation of experiments measuring the incorporation of precursors into RNA based on simple determination of radioactivity in the acid-insoluble protein nucleate fraction; such binding must also be considered in work involving other phosphate esters and anhydrides.

Zalokar[36] has concluded that all RNA in Neurospora crassa is synthesized in the nucleus on the basis of autoradiographs of centrifuged hyphae incubated with tritiated uridine. Goldstein and Micou[37] have come to the same conclusion from similar experiments with cultured human amnion cells using tritiated cytidine. The results of the experiments reported here, on pigeon liver cytoplasmic fractions, show that RNA synthesis does occur in the microsome fraction.

*Net synthesis of RNA by cell-free systems from animal cells has not been reported in any detail. For the purposes of this discussion, it is assumed that incorporation of nucleotides into polyribonucleotides represents synthesis since the rapid formation and breaking of phosphodiester bonds required of an exchange reaction appears unlikely. Synthesis, in this sense, can be de novo or may represent increase in molecular size with no increase in the number of molecules as by repeated terminal addition of nucleotides to a preexisting polynucleotide.

The work of others[1-4,6,11-13] may be interpreted to show that RNA synthesis takes place in the cytoplasm. The conclusion that RNA synthesis occurs only in the nucleus cannot be universally valid.

LITERATURE CITED

1. Goldwasser, E. J. Am. Chem. Soc., 77:6083, 1955.
2. Heidelberger, C., E. Harbers, K. C. Leibman, Y. Takagi, and V. R. Potter. Biochim. et Biophys. Acta., 20:445, 1956.
3. Herbert, E., V. R. Potter, and L. I. Hecht. J. Biol. Chem., 225:659, 1957.
4. Potter, V. R., L. I. Hecht, and E. Herbert. Biochim. et Biophys. Acta, 20:439, 1956.
5. Grunberg-Manago, M., P. J. Ortiz, and S. Ochoa. Biochim. et Biophys. Acta, 20:269, 1956.
6. Burdon, R. H., and R. M. S. Smellie. Biochem. J., 76:2P, 1960.
7. Hilmoe, R. J., and L. A. Heppel. J. Am. Chem. Soc., 79:4810, 1957.
8. Weiss, S. B. Proc. Natl. Acad. Sci. U. S., 46:1020, 1960.
9. Edmonds, M., and R. Abrams. J. Biol. Chem., 235:1142, 1960.
10. Hurwitz, J., A. Bresler, and A. Kaye. Biochem. and Biophys. Research Communs., 1:3, 1959.
11. Herbert, E. J. Biol. Chem., 231:975, 1958.
12. Chung, C. W., H. R. Mahler, and M. Enrione. J. Biol. Chem., 235:1448, 1960.
13. Hecht, L. I., P. C. Zamecnik, M. L. Stephenson, and J. F. Scott. J. Biol. Chem., 233:954, 1958.
14. Lowry, O. H., N. J. Rosebrough, A. L. Farr, and R. J. Randall. J. Biol. Chem., 193:265, 1951.
15. Dische, Z. In The Nucleic Acids, ed. E. Chargaff and J. N. Davidson, New York: Academic Press, Inc., 1955, I, p. 301.
16. Crestfield, A. M., K. C. Smith, and F. W. Allen. J. Biol. Chem., 216:185, 1955.
17. Lieberman, I., A. Kornberg, and E. S. Simms. J. Biol. Chem., 215:403, 1955.
18. Lieberman, I., A. Kornberg, and E. S. Simms. J. Biol. Chem., 215:429, 1955.
19. Cohn, W. E. J. Am. Chem. Soc., 72:1471, 1950.
20. Smith, M., and H. G. Khorana. J. Am. Chem. Soc., 80:1141, 1958.
21. Hall, R. H., and H. G. Khorana. J. Am. Chem. Soc., 76:5036:1954.
22. Emanuel, C. F., and I. L. Chaikoff. Biochim. et Biophys. Acta, 24:254, 1957.
23. Sachs, H. J. Biol. Chem., 233:643, 1958.
24. Davidson, J. N., and R. M. S. Smellie. Biochem. J., 52:594, 1952.
25. Dutta, S. K., A. S. Jones, and M. Stacey. Biochim. et Biophys. Acta, 10:613, 1953.
26. Metzenberg, R. L. J. Cellular Comp. Physiol., 54:(Suppl. 1), 15, 1959.
27. Sachs, H. J. Biol. Chem., 233:650, 1958.

28. Hoagland, M. B. Proceedings of the fourth international congress of biochemistry, Vol. VIII, Pergamon Press, Ltd., London, 1960, p. 212.

29. Bloemendal, H., L. Bosch, and M. Slayser. Biochim. et Biophys. Acta, 41:444, 1960.

30. Dunn, D. B. Biochim. et Biophys. Acta, 34:286, 1959.

31. Cohn, W. E. J. Biol. Chem., 235:1488, 1960.

32. Brachet, J. Biochim. et Biophys. Acta, 19:583, 1956.

33. Ortiz, P. J., and S. Ochoa. J. Biol. Chem., 234:1208, 1959.

34. Wyatt, G. R. Biochem. J., 48:584, 1951.

35. Littlefield, J. W., and E. B. Keller. J. Biol. Chem., 224:13, 1957.

36. Zalokar, M. Nature (London), 183:1330, 1959.

37. Goldstein, L., and J. Micou. J. Biophys. Biochem. Cytol., 6:1, 1959.

ON THE PARTICIPATION OF DNA IN RNA BIOSYNTHESIS*

By

S. B. Weiss and T. Nakamoto

We have recently described an enzyme system in rat liver nuclei requiring four ribonucleoside triphosphates for the incorporation of ribonucleotides into RNA.[1] Further work with this system showed that the incorporation of ribonucleotides occurred throughout the entire polynucleotide molecule and that this activity disappeared after treatment of the mammalian particles with DNase.[2] Subsequent experiments with DNase-treated rat liver preparations indicated that a partial reactivation of the ribonucleotide incorporating activity could be achieved with added DNA. In agreement with these observations, Stevens[3] and Hurwitz, et al.[4] demonstrated the existence of a similar system in extracts from E. coli. In addition to requiring the presence of all four ribonucleoside triphosphates in the bacterial system, Hurwitz, et al. first reported that the addition of DNA was also necessary.

More recently, Weiss and Nakamoto[5] reported the isolation of a similar enzyme system from extracts of the microorganism M. lysodeikticus, and using this preparation demonstrated net synthesis of RNA. In order to obtain some insight into the role played by DNA in this reaction, nearest neighbor sequence analysis and base composition of the newly synthesized RNA were determined. Studies of this type were conducted for a number of different "primer" DNA's and are reported herein.

Using the partially purified M. lysodeikticus enzyme, RNA was isolated from the reaction mixture at different times of incubation. Calf thymus or rat liver DNA served as "primer" for this experiment. Analysis of the RNA so prepared suggested that polynucleotides with a similar statistical arrangement of bases were formed at these different reaction times (Table 1). In consequence, it was felt that the nearest neighbor sequence analysis and base composition studies of the RNA synthesized in vitro might be meaningful.

Although little information concerning the sequential arrangement of bases in nucleic acid is available, it is probable that the arrangement of deoxynucleotides in DNA differs in DNA's isolated from different sources. If the sequence of ribonucleotides in RNA is influenced by the DNA required for this reaction, then this influence should be reflected in the position of any one ribonucleotide in the RNA chain when various DNA "primers" are used. This relative position may be conveniently determined by preparing RNA enzymatically with one P^{32}-nucleotide, and hydrolyzing the P^{32}-RNA formed with alkali. Since the labeled phosphate is transferred to the adjacent nucleotide under alkaline hydrolysis, one may then examine the relative frequency with which the labeled nucleotide occurs next to a given neighbor.

Examination of the results obtained when calf thymus, rat liver and different bacterial DNA's serve as "primers" in separate reactions, suggests that the relative position of labeled cytidylate in the newly formed RNA is different for the various "primers" used (Tables 1 and 2).

*This paper appears in Proc. Nat. Acad. Sci., 47:694, 1961. The investigation was supported in part by funds from the Joseph and Helen Regenstein Foundation.

Table 1

RATIO OF LABEL IN ALKALINE HYDROLYZED PRODUCTS FROM CMP^{32}-RNA FORMED AT DIFFERENT INCUBATION TIMES

DNA source	Reaction time (minutes)	Total hydrolyzable counts	Count ratio of isolated nucleotides*			
			2'(3')CMP	2'(3')AMP	2'(3')GMP	2'(3')UMP
Calf thymus	4	120,000	1.00	1.15	1.01	1.44
Calf thymus	15	218,000	1.00	1.13	0.99	1.51
Rat liver	4	47,400	1.00	1.19	0.80	1.30
Rat liver	15	92,000	1.00	1.13	0.78	1.30

The reaction system contained 9 μmoles of $MnCl_2$, 300 μmoles phosphate buffer of pH 7.5, 0.18 μmoles of CTP^{32} (3 x 10^7 cpm per micromole), 2.4 μmoles each of ATP, UTP and GTP, 300 μgrams of calf thymus or rat liver DNA and 1.0 mg of M. lysodeikticus enzyme. The final volume was 3.0 ml and the vessels were incubated at 25° for the time periods indicated. The reaction was stopped by the addition of 0.60 ml of 3 N $HClO_4$ with 4 mg of yeast RNA added as carrier. The precipitate was collected by centrifugation, washed four times by solution in cold 0.10 N NaOH and reprecipitation with 0.50 N $HClO_4$. The washed residue was hydrolyzed in 0.2 N KOH for 18 hours at 37°, acidified with $HClO_4$ to below pH 1 and the acid-soluble fraction saved after centrifugation. This fraction was neutralized and subjected to paper electrophoresis as described previously.[2] The separated nucleotides were assayed for radioactivity. A minimum of 90 per cent of the radioactive material placed on paper was recovered in the nucleotides eluted.

*The total radioactivity found for each isolated mononucleotide was divided by the total counts found for 2'(3')-cytidylic acid and is the value listed above. Hence, a value of 1.00 indicates a total number of counts equivalent to that found for 2'(3')-cytidylic acid for that particular experiment.

Table 2

RATIO OF LABEL IN ALKALINE HYDROLYZED PRODUCTS FROM CMP^{32}-RNA PREPARED WITH VARIOUS DNAs

DNA used in Reaction	Count ratio of isolated nucleotides*			
	2'(3')CMP	2'(3')AMP	2'(3')GMP	2'(3')UMP
Pseudomonas	1.00	0.58	0.89	0.68
Serratia	1.00	0.66	1.55	0.80
E. coli	1.00	0.81	0.82	0.89

*The reaction system and the procedure used in these experiments were the same as described in Table 1 except that Pseudomonas, Serratia and E. coli DNA were used.

Loss of the terminal nucleotide residue after hydrolysis, contamination of the enzyme or DNA with RNA, or the addition of carrier RNA should have no influence on the results obtained. A complete nearest neighbor study of this type for each labeled ribonucleotide, using a DNA which has been similarly characterized,[6] should give more detailed information as to the role played by DNA in RNA synthesis.

Further information on the participation of DNA in the synthesis of RNA was obtained by determining the base composition of the newly formed ribopolynucleotide. In a series of separate reactions using the microbial enzyme, RNA was prepared in vitro when a number of different purified microbial and salmon DNA preparations were present as "primers." The nucleic acid fraction isolated from the reaction mixture was hydrolyzed with alkali, and the products of hydrolysis separated by paper electrophoresis. No carrier RNA was added at any time. In each of the experiments conducted, a net amount of ribonucleotide material corresponding to about 20 optical density units at 260 mμ was released into the acid-soluble fraction after alkaline hydrolysis. Control incubation vessels in which one nucleotide was omitted during the reaction, but re-added after the reaction had been stopped, gave only 10 per cent of the ultraviolet material obtained with the complete system. The 2'(3')-nucleoside monophosphates, located on the paper under ultraviolet light after electrophoresis, were eluted and their concentrations determined in a Zeiss spectrophotometer at their respective absorption maxima. The results of these experiments are given in Table 3.

Examination of the base composition of the RNA formed shows a remarkable similarity to the base composition reported for the respective DNA "primers." Pseudomonas and Serratia DNA have a relatively high GC mole per cent content, while salmon DNA has a low GC mole per cent content. Similarly, it can be seen that the GC base content of the RNA formed in the presence of Pseudomonas and Serratia DNA is high, while the GC content for the RNA found when salmon DNA was used is correspondingly low. When E. coli DNA was present in the reaction mixture, the RNA formed had nearly equivalent amounts of each ribonucleotide, which also reflects the base composition of this particular DNA. In each of these experiments, experimental error does not allow for exact comparison between DNA and RNA bases. Examination of experiments 1 and 2 with Pseudomonas DNA shows the limit of error incurred. However, the DNA's used here are sufficiently different in composition to exclude experimental error in the interpretation of the results obtained.

Table 3

BASE COMPOSITION OF SYNTHESIZED RNA AS COMPARED TO PRIMER DNA

Base*	Base proportions (moles %)†								
	Pseudomonas DNA	Synthesized RNA		Salmon DNA	Synthesized RNA	Serratia DNA	Synthesized RNA	E. coli DNA	Synthesized RNA
		Expt. (1)	Expt. (2)						
G	33.0	28.2	35.0	20.8	21.0	29.0	32.6	24.1	23.4
A	18.2	18.3	16.5	29.7	29.0	21.1	18.6	25.4	23.4
C	30.0	32.8	29.5	20.4	23.0	29.0	28.0	25.7	24.8
T(U)	18.8	20.7	19.0	29.1	27.0	20.9	20.8	24.8	28.4
GC	63.0	61.0	64.5	41.2	44.0	58.0	60.6	49.8	48.2
$\frac{A + T(U)}{G + C}$	0.59	0.64	0.55	1.43	1.27	0.72	0.65	1.01	1.07

The complete system contained 30 μmoles of $MnCl_2$, 1.0 mmole of phosphate buffer of pH 7.5, 10 μmoles each of CTP, ATP and GTP, 1.0 mg of bacterial or salmon DNA and 8 to 10 mg of enzyme (absorbency ratio of 280/260 mμ = 1.54). The reaction was incubated for 1 hour at 25° in a final volume of 10 ml. After incubation, the reaction was treated as described in Table 1, except for the following modifications. No carrier RNA was added. An extraction of the washed acid-insoluble material was made with 10 per cent NaCl, pH 8, at 90° for 30 minutes. The nucleic acid was precipitated twice from the salt extract with two volumes of ethanol. This modification considerably lowered the optical density units released, after alkaline hydrolysis, in control vessels where one nucleotide had been omitted from the reaction mixture.

*Base composition of DNA as reported by Belozersky and Spirin.[11]

†The moles per cent of the bases found in RNA were calculated by assuming that the nucleotides eluted from paper, after electrophoresis, represented 100 per cent recovery. The loss of terminal nucleotide residues by this procedure, as well as endogenous RNA, account in part for the experimental error observed.

Examination of P^{32}-RNA formed after coli infection with phage, led Volkin and Astrachan[7] to conclude that the RNA synthesized in the infected cells resembled phage DNA in base ratio. Belozersky and Spirin,[8] after studying DNA and RNA composition in a number of different bacterial species, speculated that a small portion of the cellular RNA might fully correlate in its composition with that of DNA. Yčas and Vincent[9] presented evidence that a metabolically active RNA fraction in yeast had a base composition resembling yeast DNA. More recently, Hall and Spiegelman[10] reported on complex formation between denatured phage DNA and specific RNA. These authors concluded that only T2-DNA complexes with T2-specific RNA since they possess complementary nucleotide sequences. The work described in the present paper agrees with and supports the concept put forth by the above authors.

The M. lysodeikticus enzyme used in our experiments will form ribopolynucleotides when mammalian, salmon, sea urchin, bacterial and phage DNA serve as "primers." It is quite possible that in the presence of a specific DNA this enzyme will assemble complementary ribopolynucleotides. However, it should be emphasized that we have not yet proved with certainty that the RNA thus synthesized is an exact replica of the "primer" DNA. It is interesting to note that besides the above mentioned DNA's, preliminary results with Turnip yellow mosaic virus RNA indicate that it too may prime this system.

The authors are indebted to Drs. E. Peter Geiduschek and Alexander Rich for providing the purified salmon and bacterial DNA.

LITERATURE CITED

1. Weiss, S. B., and L. Gladstone, J. Am. Chem. Soc., 81:4118, 1959.
2. Weiss, S. B. These PROCEEDINGS, 46:1020, 1960.
3. Stevens, A. Biochem. and Biophys., 3:92, 1960.
4. Hurwitz, J., A. Bresler, and R. Diringer. Ibid., 3:15, 1960.
5. Weiss, S. B., and T. Nakamoto. J. Biol. Chem., 236:PC18, 1961.
6. Josse, J., A. D. Kaiser, and A. Kornberg. Ibid., 236:864, 1961.
7. Volkin, E., and L. Astrachan. Virology, 2:149, 1956.
8. Belozersky, A. N., and A. S. Spirin. Nature, 182:111, 1958.
9. Yčas, M., and W. S. Vincent. These PROCEEDINGS, 46:804, 1960.
10. Hall, B. D., and S. Spiegelman. Ibid., 47:137, 1961.
11. Belozersky, A. N., and A. S. Spirin. In The Nucleic Acids, ed. E. Chargaff and J. N. Davidson, New York: Academic Press, Inc., 1960, III, p. 147.

STUDIES ON IRON ABSORPTION I. THE RELATIONSHIPS BETWEEN THE RATE OF ERYTHROPOIESIS, HYPOXIA AND IRON ABSORPTION*

By

G. A. Mendel

Since the demonstration by McCance and Widdowson[1] of the marked limitations of human iron excretion, it has been recognized that total body iron in man is normally maintained at a relatively constant level by some mechanism which regulates the amount of iron absorbed from the gastrointestinal tract.

Despite intensive investigation, these mechanisms remain incompletely defined. The once widely accepted concept (Hahn[2] and Granick[3]) that a "mucosal block" acts as the prime regulatory mechanism whereby saturation of the mucosal cell ferritin impedes further iron absorption, no longer appears tenable in view of more recent studies. Brown[4] has shown that the "block" to absorption induced by prior iron feeding is not complete and has suggested that it is relatively unimportant as a regulatory mechanism when physiologic quantities of iron are involved. Heilmeyer[5] has demonstrated a rising ferritin content in the liver following iron ingestion at a time when mucosal ferritin content was maximal.

Other factors regarded as important in the regulation of iron absorption include the rate of erythropoiesis,[6,7] bowel hypoxia,[8] the content of total-body iron,[7] the activity of iron-containing enzymes,[9] and the state of the plasma iron-transferrin system.[10]

The rate of erythropoiesis has come to be considered one of the more important internal regulators of iron absorption in man under "physiologic" conditions. Numerous conditions are known, both in human subjects and in experimental animals, in which an acceleration of red cell production is paralleled by an increase in the gastrointestinal absorption of iron. These conditions include anoxic hypoxia,[11] cobalt administration,[12] hemolytic anemias of varied etiology[13,7] and the anemia induced by blood loss.[2] In contradistinction, iron absorption is increased in patients with hemochromatosis without measurable acceleration of the rate of erythropoiesis.[14]

It has been demonstrated repeatedly that hypoxic anoxia enhances iron absorption in <u>in vivo</u> experiments.[11,12] In <u>in vitro</u> studies using everted sacs of rat duodenum, however, anaerobic conditions were found to impede iron transport across the mucosa.[15] It has frequently been tacitly assumed that the increased absorption of iron associated with hypoxia is secondary to increased red cell production.[16] The role and importance of anoxia, hypoxic and anemic, in iron absorption remain uncertain.

The present studies were undertaken to explore further the relationships between the rate of red cell production, hypoxia and the gastrointestinal absorption of iron.

MATERIALS AND METHODS

CF No. 1 virgin female mice 9-12 weeks old, maintained on a Rockland Mouse Pellet diet,

*This report is based on a paper given on May 15, 1961 in Washington, D. C. at the Ninth Annual Meeting of the Radiation Research Society, and has been accepted for publication by "Blood."

were used in all experiments except as indicated in Table V where mice 29-30 weeks old were used. Water containing approximately 12 μg of iron per ml was given for 3 weeks prior to the beginning of an experiment.

Splenectomy was performed through a small left flank incision under intraperitoneal sodium pentobarbitol anesthesia.

Mice treated with radiostrontium were given 2 or 4 microcuries of $Sr^{89}Cl_3$ per gram of body weight intraperitoneally on the day following splenectomy and eleven days prior to the feeding of $Fe^{59}SO_4$. As shown by Jacobson et al.,[17] excretion of Sr^{89} was negligible after this 11-day period.

Mice were hypertransfused by intraperitoneal injection of 0.5 cc of washed homologous red blood cells twice daily for 2 days beginning the day after Sr^{89} administration.

Mice treated with erythropoietin were given 6 units of erythropoietin* subcutaneously daily for 3 days beginning 6 days after red cell transfusion. The 6-day interval coincides with the period of maximum suppression of erythropoiesis induced by hypertransfusion. The unit of activity is as described by Goldwasser and White.[18]

Hypoxic anoxia was induced in animals by placing them in a chamber containing a gas mixture having a concentration of 10 per cent O_2 for 24 hours before and after the administration of Fe^{59} intragastrically or intravenously.

Iron absorption was measured by total body counting in a Geiger-Mueller well counter† as described by Krantz et al.[12] Fasting mice were force-fed 0.6 cc of a solution of 0.01 N HCl containing 1.5 μc $Fe^{59}SO_4$ and 36 μg of $FeSO_4 \cdot 7\ H_2O$.

In mice treated with strontium-89, percentage absorption of Fe^{59} was calculated from the formula:

$$\% \text{ Fe}^{59} \text{ absorbed} = \frac{C - k_1 A}{k_2 (B - A)}$$

Where: A = cpm due to Sr^{89} immediately prior to Fe^{59} feeding
B = cpm immediately after Fe^{59} feeding
C = cpm 3 days after Fe^{59} feeding
k_1 = decay factor for Sr^{89}
k_2 = decay factor for Fe^{59}

Because of variations in mean iron absorption values of normal mice in different experiments, no attempt has been made to make comparisons between absolute values obtained in these various experiments. No correction was made for contamination of the Sr^{89} with Sr^{90} since calculation indicated that this contamination could introduce a maximum error of ± 0.4 per cent.

Iron incorporation into circulating red blood cells was determined by injecting 1 μc of Fe^{59} citrate into the tail vein and measuring the radioactivity in 0.2 cc of blood approximately 24 hours later. Calculations of percentage incorporation were based on assumed blood volume of 6 per cent. Changes in blood volume produced by anemia and hypoxia were considered insignificant.

---

*Prepared by Armour and Company Research Division, AEC Subcontract #21, under Contract #18-(11-1)-69 with the University of Chicago.[18,19]

†Nucleonic Corporation of America Model WC-3.

Iron absorption was measured over a 3-day period to allow time for elimination of unabsorbed radioiron from the gut. The incorporation of intravenously-administered iron was measured during the 24-hour period coinciding with the time of maximum iron absorption.

Reticulocyte counts were done on tail vein blood by the direct smear method using brilliant cresyl blue and counting 1000 red cells. Considerable variation in normal count was found to exist in groups of mice of identical age received at various times during the year. Variation within a group was not large.

Hematocrits were determined on tail vein blood collected in heparinized capillary tubes and spun in a microhematocrit centrifuge.

Histologic studies were performed on mice killed by cervical fracture. Tissues were fixed in Zenker-formol, embedded in nitrocellulose, cut at 6-8 microns and stained with hematoxylin-eosin-azure and/or Prussian blue. These preparations included whole mounts of femur and specimens of small intestine, liver and spleen.

RESULTS

The effect of erythropoietin on iron absorption in hypertransfused mice. To suppress red cell production, mice were hypertransfused. By the sixth day after hypertransfusion, erythropoiesis was markedly reduced as evidenced by a fall in the reticulocyte count to near zero and by the disappearance of proerythroblasts and normoblasts from the bone marrow and spleen.[20] When such hypertransfused mice are given 3 doses of erythropoietin at 24-hour intervals, a wave of erythropoiesis sweeps through the marrow with a maximal rise in reticulocytes during the third day and a return in the reticulocyte count to zero by the seventh day.[21] Iron absorption was measured during this period of accelerated erythropoiesis.

As indicated in Table 1, mean iron absorption in the normal controls was 28.8 per cent and the average reticulocyte count was 5.55 per cent. Iron absorption in the hypertransfused group* was reduced to a mean of 6.3 per cent and red cell production was markedly suppressed as indicated by the mean reticulocyte count of 0.03 per cent. In the erythropoietin treated hyper-

Table 1

THE EFFECT OF ERYTHROPOIETIN ON IRON ABSORPTION IN HYPERTRANSFUSED MICE

Treatment		% Fe^{59} absorbed from G-I tract	At time of Fe^{59} feeding	
			Mean reticulocyte count (%)	Mean hematocrit (%)
Normal controls	(9)*	28.8 ± 5.03†	5.55	54
Hypertransfusion	(8)	6.3 ± 3.85	0.03	69
Hypertransfusion + erythropoietin	(9)	12.1 ± 1.46	2.20	69

*Number of mice in each group.

†Standard error of mean.

*It is recognized that the iron content of the injected cells may play some role in the reduction of absorption in both hypertransfused groups.

transfused mice, the absorption of iron was increased from the mean of 6.3 per cent to 12.1 per cent, paralleling the increase in red cell production indicated by the rise in the mean reticulocyte count from 0.03 per cent to 2.20 per cent.

The effect of erythropoietin on iron absorption in hypertransfused mice with erythropoietic suppression produced by splenectomy and Sr^{89} administration. To determine whether the action of erythropoietin in enhancing iron absorption was directly on the gastrointestinal mucosa or was dependent on increased red cell production, mice were injected with 2 $\mu c/g$ of Sr^{89}* to impair the capacity of the bone marrow to respond to erythropoietin. Figure 1 illustrates the almost complete replacement of normal marrow by fibrous tissue in a Sr^{89}-treated

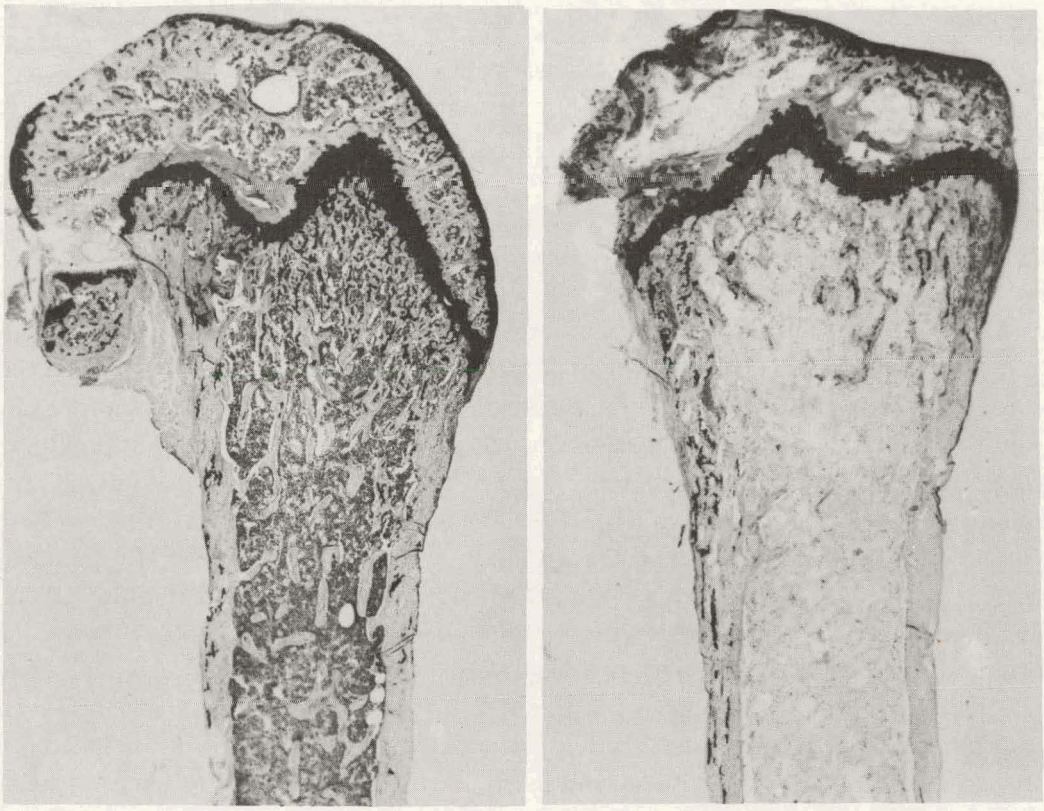

A B

Figure 1. A. Whole mount of femur of normal mouse. B. Whole mount of femur of mouse 14 days after treatment with 2 $\mu c/g$ Sr^{89}. Note almost complete replacement of hematopoietic tissue by fibrous tissue.

animal. Jacobson[17] has shown that mice given this dose of Sr^{89} rapidly develop a marked increase in erythropoiesis in the spleen. For this reason splenectomy was performed on the day prior to strontium-89 administration.

As shown in Table 2, the mean iron absorption value in the splenectomized-Sr^{89}-treated

*It is unlikely that splenectomy followed by this dose of Sr^{89} results in complete suppression of erythropoiesis. The anemia which develops in mice so treated does not become fully expressed until 4 weeks following radiostrontium administration and is only moderate in degree.

Table 2

THE EFFECT OF ERYTHROPOIETIN ON IRON ABSORPTION IN SPLENECTOMIZED-Sr^{89}* TREATED HYPERTRANSFUSED MICE

Treatment		% Fe^{59} absorbed from G-I tract	At time of Fe^{59} feeding	
			Mean reticulocyte count (%)	Mean hematocrit (%)
Normal controls	(9)†	28.8 ± 5.03‡	5.55	54
Splenectomy + Sr^{89}	(8)	18.1 ± 2.47	1.27	43
Splenectomy + Sr^{89} + hypertransfusion	(7)	7.2 ± 1.32	0.01	71
Splenectomy + Sr^{89} + hypertransfusion + erythropoietin	(8)	5.2 ± 0.91	0.25	66

*Sr^{89} 2 μc/g.

†Number of mice in each group.

‡Standard error of mean.

group was 18.1 per cent and the mean reticulocyte count was 1.27 per cent. In the splenectomized-Sr^{89} hypertransfused group, mean absorption was reduced to 7.2 per cent and the mean reticulocyte count was 0.01 per cent. In the erythropoietin-treated group, mean absorption was 5.2 per cent and reticulocytes were 0.25 per cent. Thus, in the erythropoietin stimulated, hypertransfused group pre-treated by splenectomy and Sr^{89}, there was no increase in iron absorption or in reticulocyte count comparable to that demonstrated in Table 1.

The effect of erythropoietin on iron absorption in hypertransfused mice with intact spleens treated with Sr^{89}. Figure 2 illustrates the marked increase in blood formation in the spleen that occurs in an animal treated with 2 μc/g of Sr^{89} in which the spleen was left intact. As indicated in Table 3, no significant difference in iron absorption was found between such animals with intact spleens treated with 2 μc/g of Sr^{89} and the normal controls. However, the enhancing effect of erythropoietin on iron absorption previously observed in hypertransfused mice with intact spleens (see Table 1) was not observed in hypertransfused mice with intact spleens treated with Sr^{89}. The mean absorption value with the Sr^{89} treated hypertransfused group with intact spleens was 3.7 per cent while that of the Sr^{89} treated hypertransfused group with intact spleens treated with erythropoietin was 4.7 per cent.

The effect of erythropoietin on iron absorption in hypertransfused mice pre-treated by splenectomy alone. As demonstrated in Table 4 splenectomy alone had no significant effect on iron absorption. Hypertransfused mice previously splenectomized showed a reduction in mean iron absorption from 24.8 per cent to 3.4 per cent. Splenectomized and hypertransfused mice given erythropoietin exhibited only a slight increase in mean absorption from 3.4 per cent to 4.6 per cent. While the difference is not statistically significant, it is typical of the results in several experiments.

The effect of hypoxia on iron absorption and erythropoiesis in normal and splenectomized-Sr^{89}-treated mice. To determine whether the reported effect of hypoxia in increasing iron absorption is dependent on acceleration of the rate of erythropoiesis, the effect of decreased oxy-

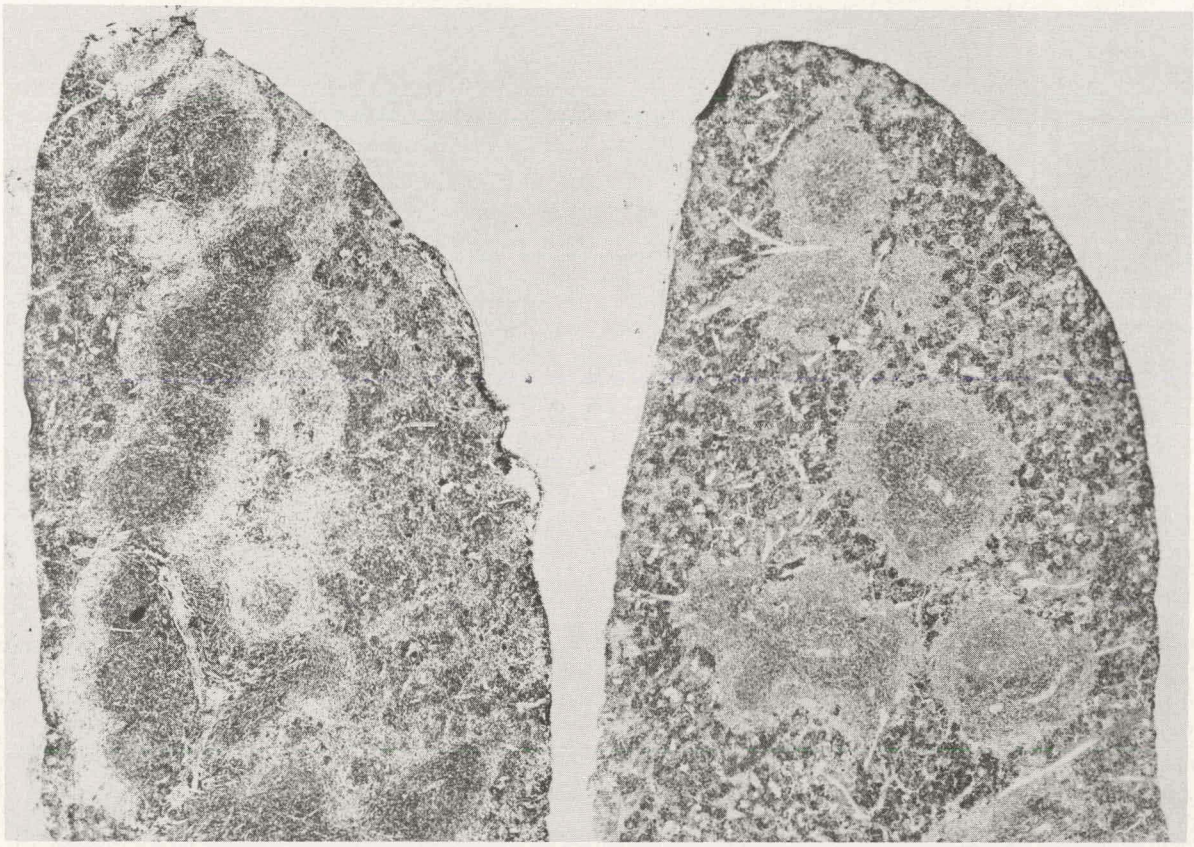

A B

Figure 2. A. Normal mouse spleen. B. Spleen removed from mouse 14 days after treatment with 2 μc/g Sr^{89}. Note marked increase in hematopoietic tissue with depletion of white pulp.

Table 3

THE EFFECT OF ERYTHROPOIETIN ON IRON ABSORPTION IN HYPERTRANSFUSED MICE WITH INTACT SPLEENS TREATED WITH Sr^{89}*

Treatment		% Fe^{59} absorbed from G-I tract	At time of Fe^{59} feeding	
			Mean reticulocyte (count (%)	Mean hematocrit (%)
Normal controls	(10)†	15.3 ± 2.40‡	2.20	51
Sr^{89}	(9)	18.0 ± 2.96	2.97	50
Sr^{89} + hypertransfusion	(8)	3.7 ± 0.60	0.00	71
Sr^{89} + hypertransfusion + erythropoietin	(10)	4.7 ± 1.10	2.01	70

*Sr^{89} 2 μc/g.

†Number of mice in each group.

‡Standard error of mean.

Table 4

THE EFFECT OF ERYTHROPOIETIN ON IRON ABSORPTION IN HYPERTRANSFUSED MICE TREATED WITH SPLENECTOMY

Treatment		% Fe^{59} absorbed from G-I tract	At time of Fe^{59} feeding	
			Mean reticulocyte count (%)	Mean hematocrit (%)
Normal controls	(10)*	24.8 ± 2.22†	1.63	50
Splenectomy	(9)	23.6 ± 1.40	2.60	48
Splenectomy + hypertransfusion	(4)	3.4 ± 0.85	0.00	72
Splenectomy + hypertransfusion + erythropoietin	(7)	4.6 ± 0.93	1.45	73

*Number of mice in each group.

†Standard error of mean.

gen tension on iron absorption and erythropoiesis in normal and splenectomized mice treated with 4 μc/g Sr^{89} was studied.

Table 5 shows that normal mice made hypoxic exhibited a marked increase in mean iron absorption from 15.5 per cent to 33.1 per cent as well as an increase in mean red cell production from 38.8 per cent* to 56.5 per cent as measured by the incorporation of intravenously administered Fe^{59} into newly released circulating red cells. The splenectomized-Sr^{89}-treated mice that were made hypoxic likewise showed a marked increase in mean iron absorption from 11.6 per cent to 30.3 per cent but no change in the rate of red cell production, which remained markedly reduced at a mean value of 4.0 per cent. Comparable results were obtained in mice treated with 2 μc/g of Sr^{89} and in which the degree of anemia was much less.

DISCUSSION

The present demonstration that iron absorption is enhanced by the hormone erythropoietin is in accord with the observations of Moore[6] and Bothwell[7] and their co-workers on the relationship which exists between the rate of erythropoiesis and iron absorption. Our data indicate that the mechanism by which erythropoietin augments iron absorption lies not in a direct action on the gastrointestinal mucosa, but is dependent on acceleration of erythropoiesis. Under the experimental conditions described, augmentation of iron absorption by erythropoietin did not occur when the ability to increase red cell production was impaired by splenectomy and radiostrontium. Radiostrontium was chosen because of its rapid localization in bone and in an attempt to avoid radiation injury to the gastrointestinal mucosa. That this attempt was successful is suggested by the finding that iron absorption was normal in animals treated with Sr^{89} in which the spleen (now the major organ of blood formation) was left intact. The rate of erythropoiesis, as measured by the incorporation of intravenously administered radioiron into newly released circulating red cells did not vary significantly from normal in this preparation.[26] These two find-

*In other experiments, 24 hour incorporation of I.V. Fe^{59} was as low as 15 per cent in normal animals of the same age.

Table 5

THE EFFECT OF HYPOXIA ON IRON ABSORPTION AND ERYTHROPOIESIS IN NORMAL AND SPLENECTOMIZED-Sr^{89}*-TREATED MICE

Treatment	% Fe^{59} absorbed from G-I tract (72 hrs)	% IV-administered Fe^{59} incorporated into circulating RBC's (24 hrs)	At time of Fe^{59} feeding	
			Mean reticulocyte count (%)	Mean hematocrit (%)
Normal controls	15.5 ± 3.98† (8)‡	38.8 ± 2.57 (8)	4.84	48
Normal hypoxia	33.1 ± 1.93 (10)	56.5 ± 4.85 (6)	4.21	49
Splenectomy + Sr^{89}	11.6 ± 1.32 (10)	4.1 ± 0.36 (6)	0.22	22
Splenectomy + Sr^{89} + hypoxia	30.3 ± 4.48 (8)	4.0 ± 0.02 (6)	0.14	26

*Sr^{89} 4 μc/g.

†Standard error of mean.

‡Number of animals in each group.

ings make it unlikely that radiostrontium itself, in the doses used, affects absorption or that a systemic inhibitor to erythropoietin exists in the radiostrontium-treated animals.

The diminution of the enhancing effect of erythropoietin on iron absorption in radiostrontium-treated animals with intact spleens and in animals subjected to splenectomy alone remains unexplained. One of several possible explanations is that this is a reflection of the reduction in the stem cell pool caused by these procedures, and one may speculate that cellular division at an immature stage in some manner influences the mucosa. Of some interest in this connection are (1) the suggestion by Mazur[22] and his co-workers that the incorporation of plasma iron into ferritin is linked to oxidative metabolism, nucleoprotein, and adenosine triphosphate synthesis and (2) their demonstration of increased incorporation of plasma iron into ferritin in animals undergoing liver regeneration as well as in animals treated with thyroxine.

The demonstration that iron absorption in hypoxic animals is greatly enhanced in the presence of profound suppression of erythropoiesis and without experimental manipulation likely to alter total body iron content, emphasizes the existence and importance of factors influencing absorption that are independent of accelerated erythropoiesis and total body iron content per se. These data clearly demonstrate for the first time, that increased absorption due to hypoxia can occur independently of acceleration of erythropoiesis. The effects of chronic iron deficiency, acute blood loss, cobalt administration, and pyridoxine deficiency in augmenting iron absorption, and the role of the concomitant acceleration of erythropoiesis warrant further exploration in the light of these findings.

The important question whether the augmenting effect of hypoxia on iron absorption is due to a direct effect on the mucosa or is a reflection of the many changes induced by hypoxia elsewhere in the organism is unanswered. Pertinent to this question are the reported effects of hypoxia in producing a decrease in serum iron concentration and elevation of the serum transferrin concentration,[23] the production of changes in iron-containing enzyme systems and other metabolites[24,25] as well as the relationship of oxidative metabolism to the internal movements of iron.[22]

There can be little doubt that multiple factors are operative in determining how much iron will be absorbed at any point in time. We believe that the splenectomized, strontium-89 treated animal will be of further use in the more precise definition of these factors.

ACKNOWLEDGMENT

The author wishes to express his gratitude to Dr. Leon O. Jacobson for his suggestions, criticism and continued interest.

LITERATURE CITED

1. McCance, R. A., and E. M. Widdowson. Lancet, 2:680, 1937.
2. Hahn, P. F., W. F. Bale, J. F. Ross, W. M. Balfour, and G. H. Whipple. J. Exptl. Med., 78:169, 1943.
3. Granick, S. J. Biol. Chem., 164:737, 1946.
4. Brown, E. B., Jr., R. Dubach, and C. V. Moore. J. Lab. Clin. Med., 52:335, 1958.
5. Heilmeyer, L. Iron in Clinical Medicine, ed. by R. O. Wallerstein and S. R. Mettier, Berkeley and Los Angeles: University of California Press, 1960, p. 24.

6. Moore, C. V. National Institutes of Health Annual Lectures, Washington, D. C., Public Health Service Publication 467, 1954, p. 38.

7. Bothwell, T. H., G. Pirzio-Biroli, and C. A. Finch. J. Lab. Clin. Med., 51:24, 1958.

8. Granick, S. Bull. N. Y. Acad. Med., 25:403, 1949.

9. Gillman, T., and M. Hathorn. Brit. Med. J., II:635, 1958.

10. Solvell, L. Acta Medica Scandinavia, Supplementum, 358:71, 1960.

11. Vassar, P. S., and D. M. Taylor. Proc. Soc. Exptl. Biol. and Med., 93:504, 1956.

12. Krantz, S., E. Goldwasser, and L. O. Jacobson. Blood, 14:654, 1959.

13. Stewart, W. B., P. S. Vassar, and R. S. Stone. J. Clin. Invest., 32:1225, 1953.

14. Peterson, A. R., and R. H. Ettinger. Am. J. Med., 15:518, 1953.

15. Dowdle, E. B., D. Schacter, and H. Schenker. Am. J. Phys., 198:609, 1960.

16. Peterson, R. E. The Metabolic Basis of Inherited Disease, ed. by J. B. Stanbury, J. B. Wyngaarden, and D. S. Fredrickson, New York: McGraw Hill Book Co., Inc., Blakiston Division, 1960, p. 856.

17. Jacobson, L. O., E. L. Simmons, and M. H. Block. J. Lab Clin. Med., 34:1640, 1949.

18. Goldwasser, E., and W. F. White. Federation Proc., 18:236, 1959.

19. White, W. F., C. W. Gurney, E. Goldwasser, and L. O. Jacobson. Recent Progress in Hormone Research XVI, ed. by G. Pincus, New York: Academic Press, Inc., 1960, p. 219.

20. Jacobson, L. O., E. Goldwasser, L. F. Plzak, and W. Fried. Proc. Soc. Exptl. Biol. and Med., 94:243, 1957.

21. Gurney, C. W., N. Wackman, and E. Filmanowicz. Blood, 17:531, 1961.

22. Mazur, A., A. Carleton, and A. Carlsen. J. Biol. Chem., 236:1109, 1961.

23. Colehour, J. K., H. Borsook, and A. Graybiel. Am. J. Physiol., 191:113, 1957.

24. Criscuolo, D., R. T. Clark, Jr., and R. B. Mefford, Jr. Am. J. Physiol., 180:215, 1955.

25. Tappan, D. V., B. Reynafarje, V. R. Potter, Jr., and A. Hurtado. Am. J. Physiol., 190:93, 1957.

26. Mendel, G. A. Unpublished observations.

METABOLISM OF GLYCOGEN IN THE SKIN AND THE EFFECT OF RADIATION*

By

K. Adachi,† D. C. Chow, and S. Rothman

Most of the little that is known about the metabolism and biological role of glycogen in the skin is based on histochemical evidence.[1] This evidence seems to indicate that certain cells of the skin accumulate glycogen when in a resting state, subsequently utilizing it as a source of energy when their metabolism is heightened in order to perform some function. For instance, all cells in the basal layer of early fetal mammalian epidermis are loaded with glycogen except those which are in mitotic division;[2] the glycogen of the secretory cells of eccrine sweat glands disappears when the glands are stimulated;[3] accumulation of glycogen in the epidermis of healing wounds is well known;[4] and this glycogen disappears at the level where the cells start to keratinize.[5] It was assumed that epithelial cells will accumulate glycogen if their metabolism is experimentally suppressed.[6]

Pure biochemical work on cutaneous glycogen has yielded contradictory results. The methods used for isolation and estimation have been crude and unreliable, and modern biochemical research methods, particularly those using radioactive tracers, have not been applied.[1]

In the present work the following method was used for the quantitative extraction and isolation of chemically pure glycogen from dog skin: the skin was lyophilized and ground to a powder which was then defatted, digested with hot 30 per cent KOH, dialyzed and deproteinized with ten per cent trichloroacetic acid. The supernatant was dialyzed, and transferred to a Dowex-1 ion exchange column to remove mucopolysaccharides. In the effluent solution glycogen was precipitated with alcohol. Chemical purity was tested by spectrography of the glycogen-iodine complex, optical rotation, phosphorylase degradation, β-amylase degradation and elementary analysis. All these data were in the range of those obtained from a pure liver glycogen preparation (Table 1). The amount of glycogen thus found in the skin was around 30 mg per 100 g dry weight, which is only 1/10 to 1/5 of the amounts previously reported.

In the last few years it has become possible to perfuse the skin of dogs in the same manner that liver, kidney and adrenal glands are being perfused. The inner surface of the thigh of the dog has a saphenous artery, the cutaneous branch of which has very few minor muscular branches and these can easily be tied off. This cutaneous artery and the saphenous vein can be cannulated, and the skin supplied by the artery can be isolated and perfused under standardized experimental conditions.[7] Metabolism in the isolated perfused skin has been maintained for eight hours at 37°C and 100 per cent humidity.[8]

This preparation was utilized to study glycogen synthesis in the skin by perfusing it with uniformly labeled C^{14} glucose. Two hundred experiments were carried out with perfusion of

*This report is abstracted from the dissertation presented by K. Adachi in partial fulfillment of the requirements for the degree of Ph.D. in Biochemistry, University of Yokohama. It will appear in the J. Invest. Dermatol.

†Present address: Department of Biochemistry, Yokohama University School of Medicine, Urafune-cho, Minami-ku, Yokohama, Japan.

Table 1

IDENTIFICATION AND PROOF OF PURITY OF CUTANEOUS GLYCOGEN

	Glycogen from liver	Glycogen from skin
Absorption of glycogen-iodine complex	470-515 mμ	490 mμ
Optical rotation $[\alpha]_D$	185-200	189-194
Phosphorylase degradation	30 ~ 40%	27-41%
β -amylase degradation	41 ~ 59%	48-51%
Elementary analysis	C 44.48 H 6.22 N none Ash none	C 44.5 H 6.45 N none Ash 0.4%
Sedimentation coefficients S_{20}(corr.) x 10^{-13}	44-94	38-53
Sedimentation pattern	Single peak polydisperse	Single peak polydisperse

20 μc of C^{14} glucose in saline, in saline containing 0.1 per cent unlabeled glucose and in heparinized dog blood respectively. In all these experiments radioactive glycogen could be isolated from the skin in chemically pure form after perfusions lasting not longer than two and one-half hours.

In one series of experiments the skin flap of one thigh was perfused with blood and that of the other thigh with saline which, in addition to labeled glucose, contained cold glucose to bring the final concentration of total glucose up to 100 mg per cent corresponding with the glucose level of blood. Three dogs were perfused in this way under standardized conditions with perfusion of 0.20 μc in 150 ml perfusion fluid in 30 minutes.

The results are given in Table 2 which shows that the specific activities of glycogen were greater by a factor of about four after perfusion with blood than after perfusion with saline-glucose. Under controlled conditions, the results were consistent.

Table 2

INCORPORATION OF C^{14} GLUCOSE INTO GLYCOGEN IN PERFUSED SKIN UNDER STANDARDIZED CONDITIONS

	Perfusion with glucose-saline cpm/mg	Perfusion with blood cpm/mg
Dog #29	720	3960
Dog #31	710	4120
Dog #33	970	3830

Degradation experiments on the radioactive cutaneous glycogen with β-amylase showed that after blood perfusion with C^{14} glucose, the specific activities of outer and inner tiers were

approximately equal, indicating true biosynthesis of glycogen in the skin. After saline perfusion, in the majority of experiments, mainly the outer branches were found to be labeled with an average relation of specific activities in outer to inner tiers of 3:1 (Table 3). In a few experiments epidermis and dermis were separated after perfusion and the radioactivity of glycogen was estimated separately in the two layers. After blood perfusion the specific activities were about equal in epidermal and dermal glycogen (Table 4).

Table 3

DISTRIBUTION OF RADIOACTIVITY MEASURED BY β-AMYLASE DEGRADATION

(Specific activity of inner tiers taken as 1. The figures indicate specific activity of outer tiers.)

Perfusion with	Number of samples	Average	Range
Saline	6	2.8 ± 1.26*	1.0 ~ 4.1
Blood	10	0.86 ± 0.53*	0.4 ~ 2.0

*Standard error of mean.

Table 4

UPTAKE OF GLUCOSE INTO GLYCOGEN BY EPIDERMIS AND DERMIS

Sample number	Epidermis (cpm/mg)	Dermis (cpm/mg)
1*	277	203
2*	638	740
3*	512	583
4*	1,030	1,120
5†	4,460	4,010
6†	2,800	2,450

*Perfusion of 20 μc of C^{14} glucose in 0.1 per cent glucose-saline solution for 30 minutes.

†Perfusion of 20 μc of C^{14} glucose in blood for 30 minutes.

Glucose incorporation into the glycogen molecules was also studied as a function of time in three modified perfusion experiments. The skin was first isolated and perfused with 20 μc of 0.1 per cent glucose-saline solution. Proximal, distal and central portions, each representing approximately 1/3 of the perfused flap were then removed at 15 minutes, 30 minutes, and one hour respectively after the beginning of perfusion while perfusion was continued at the same rate. The specific activity of each sample in three such perfusions was analyzed. The results are graphically represented in Figure 1 and show a linear increase of incorporation up to one and one-half hours.

X-rays were used to study cutaneous glycogen after experimental depression of cellular metabolism. One thigh of the dog was irradiated in vivo with a Maxitron 250 machine, 800 r, 250 kv, 30 ma and 1 mm Al filtration, a dose corresponding to an "erythema dose" in the dog.[9]

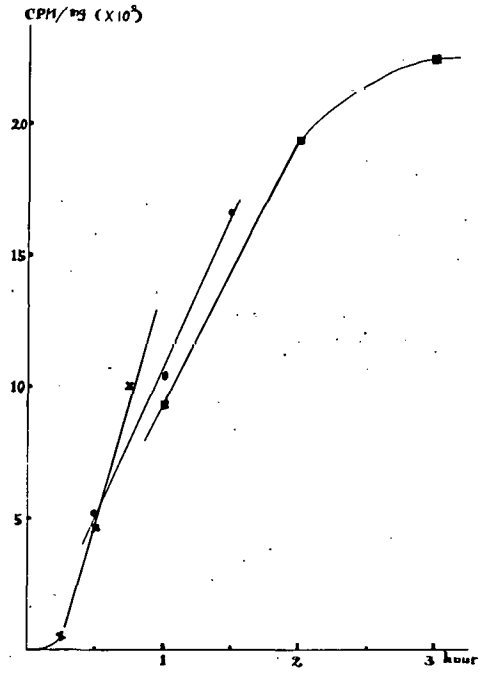

Figure 1. Incorporation of C^{14} glucose into skin glycogen as a function of time.

Twenty-four hours later, the skin flaps of both irradiated and non-irradiated thighs were perfused under identical conditions. Glycogen was isolated from both sides and specific activities were counted. Seven such experiments were performed. In all experiments the radioactive uptake into glycogen per milligram was found to be significantly greater on the irradiated side by an average of 85 per cent (Table 5). Remarkably enough, the increased glucose uptake was not associated with an absolute increase in glycogen content.

The time relations of the increase of glucose uptake into glycogen after x-ray irradiation was also investigated. Figure 2 shows that this increase starts 18 hours after irradiation reaches a maximum approximately at 24 hours and lasts for about 24 hours longer.

In four dogs the activity of phosphorylase and of UDPG-glycogen synthetase were compared on the irradiated and non-irradiated skin of the thighs. The irradiation was given 24 hours prior to perfusion. Phosphorylase activity was weaker on the irradiated side in all animals by an average of 20 per cent. The synthetase activity was assayed with an UDPG substrate labeled with C^{14} in the glucose moiety.[10] This activity was enhanced in the irradiated skin in all experiments by an average of 23 per cent (Table 6). Thus it appears that a dysbalance of phosphorylase and synthetase activities, brought about by radiation, disturbs the dynamics of glycogen metabolism.

The effect of x rays on the UDPG-glycogen synthetase of the skin was tested also in mice one, two, three, four, five and seven days after irradiation with one skin erythema dose. A progressive increase of synthetase activity was observed up to three days following irradiation with a gradual return to pre-irradiation values seven days after irradiation (Figure 3).

Recently we found that ultraviolet irradiation with a hot mercury vapor lamp may have a

Table 5

EFFECT OF X-RAYS ON INCORPORATION OF C^{14}-GLUCOSE INTO GLYCOGEN

A single dose of 800 r (250 kv, 1 mm A1, 30 ma) was given to one thigh 24 hours prior to perfusion.

A: Perfusion with saline plus C^{14}-glucose (20 μc),
B: Perfusion with blood plus C^{14}-glucose (20 μc).

	Non-irradiated skin (glycogen cpm/mg)	Irradiated skin (glycogen cpm/mg)	% increase
A.	36,900	68,200	82
	28,700	61,500	114
	26,600	49,200	85
B.	4,110	5,580	36
	2,290	3,680	60
	5,130	11,730	115
	4,730	11,440	140
			Ave. 90.3 ± 13.1*

*Standard error of mean.

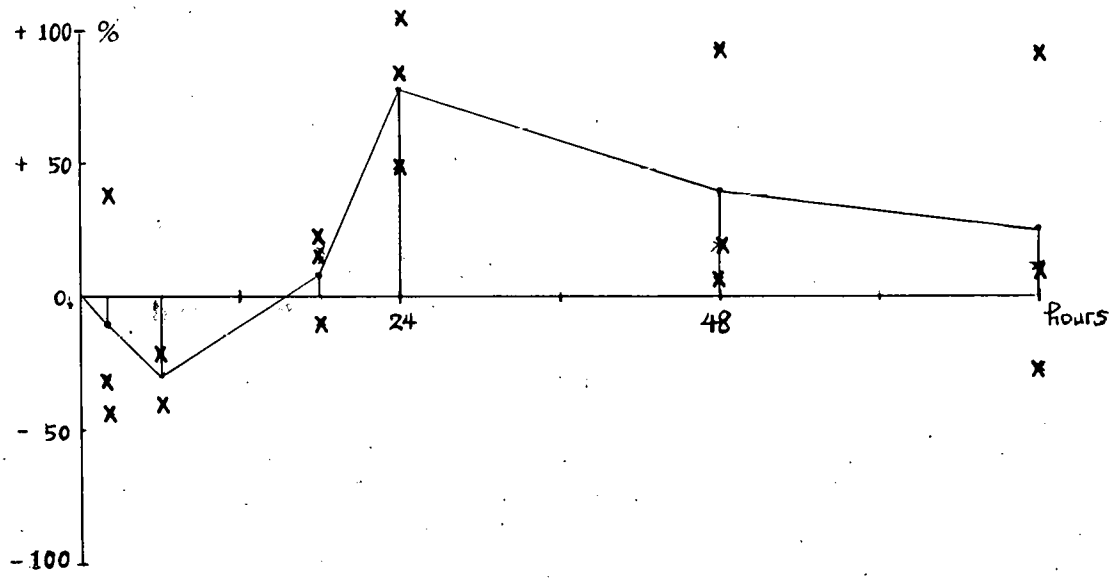

Figure 2. Effect of x rays on incorporation of glucose into skin glycogen: One thigh of the dog was irradiated with one erythema dose of x rays, prior to the perfusion experiments at different times. The non-irradiated thigh was used as control. Changes in specific activity of newly-formed glycogen in irradiated and non-irradiated skin were compared. Values are expressed as percentage ratio of specific activities of glycogen of irradiated and control sides.

Table 6

EFFECT OF X-RAYS ON PHOSPHORYLASE AND UDPG-GLYCOGEN SYNTHETASE

A single dose of 800 r (250 kv, 1 mm Al, 30 ma) was given to one thigh of dog 24 hours prior to the assay.

A: Phosphorylase activity, expressed as mμ moles/min/mg protein.
B: UDPG-glycogen synthetase, mμ moles/hr/mg protein.

	Non-irradiated skin	Irradiated skin	% increase (+) or decrease (-)
A:	24.5	16.5	-32.6
	32.9	23.6	-28.3
	16.4	14.0	-14.6
	16.1	14.5	- 9.9
			Ave. -21.4 ± 5.4*
B:	45.1	59.8	+32.6
	51.9	57.1	+10.0
	31.3	39.7	+26.8
	65.0	79.4	+22.2
			Ave. +22.9 ± 7.8*

*Standard error of mean.

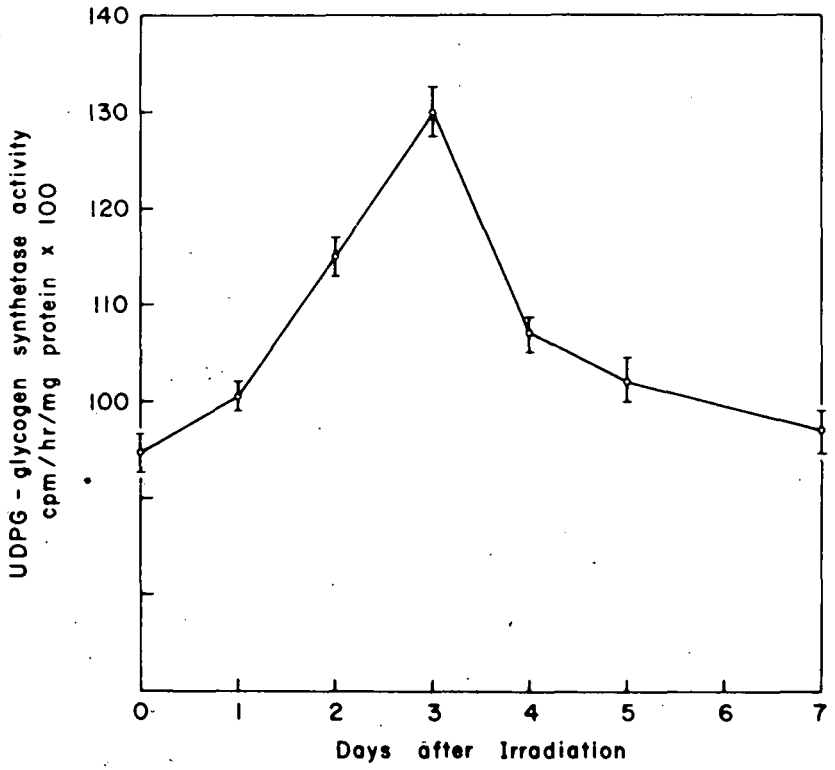

Figure 3. A single dose of 550 r (75 kv, 10 ma, no filtration) was given to the clipped back of CF No. 1 albino mice. UDPG synthetase was assayed on other homogenates according to Steiner, et al.[10]

similar effect to x rays if the skin is analyzed 24 hours after irradiation with a minimal erythema dose, but these results have not been consistent.

Experiments with an UDPG substrate labeled with C^{14} in the glucose moiety indicate that the UDPG pathway is the main route of glycogenesis in the skin. The in vivo synthesis of glycogen from labeled glucose and the in vitro synthesis of glycogen from labeled UDPG by the skin are of the same order of magnitude.

In histochemical studies of human skin performed in cooperation with the Biology Department of Brown University,[11] phosphorylase and UDPG-glycogen synthetase were found in the same sites, viz., eccrine glands, hair follicles, muscle, and epidermis.

LITERATURE CITED

1. For a review of available data, see S. Rothman, Physiology and Biochemistry of the Skin, University of Chicago Press, Chicago, 1954, p. 465.
2. Sundberg, C. Ztschr. f. Anat., 73:168, 1924.
3. Gualdi, A., and N. Baldino. Riv. di. pat. sper., 5:318, 1930; Yuyama, H., Jap. J. Dermatol. and Urol., 37:134, 1935; Shelley, W. B., and H. Mescon, J. Invest. Dermatol., 18:289, 1952.
4. Lobitz, W. C., Jr., and J. B. Holyoke. J. Invest. Dermatol., 22:189, 1954.
5. Bradfield, J. R. Nature, 167:40, 1951.
6. Montagna, W. The Structure and Function of the Skin, New York: Academic Press, Inc., 1956, p. 211.
7. Kjaersgaard, A. R. J. Invest. Dermatol., 22:135, 1954.
8. Bell, R. L., R. Lundquist, and K. Halprin. J. Invest. Dermatol., 31:13, 1958.
9. Pommer, A., and W. Mähling. North Amer. Veterinarian, 18:54, 1937.
10. The authors are greatly indebted to Dr. Donald F. Steiner, Department of Biochemistry, University of Chicago, for his advice, supervision of this work, and for supplies of radioactive UDPG preparation and other reagents. Concerning methodology, see D. F. Steiner, V. Randa, and R. H. Williams. J. Biol. Chem., 236:299, 1961.
11. Adachi, K., W. Montagna, and S. Rothman. To be published.

DISAPPEARANCE RATE OF NORMAL BACTERICIDINS IN IRRADIATED MICE*

By

L. Kornfeld† and C. P. Miller

An earlier publication from this laboratory[1] reported that normal serum bactericidal activity for a strain of Escherichia coli was lost within 9-12 hours after total-body exposure of CF No. 1 mice to a midlethal dose of X rays and remained absent for about 10 days. The disappearance of bactericidins could not be associated with development of an inhibitor demonstrable in vitro or with in vivo absorption by enteric microorganisms through the damaged intestinal mucosa.

The rapidity of the loss of bactericidins indicated that their production was promptly interrupted by irradiation and that they must have a very short biological half-life. Recent findings suggested that a block in the synthesis of bactericidins develops after x-ray exposure.[2] It is the purpose of this communication to show that normal bactericidins for E. coli disappear very quickly after passive transfer in irradiated mice.

MATERIALS AND METHODS

CF No. 1 mice were exposed to 500 or 700 r total-body x-radiation‡ and were used on the following day when no serum bactericidal activity was demonstrable. They were injected intravenously via a tail vein with pooled mouse sera of known bactericidin titer and exsanguinated at intervals thereafter. Bactericidal tests were performed with sera from individual mice. Briefly, the test consisted of mixing serially diluted mouse serum, rabbit complement and a suspension of E. coli. After incubation at 37°C, the number of microorganisms present in each tube was determined either by plating aliquots on eosin-methylene blue agar and making colony counts or by adding 5 volumes of nutrient broth and continuing incubation until the complement control became turbid. At that time, the presence or absence of turbidity in all other tubes was recorded. These readings closely paralleled the results obtained by plate counts. The reciprocal of the highest dilution of serum showing bactericidal activity was recorded as the titer. Details regarding animals, irradiation factors, bleeding and assay of bactericidins have been reported.[1] In one series of experiments, preinjection plasma samples were obtained from each mouse by a slight modification of the orbital bleeding technic described by Riley.[3]

Immune sera for sheep cells were obtained from CF No. 1 mice given 1 ml of a 1 per cent suspension of washed sheep erythrocytes intraperitoneally 12-13 days earlier. For hemagglutination tests, equal volumes (0.1 ml) of serial 2-fold serum dilutions and 1 per cent washed sheep cells were mixed and allowed to stand at room temperature for 30 minutes. The tubes were then centrifuged for 5 minutes at 1000 rpm and gently shaken. The reciprocal of the high-

*This paper appears in Proc. Soc. Exptl. Biol. and Med., 107:590, 1961. The work was supported in part under U. S. Atomic Energy Commission Contract No. AT (11-1)-46.

†Present address: Scripps Clinic and Research Foundation, Division of Experimental Pathology, La Jolla, California.

‡The authors wish to thank Mr. James Bland for irradiating the animals.

est dilution of serum showing agglutination distinctly visible to the naked eye was recorded as the titer.

EXPERIMENTAL

Disappearance of normal bactericidins following a single intravenous injection. One day postirradiation, mice were injected intravenously with 0.25 ml of mouse serum having a bactericidin titer of 128. Control mice were given 0.25 ml of negative serum (titer < 2). Table 1 lists the titers of the recipients' sera at various intervals after injection. Bactericidins were not demonstrable in sera of uninjected mice or of those given negative serum. They were present in the circulating blood for a short time after injection of positive serum but were lost so rapidly as to be undetectable 20 minutes later.

Table 1

DISAPPEARANCE OF PASSIVELY TRANSFERRED BACTERICIDINS AFTER A SINGLE INTRAVENOUS INJECTION*

Serum injected 0.25 ml	Bleeding time min. after injection	No. mice tested	No. of mice with titer of:							Geometric mean titer
			< 2	2	4	8	16	32	64	
Positive (titer 128)	1	20		2		2	9	4	3	17.1
	10	6				2	3	1		14.2
	15	6	3			1	2			
	20	6	6							
	30	10	9		1					
	45	3	3							
	60	8	8							
	120	3	3							
Negative (titer < 2)	1	11	11							
	10	6	6							
	30	3	3							
	60	3	3							
None		18	18							

*Mice were exposed to 500 r 24 hours before injection.

Disappearance of normal bactericidins following a second intravenous injection. To rule out the possibility that the rapid disappearance of bactericidins might be due to equilibration between intravascular and extravascular fluids, a second intravenous injection of bactericidal mouse serum was given 30 minutes after the first. The results of 5 separate experiments are summarized in Table 2. After one injection, passively transferred bactericidins always disappeared within 30 minutes. After two injections, passively transferred bactericidins had disappeared by 30 minutes in half of the animals, and by 60 minutes in all those tested. It is interesting to note that the mean titers of sera from mice sacrificed immediately after injection were essentially the same for both groups. In this series of experiments, a bleeding was obtained from each mouse before the first injection of serum. All initial plasma samples were devoid of bactericidal activity.

Disappearance of immune hemagglutinins after passive transfer. Dixon et al.[4] reported

Table 2

DISAPPEARANCE OF PASSIVELY TRANSFERRED BACTERICIDINS AFTER TWO INTRAVENOUS INJECTIONS 30 MINUTES APART*

No. of injections†	Bleeding time min. after injection	No. mice tested	No. of mice with titer of:						Geometric mean titer
			< 4	4	8	16	32	64	
1	1	17			3	12	2		15.3
	30	9	9						
2	1	12		1	3	4	3	1	16.0
	30	13	7	1	2	2	1		
	60	12	11	1					

*Mice were exposed to 700 r 24 hours before injection. All mice had preinjection titers of < 4.

†0.25 ml mouse serum (titer 128).

that the homologous gamma globulins (antibodies) had a half-life of 1.9 days in mice. This value differs considerably from our data on normal bactericidins. Consequently, disappearance rates of normal bactericidins and immune hemagglutinins were compared under identical experimental conditions. A mouse antiserum for sheep cells which was also bactericidal was given intravenously to irradiated mice. This serum had a hemagglutinin titer of 1024 and a bactericidin titer of 128. The recipients were sacrificed at intervals after injection and their sera were tested for the presence of both E. coli bactericidins and sheep cell agglutinins. The results are presented in Table 3. In this experiment, as in those described above, a loss of passively transferred bactericidins corresponding to about 3 serum dilutions occurred within 30 minutes. In contrast, 5 days were required for a comparable decline in sheep cell agglutinins.

Table 3

DISAPPEARANCE OF PASSIVELY TRANSFERRED BACTERICIDINS AND SHEEP CELL AGGLUTININS*

Bleeding time after injection†	No. mice tested	Bactericidins No. mice with titer of:					Hemagglutinins No. mice with titer of:					
		< 4	4	8	16	32	8	16	32	64	128	256
1 min.	5		1	1	3						3	2
30 min.	6	6									6	
6 hrs.	6	6									6	
1 day	6	6								6		
2 days	4	4							1	3		
3 days	4	4						1	1	2		
4 days	4								4			
5 days	3							1	2			
6 days	4						1	3				
7 days	4							4				

*Mice were exposed to 500 r 24 hours before injection. Uninjected mice had bactericidin and hemagglutinin titers of < 4.

†0.20 ml mouse serum (bactericidin titer 128; hemagglutinin titer 1024).

DISCUSSION

Taliaferro and Talmage[5] have pointed out that the half-life of antibodies should be calculated from disappearance rates after passive transfer, not from rates of antibody decline after immunization. Values based on the latter are generally too high as they reflect rates of synthesis as well as of decay. The same considerations apply if the half-life of naturally occurring antibodies is calculated from disappearance rates after whole body irradiation.[6]

In order to determine the rate of metabolic decay of normal bactericidins for E. coli, passive transfer experiments were carried out in irradiated mice whose sera were not bactericidal. Presumably, bactericidins were not synthesized during the period of observation, therefore their half-life could be estimated from the time of their disappearance after intravenous administration.

The data presented indicate that the half-disappearance time of homologous bactericidins after passive transfer in irradiated mice was a few minutes. Equilibration between intravascular and extravascular fluids accounted for the distribution of bactericidins immediately after intravenous injection, but not for their complete absence 20 minutes later. Estimating the plasma volume of a 25 g mouse to be 1.5-2 ml, 0.25 ml of intravenously injected serum would be diluted 6-8-fold. Thus, a serum of titer 128 should produce titers of approximately 16 in the recipients. Mice sacrificed 1 minute after injection of such a serum had mean bactericidin titers of 17.1 and 15.3 (Tables 1 and 2).

If the loss of bactericidins during the first 30 minutes after intravenous administration had been solely the result of equilibration, it should have been possible to prolong their survival considerably by reinjecting a bactericidal serum at the end of this interval. After the second injection however, bactericidins disappeared almost as rapidly as after the first.

Data obtained with the sheep cell immune serum provide additional evidence that the rapid disappearance of bactericidins is not due to equilibration. The initial dilution factors were the same for bactericidins and hemagglutinins. Thereafter, the half-disappearance times were a few minutes for the former and approximately 2 days for the latter.

Our findings with hemagglutinins are in accord with the results of Dixon, et al.[4] who reported that the half-life of homologous antibodies in mice was 1.9 days, and with those of Smith and co-workers[7] who studied passively transferred antisheep hemolysins.

Our data are consistent with the premise that the rapid disappearance of passively administered bactericidins in irradiated mice is due to metabolic decay. They do not, however, provide information on whether such decay is more rapid in irradiated than in normal mice. Hollingsworth[8] found that irradiation did not alter the rate of disappearance of passively transferred antibodies, but it is not known whether this holds true also for other serum proteins.

In an earlier publication[1] we reported that normal serum bactericidins for E. coli were lost 9-12 hours after total-body exposure of CF No. 1 mice to x-rays. The data presented here show that such bactericidins, when injected into irradiated mice, were lost in less than 1 hour. In other words, the disappearance of passively transferred bactericidins in previously irradiated mice was much more rapid than was the disappearance of normally circulating bactericidins from mice following their exposure to total-body irradiation. Similar observations on hemolysins in rabbits were made by Taliaferro and Talmage who found the mean half-disappearance time of rabbit antisheep hemolysins (large molecules), as determined by passive transfer, to be 2.8 days,[5] but that of natural hemolysins in irradiated rabbits to be 7 days.[6] If

a comparison may be made between hemolysins in rabbits and bactericidins in mice, the loss of normal serum bactericidal activity 9-12 hours after total-body exposure of CF No. 1 mice to 600 r[1] may be explained as follows: production of bactericidins is impaired shortly after irradiation, resulting in an overall rate of decline more gradual than in the absence of bactericidin synthesis. A few hours postirradiation, bactericidin production ceases altogether for approximately 10 days.

The authors are indebted to Dr. William H. Taliaferro for his interest in this work, and for many valuable suggestions.

LITERATURE CITED

1. Kornfeld, L., C. W. Hammond, and C. P. Miller. J. Immunol., 84:77, 1960.
2. Kornfeld, L., and C. P. Miller. Ibid., 86:215, 1961.
3. Riley, V. Proc. Soc. Exptl. Biol. and Med., 104:751, 1960.
4. Dixon, F. J., D. W. Talmage, P. H. Maurer, and M. Deichmiller. J. Exptl. Med., 96:313, 1952.
5. Taliaferro, W. H., and D. W. Talmage. J. Infect. Dis., 99:21, 1956.
6. Talmage, D. W., G. G. Freter, and W. H. Taliaferro. Ibid., 99:241, 1956.
7. Smith, F., M. M. Grenan, and J. Owens. J. Nat. Cancer Inst., 25:803, 1960.
8. Hollingsworth, J. W. Proc. Soc. Exptl. Biol. and Med., 75:477, 1950.

FROM PHANTOM TO ANALOG PATIENT*

By

S. W. Alderson,† L. H. Lanzl,‡ M. Rollins,** and J. Spira††

In recent years, considerable advances have been made in methods and materials for simulating many of the physical characteristics of the human body. In the field of radiotherapy, the simulated human body for dosimetry is called a phantom, and its purpose is to represent the energy absorption of ionizing radiations of the body. The simplest forms of phantoms are boxes containing water and solid materials whose density is equal to that of water. Radiation measuring devices are inserted into these preparatory to working out radiation treatment plans. Such homogeneous phantoms, however, do not accurately represent the structural differentiation of the human body.

More recently, phantoms have become available which contain such differentiation and which suggest the possibility of achieving an accurate and practicable patient analog. This paper describes a phantom developed for this specific purpose, followed by some preliminary studies in the new field of analog dosimetry.

Various pertinent methods of dosimetry are also discussed. It will be seen that a very substantial amount of research, development, and clinical testing lies ahead before a full-scale analog dosimetry system may be added to the armamentarium of radiotherapy; however, within certain restricted limits, analog dosimetry has now become a practical tool for the radiotherapist.

Various forms of simple phantoms are presently in regular use for the derivation of the depth-dose tables and isodose curves which are basic to treatment planning. These data are used to compute specific treatments which can be administered to the patient. Although data for patient entrance and exit doses are available, as are occasional intracavitary measurements, detailed systematic distribution measurements within the body of the patient are limited. As a result, a generalized distribution produced within a simplified and usually homogeneous phantom becomes the foundation upon which a patient of complex and non-homogeneous composition is irradiated at a different place and with different equipment than was used for the original phantom dose distributions.

It is not surprising that many studies[1,2] show a variety of substantial errors between depth-dose data and their final utilization within the patient. There are many sources of error, including uncertainties in the basic data, in machine calibration and output, in computation, in

---

*Another version of this paper has been accepted for publication in the Am. J. Roentgenol., Rad. Therapy, and Nuclear Medicine under the title "An Instrumented Phantom System for Analog Computation of Treatment Plans."

†Alderson Research Laboratories, Inc., New York City, New York.

‡Department of Radiology, University of Chicago, and Argonne Cancer Research Hospital.

**Radiotherapy Departments, Lutheran Hospital and Western Reserve University, Cleveland, Ohio.

††Radiotherapy Department, Montefiore Hospital, Bronx, New York.

inadequate correction for bone, air, and fat, in positioning, and so on.

A basic source of error is the difference between data usually taken in a homogeneous phantom under research conditions, and their later application to a patient. It is obvious that every diminution of the gap between phantom and patient will decrease the chain of potential error and reduce the burdens of computation. If, for example, a depth-dose table were derived under the conditions of a given treatment, and using the same therapeutic apparatus, variations due to beam quality and machine output would be decreased substantially as error sources.

If the structure and composition of a phantom could be brought into much closer correspondence with a specific patient, the number of cumulative errors would be substantially reduced. If such a phantom included ample and flexible provisions for dosimetry, it would be possible by first ascertaining the actual dose distribution for a given treatment plan within the phantom, then empirically correcting it to obtain an optimal distribution, and finally applying it directly to the patient, to obtain an appreciable increase in accuracy. Thus almost all dosage, beam direction, and field selection problems could be worked out in the phantom, and laborious and complex computations would be replaced by direct observation of specific treatments. The phantom might then be regarded as an analog to the patient, and treatment planning might be replaced by analog dosimetry.

BACKGROUND FOR PHANTOM DEVELOPMENT

A number of basic criteria were established for the design of the first analog phantom.

a: It must include natural bone, and materials equivalent to soft tissue and lung tissue. Fat could be considered at a later time.

b: It must have a composition such that the absorbed dose corresponds accurately to that in the human body over the entire range of x-ray and electron energies in therapeutic use.

c: It must be compatible with systems of dosimetry in general use by radiotherapy departments.

d: It must be rugged and serviceable; it must be capable of placement upon a treatment table in a variety of standard positions.

e: It must be constructed by production processes.

The problem of correspondence to a broad range of patients was reserved for later consideration. Existing phantoms were now surveyed on the basis of these criteria.

MATERIALS FOR PHANTOM CONSTRUCTION

Bone. Natural human skeletons were found to be indispensable; plastic skeletons were available commercially, but their specific gravities were of the order of 1.1 rather than the 1.8 - 1.9 range of the human skeleton. Efforts were made to compact plastic materials to achieve the required specific gravity, but sintering methods were necessary, and extremely high costs of molds forced the rejection of this approach.

It was found that available skeletons had frequently been contaminated in the course of preparation, particularly with sodium from bleaching compounds. When we specified the processing methods, skeletons were obtained in a dried, but uncontaminated condition. Restoration to the radioabsorptivity of living bone required vacuum impregnation with a soft tissue equivalent material, perhaps adjusted for the fat content of yellow marrows and oils.

Soft tissues. Water is a commonly used material, and water solutions can be chemically

equivalent to composite soft tissues of the body. Formulae of tissue-equivalent solutions were derived by Langham[3] and others. Pure distilled water, however, has an effective atomic number for absorption of ionizing radiation of 7.42, and a specific gravity of 1.00. This makes it equivalent to muscle tissue in regard to absorption.

Two general types of phantoms are those filled with liquids and those made of solid materials. Open, geometrically regular tanks are obviously unsuited for analog dosimetry. Liquid-filled, sealed structures with human contours could be considered. One such phantom was developed by Rundo[4] on a laboratory basis for specific research purposes; another was produced for commercial use under the trade name REMAB. Considerable field experience with the latter indicated that structural stability could be attained, but it was difficult to utilize it for the measurements needed in radiotherapy, although pre-selected dosimetry points could be provided readily. Water or other liquids have the general disadvantage, moreover, of limiting dosimetry to instruments which can be immersed without leakage or other adverse effects.

For the construction of solid phantoms, one of the most common materials now being used regularly is "Presdwood," which has an effective atomic number and a specific gravity close to that of water. However, since this is essentially a building material, it is not controlled closely for these characteristics, which therefore vary considerably. It is obtained commercially in sheet form and then sawed into laminations for assembly into phantoms.

An important defect of Presdwood is the difficulty of inserting skeletons into such phantoms. This procedure was actually carried through by Laughlin,[5] but the processes involved were extremely laborious and not suited to production methods.

A number of powdered materials had been developed, such as a mixture of rice flour and sodium bicarbonate by Spiers,[6] but for practical purposes such materials introduce problems similar to those encountered with water, except that water absorption and infestation replace instrument leakage as problems.

The field of cast plastics appeared to offer the most promise. A number of formulations suitable for use in a phantom have been developed. One of the best known of these is Mix-D, developed by Jones and Raine,[7] which is based upon polyethylene and wax, and uses high-Z materials to adjust to the effective atomic number. A reasonable phantom might be developed using this formulation, but better mechanical properties were thought desirable. Mix-D is a thermoplastic, and subject to softening under local heating, and to cold-flow distortion under stress. It is also subject to cracking, chipping, and fracturing.

A material had been developed by Alderson[8] which is based upon a thermo-setting isocyanate compound, and adjusted by physical and chemical processing to the effective atomic number and specific gravity of soft tissue. This had been used in the Picker-Alderson Pelvic Phantom for diagnostic x-ray applications. The material is essentially a tough, hard rubber, similar to that used for rubber heels. It is dimensionally stable, resistant to chipping, abrasion, and laceration, and can be readily restored if holes are drilled or cuts made in a phantom for special research purposes. This material, designated as TEP-7, was taken as the starting point of the development.

Fat. For fat, Spiers[9] gives values of 5.6 - 5.92 for effective atomic number and 0.90 - 0.91 for specific gravity. Polyethylene has values of 5.42 and 0.92 - 0.95, respectively. With very minor modifications, this could serve as a fat-equivalent material.

CONSIDERATIONS IN MECHANICAL DESIGN OF A PHANTOM

Anthropometry. Anthropometric considerations include the method of selecting the body form of a proper population group. In the construction of a phantom to serve as an analog for as broad a population as possible, many new complications emerged. Medians for the human race are not available, and they would be of questionable significance in any event. An analog phantom must correspond to a patient within certain undefined, but probably narrow, limits in size and contour; the range might be extended by correction factors, but these would have to be minor if the basic philosophy of analog dosimetry was to be maintained. Multiple-size or matching techniques would be required. Thus, the principal effect of a truly global anthropometric mean would merely be to modify to a slight degree the range of the patient-matching problem.

A second difficulty lay in the treatment of body fat, variations in the amount of which can be as great as 25 to 1 among otherwise normal individuals, as reported by Damon et al.[10] Thus, fat matching is a problem for normal body fat deposits, and new techniques have to be developed.

Essentially, then, an anthropometric standard for the first phantom was not a critical issue. An "average man" was taken from a United States Air Force study,[11] and modified to correspond in over-all stature (5 ft. 8 ins. or 1.73 meters, weight 162 lbs. or 73.5 kg) to a civilian population of railroad travelers as reported by Hooton.[12]

Articulations. Prior work by Alderson[13] had shown that articulations were severely disturbing factors in achieving accurate and artifact-free phantoms. Although of some limited utility in certain therapeutic positions, articulations would have introduced maximum error in such cases. A rigid phantom was therefore chosen.

Appendages. Since radiotherapy is concerned to an overwhelming degree with the head, neck, and trunk, the phantom was terminated at the shoulders, enclosing the full scapulae. The upper thirds of the thighs were included, with a guillotine cut at that level to establish a square base.

Access for dosimetry. Dosimetry systems must be capable of being installed readily anywhere with the phantom. Pre-selected dosimetry points, such as those used in the REMAB phantom, were unsuitable here. A transversely sectioned phantom appeared most flexible for this purpose.

Presdwood phantoms based on this principle have been used widely for both film and ion chamber dosimetry, film sheets being clamped between segments, and ion chambers inserted in holes or ducts. One convenient approach, used by Laughlin[5] but not adopted in our system, was based on drawers inserted into the phantom. The principle of transverse sectioning was regarded as the most reasonable approach.

The problem of segmentation. There were two choices to be made in the construction of a segmented phantom: either to segment the skeletons and mold them into discrete transverse phantom slabs, or to mold a complete phantom with an intact skeleton inserted, and subsequently saw it into slabs. Both procedures present many technological difficulties, but experimental work soon demonstrated that the latter approach could be organized on a production basis. Presegmentation of the skeleton did not seem adaptable to any reasonable production procedure.

DOSIMETRY SYSTEMS

The precise determination of the optimal dose distribution within the phantom for the proper planning and carrying out of a treatment course is the essential purpose of the analog.

The importance of a knowledge of the absorbed dose was first pointed out by T. Christen (1914-1915) and remains a central problem in radiotherapy. Skin erythema was used in the early years, and is still used widely as a qualitative indicator of dose. Its application is crude and highly inadequate, and cannot be applied to such techniques as moving field and multiple cross-fire therapy, which have high tumor-to-skin dose ratios. Moreover, the build-up effect has rendered skin erythema useless as an indicator in supervoltage therapy, sometimes with serious consequences, as reported by Paterson.[14]

Instead, detailed and precise quantitative data at many points within the patient's body are required. A common starting point for treatment planning is a body cross section which passes through the tumor, although this gives no information about dose distributions in planes above or below this section.

Two to three cross sectional planes passing through various levels of the tumor would appear to be desirable and practicable in analog dosimetry. An optimum treatment requires that the minimum tumor lethal dose be achieved within the tumor area in each plane, without "hot" spots or "cold" spots. The maximum isodose curve should be well within the area of the tumor in order that dose to normal tissues be minimized. Hemopoietic tissues, the spinal cord, scar tissue, the rectum, and other sensitive tissues should, of course, receive minimal doses, and the integral body dose should be as small as possible.

These requirements indicate the need for multiple points for dose measurement, and a high degree of flexibility in the location of these points. An initial survey of various possibilities was made, bearing in mind the problems associated with their clinical use.

The general dosimetry requirements for phantom measurements are as follows:

(1) A given dosimeter or group of dosimeters should have a small volume to insure a minimum distortion of the radiation field due to its presence in the phantom.

(2) It should be capable of being calibrated for a given energy of radiation within the phantom so that it registers absorbed dose, i.e., energy absorbed per unit mass of the material in question. If this is not possible, the dosimeter reading should be capable of simple conversion to absorbed dose. In most cases, it is adequate to calibrate the dosimeter in muscle or muscle-equivalent tissue, since, in general, tumors are composed of soft tissue.

(3) The dosimeter most generally useful in phantom work is of an integrating type. In a single fixed-field irradiation, a dosimeter which measures dose rates is frequently used. This is often done in the measurement of isodose curves in simple water phantoms, where an ion chamber is moved about within the water while a fixed beam irradiates the field. Rate dosimeters are not called for in cross-fire and especially in moving-field dose determinations. In these cases, the dosimeter must be confined to a fixed position within the phantom to "add up" the dose delivered to that given point.

(4) The dosimeter should be wavelength- or energy-independent, as far as possible, to give a proper reading for both the primary radiation and any secondary or degraded radiation which reaches the point where the measurement is being made.

(5) The dosimeter should be of high reliability, rugged in construction, stable in its radiation response, and easy to use and read.

(6) The dosimeter response should be independent of dose rate. With some radiation sources, the radiation is emitted in short bursts or pulses. Under this mode of radiation, also, dosimeters should be capable of giving a true reading of the total dose.

In principle, the most direct method of measuring absorbed dose (in rads) is to measure the heat produced at points within the phantom, since most of the absorbed energy appears as heat. The type of dosimeter which comes to mind then is a calorimeter; but calorimeters are not suited for clinical work within phantoms, measurements with them being difficult and tedious.

In recent years, chemical methods of dosimetry have gained wide use in the measurement of absorbed dose. Chemical dosimeters[15] are of an integrating type and cover the range of doses useful in therapy, including single doses as well as total treatment doses. They are in liquid form, require glass-like containers, and can be calibrated directly on an absolute basis. However, their usefulness for routine clinical work is limited because of a relatively short shelf life and because of the detailed chemical precautions and procedures which are required.

More amenable for our purpose are such dosimeters as ionization chambers, solid-state detectors of the radiophotoluminescent type, and photographic film.

Ionization chambers. The use of ionization chambers for radiation dosimetry goes back to the very early days of the discovery of x- and gamma radiation. The ability of radiation to ionize air, or any other gas, with subsequent measurement of the amount of ionization produced, is the principle on which this dosimeter is based. The impact of ionization methods for radiation measurement becomes evident when one realizes that it was through this type of detector that the concept of exposure dose, with its unit of measurement the roentgen, came into being and continues to play a leading role in patient dose prescription.

The use of ion chambers with phantoms has been the subject of many studies. The central axis depth-dose curves in water which are available in numerous present-day books on radiation therapy were derived almost exclusively from ionization measurements, either in water or water-like phantoms. Ionization chambers and their concomitant electronic circuits can be used as rate dosimeters or as integrating types.

For use in a phantom, ion chambers should be small in size. Some presently available commercially, for example, have dimensions of the order of 5 mm x 2 cm.[16,17]

The integrating ionization chamber is first charged electrically by means of an external charger-reader device. Following irradiation in the cavities provided within the phantom, the chambers are removed and the final electrical potential is read, the difference in potential being a measure of the dose received. The absorbed dose can then be determined from the ionization measurement by means of the cavity ionization relationship. In some instances, reading devices are calibrated in roentgens.

One common procedure in determining dose distributions in a phantom is to have a series of holes in the form of a lattice within the phantom, and to place a series of ion chambers within them. If a hole is not in use, it is filled with the phantom material. After a treatment plan (i.e., a single exposure, cross-fire fields, or a moving-beam field) has been carried out on the phantom, the dosimeters are removed, read, and the results plotted to give the isodose distribution. Among the many phantom studies using this technique is an especially careful one by Dahl and Vikterlöf.[18]

In a phantom which contains differentiated structures such as lung and bone, the final iso-

dose distribution may then be obtained directly, without recourse to correction factors.

Film dosimetry. The effect of x-rays and gamma rays in producing blackening of a photographic film is also used in dosimetry, the blackened film emulsion being measured with a photo-densitometer.

The optical density of the film exposed to radiation depends on the type and thickness of the film emulsion, on the energy of the radiation, development conditions, etc. The method of film dosimetry has been used extensively (Lanzl and Skaggs,[19] Loevinger and Spira,[20] and Dudley[21]).

The response of the film emulsion per roentgen of x-rays is practically independent of photon energy above 0.3 Mev. Below this energy, however, sensitivity increases sharply due to the photoelectric effect in silver at lower energies. If film is used in higher-energy ranges, where its response is equivalent to that of soft tissue, and if careful developing and calibration techniques are established, this is a very useful method. It has the advantage of occupying a very small volume of the phantom, and thus has a negligible effect on the original radiation field. Continuous data are available in the plane of the film, enabling one to make measurements at any set of points in that plane. It is possible to detect the presence of "hot spots" at a glance. An examination of dose distributions shows that significant changes can occur over very short distances, especially for small fields. These are not observable by means of ionization chambers unless extremely small spacings are used. Finally, film provides a permanent record of any given treatment plan.

Glass dosimetry. The newest type of dosimeter available for use within the phantom for the detection of x-rays, gamma rays, or high-energy electrons is based on the effect of radiophotoluminescence. Irradiation of the dosimeter material creates stable luminescent centers, which are believed to be caused by the trapping of high-energy electrons liberated by the radiation in ions within the dosimeter. The luminescence occurs upon excitation in the near ultraviolet region.

The luminescence of the glass, which has been exposed to radiation within the phantom, is read on a reader which contains the exciting near-ultraviolet lamp and the sensitive luminescence detector, which is in the region of orange light. Presently, several commercial readers are available.

One dosimeter using this principle is made of a silver-activated phosphate glass, discovered a little over a decade ago by Weyl, Schulman, Ginther, and Evans,[22] and now being tested and used in a variety of ways, including clinical evaluation of dose by interstitial placement in animals during experimental irradiation.[23]

The use of the glass dosimeters within a phantom has definite advantages. The glass pieces now being manufactured by Bausch and Lomb Company are small, and have the shape of right cylinders of 1 x 6 mm.

Two types of glass are being manufactured for this purpose: a so-called high-Z, i.e., high atomic number, and a so-called low-atomic number type.[24] In each case, the small size of the glass piece in relation to the size of the phantom means that its presence will perturb a radiation field very little. Thus, one can immerse a large number of the dosimeters in a lattice of small holes within the phantom.

PRESENT STATUS OF RESEARCH AND DEVELOPMENT

Two prototypes of a phantom analog were completed in October, 1960 and have been utilized extensively in research into the methods of analog dosimetry. Inadequate control of specific gravity and effective atomic number in these initial phantoms precludes presentation of the data derived from them. These preliminary phantoms served, however, to define and clarify many of the problems encountered.

The phantom shown in Figure 1 embodies many of the findings of this initial research. It also signals a significant step towards a practical system in that it has been manufactured by rational production methods.

This phantom is molded to the anthropometric standards discussed above. Skeletons are selected to fit in a reasonable manner within body contours, and jig-fitted to give normal intervertebral spacings and thicknesses of soft tissue over bony landmarks. The phantom includes lungs molded to a volume corresponding to a neutral respiratory state, the left lung being appreciably smaller than the right because of the heart-space allowance. The air content of the trachea, stem bronchi, and esophagus are reproduced (Figure 2). Considerable difficulty was

Figure 1. Complete phantom before splicing.

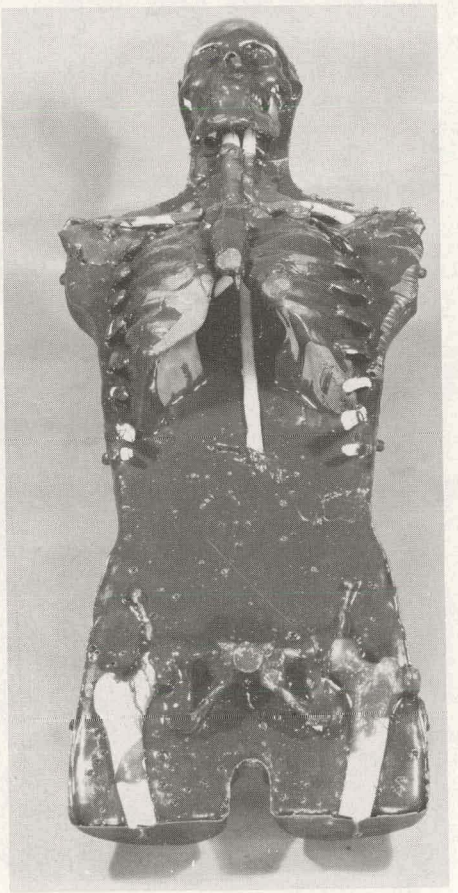

Figure 2. Partially completed phantom during manufacture. The skeleton and lung inserts are visible.

encountered in establishing optimal values for the effective atomic number and specific gravity of composite soft tissues, including fat. Most studies of the chemical content of the human body are based on an inadequate number of specimens,[10] and for optimum phantom standards (and hence, optimum treatment) considerable additional research will be needed. Data on The Standard Man of the International Committee on Radiological Units and Measurements[25] were used after deduction of dense bone constituents, yielding a value of 7.30 for effective atomic number and 0.986 for specific gravity. Processing controls were established to hold these values to within 0.50 per cent for the former and 1.25 per cent for the latter. Lung values were taken as 7.30 for effective atomic number and 0.3 for specific gravity.

Machine methods were developed for sawing the phantom into precise transverse slabs, a registration bed and indexing system assuring that cuts were made at closely corresponding levels on all phantoms. Representative "as-cut" slabs are shown in Figure 3. Approximately

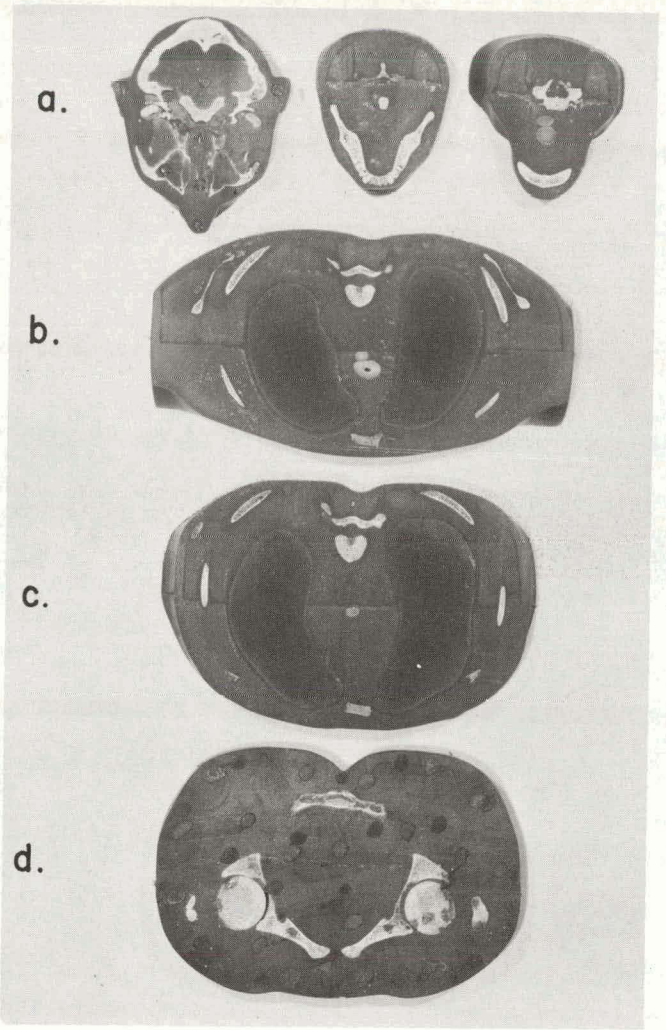

Figure 3. Sections of sliced phantom showing

a) Teeth and skull
b and c) Lung equivalents and bone in the thorax
d) Skeleton in the pelvis

0.035 in. of material is removed in the sawing operation, with only 0.018 in. restored in finishing operations to minimize soft-tissue coating over bones.

The slabs are vacuum-impregnated with TEP-7 to restore soft-tissue and marrow constituents of the bone, to establish flat, smooth surfaces which avoid air spaces when the slabs are clamped together, and to ensure uniform and intimate contact with films inserted at the interfaces. The impregnation process also creates a system of spherical bosses and recesses to register the slabs to each other in accurate alignment. The clamping device shown in Figure 4 is capable of receiving from one to all thirty-five slices as well as the base of the completed phantom. Rotation of the ribbed central wheel creates uniform tension in the nylon cords at each corner, assuring even clamping pressure. If x-ray cones must contact the phantom in the vicinity of a cord, one may be removed, and the system still remains stable.

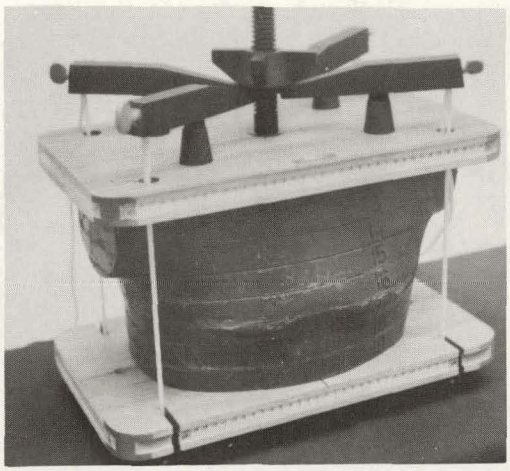

Figure 4. Sections of phantom held by clamping device. Nylon cords are used in tension to hold sections rigid during irradiation. Scales have been added to assist in reproducing phantom position under irradiation.

The phantom is designed around a coordinate system to facilitate the establishment of positional relationships on the treatment table and with the patient. Slabs are uniformly 2.5 cm thick to a level 2 cm above the crotch, while the top of the head is 3 cm thick.

The clamping device contains a series of registrations to match those of all slabs, so that any desired body section may be inserted readily. This device is so proportioned that the phantom's principal planes are always parallel to the plane of the treatment table.

Several radiographic views are shown in Figure 5. These include the skull and abdomen.

Provisions for ion chamber dosimetry. Two suitable types of miniature ionization chambers are available commercially, both of which may be inserted in 5-mm diameter holes drilled through the slabs. Injection-molded plugs of Mix-D can be used to close holes when chambers are not in use. Ion chamber holes may be drilled readily, so that additional chamber spacings may be added at will (see Figure 6).

Provisions for film dosimetry. Standards for loading, development, and read-out are be-

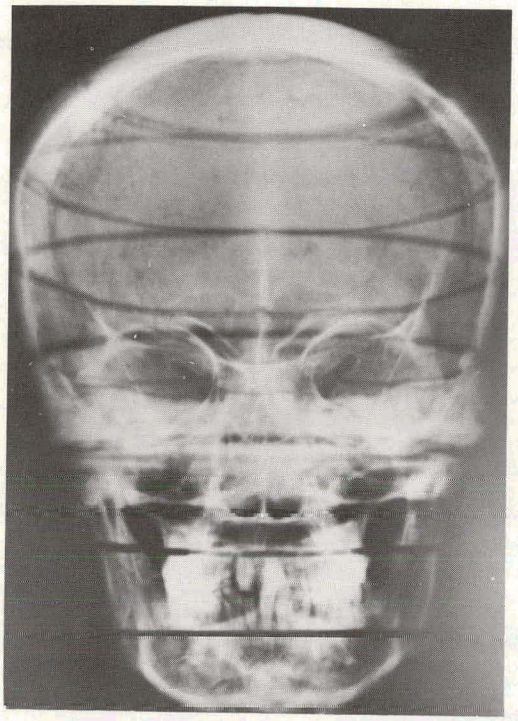

Figure 5a. Frontal view of skull of phanton.

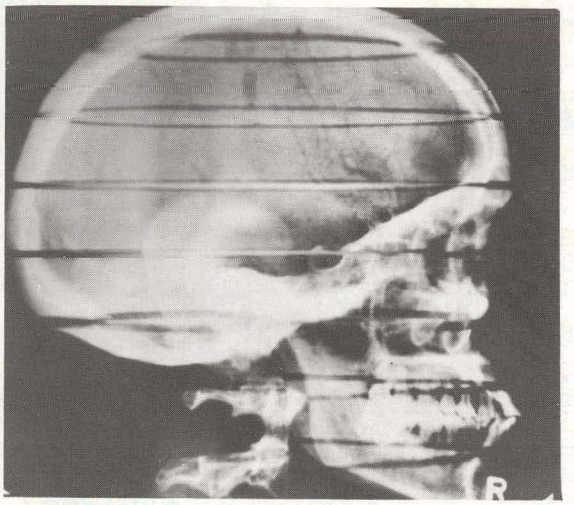

Figure 5b. Lateral view of skull of phanton.

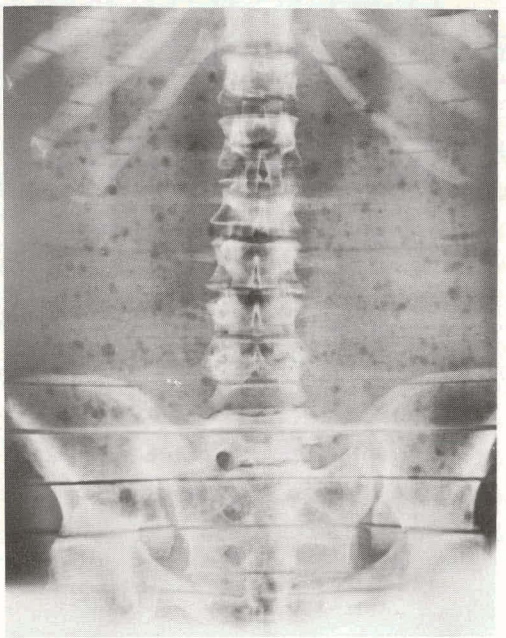

Figure 5c. View of abdomen (small air pockets are visible in first phantom).

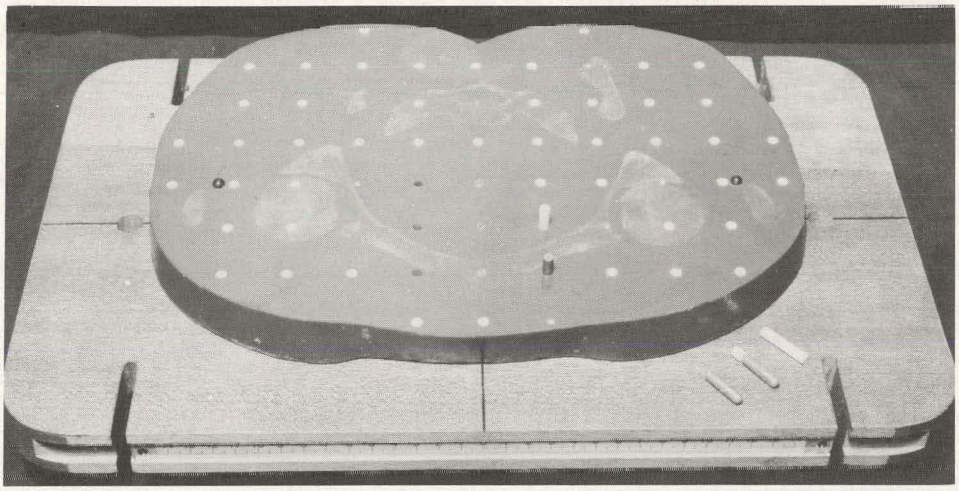

Figure 6. Section of phantom with holes drilled for ion chambers in a grid array. Some of the holes are filled with Mix-D plugs or Sievert ion chambers. In the lower right hand corner of the figure are a plug, an ion chamber and an ion chamber with a short Mix-D plug used to avoid an air gap.

ing established for a variety of commercial films of high dose capacity.

Variations in size, contour, and sex. Initial studies are being conducted to extend the analog range of this phantom by fat or muscle-equivalent build-ups to match the patient, or the converse. A female phantom is being processed, including specialized devices for conforming breasts to graded and interchangeable phantom standards and means for achieving analog dosimetry for a variety of radium applicators. Research is being initiated into the basic problems of multiple sizes.

CLINICAL APPLICATIONS OF ANALOG DOSIMETRY

Chief among the problems which beset the practitioner as he attempts to arrive at his ultimate determination for the treatment of each patient is the delivery of an absorbed lethal tumor dose with no complications or sequelae to the patient. An accurate preliminary determination of the exact dose that actually reaches the tumor, particularly tumors lying deep within the body, is of the first importance. The method of analog dosimetry holds forth the promise of solving this problem.

Another important application of analog dosimetry is in the use of tangential fields for the treatment of inoperable carcinomas of the breast, where the entire chest wall, breast, sternum, and internal mammary fields need to be irradiated. As every radiotherapist knows, tangential field therapy has never been worked out thoroughly, and there are few depth-dose charts or isodose curves which can be applied with any reasonableness.

In actual practice, one of the ways of circumventing this difficulty is to use ordinary isodose curves, with bolus material applied to the patient. In many instances, it is difficult to obtain an idealized bolus set-up. With analog dosimetry, however, the chest wall and breast could be conformed to the patient's chest wall and breast, and dosimetric measurements could be made in the necessary positions in the phantom breast, chest wall, and adjacent lung field. Any modifications necessary in the alignment or size of the fields to ensure homogeneity of the dose

throughout the tumor and to eliminate "hot spots" could then be made; this set-up could be transferred readily to the patient for the actual treatment.

In this way both patient and radiotherapist would be spared the pressures and discomforts of a long and tedious planning session.

Another example which well illustrates the need for an inhomogeneous human substitute is the treatment of carcinoma of the lung. Much information has been published on correction factors to allow for diminished absorption and scatter in lung. A perusal of such tables leads the reader to the inescapable conclusion that considerable error is likely to arise in estimating dose distribution within tumor and surrounding tissue, particularly when oblique or tangential fields are utilized. A much more precise dose distribution is attained by placing dosimeters within an accurate, patient-adjusted phantom, and actually measuring the doses from the various fields to be used. Corrections can then be made, and the final results, including beam alignment, readily transferred to the patient.

The above are but two examples of the many in which a phantom analog may be of great utility. Other problems that could be readily solved are the measurement of dosages for head and neck tumors located behind bone, and for tumors which require treatment by centered or off-centered arc or full rotation therapy.

An analog phantom is in no sense of the word a substitute for an astute clinical radiotherapist, but such a phantom has the potential for becoming an easily accessible and useful tool in every-day treatment planning for the clinical radiotherapist.

LITERATURE CITED

1. Report of the International Commission on Radiological Units and Measurements, National Bureau of Standards Handbook 78, 1961 (U. S. Government Printing Office, Washington, D. C.).
2. Martin J. H., E. A. Evans, and F. J. Anderson. Radiology, 75:552, 1960.
3. Langham, W. H. Private communication.
4. Rundo, J. Acta Radiol., 47:65, 1957.
5. Laughlin, J. S., M. L. Meurk, I. Pullman, and R. S. Sherman. Am. J. Roentgenol., Rad. Therapy, and Nucl. Med., 78:961, 1957.
6. Spiers, F. W. Brit. J. Radiol., 16:90, 1943.
7. Jones, D. E. A., and H. C. Raine. Brit. J. Radiol., 22:549, 1949.
8. From Heels to Wheels. DuPont Magazine. E. I. DuPont de Nemours and Co., Wilmington, Del., 21-23, November-December 1960.
9. Spiers, F. W. Brit. J. Radiol., 19:52, 1946.
10. Damon, A., H. W. Stoudt, and R. A. McFarland. To be published.
11. Hertzberg, H. T. E., G. S. Daniels, and E. Churchill. WADC Tech. Report 52-321, Wright Air Development Center, Wright-Patterson Air Force Base, Ohio, 1954.
12. Hooton, E. A., et al. A survey in Seating, Heywood-Wakefield Co., Gardner, Mass., 1945.
13. Alderson, S. W. Report to the Walter Reed Army Medical Center: Alderson Research Laboratories, Inc., June, 1959.

14. Paterson, R. The Treatment of Malignant Disease by Radium and X-Rays, London, England, Edward Arnold, Ltd., 1956.

15. Taplin, G. V. In Radiation Dosimetry, eds. Hine, G. J., and G. L. Brownell, New York, Academic Press, Inc., 1956, Chapter 8.

16. Sievert, R. M. Acta Radiol., Suppl. 14:1, 1932.

17. Sievert, R. M. Acta Radiol., 15:193, 1934.

18. Dahl, O., and K. J. Vikterlöf. Acta Radiol., Suppl. 171, 1958.

19. Lanzl, L. H., and L. S. Skaggs. Am. J. Roentgenol., Rad. Therapy, and Nucl. Med., 80:851, 1958.

20. Loevinger, R., and J. Spira. Am. J. Roentgenol., Rad. Therapy, and Nucl. Med., 77:869, 1957.

21. Dudley, R. A. In Radiation Dosimetry, eds. Hine, G. J., and G. L. Brownell, New York, Academic Press, Inc., 1956, Chapter 7.

22. Weyl, W. A., J. M. Schulman, R. J. Ginter, and L. W. Evans. Electrochem. Soc., 95:70, 1949; Ceram. Abstracts, p. 841, 1950.

23. Amato, C. G., S. J. Malsky, V. P. Bond, and B. Roswit. Radiology, 76:292, 1961.

24. Blair, G. E. J. Am. Ceram. Soc., 43:426, 1960.

25. Report of the International Committee on Radiological Units and Measurements. National Bureau of Standards Handbook 62, p. 12, 1956.

USE OF A HETEROGENEOUS PHANTOM WITH A LINEAR ACCELERATOR

By

L. H. Lanzl

The following note is not intended to describe the range of treatment plans that are possible with the Argonne Cancer Research Hospital's Linear Accelerator[1] and its deflecting system,[2] but to illustrate the use of the heterogeneous phantom described in the previous paper.

In many radiation therapy centers, the phantoms hitherto in use have been of the homogeneous type. With these, errors in dosage as large as 40 per cent may be made if standard depth dose tables are used without corrections for the presence of air cavities and bony structures.[3] Such a homogeneous phantom, constructed of elliptical masonite slabs 1 cm thick and having major and minor axes of 34 and 24 cm respectively, was used extensively with the cobalt unit of the Argonne Cancer Research Hospital. Results for cobalt gamma rays have previously been published.[4,5] The radiation detector was Eastman Kodak Industrial AA photographic film, the blackening of which serves as an indicator of the dose.

Using this film with the linear accelerator, it has been found that there is a linear relationship between exposure and net optical density of the film for doses of electrons from five to over 40 Mev. Measurements of this relationship were made by exposing the film to different numbers of electron pulses, always at the same instantaneous current. The measured isodensity distribution therefore corresponds to the isodose distribution.

Figure 1 shows a film exposed in the homogeneous phantom to electrons during a combination of field and arc therapy. The beam was directed parallel to the film surface, as illustrated in Figures 2 and 3, in which the isodose curves are plotted. An arc of 93° was used with a field width of 8 cm. In both Figures 2 and 3, the energy of the electrons for the arc portion

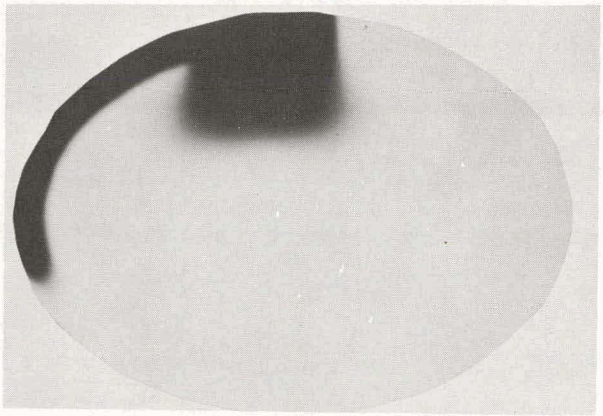

Figure 1. Photographic blackening of film exposed to five and ten Mev electrons. Homogeneous Phantom. Linear Accelerator. See Figure 2 for dose distribution.

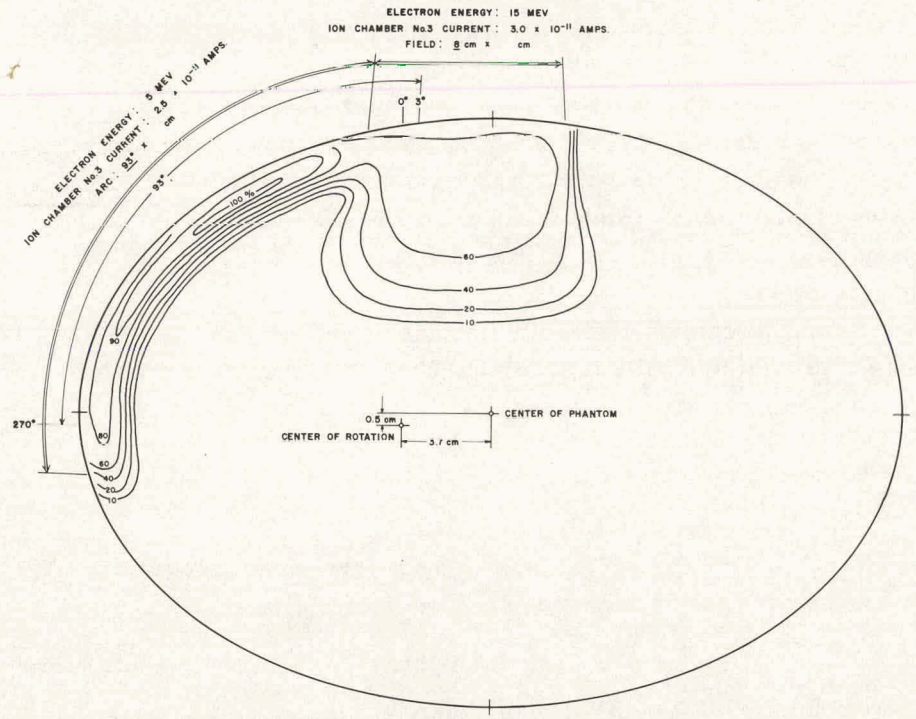

Figure 2. Isodose distributions for combined arc and field therapy. Homogeneous Phantom. Linear Accelerator.

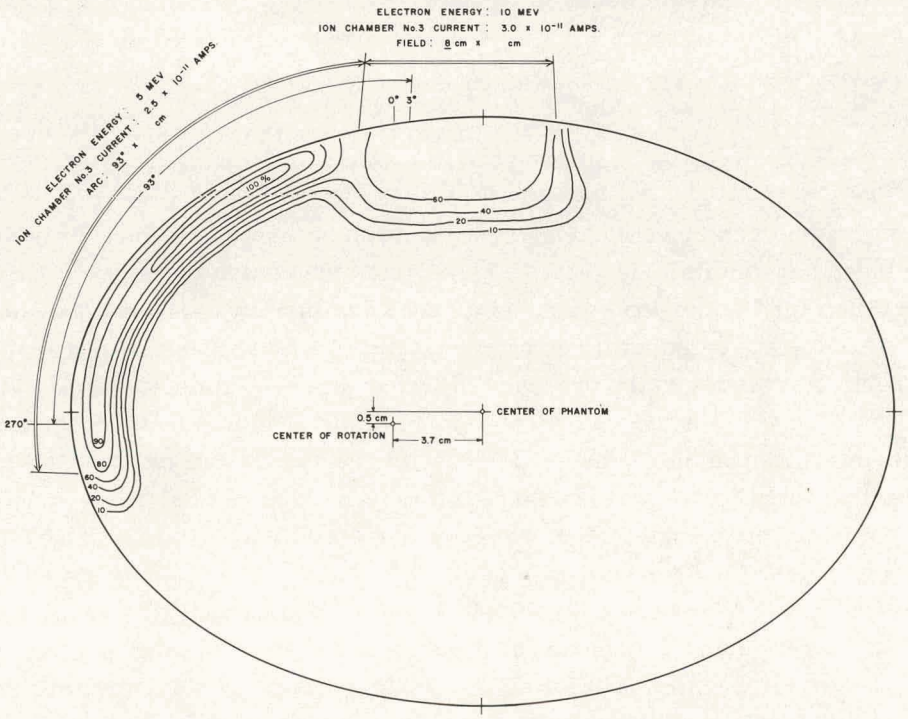

Figure 3. Isodose distributions for combined arc and field therapy. Homogeneous Phantom. Linear accelerator.

is 5 Mev. In Figure 2, the energy for the field portion is 15 Mev and in Figure 3, 10 Mev. The sharp cut-off of dose at the end of the electron range is clearly visible. It is of interest to note that the convergence of the electron beam in arc therapy requires less beam current to deliver a given dose than is necessary in field therapy. The beam current as indicated by a transmission ion chamber is shown on the various isodose distribution curves. Since the phantom used has the shape of an elliptical right cylinder, the distribution is independent of the width of the beam normal to a cross-sectional plane, except at very narrow beam widths. (Figures 2 and 3 are for wide beams.)

We turn now to measurements made with the heterogeneous phantom shown in Figure 4, which represents the thoracic region of a patient. The phantom is loaded with film cut to shape and inserted between the sections. The edges of the film are then sealed with light-proof tape.

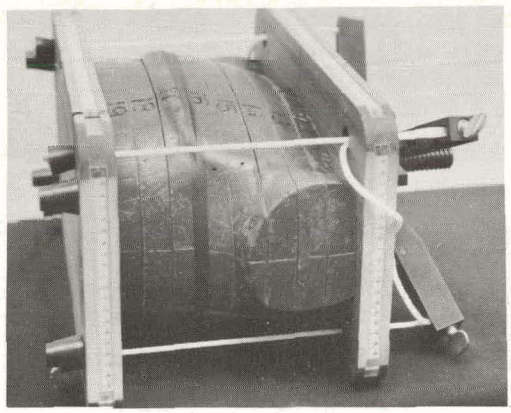

Figure 4. Heterogeneous phantom with film loaded between two sections. Edge of film protected with light-proof tape.

(This particular phantom contained no holes for ionization chambers.) Figure 5 shows a film exposed to combined arc and field therapy. C.P. indicates the center of the phantom, and C.R. the center of rotation for the portion of the beam under arc therapy. Although the combination of energies delivered is the same as illustrated in Figure 1, the appearance of the film is markedly different. This is due to the presence of lung-equivalent material which, while having the same effective Z as the muscle-equivalent portion of the phantom, has a density of 0.3. In addition, the sternum absorbs more energy per unit thickness than muscle. These inhomogeneities are responsible for the two-pronged shape of the irradiated region. The striations are caused by the type of developer used. They can be eliminated by the use of standard developer for Eastman Kodak Industrial AA films.

Figures 6, 7, and 8 represent isodose distributions at various positions in the heterogeneous phantom. Lungs are indicated by means of dashed lines, bones by solid lines. The dotted line in Figure 6 shows the position of the trachea. Comparing Figures 6 and 7 with Figure 5, it will be noted that the blackened prongs on the film correspond to the lungs. Comparing Figures 5 and 8, the prong on the right indicates the position of the heart, which has a density higher than that of the lung.

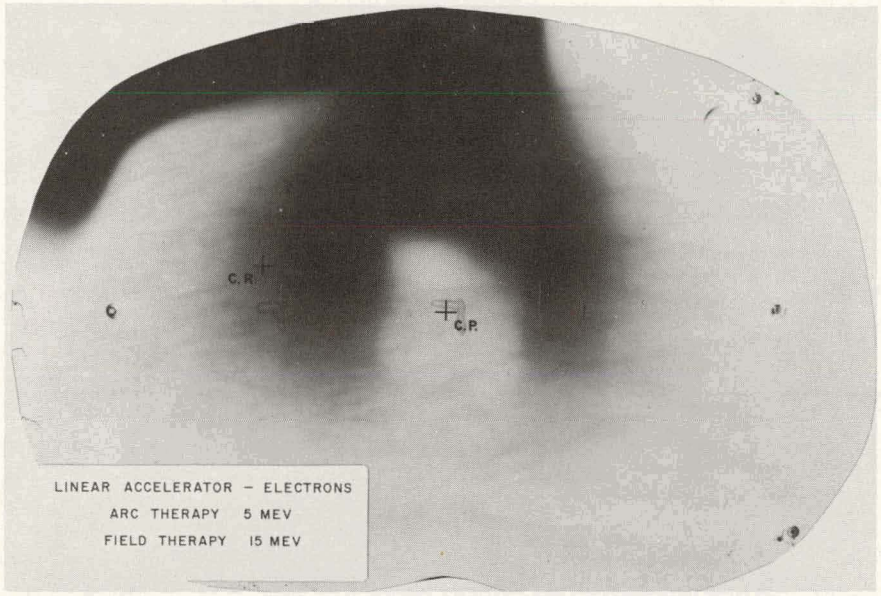

Figure 5. Photographic blackening of a film by fast electrons. Heterogeneous Phantom. Linear Accelerator.

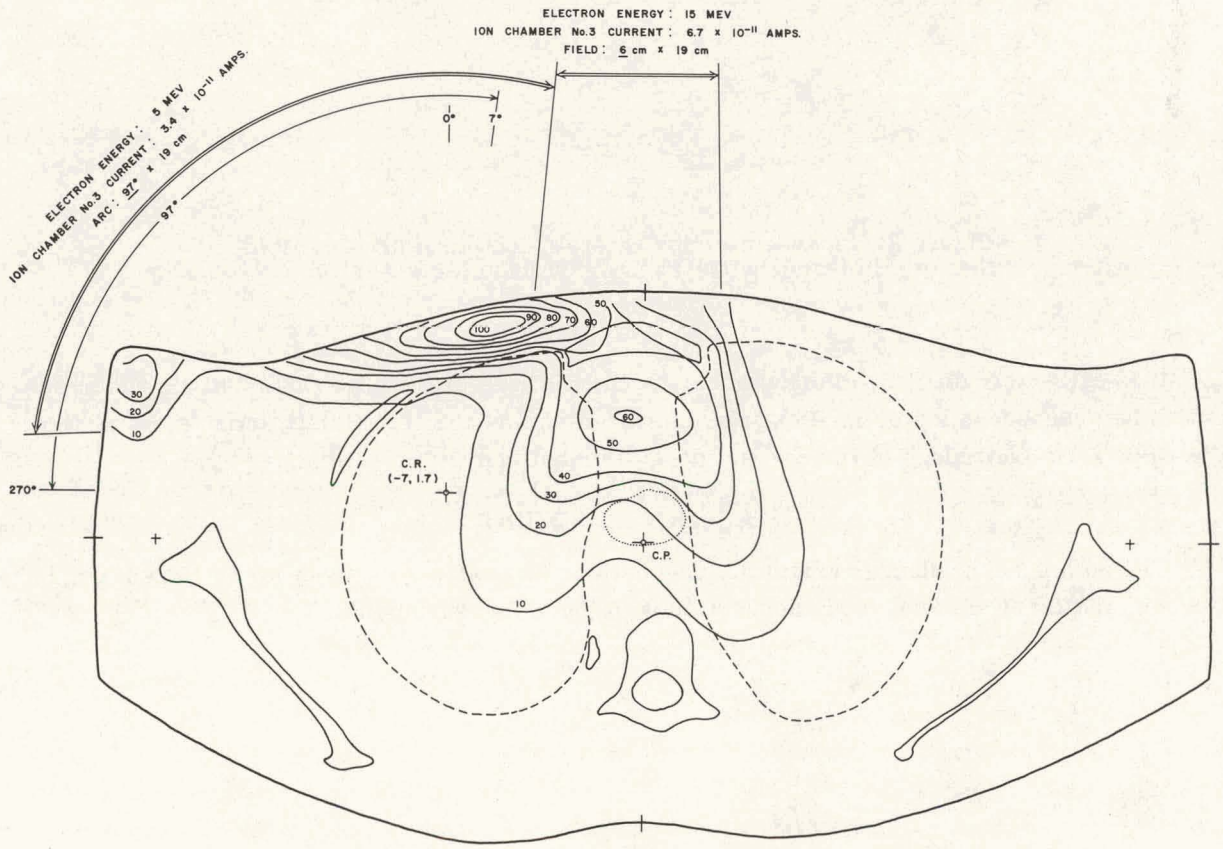

Figure 6. Isodose distributions for combined arc and field therapy. Heterogeneous Phantom. Linear Accelerator.

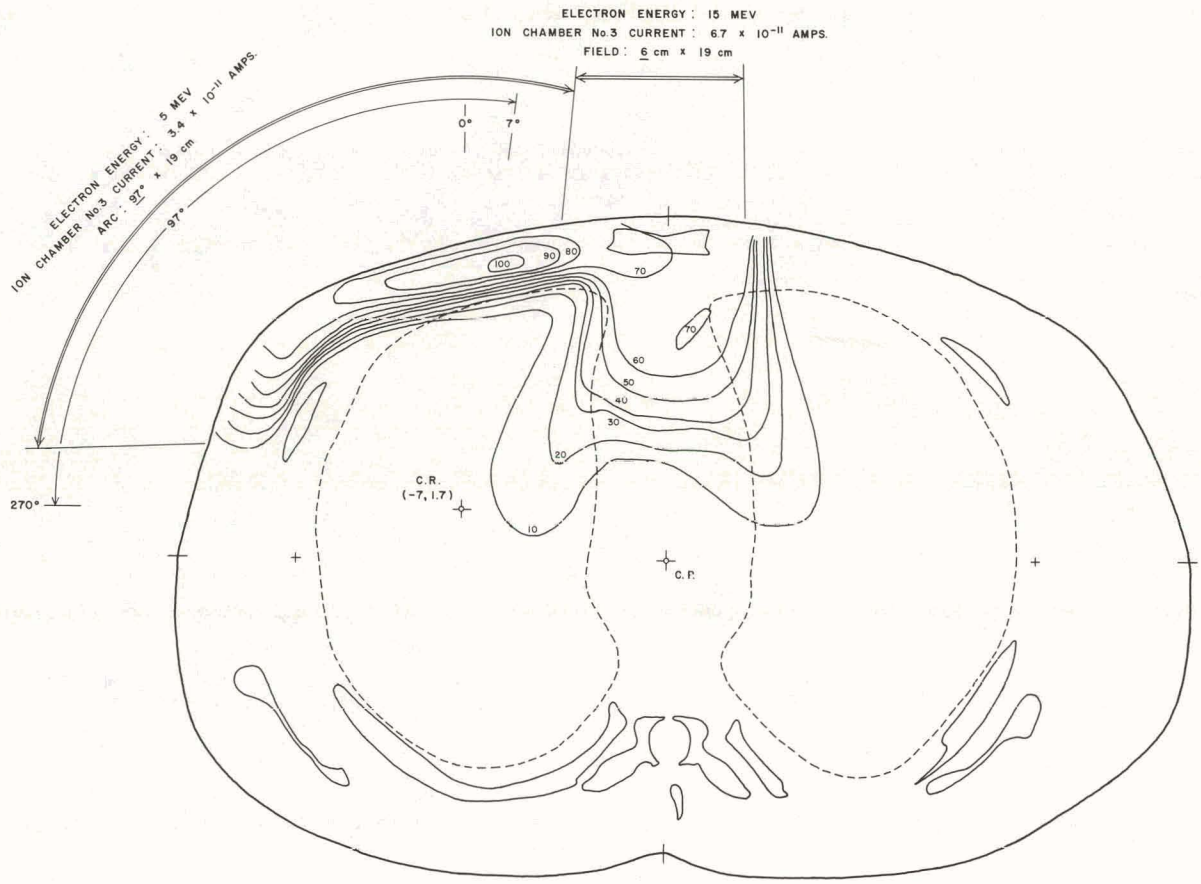

Figure 7. Isodose distributions for combined arc and field therapy. Heterogeneous Phantom. Linear Accelerator.

It is extremely difficult to make accurate calculations of the dose distributions which occur in heterogeneous material. Phantom measurements of the type illustrated are of inestimable value for a knowledge of the correct dose distributions within patients.

ACKNOWLEDGMENT

The author acknowledges gratefully suggestions and assistance from M. L. Rozenfeld, E. Person, and Dr. L. S. Skaggs, in connection with these measurements.

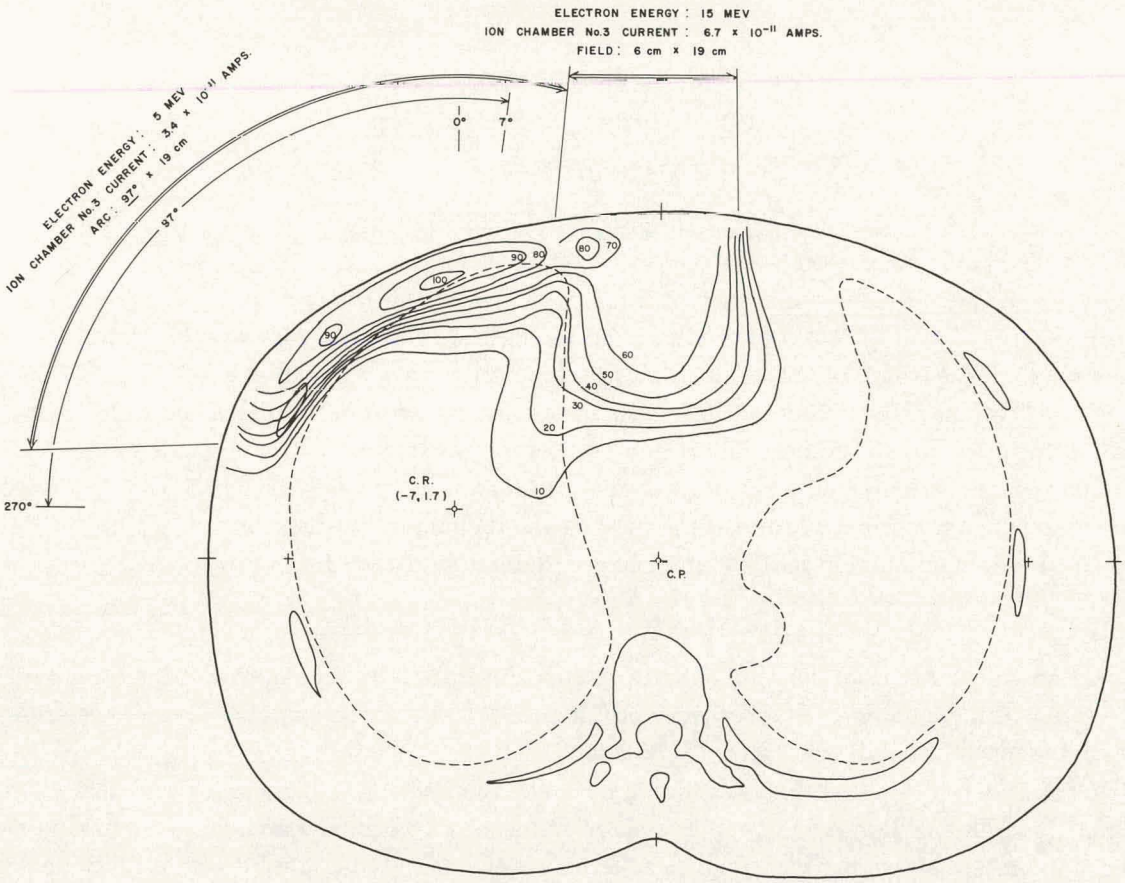

Figure 8. Isodose distributions for combined arc and field therapy. Heterogeneous Phantom. Linear Accelerator.

LITERATURE CITED

1. Skaggs, L. S., J. C. Nygard, and L. H. Lanzl. Radiology, 64:113, 1955.

2. Skaggs, L. S., L. H. Lanzl, and R. T. Avery. Proc. 2nd Int. Conf. Peaceful Uses of Atomic Energy, 26:312, 1958.

3. Report of the International Commission on Radiological Units and Measurements (1959, National Bureau of Standards Handbook 78, issued January 16, 1961 (U. S. Government Printing Office, Washington, D. C.)).

4. Lanzl, L. H., D. D. Davison, and W. J. Raine. Am. J. Roentgenol. Rad. Therapy and Nucl. Med., 74:898, 1955.

5. Lanzl, L. H., and L. S. Skaggs. Am. J. Roentgenol. Rad. Therapy and Nucl. Med., 80:851, 1958.

A WHOLE-BODY COUNTING FACILITY FOR BIOLOGICAL AND MEDICAL RESEARCH*

By

D. B. Charleston

The high sensitivity and selectivity of a large-crystal whole-body counting facility introduces a powerful tool to the field of medical and biological research. Among other advantages, it makes feasible the study of tracer levels of isotopes in vivo with good statistical information. Such an instrument stimulates the imagination and taxes the ingenuity of the worker. Many direct applications become evident immediately; other more exotic demands can be satisfied with proper design consideration. The use of a single large sodium iodide crystal detector for these purposes was already a well established technique when we began to plan the development of a human counter facility at Argonne Cancer Research Hospital.

CONSTRUCTION OF THE COUNTING CELL

Space restrictions, floor loading conditions, and limitation of access within the hospital were best accommodated by the construction of a shield room of the laminated steel type designed at Argonne National Laboratory[1] (Figure 1).

Mill-cut sheets of cold rolled steel were obtained from a single production run at a local mill. Small samples of this steel were evaluated at Argonne National Laboratory and found to be of acceptable standard. Such fall-out products as were detected could be removed by shot-blasting and by meticulous hand scrubbing.

The inner walls, ceiling, and floor were lined with virgin lead sheet, one-eighth inch thick. Ceiling and floor were protected with stainless steel sheets to prevent the lead from damage and sagging, and to facilitate cleaning. As an added protection against accidental spills and build-up from air-borne contamination, the inside of the cell was lined with a replaceable heavy plastic sheet. This plastic liner also acts as an air seal and restricts the passage of the iron room ventilating air to the openings around the cell door.

When the facility is in operation, air which has been stored in pressure tanks until the short half-life products have decayed to a low level is introduced into the rear of the cell and used to keep the room at a slightly positive pressure compared to the surrounding area (Figure 2). Outside, or make-up air to the cell area room (B) is filtered through a coarse particle filter and a CWS air filter before being conditioned and introduced to the cell area. Meanwhile, a decreasing gradient in pressure is maintained from the cell (A) to the cell area (B) to the adjacent rooms (C) and (D), thus assuring an outward flow of air from the counting cell. The data room area (D) air is treated with a recirculating type of air conditioner.

Showers and locker room facilities are provided (C) for subjects coming to be "counted." Street clothing is removed; showering is required; and hospital gowns and disposable slippers

*This report is taken from a paper delivered at the International Atomic Energy Agency's Whole-Body Counting Symposium in Vienna, Austria, June 12-16, 1961, and will appear in the Proceedings of this symposium.

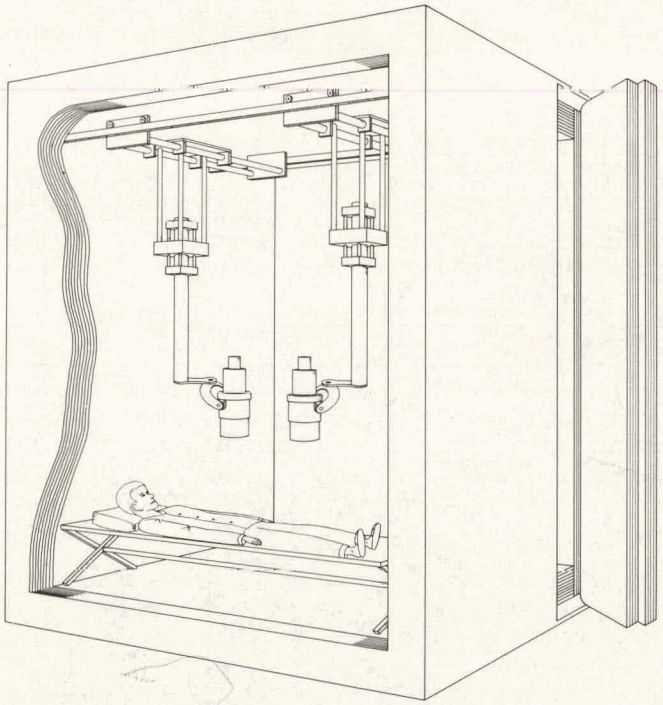

Figure 1. Counting cell. Only two of the five detectors are shown in this drawing.

are worn by each subject. When the door is closed, the counting cell is a complete enclosure without viewing ports or windows. Music is piped into the cell to distract the subject, and a two-way intercommunication system is in operation at all times.

SOME APPLICATIONS OF MULTIPLE DETECTOR SYSTEMS

Previous biological investigations involving differential uptake and diffusion had been made with conventional equipment which left much to be desired regarding patient dose and length of time over which sensitive and accurate measurements could be made. We were aware that more sensitive large-volume detectors, properly shielded from background, would permit detection of tracer levels of activity and extend the period of study. A human counter designed to accommodate studies of this type was made possible by the work of R. N. Beck,[2] who formulated a rigorous mathematical theory and made the experimental evaluations necessary to the design of optimum focusing collimators for detectors employing sodium iodide crystals. This study permitted incorporation into the design consideration the possibility of examining various well-defined regions of view within the human body.

As a consequence, the Argonne Hospital's multiple-crystal array can be used to perform compartment studies which will permit the observation of as many as five regions of view within the body using any gamma-emitting isotope from 30 Kev to 500 Kev. (Above 500 Kev, focusing collimators become extremely bulky and inefficient for gamma energies.) Studies have been made using two detectors with focusing collimators for calcium-47, iron-59, iodine-131, and strontium-85; these are long-term investigations and will be reported at a later date.

Another program presented for design consideration involves the administration of two sep-

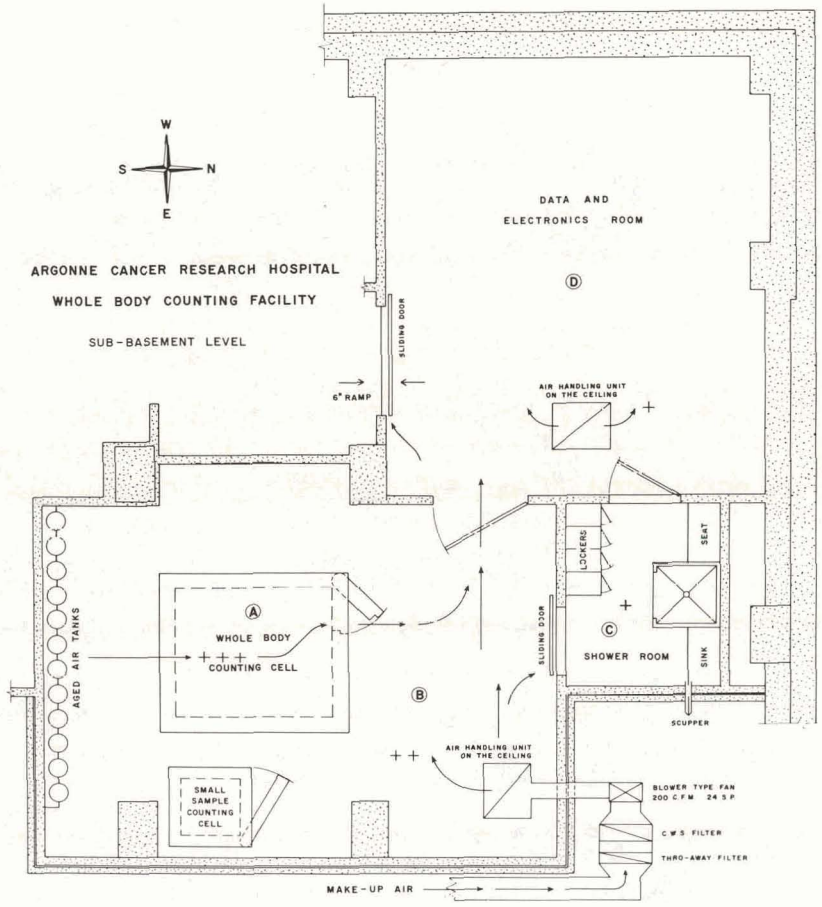

Figure 2. Floor plan showing (A) whole-body counting cell; (B) clean area; (C) shower and preparation room; and (D) data and electronics room.

+++ Most positive air pressure
++ Intermediate air pressure
+ Least positive air pressure

arate compounds, each labeled with a different isotope. This experiment requires multiple detectors and two different sizes of focusing collimators. Our array of equipment makes it possible to observe uptake, diffusion, cross-diffusion, and elimination for specific regions in the body. Compartmental behavior studies in vivo can be made at tracer or therapeutic levels of radioactivity.

An important and obvious advantage of the multiple detector system is its inherent stepwise sensitivity. High levels of radioactivity are frequently encountered in humans to whom therapeutic dosages have been administered. The use of all large-crystal detectors of a multiple array is not necessary or even possible in many cases because the counting rates involved may exceed the resolving time of the associated electronics equipment. (Such would be the case with a single large-crystal detector counting facility which contains the entire crystal volume in one unit.)

As the isotope decays and as biological elimination progresses, the levels of activity fall.

The multiple array then makes it possible to introduce additional detectors for step-wise increases in sensitivity until all detectors are in use.

A feature which might be called "semi-scanning" is a natural by-product of the multiple detector array. By this means it is simple to determine the portion of the total count contributed by each detector position.

Most of the subjects studied at the hospital installation are sick people, and for their comfort it is desirable that measurements should take a minimum of time, and that they should be permitted to recline during the counting period.

A short counting time implies a large crystal volume, and the reclining position can be most easily satisfied by distributing this large crystal volume along the body axis. While a single large crystal fulfills the large detector volume requirement, it does not present good geometry to the reclining position; nor does it satisfy the demands for the other proposed studies.

A summation of these varied proposals makes rigorous demands on the system design—both in the mechanical components and in the necessary electronics.

DESIGN AND CONSTRUCTION OF THE MULTIPLE DETECTOR SYSTEM

In our system, each detector is suspended from a support elevator which is in turn attached to a "trolley" having two-dimensional freedom of motion at the ceiling of the iron cell. The support elevator rod may be used to raise and lower this detector from limits of 36.5 inches to 55 inches above the floor of the room. A further degree of freedom is obtained by a support yoke which allows the detector to be inclined at any angle between the vertical and horizontal. These mechanical adjustments permit maximum freedom of position within the cell. While an infinite number of position configurations is attainable, routine survey information can be gathered from a few standardized geometrical placements. It is always possible to correlate counting information to other large single detector installations by counting for a longer period of time with a single crystal of the array or a detector "cluster" at approximate geometry (Figure 3).

Observations made with the detector in an in-line arrangement over the patient show that constant counting geometry is maintained over all in spite of migration and localization of the isotope within the body (Figure 4).

The determination of crystal size for a multiple array was made after consideration of many factors. From the published work of W. F. Miller et al.[3] it was determined that a minimum crystal thickness of 4 inches would be required for effective counting of gamma energies up to 1.5 Mev. Better light collection, or better resolution, is obtained as more of the crystal surface is covered by photomultiplier tube photocathode. Calculations of relative light collection efficiencies for various sizes of right circular cylinder crystals which were made by J. Van Sciver[4] indicate that an 8-inch by 4-inch crystal (if it could have one circular surface completely covered by photocathode) would have an idealized light collection efficiency of 58 per cent. A 4- by 4-inch crystal would have an efficiency of 56 per cent; a 5- by 4-inch crystal, of 59 per cent; and a 5- by 5-inch crystal, of approximately 52 per cent. These variations are not great enough to exclude any one of the sizes mentioned. The calculations are most helpful as an aid to visualizing the optical behavior within a crystal, and to indicate size and configuration. It is difficult to cover completely an 8-inch-diameter crystal surface with presently available photomultiplier tubes. A 4-inch-diameter crystal can be covered with a 5-inch tube,

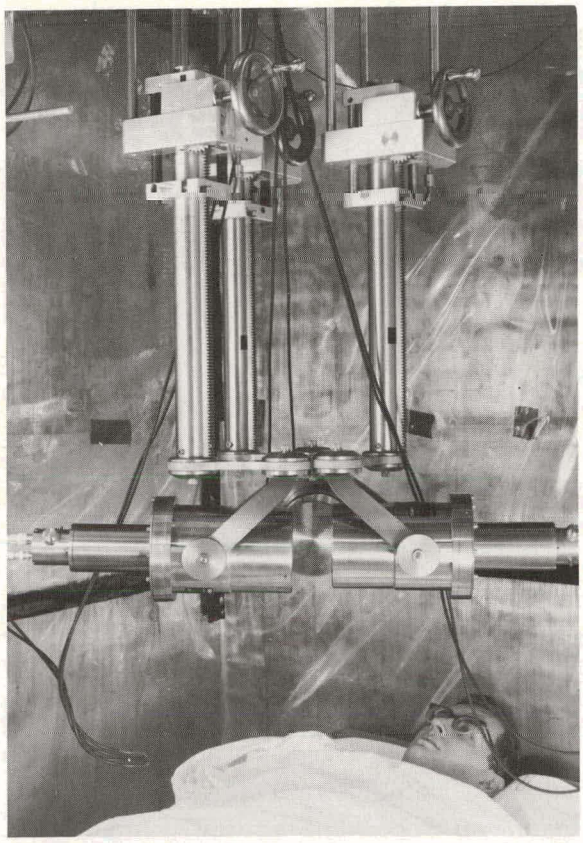

Figure 3. Detector cluster arrangement. Only three of five detectors are shown.

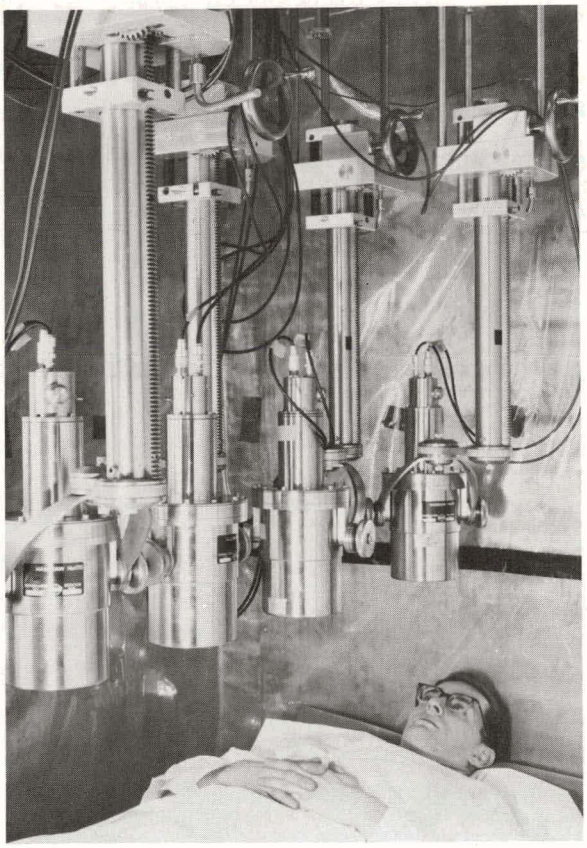

Figure 4. Detectors in line over body axis.

but the coupling becomes difficult and the package is awkward. A survey of the market for photomultiplier tubes of large size with low internal radioactivity revealed that no 4-inch phototube was available.

It was found that E.M.I. of England manufactured a 5-inch-diameter venetian-blind eleven-stage photomultiplier tube with a quartz envelope—the 9530 BQ, which proved to be acceptable in all respects. One such tube, broken in shipment, was separated into various components (faceplate, internal structure, tube base, and side envelope) for counting purposes. The counting breakdown up to and including the potassium peak gave the following information: Faceplate, no detectable count; side envelope, 3 counts per minute; internal dynode structure, 4 counts per minute; base structure (glass), 6 counts per minute—a total of 13 counts per minute. Since other available 5-inch tubes gave counts ranging from 180 to 235 per minute, this tube was selected for our use.

The tube size selected determined the diameter of the crystal—5 inches. A 5-inch by 4-inch size was considered, but because of the many geometric arrangements possible with the detectors, it was decided to use a crystal 5 inches by 5 inches so as to present as uniform a profile as possible to the source no matter in what position the detectors might be placed. Since two such units, butted end to end, will essentially duplicate the configuration of a single 10-inch by 5-inch crystal, this position arrangement has been incorporated into the design.

The direct coupling of a photomultiplier tube cathode face to the crystal surface reduces the number of possible interface reflections and tends to improve resolution by a few per cent. In order to provide optimum resolution, the phototubes were integrally mounted to the crystal by the Harshaw Chemical Company of Cleveland, Ohio. The crystals were enclosed in a stainless steel can having 0.010-inch-thick walls.

ANALYSIS OF DETECTORS

In the analysis of individual detectors, careful and somewhat tedious measurement revealed that the optimum resolution of each detector must be determined independently. Acceptable resolution was obtainable without difficulty (11.5 per cent to 13 per cent for the cesium line), but improvements of 25 per cent were attained by careful adjustment of the cathode to first dynode voltage, and the focusing electrode voltage.

For three of the five tubes tested, optimum resolution was observed not at the point of adjustment on the focus electrode which gave maximum pulse heights, but slightly higher (closer to first dynode potential).

Families of curves were plotted for each detector. Resolution was plotted against focus electrode voltage for various cathode to first dynode voltages (Figure 5).

Fixing the optimum resolution voltages for each tube presented a problem in electronics design. It was necessary to provide an individual linear amplifier of high stability which could be adjusted to compensate for the amplitude variations from each detector to match them precisely for presentation to the mixer circuit.

The output signal from each photomultiplier tube is fed to an emitter follower circuit which is contained in the detector housing base. The "followers" drive approximately 30 feet of cable into the linear amplifier mixer circuit. The mixer circuit is essentially a summing network.

The probability of chance coincidence from the source is quite small at the counting rates

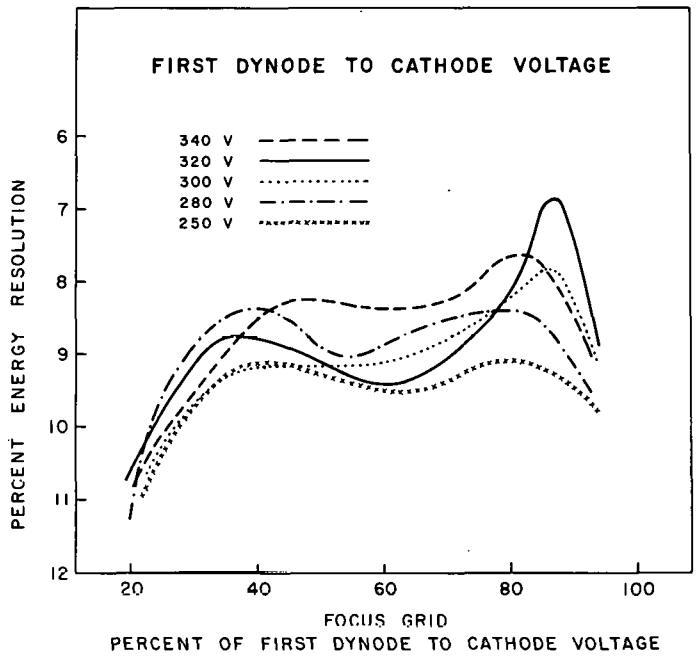

Figure 5. Plot of focus electrode setting vs. resolution.

encountered, but the probability of coincidence pulses of large amplitude from cosmic showers is quite high. Since the pulses are summed before being presented to the multi-channel analyzer, most summed coincidence pulse heights are too high to be registered on the spectrum presentation. When introduced to the 512-channel analyzer, these high pulses "paralyze" the unit for the duration of the pulse only, and no error is introduced in the counting statistics or the "live time."

Each linear amplifier has an auxiliary follower output which presents the matched signal directly to a high stability transistorized single-channel pulse height analyzer of our own design (Figure 6). Each analyzer has both an "integral" as well as a "differential" mode of operation, thus permitting maximum flexibility of operation.

The output of any or all the pulse height analyzers can be used as gate signals, to route any detector output to one of four 128-channel sections of the 512-channel analyzer for storage, for coincidence or anti-coincidence presentation to the multi-channel analyzer, or as input to any of five high accuracy transistorized linear ratemeters of Argonne Hospital design. Switching networks permit all single-channel analyzers to be used either on one detector or on any combination desired.

The ratemeter outputs are recorded on a switched multi-position potentiometer recorder.

The output of each single-channel analyzer may be stored by means of a scaler for gross count accumulation over any set period of time.

Standard scalers borrowed from other projects are being used at the present time; but, because they are expensive and bulky, a design program has been initiated to utilize a memory core storage system for a six-channel scaling unit that will be compatible with our planned data storage system.

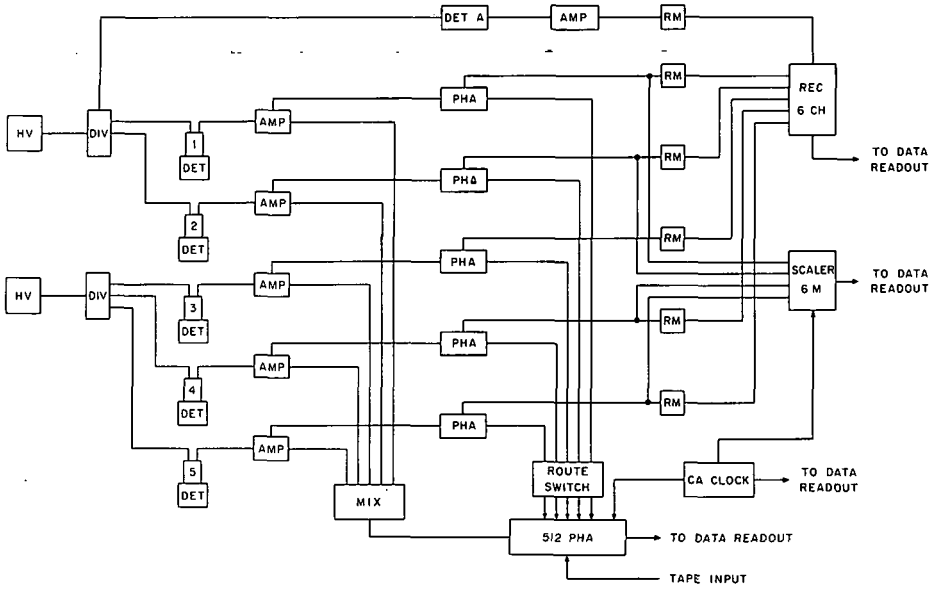

Figure 6. Block diagram of electronics.

HV	John Fluke Model 405 high voltage supply.
DIV	Voltage dividers, one for each detector.
DET-A	Area monitor 2- by 2-inch crystal detector (outside cell).
DET-1-2-3-4-5	5- by 5-inch NaI crystal detectors in cell.
AMP	Linear amplifier, Argonne Hospital design.
MIX	Summing mixer.
PHA	Transistorized single-channel analyzer, Argonne Hospital design.
ROUTE SWITCH	Switching facility for coincidence-anticoincidence signal selection and routing to multi-channel analyzer.
512 PHA	512-Channel spectrum analyzer transistorized Nuclear Data Model ND-130.
RM	Transistorized linear ratemeter, Argonne Hospital design.
CA CLOCK	Channel advance clock used with 512 PHA and accumulate scalers.
SCALER 6M	6-Channel memory scaler for accumulate mode.
REC 6CH	6-Channel switched potentiometer recorder, Wheelco.
DATA READOUT	IBM typewriter, Mosley X-Y recorder, Friden paper tape punch, Tektronix display oscilloscope.

A program of importance to the Argonne Hospital high-energy machinery group is the detection and evaluation of induced radioactivity in humans after therapy. Since the whole-body counting facility is on the same floor level as our 50-Mev linear accelerator, it is convenient to "count" a patient in the iron cell before therapy, store this "background" information, and then study the subject again after therapy. As short half-life peaks are seen on the multi-channel analyzer, the single-channel analyzers can be set up to follow these peaks, and the multi-channel analyzer can then be switched over to the multi-scaler mode of information storage for observation of the decay curve.

If one energy level is to be investigated, all the outputs of the single-channel analyzers can be fed into the multi-channel analyzer, and counts can be accumulated in the first channel before being advanced by a timing pulse to the next channel or "scaler," and so on, until a plot of the half-life decay curve will be evident for display and computation.

If as many as four peaks are under investigation, the multi-channel analyzer can be switched to the routed access mode, and the unit will then accept routed pulses from each single-channel analyzer to be stored in its own block of 128 channels or "scalers." The channel advance clock will advance channels in all four storage blocks simultaneously, making it possible to study four different short half-life decay patterns at one time. A transistorized channel advance clock of our own design will be used for the short half-life studies.

A transistorized Nuclear Data Model ND-130 512-channel analyzer is used as the basic spectrum analyzer. This unit presents its stored data to an IBM typewriter, a Friden paper tape punch, an oscilloscope display, and a Mosley X-Y plotting recorder.

Background "stripping" can be accomplished by a punched paper tape "read in" presentation to the analyzer of a previously recorded background spectrum.

CALIBRATION OF MULTIPLE CRYSTAL ARRAY

The over-all "absolute" calibration of the multiple crystal array is admittedly more complex than for a single large-crystal detector, but the problem is simplified somewhat in a hospital installation because of the wide variety of investigations under way at one time. A patient who has received a known amount of isotope for diagnostic or therapeutic purposes, can act as a calibrating standard and thus aid in standardizing counting procedures.

The use of phantoms, the possibility of counting with a single crystal or a cluster of crystals to duplicate single-crystal geometry, and the number of subjects having known levels of administered isotope who are available for study are direct aids to absolute calibration.

It should be noted that most of the work at the hospital requires that relative rather than absolute counting statistics be accumulated. If a known tracer level in vivo is evaluated and the geometry remains consistent, the study can be carried on with good statistical information and will tend to be very nearly absolute.

An in vivo study of the cesium-137 and potassium-40 peaks in normal humans was undertaken to determine the sensitivity of the multiple array to bodily configuration when the detectors are oriented with the long axis of the reclining person. The subject was placed in a reclining position and counted for long periods in order to obtain statistics with standard deviation in the order of 3 per cent. Four detectors were used, placed 19.5 inches from the cot surface and arranged so that one crystal was over the sternum, one over the pelvis, one over the thigh, and the fourth over the shin. It was found that for geometric compression of the system (axially)

over a 9-inch range, the K^{40} count changed to new mean values (with the same standard deviation) all within 6 per cent to the maximum mean value. The Cs^{137} count variations remained within the standard deviation limits of 3 per cent for all positions.

If the crystals are arranged so that individual alignment is directly over the sternum, pelvis, knee, and a point half-way between the knee and pelvis, the units may be raised or lowered as well as displaced axially and still maintain variations within 5 per cent limits for K^{40} and 3 per cent limits for Cs^{137}. Experiments with lower energy isotopes are under way to evaluate further the effect of body build on counting statistics.

The data logging system is still in the planning stage, and a fairly comprehensive system design is anticipated in order to accumulate, store, classify, cross-index and identify information for analysis and for presentation to a digital computer facility.

Several specifically oriented investigations are in progress, the primary intent being to collect and store all available information derived by use of the counter, even though it may not be immediately pertinent to a given experiment. In this way, we expect to accumulate a "stock pile" of counting data on humans for future statistical reference.

ACKNOWLEDGMENTS

The author is pleased to acknowledge his indebtedness to Dr. R. J. Hasterlik for his valuable assistance and guidance; to Mr. R. N. Beck for his excellent work on focusing collimator theory and his active participation in the design study; and to Mr. J. Stupka, supervisor of the Argonne Cancer Research Hospital Machine Shop, for his direction of the design and construction of the probe supports and construction of the iron room cell.

LITERATURE CITED

1. Miller, C. E., L. D. Marinelli, R. E. Rowland, and J. E. Rose. IRE Transactions on Nuclear Science NS-3 No. 4, 1956.
2. Beck, R. N. "A Theoretical Evaluation of Brain Scanning Systems," accepted for publication in The Journal of Nuclear Medicine.
3. Miller, W. F., J. Reynolds, and W. J. Snow. ANL-5902, 1958.
4. Van Sciver, J. APEX-471:28, 1958.

EFFECT OF PREGNANCY ON THE METABOLIC INFLUENCE OF ADMINISTERED PROGESTERONE*

By

R. L. Landau, E. J. Plotz,† and K. Lugibihl‡

It has been shown that intramuscularly administered progesterone will increase the net rate of protein catabolism and enhance the urinary excretion of sodium and chloride in non-pregnant women and in men.[1-3] This mild to moderate catabolic process can be distinguished qualitatively from those resulting from excesses of adrenocortical and thyroid hormones.[2,4] The natriuresis and chloruresis have been ascribed to an inhibition of the renal tubular effects of aldosterone and other sodium-retaining adrenal secretions.[2,5] The influence of progesterone on both protein and electrolyte metabolism was detectable when as little as 12.5 mg per day was administered. The catabolic response was maximal at a daily dosage of about 25-50 mg, but the intensity and duration of the natriuresis continued to increase until a dosage level of at least 200-300 mg per day had been reached.[6]

It appears likely that these metabolic properties of progesterone will prove to be important during pregnancy when very large amounts of the hormone are secreted. Estimates based on the fact that about 15 per cent of administered progesterone is excreted as urinary pregnanediol indicate that about 25-75 mg of progesterone may be secreted each day during the first trimester of pregnancy, with a progressive increase of 200-400 mg per day before delivery.[7,8] More direct measurements of the rate of progesterone secretion indicate secretory rates of 20 and 41 mg per day in the first and second trimesters,[9] and 190-280 mg per day in the third trimester.[10,11] From the dose-response relationships noted previously,[6] it could be assumed that the pregnant women are under the influence of the maximum catabolic stimulus of progesterone during most of the period of gestation. The progressively increasing rate of progesterone secretion would also be expected to result in greater capacity for inhibition of aldosterone, but the rate of aldosterone secretion also rises during pregnancy.[12,13]

In these circumstances one would anticipate that, after the first few weeks of gestation, administered progesterone would have no effect on nitrogen metabolism, and that its influence on urinary sodium excretion would be dependent in large measure upon the pre-existing balance of endogenous progesterone and aldosterone. As a partial test of these suppositions the metabolic effects of progesterone in a dosage of 50-100 mg per day was determined in 3 women during the second and third trimesters of pregnancy. Such amounts of progesterone have frequently been administered to pregnant women to prevent abortion.[14]

METHODS

The 3 subjects studied were in the fourth, seventh and eighth month of pregnancy, respectively. All of the pregnancies were uncomplicated and without excessive weight gain. The women

*This report appears in J. Clin. Endocrinology & Metabolism, 20:1561, 1960.

†Department of Obstetrics and Gynecology, University of Chicago.

‡Department of Medicine, University of Chicago.

lived in the metabolic ward of the hospital and consumed adequate constant diets in the usual manner. Urine was collected in 24-hour specimens as soon as sufficient time had elapsed for metabolic equilibration. The 24-hour collections were usually combined in 48-hour pools for analysis. Completeness of collections was checked by urinary creatinine determinations. The urine specimens were also analyzed for total nitrogen, inorganic phosphorus, sodium and potassium by methods previously noted.[2] Pregnanediol was determined by the procedure of Bongiovanni and Clayton,[15] after glucuronidase hydrolysis and extraction.

Subject B.Pe (Figure 1) received progesterone in a dosage of 50 mg per day intramuscularly for eight days. Subjects J.H. (Figure 2) and D.W. (data not illustrated) were given 100 mg per day.

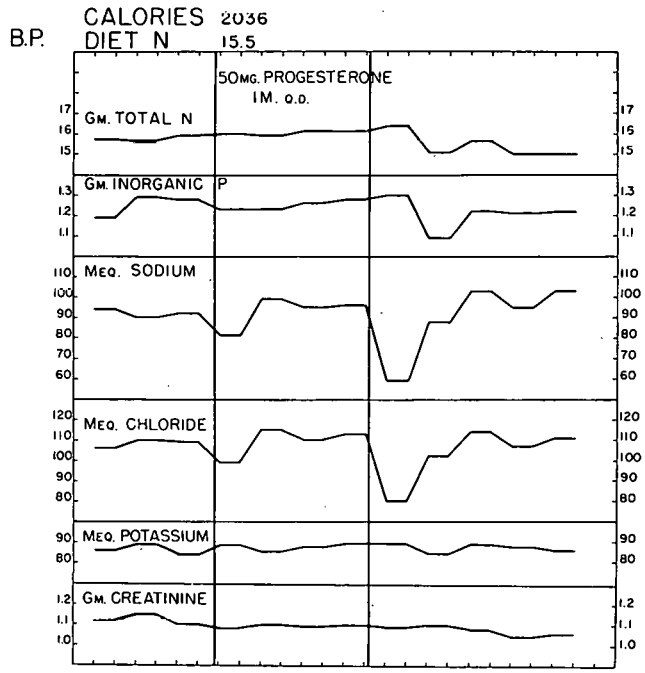

Figure 1. Effect of progesterone (50 mg per day) on the urinary excretion of total nitrogen, inorganic phosphorus, sodium, chloride and potassium in Subject B.Pe., a normal woman in the fourth month of pregnancy.

RESULTS

In none of these pregnant women was there conclusive evidence that nitrogen excretion was influenced by treatment with progesterone. In Subject B.Pe. (Figure 1), urinary nitrogen excretion continued at the control level throughout the treatment period. Although nitrogen excretion dropped slightly at the conclusion of treatment, this can hardly be regarded as evidence of a prior catabolic process. During the seventh month of gestation in Subject J.H. (Figure 2), 100 mg of progesterone daily failed to induce even a suggestion of an effect on nitrogen excretion. The excretion of nitrogen was also uninfluenced in Subject D.W. (data not shown). Urinary

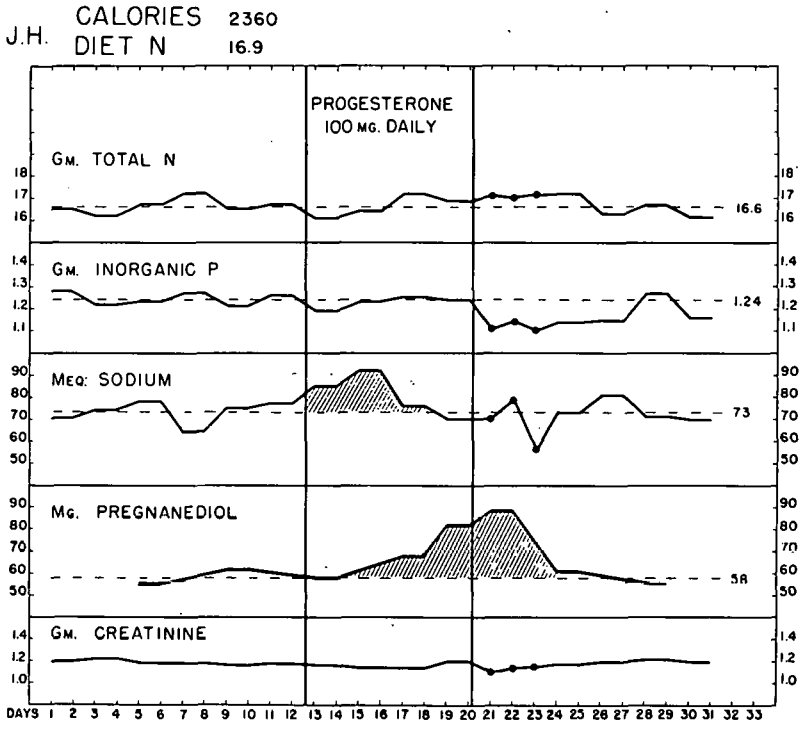

Figure 2. Effect of progesterone (100 mg per day) on the urinary excretion of total nitrogen, inorganic phosphorus, sodium and pregnanediol, in Subject J.H., a normal woman in the seventh month of pregnancy. Broken horizontal lines indicate the control levels (averages); significant changes are indicated by cross-hatched areas.

inorganic phosphorus excretion was likewise unaffected in these subjects. Thus there was no evidence that protein metabolism could be influenced by administered progesterone in the middle or last trimesters of pregnancy.

When examined in the light of other experiences with progesterone, the results obtained in Subject J.H. (Figure 2) suggest that the 100-mg dosage of the hormone may have induced a mild sodium diuresis which lasted the first four days of treatment. The estimated sodium loss totaled only 65 mEq, and except for a single low value on the third post-treatment day, there was no distinct post-treatment retention of sodium. In Subject B.Pe. (Figure 1), 50 mg of progesterone each day induced no sodium loss, but sodium retention was observed during the first two days after progesterone was discontinued. In Subject D.W., who also received 100 mg daily, there was no loss or post-treatment retention of sodium.

The basal body temperatures did not rise during treatment with progesterone in any of the subjects. Pregnanediol excretion in Subject J.H. rose from a pre-treatment level of 58 mg to a peak of 90 mg per twenty-four hours, about 10 to 15 per cent of the administered progesterone being recovered as pregnanediol. In the other 2 women the course of pregnanediol excretion during treatment was not followed in such detail, but in each case the excretion increased as a result of progesterone therapy.

DISCUSSION

These failures of administered progesterone to enhance urinary nitrogen excretion were the first to be observed in about 75 such studies in men and women under a variety of circumstances. On the assumption that endogenous progesterone acts like the administered hormone, this lack of response had been anticipated. As noted previously, 50 mg of progesterone per day usually induced the maximum catabolic effect. These 3 pregnant women were almost certainly under the influence of at least that quantity of endogenous progesterone when treatment was started (urinary pregnanediol excretions were 14, 58 and 45 mg per twenty-four hours, respectively). The negative results are accordingly consistent with, and indeed support, the view that during the latter two-thirds of pregnancy progesterone is exerting its maximal catabolic influence.

These studies also provide controls of a sort for the numerous instances in which progesterone did act as a catabolic agent. The remote possibility that in some manner the mild inflammatory reaction sometimes noted at the site of progesterone injection could have accounted for the catabolic response had been considered. However, the failure of progesterone to enhance nitrogen excretion during pregnancy, when the potential for local irritation was as great as ever, would seem to eliminate this consideration. Thus the concept that the enhancement of protein catabolism is a physiologic influence of the hormone has been strengthened.

The conclusion that during pregnancy—a time of fetal and selective maternal growth—protein catabolism of the maternal organism as a whole is being enhanced by one of the principal female hormones is indeed surprising. To be sure, estrogens are anabolic,[16,17] and the two female hormones may thus counteract each other. Recent studies have suggested that the catabolic influence of progesterone is not exerted directly upon peripheral tissues but, rather, is the result of an acceleration of aminoacid utilization by the liver.[18] If this be the case, this influence of progesterone would probably have a less obvious significance in the economy of the organism than the mere balancing of the effect of the anabolic estrogens.

The importance of progesterone in the regulation of electrolyte and water metabolism during pregnancy is more apparent. The huge quantities secreted in pregnancy have generally been thought to be required primarily for the preservation of the placenta and an optimum state of myometrial contractility. However, the fact that progesterone is a potent inhibitor of the sodium-retaining action of aldosterone would seem to assign to it a key position in the hormonal regulation of urinary sodium excretion during pregnancy as well. If the amount of aldosterone secreted throughout pregnancy were relatively constant, the rising rate of progesterone secretion would probably induce a serious sodium diuresis like that observed when progesterone is administered to adrenal-deficient patients managed with constant doses of aldosterone or desoxycorticosterone.[2] Accordingly the enhancement of aldosterone secretion which occurs during pregnancy could reflect, at least in part, a compensatory response to the inhibitory action of progesterone. It is also possible, however, that this increased secretion of aldosterone is causally related to other phenomena.

The minimal natriuresis induced by progesterone in Subject J.H. (Figure 2) and the absence of a significant loss of sodium in the other 2 subjects suggest that insufficient aldosterone was inhibited to induce a deficiency of mineral corticoids. This suggestion implies that there is more unopposed aldosterone circulating or very readily available in the pregnant organism than in other normal subjects who have been studied. It is also appreciated, however, that other

endocrine and metabolic changes could impair the natriuretic response to progesterone. In physiologic amounts, estrogen does not interfere with the natriuresis,[19] but other possibilities have not been investigated.

It is thus possible that the enhancement of aldosterone secretion in pregnancy is not merely a compensatory reaction to the large quantity of circulating progesterone. In this circumstance it would not be unreasonable to propose that endogenous progesterone plays a dynamic role in the daily regulation of salt metabolism by inhibiting the action of possible excesses of adrenal salt-retaining hormones.

LITERATURE CITED

1. Abels, J. D., and K. M. Dobriner. Effect of progesterone on nitrogen balance in man, in Transactions of the 7th Conference on Metabolic Aspects of Convalescence Including Bone and Wound Healing, ed. by E. C. Reifenstein, Jr., New York, Josiah Macy, Jr. Foundation, 1944, p. 122.
2. Landau, R. L., D. M. Bergenstal, K. Lugibihl, and M. E. Kascht. J. Clin. Endocrinol. & Metab., 15:1194, 1955.
3. Kyle, L. H., and W. C. Hess. J. Lab. & Clin. Med., 47:278, 1956.
4. Bergenstal, D. M., and K. Lugibihl. J. Clin. Endocrinol. & Metab., 12:929, 1952.
5. Landau, R. L., and K. Lugibihl. J. Clin. Endocrinol. & Metab., 18:1237, 1958.
6. Landau, R. L., K. Lugibihl, D. M. Bergenstal, and D. F. Dimick. J. Lab. & Clin. Med., 50: 613, 1957.
7. Sommerville, I. F., and G. F. Marrian. Biochem. J., 46:290, 1950.
8. Guterman, H. S. Progesterone metabolism in the human female, in Recent Progress in Hormone Research, New York, Academic Press Inc., 1953, vol. 8, p. 293.
9. Plotz, E. J. Unpublished studies.
10. Pearlman, W. H. Biochem. J., 67:1, 1957.
11. Zander, J., and A. M. von Munstermann. Klin. Wchschr., 32:894, 1954.
12. Venning, E. H., T. Primrose, L. C. S. Caligaris, and I. Dyrenfurth. J. Clin. Endocrinol. & Metab., 17:473, 1957.
13. Jones, K. M., R. Lloyd-Jones, A. Riondel, J. F. Tait, S. A. S. Tait, R. D. Bulbrook, and F. L. Greenwood. Acta Endocrinol., 30:321, 1959.
14. Davis, M. E., and E. J. Plotz. The metabolism of progesterone and its clinical use in pregnancy, in Recent Progress in Hormone Research, New York, Academic Press Inc., 1957, vol. 13, p. 347.
15. Bongiovanni, A. M., and G. W. Clayton. Bull. Johns Hopkins Hosp., 94:180, 1954.
16. Thorn, G. W., and L. L. Engel. J. Exptl. Med., 68:299, 1938.
17. Knowlton, K., A. T. Kenyon, I. Sandiford, G. Lotwin, and R. Fricker. J. Clin. Endocrinol., 2:671, 1942.
18. Landau, R. L., and K. Lugibihl. Unpublished studies.
19. Landau, R. L., D. M. Bergenstal, K. Lugibihl, D. F. Dimick, and E. Rashid. J. Clin. Endocrinol. & Metab., 17:177, 1957.

NUCLEIC ACID-SPLITTING ENZYMES IN HUMAN EPIDERMIS AND THEIR POSSIBLE ROLE IN KERATINIZATION*

By

P. Santoianni† and S. Rothman

The disappearance of nuclei from cells undergoing cornification is one of the most characteristic features of the keratinization process. As an indication of nuclear breakdown, water-soluble degradation products of nucleic acids have been demonstrated in keratinized structures.

It is not known whether enzymes hydrolyzing nucleic acids participate in this breakdown. A ribonuclease has been found in guinea pig epidermis by Tabachnick and Freed;[1] Steigleder and Raab[2] found that human epidermis is able to split nucleic acids.

The present work deals with the problem whether the disappearance of nuclei in keratinization could be due to an enzymatic process, and the biochemical behavior of the enzymes involved, if any. Human and rat epidermis were studied. Studies on the effects of feeding vitamin A were also carried out in an attempt to connect the presence of DNase in the epidermis with the keratinization process.

MATERIALS AND METHODS

Normal human skin was obtained from the breast, legs and abdomen of fresh surgical specimens. The epidermis was separated from the dermis by the stretch method.[3] Rat epidermis was obtained, after clipping of the hair, by scraping of the stretched skin.

For the deoxyribonuclease assay we used a method based on the formation of DNA acid-soluble products,[4] with subsequent determination of deoxyribose by indole.[5] A microprocedure, developed for the study of non-purified preparations, such as epidermis homogenates, will be described in detail below. Ribonuclease was detected and studied by a microprocedure based on the method of Dickman et al.[6] Protein concentration was determined by the method of Lowry et al.[7] DNA was estimated by a micromethod based on the extraction method of Ogur and Rosen[8] and on the indole reaction for deoxysugars.[5]

The following substrates were used: highly polymerized calf thymus DNA (Worthington Biochemicals Corporation, Freehold, New Jersey), yeast RNA (Pabst Laboratories, Milwaukee, Wisconsin). DNase I crystalline, and pancreatic RNase (Worthington Biochemicals Corporation, Freehold, New Jersey) were applied in control experiments.

Vitamin A palmitate, water dispersible, was obtained from Nutritional Biochemicals Corporation, Cleveland, Ohio.

Sulwer-Hall white rats of both sexes were used for the in vivo experiments.

Epidermis extracts for the enzymatic assays were prepared in the following way. Human

---

*This paper was presented at the 22nd Annual Meeting of the Society for Investigative Dermatology June 27-29, 1961 and will appear in J. Invest. Dermatol.

†Section of Dermatology, Department of Medicine, University of Chicago. Present address: Clinica Dermatologica Policlinico, Napoli, Italy.

epidermis was finely minced and then homogenized with 0.15 M NaCl in the approximate ratio of 1 ml per 100 mg of fresh tissue. A conical glass homogenizer with motor driven pestle was used and the operation was carried out at 0°C for about 1 minute.

In some experiments an acetone powder was prepared: the minced tissue was rapidly stirred with about 50 volumes of acetone (prechilled to minus 12°C) for three minutes in a cold room. The mixture was then sucked in a Buchner funnel, washed with about 100 volumes of acetone and dried in a stream of nitrogen. The powder was extracted with 0.15 M NaCl, in the approximate ratio of 2 ml per 100 mg of powder.

The "homogenates" obtained in both ways were centrifuged at about 5000 rpm for 10 minutes at 4°C; the supernatant was set aside and the remaining tissue was again extracted by homogenization with an equal volume of saline solution. The suspension was agitated for 12-16 hours at 4°C, and after centrifugation, the supernatant was combined with the supernatant of the first homogenization. The supernatants, containing the epidermal "soluble proteins"[9] were dialyzed against 5 mM acetate buffer (pH 6) for three hours, with agitation.

The extracts from rat epidermis were prepared by homogenization of minced epidermis in a glass homogenizer with a Teflon pestle, and by subsequent extraction with saline solution. The extraction was followed by dialysis.

Deoxyribonuclease activity. For DNase II assays, the following procedure was developed. The standard assay mixture contained, in a total volume of 150 μl:100 μg of DNA; 10 μ moles of sodium acetate buffer pH 5.0; 10 to 30 μl of epidermis extract. The mixtures were incubated at 37°C for 1 hour. Blanks containing only epidermis extract and buffer were incubated at the same time. Inactivated tissue blanks were carried out with extracts boiled for 15 minutes.

The reaction was stopped by adding 50 μl of ice-cold 10 per cent perchloric acid. After mixing, the tubes were left for five minutes in an ice-bath, then centrifuged at 3000-5000 rpm for five minutes. One hundred μl of the filtrates were used for the deoxypentose estimation with the indole reaction.

The use of the indole reaction for deoxypentose has been introduced in the determination of deoxyribonuclease because its sensitivity is higher than the diphenilamine method used by Allfrey and Mirsky.[4] The use of perchloric acid as precipitant instead of trichloracetic acid, made possible the estimation of DNase also by U.V. measurement of the degradation products of DNA. For spectrophotometry 50 μl aliquots of the perchloric acid filtrates were diluted 5-fold with water and the absorbency was measured in 100 μl cuvettes in a Beckman D.U. spectrophotometer, equipped with the Lowry and Bessey[10] micro-attachment.

Deoxyribonuclease activity was expressed in micrograms of deoxyribose-P released per hour of incubation and per milligram of protein. In addition the enzyme activity was expressed per microgram of DNA-P and per milligram of dry defatted tissue (acetone powder).

RESULTS

Deoxyribonuclease II. DNase II could be demonstrated and quantitated in both human and rat epidermis. The data shown in Table 1 reveal that comparatively much higher activity is present in the rat epidermis, the values approaching those of the spleen.

In an attempt to demonstrate the presence of this enzyme also in the dermis, the epidermis of rat skin was carefully separated from the corium by the stretch method and homogenized in a glass homogenizer. Subsequently, the denuded skin was scraped to make sure that all the epi-

Table 1

DEOXYRIBONUCLEASE II ACTIVITY

	Micrograms of deoxypentose—P liberated per hour		
	Per mg of protein	Per mg of dry tissue	Per μg of DNA-P
Human epidermis	7.6	0.4	0.5
Rat epidermis	53.0	3.1	3.4
Rat spleen	61.0	9.0	4.2

dermal cells were removed. Strips of dermis were minced and homogenized in a "Virtis 45" homogenizer with 0.15 M NaCl. Table 1 shows that no activity was found in the dermis extract.

The activity of the epidermal DNase was found to have a sharp optimum at pH 5 (Figure 1).

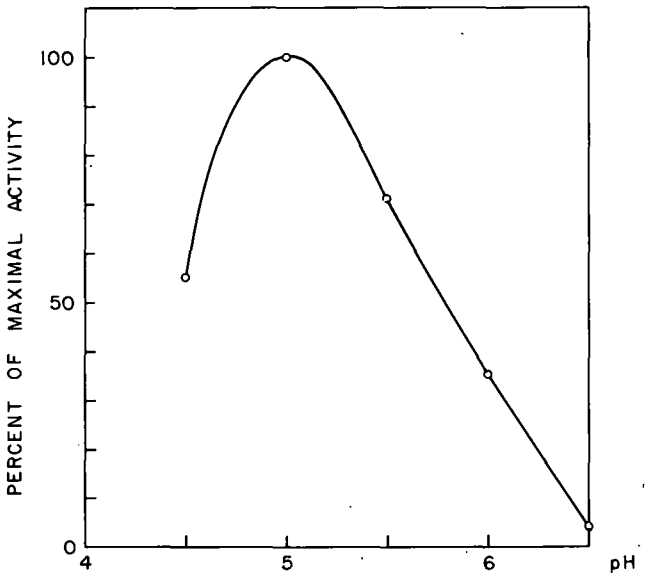

Figure 1. Effect of pH on epidermal DNase. The reaction mixtures contained 100 μg of DNA; 10 μmoles of sodium acetate buffer, and human epidermis extract in a total volume of 150 μl.

The activity of epidermal DNase as a function of time is shown in Figure 2. The slope representing the initial velocity of the reaction is less steep than that representing the subsequent time course of the reaction. A similar lag period has been observed for DNase of other tissues.[11] The two curves in Figure 2 represent two series of experiments carried out with different amounts of extract. They show that under these conditions the method used yields good proportionality in a wide range of extract concentrations.

The effect of physiological ions was tested on human epidermal DNase II. The addition of 100 mM NaCl to the standard assay resulted in activation by 15 per cent. The activity was inhibited by $MgSO_4$ in 33 mM concentration. This inhibitory effect may explain the low values

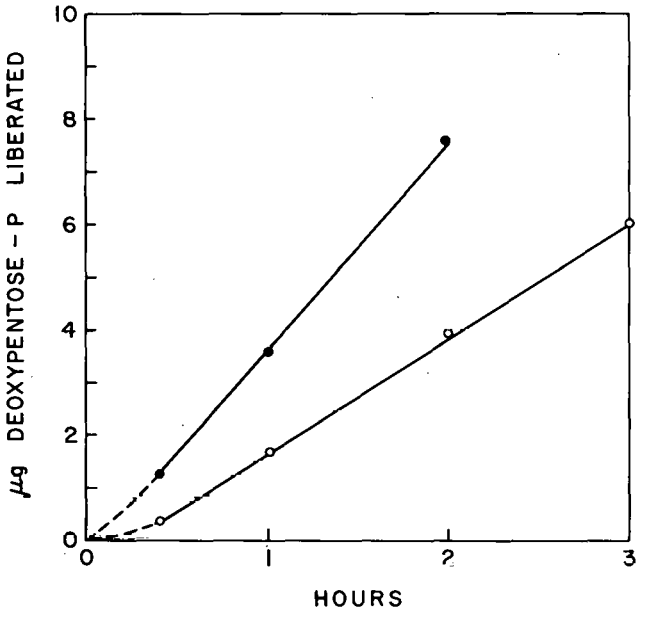

Figure 2. Enzymic hydrolysis of DNA by epidermal extract as a function of time. Total volume of reaction mixtures, 0.6 ml o ml 0.1 extract, • ml 0.2 extract.

initially obtained by us when experiments were carried out with not completely de-ionized water.

Deoxyribonuclease I. "Neutral" deoxyribonuclease activity was tested by a procedure similar to that for DNase II, but in presence of 100 mM Tris buffer, pH 7.2, and $MgSO_4$ (in concentrations up to 33 mM Mg^{++} is required for DNase I activity).

No activity could be demonstrated by this procedure, even in absence of Na ions, which reportedly are inhibitory.[12]

Ribonuclease. Ribonuclease was detected in human and rat epidermis extracts. For the assay the reaction mixture (100 μl) contained 2.5 μ moles of Tris buffer, pH 7.5; 10 μ moles NaCl; 0.75 mg of RNA (neutralized and dialyzed) and 10 to 30 μl of epidermis extract.

The mixture was incubated at 37°C for 30 minutes. Three hundred μl of glacial acetic acid-tert. butanol (1 to 2 parts) were added to stop the reaction. The tube was kept in an ice-bath for

Table 2

DEOXYRIBONUCLEASE ASSAY IN EPIDERMIS AND DERMIS OF RAT

Determinations in duplicate on 10 μl of extracts.

	Protein concentr. mg/ml	μg deoxypentose-P liberated/h/ mg protein
Epidermis	7.0	34
Dermis	3.8	0
Epidermis	6.0	41
Dermis	5.6	0

five minutes and the precipitate was removed by centrifugation. Finally 100 μl of the supernatant solution were diluted to 600 μl in water and the absorbency of the solution was determined in a Beckman D.U. spectrophotometer at 260 mμ.

The experimental readings were corrected in relation to a blank determined by incubating only buffer and extract and adding first acetic acid-butanol, and afterwards RNA. The values obtained with this blank system were further corrected by those of a substrate blank. Standards with crystalline RNase were also run.

A unit of activity corresponds to the amount of enzyme causing an increase in absorbency of 260 mμ of 1.0 as compared with the blank. Table 3 shows the average RNase activity of human and rat epidermis.

Table 3

RIBONUCLEASE ACTIVITY

	units/mg of protein	units/ μg of DNA-P
Human epidermis	7.0	0.46
Rat epidermis	11.6	0.78

Divalent cations, e.g., Zn^{++} and Cu^{++} reportedly inhibit ribonuclease.[13] Since these ions may come in contact with human skin (occupational diseases, therapeutic use of d'Alibour solution), we have investigated the influence of Zn and Cu ions on epidermal ribonuclease.

Inhibition was found even with extremely low concentrations (Table 4). The epidermal RNase was found sensitive also to heparin, corresponding with other findings concerning the inhibitory effect of anionic polymers.[14]

Table 4

INHIBITORS OF EPIDERMIS RIBONUCLEASE

For the assay the reaction mixture (100 μl) contained 2.5 μ moles of Tris buffer, pH 7.5; 10 μ moles NaCl; 0.75 mg of RNA and 10 μl epidermis extract

Addition of	Inhibition %
$ZnCl_2$ 1 m M	70
$CuSO_4$ 1 m M	53
Heparin (1 mg)	10

The maximal activity of this enzyme was found to be at pH 7.5 (Figure 3).

The enzymatic nature of the RNA depolymerization was further established by the relation between concentration of extract and activity. In our assay linearity was present in a wide range (Figure 4).

Influence of vitamin A on epidermal DNase activity in vivo. After having demonstrated the presence of DNase in the epidermis, the question arises whether this enzyme plays any role in the disappearance of cell nuclei during keratinization.

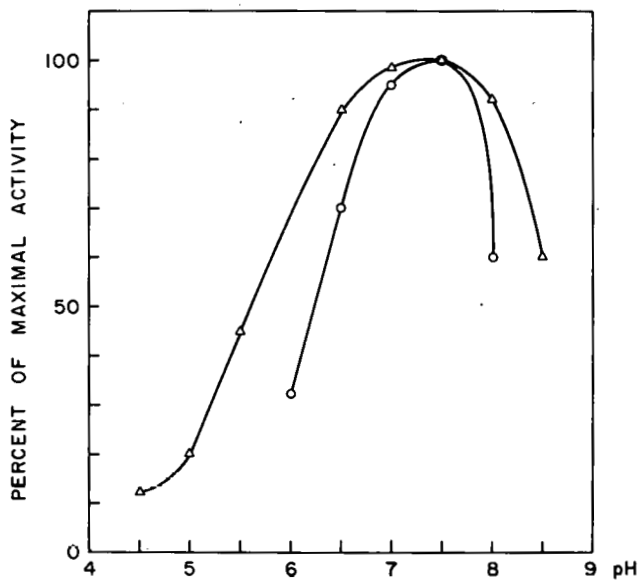

Figure 3. Effect of pH on epidermis RNase activity. The reaction mixtures contained 6 μ moles of acetate-borate-cacodylate buffer; 0.75 mg of RNA and epidermal extract in a total volume of 100 μ l. Δ - Human epidermis RNase. O - Rat epidermis RNase.

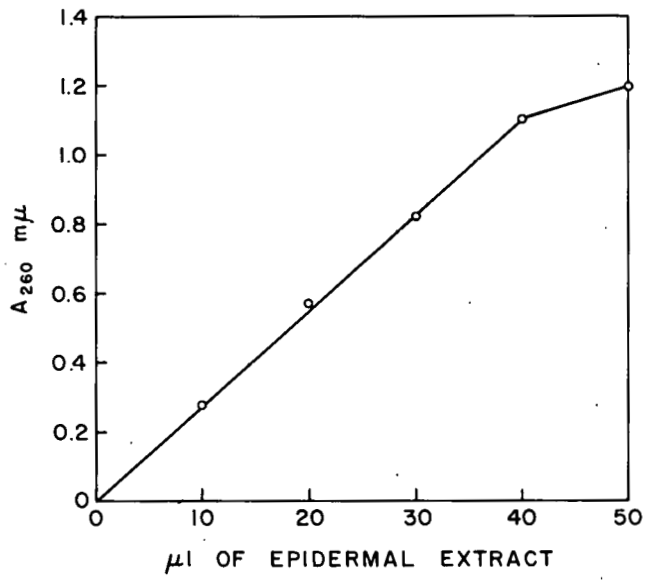

Figure 4. RNase activity of rat epidermis extract as a function of concentration.

We tried to approach this problem by feeding vitamin A to rats. Vitamin A is known to be a powerful antikeratinizing factor and as such hinders the loss of nuclei in normally keratinizing epidermis. This may take place by inhibiting DNase. We therefore tested whether feeding of excess vitamin A has any inhibitory influence on epidermal DNase activity.

In a first series of experiments, three pregnant rats were fed a diet containing 40.000 units per day of vitamin A palmitate. An equal number of pregnant animals were given a normal diet as controls.

After one week of feeding, both experimental and control mothers delivered. The administration of vitamin A was continued for two more weeks by giving 40.000 units per day to the mother rats as well as to the eight newborn rats in the experimental group. The animals were then sacrificed, the total feeding period being 3 weeks.

The shaved dorsal skin was excised, and extracts were prepared as described. Separate enzymatic assays were performed on pooled extracts from adult and from newborn animals. A decrease of DNase activity of 50 per cent was observed in the treated animals, as compared with the control groups (Table 5). There was no difference in this decreased activity between adult and young.

Table 5

DEOXYRIBONUCLEASE ACTIVITY OF RAT SKIN TREATED WITH VITAMIN A

Determinations in triplicate. Activity expressed as μg of deoxypentose-P liberated/mg of protein/hour.

	Control animals	Treated animals
Adult*	56.5	22
Young*	42.5	20

*Average weight at end of experiment: Control adults: 230 g; Treated adults: 230 g; Control young: 48 g; Treated young: 43 g.

In a second experiment 15 rats, 6 weeks old and weighing 80-90 g were fed the vitamin A diet, and 15 others were used as controls. After three weeks all the animals were sacrificed, the hair shaved, and the dorsal skin excised. The spleen of each animal was also removed.

The epidermal extracts were prepared in the usual way and pooled so that the analysis for DNase was done in 5 groups of 3 animals each. The enzymatic activity of spleen extracts was determined in order to see whether the effect of vitamin A is specifically directed against the epidermal enzyme or is general. The results are given in Table 6, and show that the DNase activity of the epidermis in the vitamin-fed animals was depressed on an average 25 per cent, while in the spleen such depression did not occur or was minimal.

Deoxyribonuclease activity and x-ray effect. It has been reported by Douglass et al.[15] that x-irradiation causes an increased activity of the enzyme in rat spleen. Kurnick et al.[16] have shown that total-body irradiation results in marked increase in the acid DNase activity of the spleen, liver, thymus and nucleated bone marrow cells of the mouse. This phenomenon was explained as being due to destruction of an enzyme inhibitor by x-rays.[16]

To test whether the epidermal DNase is sensitive to x-rays, ten rats were exposed to 500 r of total-body x-irradiation, at the rate of 30.8 r/minute, with 200 kv, 15 ma, inherent filtration only, HVL 0.25 mm Cu, 95 cm target distance. Twenty-four hours after irradiation the animals were sacrificed. No difference of DNase activity was found between these animals and con-

Table 6

EFFECT OF VITAMIN A ON DEOXYRIBONUCLEASE

Determinations in triplicate. Activity expressed as μg of deoxypentose-P liberated/mg of protein/hour

Group	Control animals		Treated animals	
	Epidermis	Spleen	Epidermis	Spleen
1	48	63	40	58
2	55	60	36	60
3	52	62	37	56
4	55	58	41	60
5	50	60	38	61
Average	52	61	38	59
% Decrease	--	--	26	3.5

trols. A possible explanation for this may be that the epidermis of rat lacks the inhibitor which is present in other tissues.

DISCUSSION

It is interesting to note that human epidermis contains type II deoxyribonuclease with an optimum pH of 5 (and no type I with a pH 7.5 optimum) because the pH of the subcorneal barrier where keratinization starts is around pH 5.[17]

Both type I and type II enzymes are endonucleases acting on the center of the polymer chain.[18] Both preferentially hydrolyze the bonds between purine and pyrimidine nucleotides, but while for DNase I the products of hydrolysis are oligonucleotides carrying the monoesterified phosphoryl group on carbon 5', DNases II yield fragments carrying the phosphoryl group on carbon 3'.[19]

Furthermore, the two types of DNases differ in their sensitivity to inhibitors and activators: DNases of type II have a requirement for high concentrations of monovalent cations such as Na^+, K^+,[19,20] while DNases of type I are inhibited by high concentrations of Na ions.[12]

DNases II are inhibited by concentrations of Mg^{++} higher than 1 mM[19,21] and by polyvalent anions (e.g. SO_4^{--}) at 5 mM,[19] whereas DNases I require Mg^{++} for their activity, and are inhibited by anions which remove Mg ions, as citrate, arsenate, fluoride, and EDTA.[22] The human and rat epidermis DNases share the principal properties of other DNases II.

Many tissues contain a thermolabile inhibitor for DNase I and a thermostable activator.[23] Identification of DNase I may therefore require the use of methods designed to inactivate the inhibitors.

Concerning the physiological significance of the tissue DNases, the data reported by Allfrey and Mirsky suggest that there is some correlation between the deoxyribonuclease activity of a tissue and its capacity for proliferation and regeneration. Tissues capable of high mitotic activity have higher deoxyribonuclease concentrations. The incorporation of N^{15} glycine into the deoxypentose nucleic acids of the chromosome is most rapid in tissues with high DNase concentrations.[4]

The ribonucleases of animal tissues exhibit specificity for those phosphodiester bonds that involve the nucleosides of cytosine and uracyl, producing RNA fragments rich in purine bases, and pyrimidine nucleoside-3'-phosphates.[2]

Since we have found RNase and DNase II in human and rat epidermis we must assume that nucleoside-3' phosphate fragments are formed there. Other enzymes acting on these fragments may further break down these split products.

The epidermis has a high ribonuclease content and a high mitotic rate. This agrees with the finding of other authors[25] that ribonuclease content and rate of cell proliferation are related.

Hypervitaminosis A produced thickening of the epidermis in the rat.[26] While in normal epidermis tritiated thymidine is taken up only by basal cell nuclei, in vitamin A-treated tissues it is incorporated also into nuclei of cells of the outer epidermal layers.[27] We may assume that vitamin A hinders depolymerization of the nuclei as it physiologically should occur in the outer layers. Therefore, the incorporated thymidine may be retained. The recent findings of Pelc and Fell[27] are in agreement with our working hypothesis that the antikeratinizing effect of vitamin A might be brought about by a depressing action on DNase activity or by inhibition of the synthesis of the enzyme.

The results of our vitamin A experiments do not directly answer our original question whether the epidermal DNase plays a role in the disappearance of nuclei during physiological keratinization. Nevertheless, the highly suppressive effect of vitamin A on the activity of this enzyme in vivo can be regarded at least as strong presumptive evidence that DNase plays an important role in the decomposition of epidermal nuclei in the cornifying layers.

LITERATURE CITED

1. Tabachnick, J., and R. Freed. Federation Proc., 19:51, 1960.
2. Steigleder, G. K., and W. P. Raab. J. Invest. Dermat., in press.
3. Van Scott, E. J. J. Invest. Dermat., 18:377, 1952.
4. Allfrey, V., and A. E. Mirsky. J. Gen. Physiol., 36:227, 1952.
5. Keck, K. Arch. Biochem. Biophys., 63:446, 1956.
6. Dickman, S. R., J. P. Aroskar, and R. B. Kropf. Biochim. et Biophys. Acta, 21:539, 1956.
7. Lowry, H. O., N. J. Rosebrough, A. L. Farr, and R. J. Randall. J. Biol. Chem., 193:265, 1951.
8. Ogur, M., and G. Rosen. Arch. Biochem. Biophys., 25:262, 1950.
9. Matoltsy, A. G., and F. S. M. Herbst. J. Invest. Dermat., 26:339, 1960.
10. Lowry, O. H., and O. A. Bessey. J. Biol. Chem., 163:637, 1946.
11. Brody, A. Acta Chem. Scand., 7:721, 1953.
12. Kunitz, M. J. Gen. Physiol., 33:363, 1950.
13. Kaplan, H. S., and L. A. Heppel. J. Biol. Chem., 222:907, 1956.
14. Roth, J. S. Arch. Biochem. Biophys., 44:265, 1953.
15. Douglass, C. D., and P. L. Day. Proc. Soc. Exptl. Biol. and Med., 89:616, 1955.

16. Kurnick, N. B., B. W. Massey, and G. Sandeen. Ann. N. Y. Acad. Sci., 75:61, 1958.

17. Szakall, A. Hautphysiologische Forschung und Gesunderhaltung der Haut., 53:399, 1951.

18. Laskowski, M. Ann. N. Y. Acad. Sci., 81:776, 1959.

19. Koerner, J. F., and R. L. Sinsheimer. J. Biol. Chem., 228:1039, 1957.

20. Shimomura, M., and M. Laskowski. Biochim. et Biophys. Acta, 26:198, 1957.

21. Oth, A., E. Fredericq, and R. Hacha. Biochim. et Biophys. Acta, 29:287, 1958.

22. Laskowski, M. The Enzymes, edited by P. D. Boyer, H. Lardy, and K. Myrback, New York, Academic Press, Inc., 1961, p. 123.

23. Feinstein, R. N. J. Biol. Chem., 235:733, 1960.

24. Anfinsen, C. B., and F. H. White. The Enzymes, edited by P. D. Boyer, H. Lardy, and K. Myrback, New York, Academic Press, Inc., 1961, p. 95.

25. Brody, S. Biochim. et Biophys. Acta, 24:502, 1957.

26. Studer, A., and J. R. Frey. Schweiz. med. Wochenschr., 79:382, 1949.

27. Pelc, S. R., and H. B. Fell. Exptl. Cell. Research, 19:99, 1960.

STAFF PUBLICATIONS

Dukes, P. P., and E. Goldwasser. Inhibition of erythropoiesis by estrogens. Endocrinol., 69: 21, 1961.

Goepp, R., and F. Fitch. Oral radiation death. Rad. Res., 14: April 1961 (Abstract).

Griem, M. L., and K. Ranniger. Potentiation of the radiation effect on the hair roots of the mouse using Actinomycin D. Rad. Res., 14: April 1961 (Abstract).

Griem, M. L., J. A. Stein, R. P. Reinertson, R. Reinertson, and B. R. Brown. Comparison of effects of I^{131}-induced hypothyroidism and L-triiodothyronine on irradiated hair roots in mice. Rad. Res., 15:202, 1961.

Gurney, C. W., and N. Wackman. Impairment of erythropoiesis by irradiation. Nature, 190: 1017, 1961.

Gurney, C. W., N. Wackman, and E. Filmanowicz. Studies on erythropoiesis. XVII. Some quantitative aspects of the erythropoietic response to erythropoietin. Blood, 17:531, 1961.

Harper, P. V. Characteristics and manufacture of radioisotopes for medical purposes at the Argonne Cancer Research Hospital - Chicago, Illinois, V° Congresso Internazionale per L'Energia Nucleare, 2:245, 1960 (Guigno).

Jacobson, L. O., C. W. Gurney, and N. Wackman. Radiation damage to stem cells. Rad. Res., 14: April 1961 (Abstract).

Jacobson, L. O. The nature of radiation anemia. Acta Haematol. Jap., 23:36, Suppl. 1960.

Jones, R. J., O. K. Reiss, and M. F. Golden. Influence of a brain extract upon cholesterol metabolism. Reprinted from: Drugs Affecting Lipid Metabolism, Proceedings of the Symposium on Drugs Affecting Lipid Metabolism, eds. S. Garattini and R. Pagletti, pp. 212-20, 1961. Publisher: Elsevier Publishing Company, Amsterdam.

Kabara, J. J., and G. T. Okita. Brain cholesterol: biosynthesis with selected precursors in vivo. J. Neurochem., 7:298, 1961.

Kappas, A., R. H. Palmer, and P. B. Glickman. Steroid fever (editorial). Am. J. Med., 31:167, 1961.

Marks, E. K. Erythropoietin: the red blood cell regulating hormone. Am. J. Med. Technol., July-August, p. 233, 1961.

Marver, H. S. Studies on tryptophan metabolism. I. Urinary tryptophan metabolites in hypoplastic anemias and other hematologic disorders. J. Lab. Clin. Med., 58:425, 1961.

Mendel, G. A. Studies on the relationship between erythropoietic activity and iron absorption. Rad. Res., 14: April 1961 (Abstract).

Rothman, S., and A. L. Lorincz. Pharmacology of topical therapy. The Pediatric Clinics of N. Amer., 8:697, 1961.

Spratt, J. L., and G. V. LeRoy. Immediate decrease in respiratory $C^{14}O_2$ excretion following simultaneous intravenous administration of $NaHC^{14}O_3$ and acetazoleamide in the rat. Proc. Soc. Exptl. Biol. Med., 107:387, 1961.

Thompson, J. S., D. Hofstra, and E. L. Simmons. Immunologic unresponsiveness of homologously-treated x-irradiated mice during the secondary disease period. Rad. Res., 14: April 1961 (Abstract).

Weiss, S. B., and T. Nakamoto. On the participation of DNA in RNA biosynthesis. Proc. Nat. Acad. Sci., 47:694, 1961.